Title

Bare Soil Evaporation at Kesterson Reservoir, Merced County, California: Estimation by Physical and Chemical Methods

Author

Zawislanski, Peter T.

Publication Date

1989-12-01

Thesis/dissertation

LBL-28207

Lawrence Berkeley Laboratory

UNIVERSITY OF CALIFORNIA

EARTH SCIENCES DIVISION

Bare Soil Evaporation at Kesterson Reservoir, Merced County, California: Estimation by Physical and Chemical Methods

P. T. Zawislanski
(M.S. Thesis)

December 1989

Prepared for the U.S. Department of Energy under Contract Number DE-AC03-76SF00098.

DISCLAIMER

LBL-28207

Bare Soil Evaporation at Kesterson Reservoir, Merced County, California: Estimation by Physical and Chemical Methods

Peter Thomas Zawislanski

(M.S. Thesis)

Earth Sciences Division
Lawrence Berkeley Laboratory
1 Cyclotron Road
Berkeley, California 94720

December 1989

This work was supported by the U.S. Bureau of Reclamation, under U.S. Department of Interior Interagency Agreement 9-AA-20-07250, through U.S. Department of Energy Contract DE-AC03-76SF00098.

BARE SOIL EVAPORATION AT KESTERSON RESERVOIR, MERCED COUNTY, CALIFORNIA: ESTIMATION BY PHYSICAL AND CHEMICAL METHODS

Peter Thomas Zawislanski

ABSTRACT

As a result of ponding of agricultural drainage water at Kesterson Reservoir, highly saline and seleniferous water entered the soil-water system. Concentrations of salts, boron, and selenium in the ponds, and biological accumulation and magnification of those species, particularly selenium, caused the deaths and deformities of thousands of waterfowl since 1983. After several years of drainage water delivery to the reservoir, concentrations of most species present, including selenium, were found to be highest near and at the soil surface, but were also elevated in soil water, and slightly elevated in groundwater. The speciation and fluxes of salts, boron, and selenium are of interest in order to assess the likely future of surface and subsurface conditions at Kesterson Reservoir. Among processes which control the physical redistribution of species in the subsurface, and near the soil surface, is evaporative concentration. The magnitude and nature of this process were studied through direct flux measurements as well as changes in the chemical composition of a defined near-surface soil interval. Direct evaporation flux measurements were made using a lysimetric (gravimetric) approach. Surface soil was sampled periodically and concentrations of species in a 10:1 water:soil extract were measured. Temporal changes in chloride concentrations and in soil moisture content were used in a quantitative assessment of a mean seasonal surface evaporative flux. All measurements were performed in a salt-crust-covered playa-like environment within two ponds which received moderate amounts of drainage water.

Results of both direct and indirect measurements are indicative of low bare soil evaporation rates at both test plots. Directly measured rates ranged between 0.10 and 1.36 mm day^{-1}. These rates were measured in the summer and fall of 1988 and the late spring and early summer of 1989. Estimates of mean seasonal bare soil evaporation rates were between 0.36 and 0.66 mm day^{-1} for one of the two plots and between 0.51 and 0.73 mm day^{-1} for the other. These values fall within the range of values measured directly. In

addition, an empirical equation based only on potential evaporation and the moisture content of a defined near-surface soil interval was fit to the directly measured bare soil evaporation data. The satisfactory fit of this equation suggests that trends in bare soil evaporation are dependant mostly on the two variables used. If this is the case, then the low magnitude of bare soil evaporation rates in this setting may correspond to rates of water vapor diffusion. The high porosity, low bulk density salt-crust covering the soil surface may have hydrologic effects similar to those of a surface mulch in limiting the water flux to predominantly a vapor flux. This supposition was tested somewhat more quantitatively using a numerical model to simulate evaporative fluxes with and without accounting for vapor diffusion. The greater sensitivity of the model to external conditions when vapor diffusion was taken into account, resulted in the model more accurately reproducing the relative changes in evaporation rates, if not the absolute rates per se.

In agreement with the observed changes in salt and selenium concentrations near the soil surface, the low bare soil evaporation rates are not likely to cause a significant increase in species concentrations during the coming years. Nevertheless, the sensitivity of soluble species to both an evaporative flux and infiltration is considerable, and while net changes in concentrations from one year to another may be slight, seasonal variations in salts and, to a lesser degree, selenium concentrations are an important component in the soil system at Kesterson Reservoir.

TABLE OF CONTENTS

LIST OF FIGURES

LIST OF TABLES

NOMENCLATURE

A	area, L^2
C	mass concentration of solute per volume of solution, ML^{-3}
$C_{A,v}$	gas phase vapor concentration per volume of air, ML^{-3}
D_{hd}	solute hydrodynamic dispersion coefficient in a porous medium, L^2T^{-1}
D_{lm}	distance between nodal points l and m, L
D_m	solute mechanical dispersion coefficient in a porous medium, L^2T^{-1}
D_0	solute diffusion coefficient in pure water, L^2T^{-1}
$D_{A,v}$	water vapor diffusion coefficient in air, L^2T^{-1}
$D_{S,v}$	water vapor diffusion coefficient in soil air, L^2T^{-1}
e_A	saturation vapor pressure at air temperature, $ML^{-1}T^{-2}$
e_D	saturation vapor pressure at dewpoint temperature, $ML^{-1}T^{-2}$
E_{bs}	bare soil evaporation rate, LT^{-1}
E_P	potential evaporation rate, LT^{-1}
E_{pan}	pan evaporation rate, LT^{-1}
$f(u)$	an empirically determined function of wind velocity u, L^2TM^{-1}
g	acceleration due to gravity, LT^{-2}
h	relative air humidity, as fraction of saturated water vapor concentration, 1
h_S	relative soil air humidity, as fraction of saturated water vapor concentration, 1
J_{adv}	advective mass flux of solute across a unit cross-sectional area of medium per unit time, $ML^{-2}T^{-1}$
J_{diff}	diffusive mass flux of solute per unit area per unit time in porous medium, $ML^{-2}T^{-1}$
J_{hd}	mass flux of solute per unit area per unit time in porous medium due to hydrodynamic dispersion, $ML^{-2}T^{-1}$
J_m	mass flux of solute per unit area per unit time in porous medium due to mechanical dispersion, $ML^{-2}T^{-1}$
J_w	diffusive mass flux of solute per unit area per unit time in pure water, $ML^{-2}T^{-1}$
$J_{A,v}$	vapor mass flux per unit bulk area in air, $MT^{-1}L^{-2}$
$J_{S,v}$	vapor mass flux per unit bulk area in soil air, $MT^{-1}L^{-2}$
k	intrinsic permeability, L^2
K	hydraulic conductivity, LT^{-1}
K_{sat}	saturated hydraulic conductivity, LT^{-1}
M_c	fluid mass capacity, ML^{-1}

M_{charge}	molar charge concentration of solute molecules, moles L^{-3}
M_{solid}	mass of solid, M
M_w	mass of water, M
n	porosity, 1
$\bar{n}$	unit outward normal vector, 1
P	pressure, $ML^{-1}T^{-2}$
q	specific flux, LT^{-1}
$q_{S,v}$	diffusive vapor specific flux, LT^{-1}
$q_{w,adv}$	specific flux of water due advection, LT^{-1}
$q_{w,ebs}$	evaporative flux of water at the soil surface, equivalent to E_{bs}, LT^{-1}
Q	volumetric flow rate, L^3T^{-1}
r	pore radius, L
R	universal gas constant, $ML^2T^{-2}moles^{-1}Kelvin^{-1}$
R_A	areal net radiation, LT^{-1}
S	relative liquid saturation, 1
t	time, T
T	temperature, Kelvin or °C
U_{lm}	conductance of the interface between volume elements l and m, $ML^{-1}T^{-1}$
V	volume, L^3
z	elevation relative to a plane z_0, L
Δ	rate of saturation vapor pressure change with respect to temperature, $ML^{-1}T^{-2}degrees\ Celsius^{-1}$
γ	psychrometric constant, $ML^{-1}T^{-2}degrees\ Celsius^{-1}$; also, surface tension, MT^{-2}
Γ_l	surface area of element l, L^2
μ	dynamic viscosity of water, $ML^{-1}T^{-1}$
Π	osmotic pressure, $ML^{-1}T^{-2}$
ϕ_g	gravitational potential, L
ϕ_h	total hydraulic potential, L
ϕ_p	pressure potential, L
$\phi_{p,air}$	air-entry pressure potential, L
Φ_g	gravitational potential, L^2T^{-2}
Φ_o	osmotic potential, L^2T^{-2}
Φ_p	pressure potential, L^2T^{-2}
Φ_t	total potential, L^2T^{-2}
ψ	pressure potential, pressure head, L

ρ	fluid density, ML^{-3}
ρ_{bulk}	dry bulk soil density, ML^{-3}
τ	liquid-filled tortuosity factor, 1
τ_a	air-filled tortuosity factor, 1
θ	volumetric moisture content, 1
θ_{grav}	gravimetric moisture content, 1

ACKNOWLEDGEMENTS

The completion of this project could not have been possible without the technical and/or moral support of a number of people. Thanks go out to Prof. T.N. Narasimhan, my chief thesis advisor, who both in the classroom and on a more independent level of inquiry expected and encouraged creative thinking and clear expression. His instruction and direct help in my numerical modeling efforts are greatly appreciated. I also owe him the opportunity of being involved with the Kesterson Reservoir project and another research project in the past. Thanks to his persistent efforts and zeal, I was able to gain financial support for my work over the last two years. Another person instrumental in making my research at Kesterson possible is Dr. Sally Benson, of Lawrence Berkeley Laboratory, the Director of the Kesterson Program. She helped define my research topic and provided a number of helpful suggestions along the way.

I am forever indebted to Dr. Tetsu Tokunaga, of Lawrence Berkeley Laboratory, for his unparalleled generosity and insight. Without his assistance in setting up field equipment and instrumentation, his instruction in laboratory methods, and his willingness to explain in the greatest required detail numerous concepts and ideas, this project would have taken twice as long to complete while the final product would have undoubtedly been less. I admire his unmatched dedication to quality and objectivity: I hope at least some of his values have rubbed off on me.

Dr. Andy Yee and Joan Oldfather, both of Lawrence Berkeley Laboratory, performed all of the chemical analyses of soil water and groundwater, except for chloride analyses. Leon Tsao prepared standards and spiked samples for the quality control of the above analyses. I am very fortunate to have had their high quality services available to me throughout this study.

Also appreciated is the input of Prof. Kenneth Tanji and Dr. Greg Smith, of the University of California, Davis, on aspects of evaporite formation. Dr. Smith performed XRD analyses of salt crust material in one of the plots involved in this study.

The following people have read my thesis and provided many useful comments: Prof. Narasimhan, Prof. William Dietrich, Prof. David Jones, and Prof. Tanji, all of whom are members of my thesis committee; Dr. Tokunaga and Dr. Benson.

Finally, on a more personal level, I am grateful to all members of my family: my wife Suzanne, who probably had more confidence in my ability to complete this project than I did and who generously postponed her further education to allow me to finish mine; my parents, who have always expected me to do my best and made sure that my early educational experience was a rich one; and my two sons, Andrew and John, who helped put everything in proper perspective. The following qoute from Andrew, $3\frac{1}{2}$, exemplifies the kind of insight he had to offer:

"When you have wetness, and add hotness, you get dryness." (1989)

1.0 INTRODUCTION

Soil and water contamination at Kesterson Reservoir, Merced County, California (Fig. 1.1), by selenium and salts has been an environmental concern for several years. The complex speciation and transport paths of these contaminants in the soil system have been the subject of intense research. The potential for further salt and selenium redistribution in the soil profile due to evaporation, transpiration, and infiltration of water needs to be seriously considered in evaluating the present and future environmental risks. This research project was designed to focus on the process of bare soil evaporation as a likely mechanism for concentrating species at and near the soil surface. To that end, bare soil evaporation rates were measured directly in the field and estimated based on chemical changes in the soil system. The nature of the bare soil evaporation process was examined through empirical and numerical means. Based on changes in near-surface concentrations of salts and selenium over a twelve month period, predictions have been made for likely future changes in species distribution.

1.1 HISTORICAL BACKGROUND

The Kesterson Reservoir was constructed between 1968 and 1975. It was to serve as a flow regulating facility for agricultural drainage water flowing in the San Luis Drain from subsurface drains underlying irrigated fields of the Wetlands Water District to the San Francisco Bay Delta. For a score of reasons, amongst which budgetary constraints and concerns about the impact of such drain water on the biota of the San Francisco Bay were most prominent, the construction of the San Luis Drain was terminated at Kesterson Reservoir. As a result, instead of serving as a controlling reservoir, Kesterson became the terminal receptacle of high salinity drain waters. Instead of draining into the San Francisco

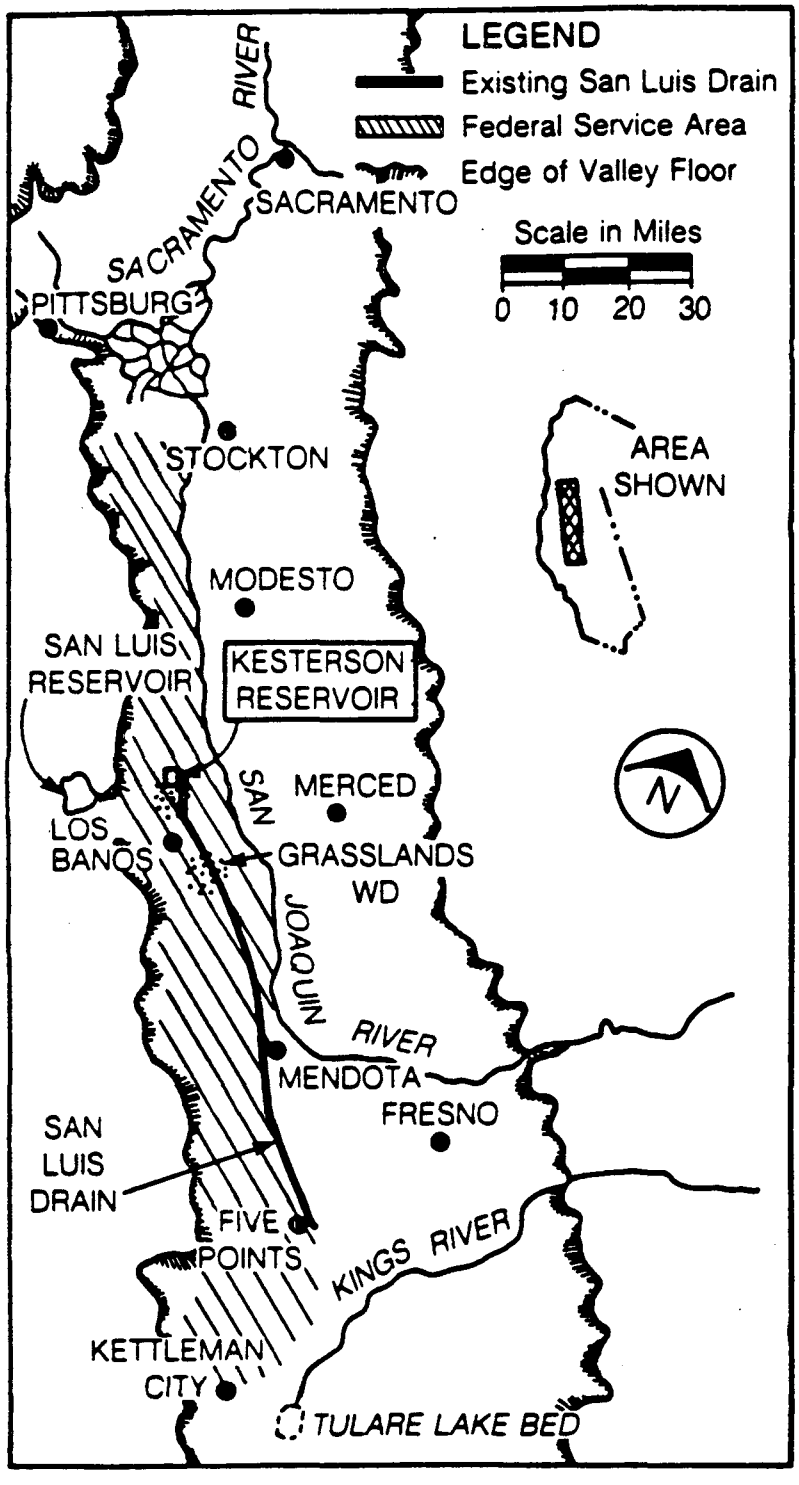

Figure 1.1 Location of Kesterson Reservoir within California and the San Joaquin Valley.

Bay, waste water was to be evaporated in a series of twelve unlined ponds at Kesterson Reservoir (Fig. 1.2). By 1981, the subsurface drainage system was connected to the San Luis Drain. By 1983, it became apparent that wildlife at Kesterson was being adversely affected by chemical species dissolved in the waste water. Fish and birds were dying and bird embryos were found to be deformed (Presser and Barnes, 1985). It was soon discovered that besides high concentrations of salts and boron (total dissolved solids ≈ 10,000 ppm), the drain water also contained very high concentrations of selenium (≈300 ppb, far exceeding the EPA drinking water standard of 10 ppb) (LBL Annual Report, 1987). It is selenium poisoning which has been singled out as the cause for the ecological disaster. Selenium is a natural component of soils derived from Cretaceous shales of the Coastal Ranges (Tidball and others, 1986). Selenium is an essential nutrient in trace amounts; 50-200 μg Se/day has been defined as the essential requirement for humans by the National Academy of Sciences (1980). However, only 500 μg/day is considered toxic to adults (Presser and Ohlendorf, 1988). While the main purpose of subsurface agricultural drainage is to prevent water logging of the crop root zone and the accumulation of salts in soil overlying a low permeability aquitard, the flushing out of selenium from the soils was not expected to result in as high a concentration in the drain water. The high evaporation rates prevalent in the San Joaquin Valley made Kesterson Reservoir an effective evaporation pond which led to rapidly increasing concentrations of both salts and selenium in the pond waters.

To prevent further wildlife contamination, the delivery of drain water to Kesterson was first curtailed and finally ceased completely by August 1986 (Long, 1988). Since then, several groups of researchers affiliated with the University of California have been investigating the nature and extent of selenium contamination at Kesterson Reservoir and attempting to devise the best way to remedy the situation. A number of plans have been proposed; these include an early suggestion by Lawrence Berkeley Laboratory researchers

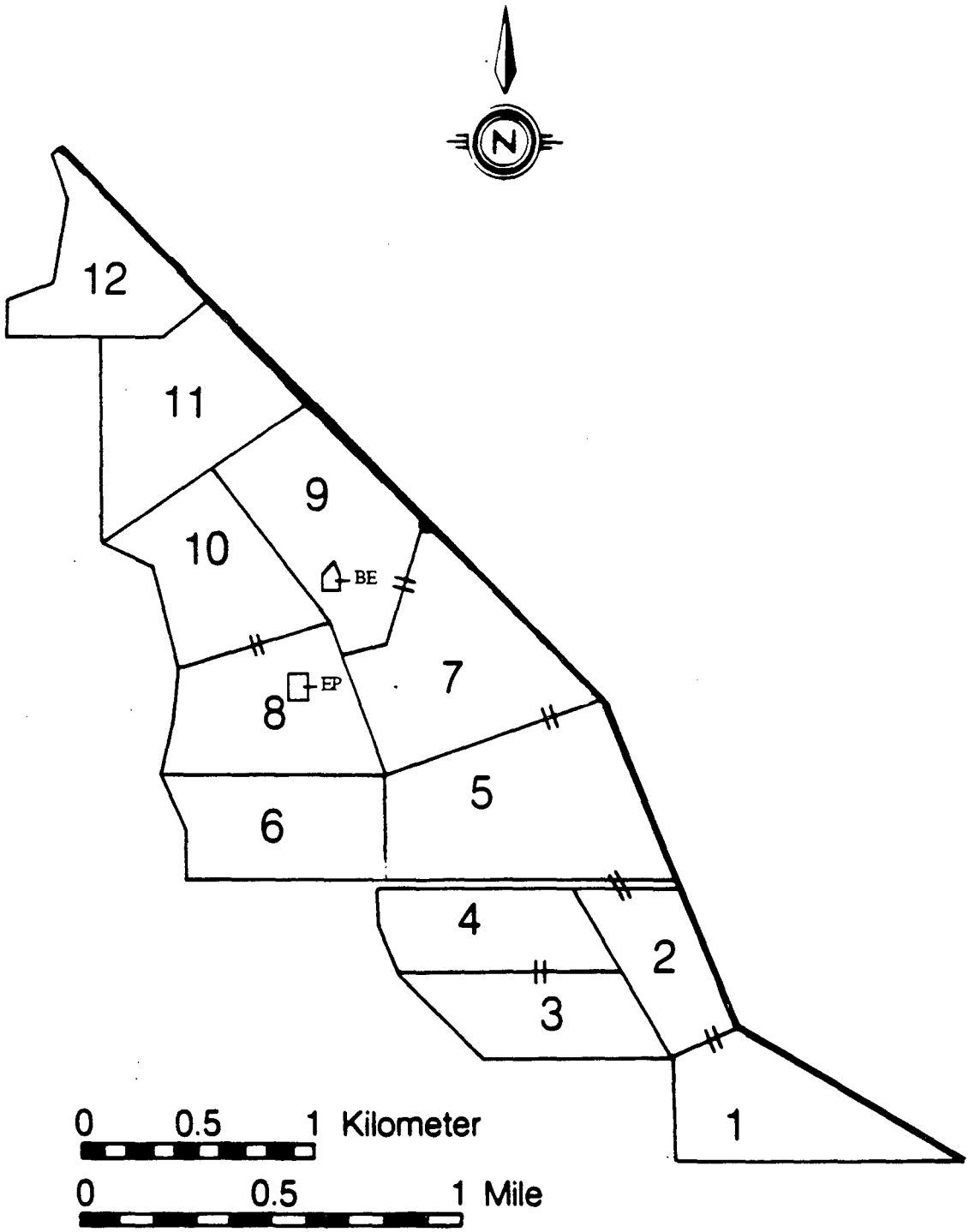

Figure 1.2 Distribution of ponds within Kesterson Reservoir. Plots 8EP and 9BE are marked.

of the Flexible Response Plan under which the Reservoir would be flooded with non-contaminated water. Because selenium is relatively immobile under reducing conditions, it was expected to precipitate and/or adsorb onto the soil in the pond bottoms, thereby not entering the food chain as readily as had oxidized forms of selenium (Weres and others, 1985; LBL Annual Report, 1987). This plan was rejected by the State Water Resources Control Board (SWRCB) as being too experimental. In March of 1987, the SWRCB ordered the Bureau of Reclamation (BOR), the operator of Kesterson Reservoir to implement the Onsite Disposal Plan which would involve the scraping off of 15 cm of the most contaminated top soil at the Kesterson Reservoir and placing it in an on-site hazardous waste landfill. After field experiments by LBL researchers showed that this could result in the evaporative reconcentration of salts and selenium in excavated test plots which would be subject to periodic flooding due to rainfall and a rising groundwater table, this remedial option was abandoned. In 1988, a decision was made by the SWRCB to fill with spoils from the construction of the Delta-Mendota Canal those parts of the Reservoir which were likely to become filled with water during the winter. The dual source of this water, rainfall and the rising water table, made it difficult to estimate the actual extent of seasonal pond formation; therefore, areas were filled to six inches above where the water table was expected to be under extreme conditions. The filling operation was completed by the end of November 1988. Currently, approximately 50% of the Reservoir's 1283 acres are covered with between 10 cm and 1 meter of fill material.

1.2 IMPETUS FOR RESEARCH

The soils of Kesterson Reservoir and the surrounding fields were salt-rich long before they were cultivated by humans. Early soil surveys performed from 1939 on by the U.S. Department of Agriculture and the University of California classified soils of the area

as slightly to strongly salt-affected (USDA Soil Conservation Service, 1952). The salinization of soils is a feature typical of regions characterized by high pan evaporation rates, low rainfall, and shallow ground-water tables, all of which are common to the San Joaquin Valley. Soil salinity is a valley-wide problem (Harradine, 1950); the proximity to shallow, highly saline groundwater has long been recognized (Fig. 1.3). Soils become salinized due to the evaporation of water at and near the soil surface and the transpiration of water by plants. The former results in the accumulation of salts at the surface while the latter process concentrates salts in the root zone (Hillel, 1980). Both processes lead to the degradation of soil from an agricultural standpoint. Evaporation of water from the soil surface creates an upward soil water potential gradient; in response to this gradient, water is transported from deeper in the profile towards the soil surface where it evaporates and the species dissolved in it precipitate. Along with the major ions (Na, Ca, Mg, SO_4 and Cl) any dissolved element, including trace elements will be subject to such redistribution. Evaporative concentration of naturally occuring selenium has been documented to occur in the Western San Joaquin Valley (Deverel and Fujii, 1989; Fujii and others, 1988; Fio and Fujii, 1988). Researchers from the U.S. Geological Survey found a close correlation between salinity and selenium (r^2=0.68) which suggested that the soluble selenium fraction (mostly selenate, SeO_4^{2-}) is fairly mobile in the soil/sediment system and may behave similarly to sulfate (SO_4^{2-}) and other major ions. These studies were performed in agricultural fields in the Panoche Creek alluvial fan area, an area assumed to be the source of much of the selenium which found its way into agricultural drains and eventually into Kesterson Reservoir.

While selenium is concentrated in soils in several areas of the San Joaquin Valley, it has caused greatest problems when further reconcentrated through human activity. The soil salinity problem was compounded at Kesterson Reservoir by the introduction of agricultural drain water containing selenenium. Due to the continuous evaporation of pond

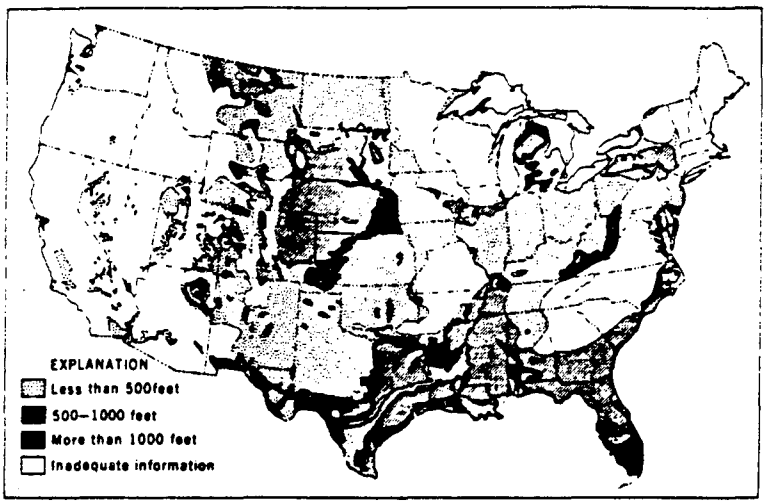

Figure 1.3 Distribution of shallow saline (more than 1000 mg/L) water in the United States (from Kohout, 1970).

water during the years of Reservoir operation, salts precipitated at the bottom and shorelines of the ponds and were incorporated into what is now a salt crust. The entire soil water profile is either saturated or nearly saturated with respect to gypsum ($CaSO_4 \cdot 2H_2O$) and calcite ($CaCO_3$). Selenium is incorporated into the salt crust; in the soil-water system, selenium concentrations range from background in the groundwater ($\approx$ 5 ppb) to thousands of ppb of dissolved selenium near the soil surface and several ppm of total selenium in the top few centimeters of soil. Field experiments performed by LBL personnel in March of 1988 involved the scraping off of 15 and 30 cm of top soil in Pond 6. As noted in the previous section, this resulted in the reconcentration of selenium and salts from below to near the soil surface. Excavation of a layer of soil accelerated the reconcentration process by decreasing the depth to the water table (LBL Annual Report, 1988). The rapidity of this process drew attention to the importance of bare soil evaporation in redistributing species near the soil surface. The nature and magnitude of this process are currently of interest to those concerned with the management of Kesterson Reservoir. It is the goal of this research to estimate bare soil evaporation rates (Chapter 3) and the resultant salt and selenium accumulation rates (Chapter 4) over an annual cycle. While selenium will not, on the whole, behave in the soil-water-air environment in the same fashion as major ions, its water-soluble fraction (SeO_4^{2-}) will be strongly affected by moisture fluxes near the soil surface. Due to the uncertainties involved in selenium extraction from soils, interference in selenium analysis (Section 4.3.3), selenium's complex redox chemistry, and the great spatial variability of selenium as compared with major ions, it is far more feasible to estimate evaporation rates and track temporal changes in concentration based on these changes amongst the major ions. This approach was the one taken and is described in the following chapters. In addition, the nature of the evaporation process was studied with the hope of gaining an understanding of the conditions which control its magnitude. To this end, numerical simulations have been performed. The results of these simulations have shed some light on the factors and processes which are dominant in bare soil evaporation.

2.0 REGIONAL AND LOCAL GEOLOGY AND HYDROLOGY

2.1 GEOLOGY

2.1.1 Regional Geologic Setting

The San Joaquin Valley comprises the southern two-thirds of the Great Central Valley of California (Fig. 2.1). It is a structural trough bounded to the west by the Coast Ranges and to the east by the Sierra Nevada. The northern half of the San Joaquin Valley is divided into western and eastern parts by the San Joaquin River, which originates in the Sierra Nevada, flows westward from Fresno to Mendota, where its course turns northwestward, and drains into the Sacramento-San Joaquin River Delta. The San Joaquin Valley is a relatively undeformed basin filled with sedimentary material up to a thickness of more than 3,600 m (12,000 ft) (Hotchkiss & Balding, 1971). In the eastern and central parts of the valley, gently dipping to horizontal strata overlie the Jurrasic-Cretaceous granitic basement of the Sierra Nevada (Gilliom, 1989). In the western part of the valley, more steeply dipping beds overlie the core of the Coast Ranges (specifically, the Diablo Range in the northern part of the San Joaquin Valley), composed chiefly of the Franciscan Assemblage of late Jurassic to late Cretaceous or Paleocene age (Bailey and others, 1964). Structurally overlying the Franciscan Assemblage is the Upper Jurassic to Upper Cretaceous or Paleocene (Lettis, 1982) Great Valley Sequence composed of unmetamorphosed, well-bedded shale, siltstone, sandstone and conglomerate (Blake & Jones, 1981). Overlying the Great Valley Sequence is a number of thin bedded, discontinuous Tertiary formations representing a variety of marine and nonmarine depositional environments (Lettis, 1982).

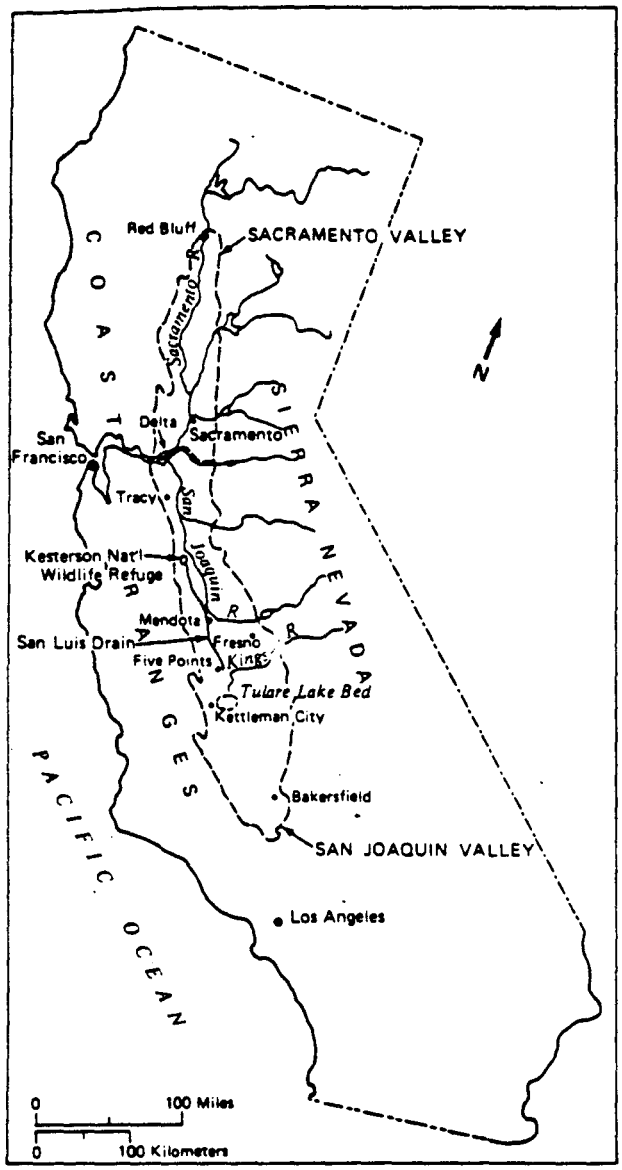

Figure 2.1 Geographic location of San Joaquin Valley in California (from Presser & Ohlendorf, 1988).

The Late Cenozoic deposits of the western and west-central San Joaquin Valley are composed of weakly consolidated and unconsolidated, poorly-sorted to well-sorted deposits of gravel, sand, silt, and clay. These sediments, derived primarily from the Diablo Range, formed a series of alluvial fans. The floodbasin of the San Joaquin River contains sediments derived from the Sierra Nevada (Lettis, 1982). The Pliocene-Pleistocene Tulare Formation of Diablo Range origin consists of two sections, separated by the diatomaceous Corcoran Clay Member of Pleistocene age. The Upper and Lower sections of the Tulare Formation consist of unconsolidated sands, silts, and clays and are generally highly to variably permeable, while the Corcoran Clay, which is up to 39 m (127 ft) thick, is an impermeable confining stratum (Hotchkiss & Balding, 1971). Overlying the Tulare Formation are Quaternary terrace deposits, flood-plain deposits, and alluvium. The flood-plain deposits are of mixed Diablo Range and Sierran origin, while the alluvium and terrace deposits, which dominate the west-central valley, are of Diablo Range origin.

2.1.2 Regional Sources of Salts and Selenium

The source of most of the selenium in the western and central parts of the San Joaquin Valley are marine sedimentary formations of the Coast Ranges. The three areas where selenium concentrations in soil often exceed 0.36 mg/kg are the alluvial fans near Panoche and Cantua Creeks, an area west of the town of Lost Hills, and the Buena Vista Lake Bed area; all three are adjacent to exposures of marine sedimentary formations (Tidball and others, 1986). The median soil selenium concentration in alluvial sediments derived from Coast Range formations is 0.13 mg/kg (Gilliom, 1989). Lund and others (1987) have isolated the Eocene Kreyenhagen Shale as one of the main sources of selenium, based on the finding that it contains between 3.1 and 18.6 mg/kg selenium and crops out to the west of all three areas mentioned above. Similarly, movement of water

from the Coast Ranges eastward is considered to be the main mechanism of salt transport into the Central Valley (Presser & Ohlendorf, 1988). The further concentration of salts due to high evaporation rates and a shallow aquifer along with agricultural practices have made soil and water salinity a pervasive and valley-wide problem.

2.1.3 Local Stratigraphy

The surface soils of Kesterson Reservoir are assigned to the Waukena Series (USDA Soil Conservation Service, 1952), which contain high concentrations of soluble salts, thereby restricting the vegetation to salt-tolerant grasses and weeds. Most of the surficial deposits of the Kesterson Reservoir area have been mapped as part of the Dos Palos alluvium (Lettis 1982; Flexser 1988), as consisting predominantly of moderately to well sorted, moderately to well bedded unconsolidated sand, silt, and clay, as well as gravel and clayey silt; a plutonic (Sierran) origin for these sediments is indicated by its arkosic composition. Although stratigraphy varies greatly within the Reservoir, a generalized cross-section (Fig. 2.2) identifies the major stratigraphic units present. The top unit, C1 (3 to 6 m) is a sandy to silty loam often covered with a thin veneer of a clay loam. The unit S2 is a medium to coarse sand, occasionally with associated gravel. At a depth of 20 to 25 meters, a low-permeability clay layer (C2) is present throughout the Reservoir. This layer is approximately 3 m thick. Unit C2 is underlain by a highly permeable sand unit (S2) which extends down to the Corcoran Clay (C3), which has not been mapped in as much detail as the upper units, but in most parts of the Reservoir is 3 to 9 m thick. Cores from a small number of wells indicate the presence of a third layer of high permeability sand, S3. Its thickness is not known (Flexser, 1988, LBL, 1987).

This study concentrates on the soil-sediment system of the top 2.5 m of unit C1. It is this interval which encompasses the vadose (unsaturated) zone, the extent of which

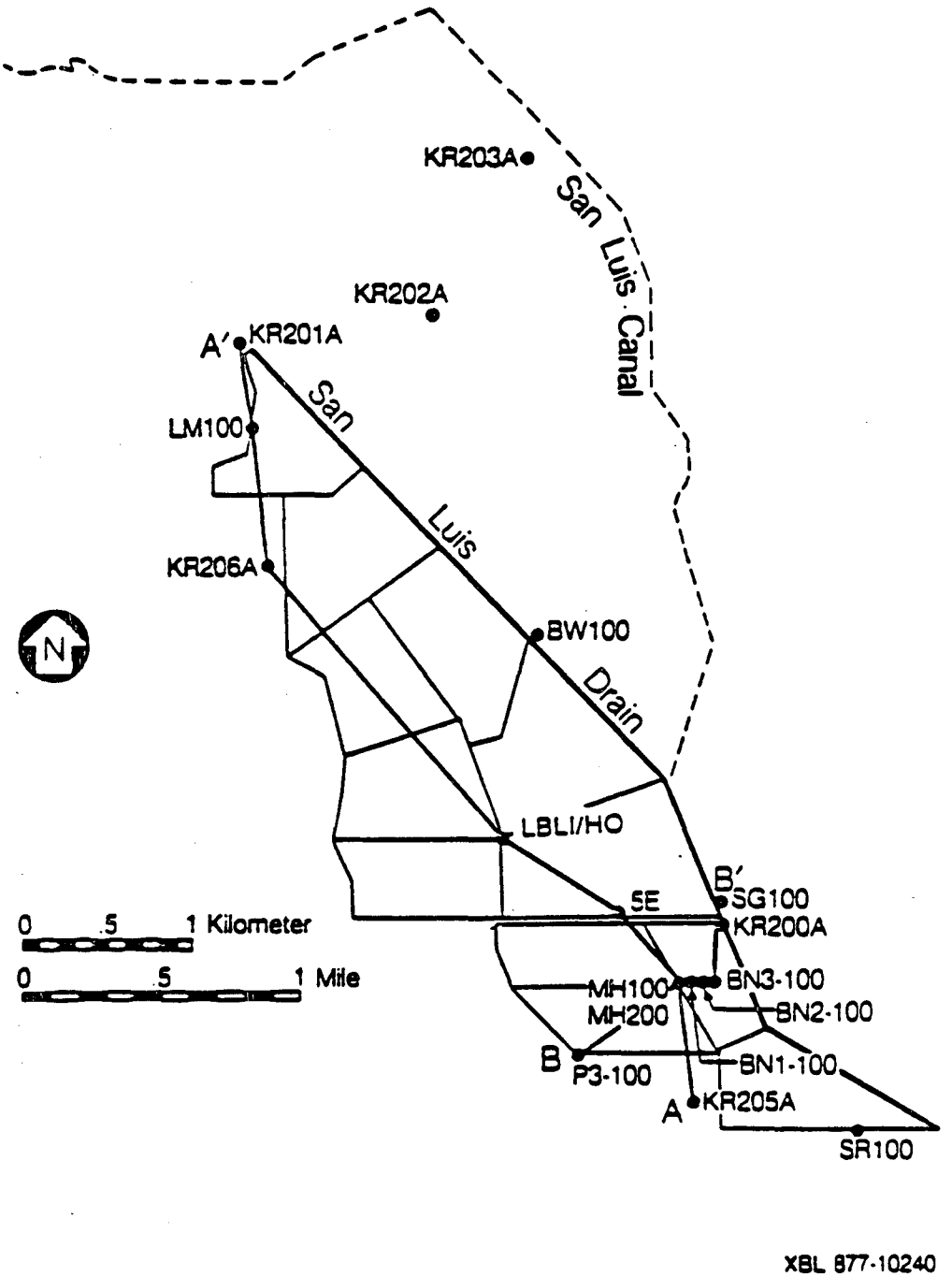

Figure 2.2a Location map showing wells from which data for the compilation of cross-section A-A' (Fig. 2.2b) were obtained.

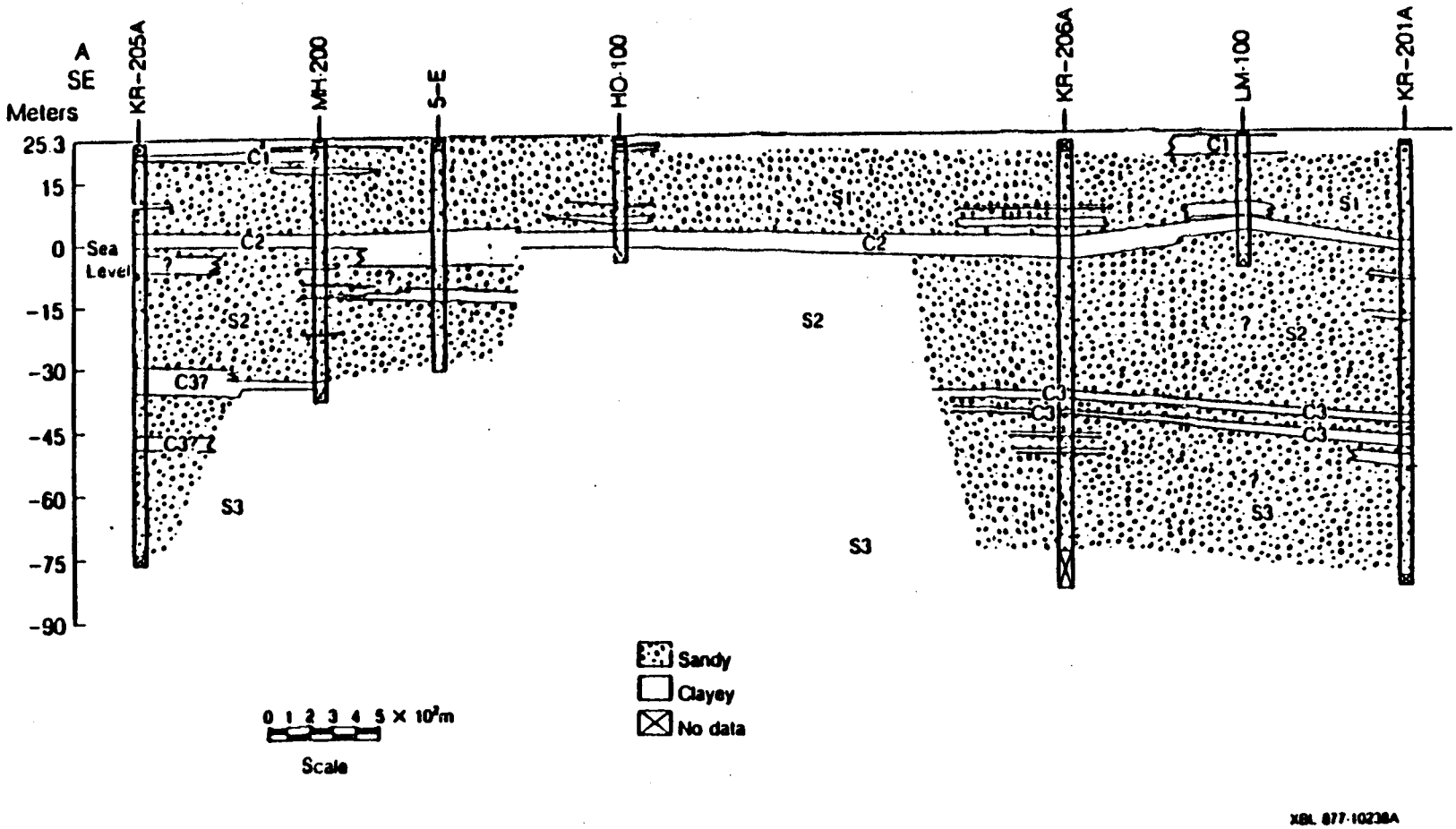

Figure 2.2b Cross-section A-A': general stratigraphy.

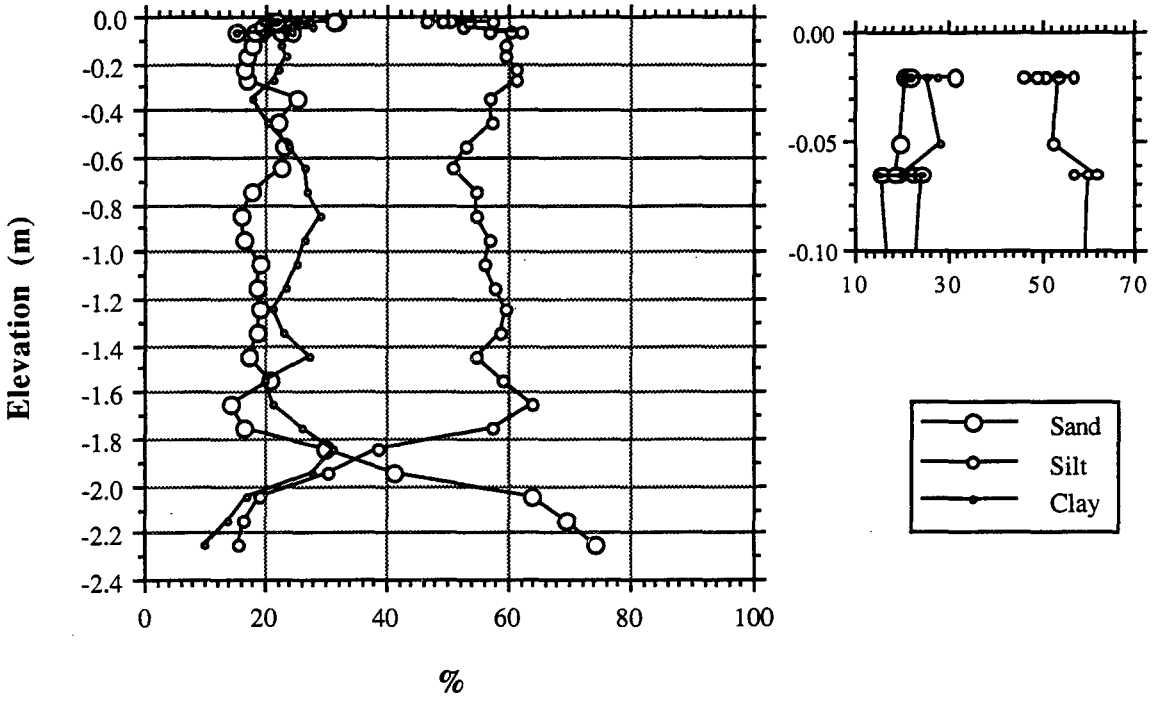

Figure 2.3a Sand, silt, and clay depth profiles in vadose zone of plot 8EP. Close-up view shown in inset graph. Elevation in this and subsequent figures is relative to the soil surface.

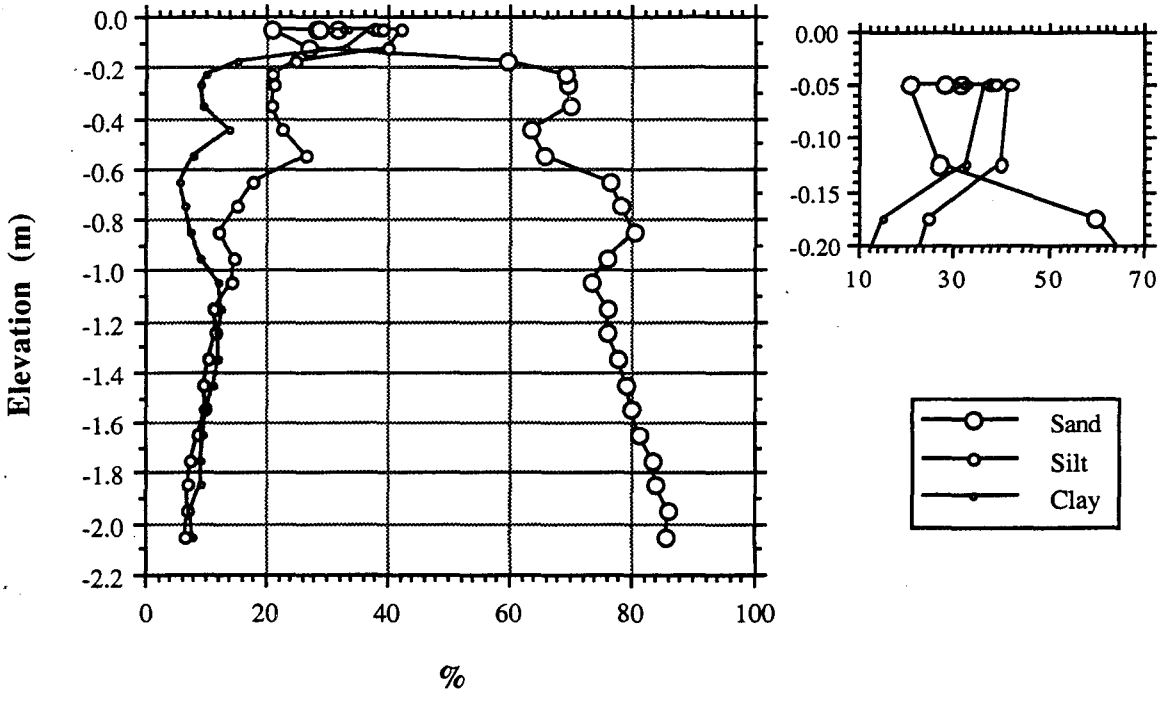

Figure 2.3b Sand, silt, and clay depth profiles in vadose zone of plot 9BE. Close-up view shown in inset graph.

varies with the seasonal rise and fall of the water table. In particular, this study focuses on the vadose zone in sites 8EP (Pond 8) and 9BE (Pond 9). The particle-size distribution at those two sites, as determined using the hydrometer method (Day, 1965), is presented in Fig. 2.3.

2.2 HYDROLOGY

2.2.1 Regional Hydrologic Setting

With variations dependent on the proximity to the surrounding mountain ranges, the San Joaquin Valley is underlain by thousands of feet of unconsolidated sediments. In most parts of the western side of the valley, the groundwater system is grossly divided into a lower, confined aquifer and upper, unconfined or semiconfined aquifer by the Corcoran Clay Member of the Tulare Formation (Belitz & Heimes, 1989). The lower unit ranges in depth from 27.5 to more than 425 meters (90 to 1400 feet) and is composed of numerous beds, lenses, and tongues of gravel, sand and clay. The upper aquifer system ranges in thickness from 30.5 to 152.5 m (100 to 500 feet), with thickness increasing southward. Its composition is similar to that of the lower aquifer (Hotchkiss, 1972). In many areas of the northern San Joaquin Valley, the upper aquifer may be further subdivided into an upper water-bearing zone which includes alluvial, flood basin, and terrace deposits, and a shallow water-bearing zone within 3 meters of the land surface (Hotchkiss & Balding, 1971).

The movement of subsurface water in the San Joaquin Valley, as in the Central Valley as a whole, has been severely altered over the last seven decades due to the extensive pumpage of water, especially from the lower aquifer. The effects of this water

use have manifested themselves over the years in various ways, the best known of which is the drawing down of the potentiometric surface of the confined aquifer by over 100 meters and the resultant land subsidence in most parts of the valley of more than 60 cm (2 ft) and in certain parts by as much as 8.5 m (28 ft) (Poland and others, 1975). Nevertheless, between the Coastal Ranges to the west and the San Joaquin River, the general northeastward direction of groundwater flow has been preserved, although many local depressions and flow direction reversals are found throughout the valley (Belitz & Heimes, 1989). The valley-wide drawdown of water in the lower aquifer has resulted in a downward leakage of water from the upper water-bearing zone. This has been shown through measurements of tritium concentrations in the confined aquifer; results of these studies showed the presence of post-1952 irrigation water below the Corcoran Clay (Dubrovsky, 1989). While the potentiometric head in the confined aquifer has fallen, the groundwater table of the unconfined and semiconfined aquifer has risen due to percolation of irrigation water (Hotchkiss & Balding, 1971). The shallow groundwater table fluctuates annually due to seasonal variations in runoff, precipitation, pumpage, and irrigation schedules. In addition, large areas close to the San Joaquin River, in the vicinity of Los Banos are flooded in the late fall and winter seasons to create wetlands for migratory bird habitat and duck hunting.

Potential evaporation far exceeds rainfall on an annual basis in the San Joaquin Valley. Average rates vary depending on the distance from the valley axis; annual evaporation ranges from 1500 to 2200 mm/year while annual rainfall averages around 150 to 360 mm/year (Davis and others, 1959; LBL Annual Report 1988). Most of the rainfall occurs during the months of November through April.

2.2.2 Salt and Selenium Distribution in Regional Groundwater

Water quality in the confined aquifer varies greatly both laterally and with depth. The concentration of dissolved solids ranges from 400 to over 6,000 mg/L (Hotchkiss & Balding, 1971), while ≈1000 mg/L is considered the maximum "fresh water" concentration (Freeze & Cherry, 1979). Selenium concentrations in the confined aquifer are found to be, in general, at or below the detection limit of 1 µg/L (Dubrovsky & Deverel, 1989).

The concentrations of total dissolved solids in the upper aquifer range from 130 to 86,500 mg/L (for reference, in seawater, TDS ≈ 35,000 mg/L). Wells in the vicinity of Kesterson contain over 1,600 mg/L of chloride and sodium combined (Hotchkiss & Balding, 1971), which suggests that almost all of the shallow groundwater in the area is brackish and in some areas, saline (TDS > 10,000 mg/L). The concentrations of selenium in the semiconfined upper aquifer are on the order of 1 to 5 µg/L, with local highs of 15 µg/L. Selenium concentrations in the shallow, unconfined aquifer vary depending on the relative distance to selenium source areas (see Section 2.2.4), with concentrations highest in the alluvial fans of the Panoche Creek (up to 1000 µg/L ten miles south of Mendota) and decreasing northward (< 10 µg/L in Kesterson area) (Fig. 2.4). Where selenium concentrations are high, their spatial variability is well correlated with salinity (Dubrovsky & Deverel, 1989; Dubrovsky, 1989).

2.2.3 Local & Site-Specific Hydrology

Local hydrologic conditions in the vicinity of Kesterson Reservoir are typical of the valley-wide conditions described above, with a few site-specific deviations. The local stratigraphy is described in Section 2.1. A layer of clayey sediments at a depth of about 20-25 meters (Yates, 1988) forms a lower boundary to a shallow aquifer which

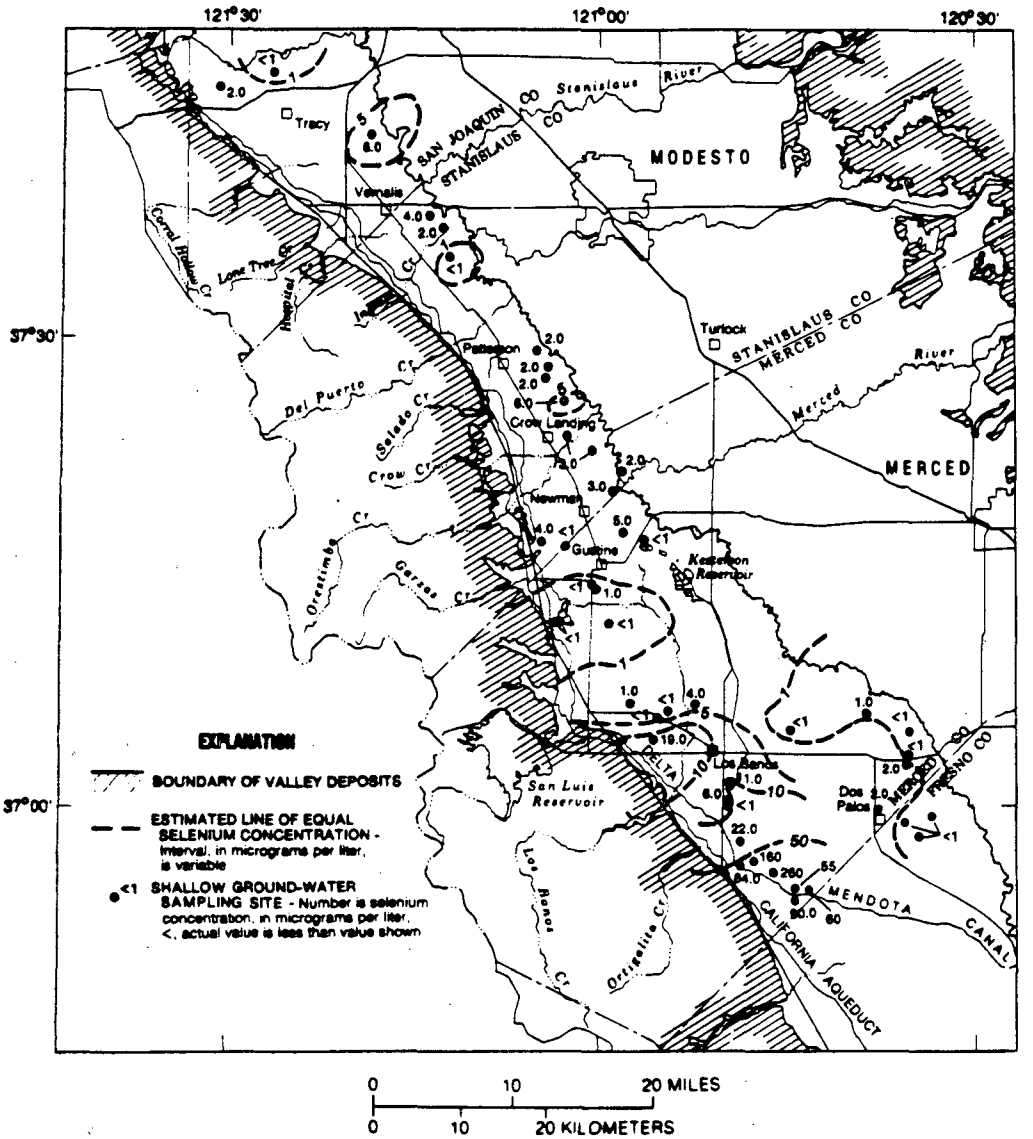

Figure 2.4 Selenium concentrations in shallow groundwater of the northwestern San Joaquin Valley (from Dubrovsky, 1989).

corresponds to the regionally described shallow aquifer. This aquitard is found to occur throughout the Reservoir and is approximately 3 meters thick (LBL Annual Report, 1987). In addition, local lenses of clayey material likely create bodies of perched water. The upper, semiconfined aquifer extends to the Corcoran Clay at a depth of approximately 55-60 meters below the soil surface. The confined aquifer, below the Corcoran Clay, has not been studied extensively in the Kesterson Reservoir area.

Prior to the flooding of the Reservoir, the depth to the shallow water table ranged from 0 to 3.7 meters (0-12 feet) (Yates, 1988). Flooding created a groundwater mound, which caused groundwater to flow radially away from the Reservoir. Since the draining of Kesterson Reservoir in 1986, groundwater flow has slowly returned to its original northeastward direction. The elevation of the water table in the Kesterson area is strongly influenced by seasonal flooding of duck ponds to the west and south of the Reservoir. This results in a fluctuation of $\pm$ 0.5 m around an annual mean (Fig. 2.5) with the water table at its highest in March and at its lowest in October. As described in Section 2.1, the lateral and vertical variability in soil and sediment properties on a reservoir-wide scale is very large. The hydraulic permeability of near-surface materials varies from pond to pond, although in most ponds a low permeability surface unit is recognized from 0 to 2 m. The saturated hydraulic conductivity (K_s) of this unit has been measured at between 3.2×10^{-8} to 3.2×10^{-7} m/s (LBL, 1987). Between depths of 2 and 12 m, the hydraulic conductivity is found to increase. A mean horizontal K_s of the upper aquifer has been measured at around 10^{-4} m/s (Benson, 1988).

This study was concentrated in ponds 8EP and 9BE (see Fig. 1.2 for locations); in order to characterize the soil/sediment profile, soil was augered in 5 and 10 cm intervals and particle size analyses were performed; also, a Guelph Permeameter was used to determine saturated conductivities in the field. The lateral and vertical variabilities are

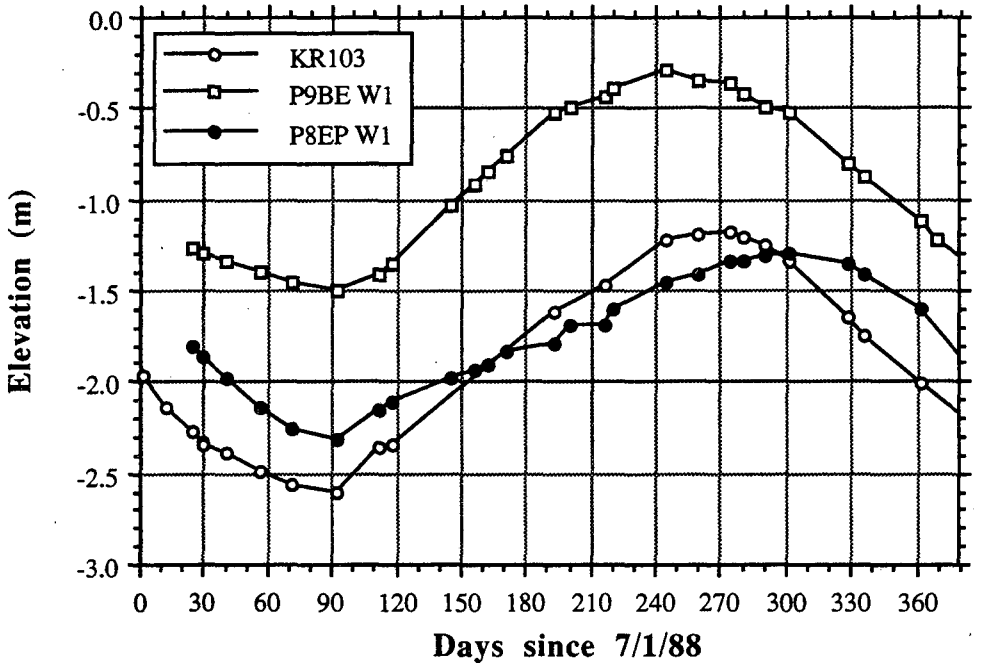

Figure 2.5 Depth to water table in three wells: P8EP W1, P9BE W1, and KR103. See text for locations of wells.

apparent from these data. In addition to the near-surface low permeability layer, the soil surface in most ponds is covered by a thin veneer of organic matter which is a remnant of shallow ponds. This organic matter, together with a salt crust up to 2 cm thick, is difficult to describe hydrogeologically and may have a unique effect on near surface moisture fluxes. High permeabilities measured near the soil surface of pond 8EP (0-20 cm) correspond most likely to macropore and fracture flow.

Climatic conditions at Kesterson Reservoir are typical of the San Joaquin Valley. Daily climatological conditions over the twelve month period from July 1988 through June 1989 at Kesterson Reservoir are depicted in Figures 2.6 and 2.7. The air temperature and humidity were measured by an electronic weather station in Los Banos. Precipitation was measured at a weather station at Kesterson Reservoir; evaporation rates presented in Fig. 2.7 were measured at the Los Banos Reservoir (from day 0 until day 180 and again from day 216 until day 366) and at Kesterson Reservoir (from day 181 through day 215). (The Bureau of Reclamation failed to record pan evaporation rates at Kesterson Reservoir from July 1988 through November 1988; therefore, evaporation rates at Kesterson were estimated from rates measured at Los Banos Reservoir, based on historical records of evaporation at the two sites. Pan evaporation was not measured at the Los Banos Reservoir during the 34 day period and rates measured at Kesterson were used.) The combination of reduced temperatures and elevated humidities during the late fall and winter lead to a reduction in measured pan evaporation. Fig. 2.7 highlights the disparity between pan evaporation and precipitation; over the twelve month period, total precipitation was measured at 162 mm, while the cumulative annual pan evaporation was 2234 mm.

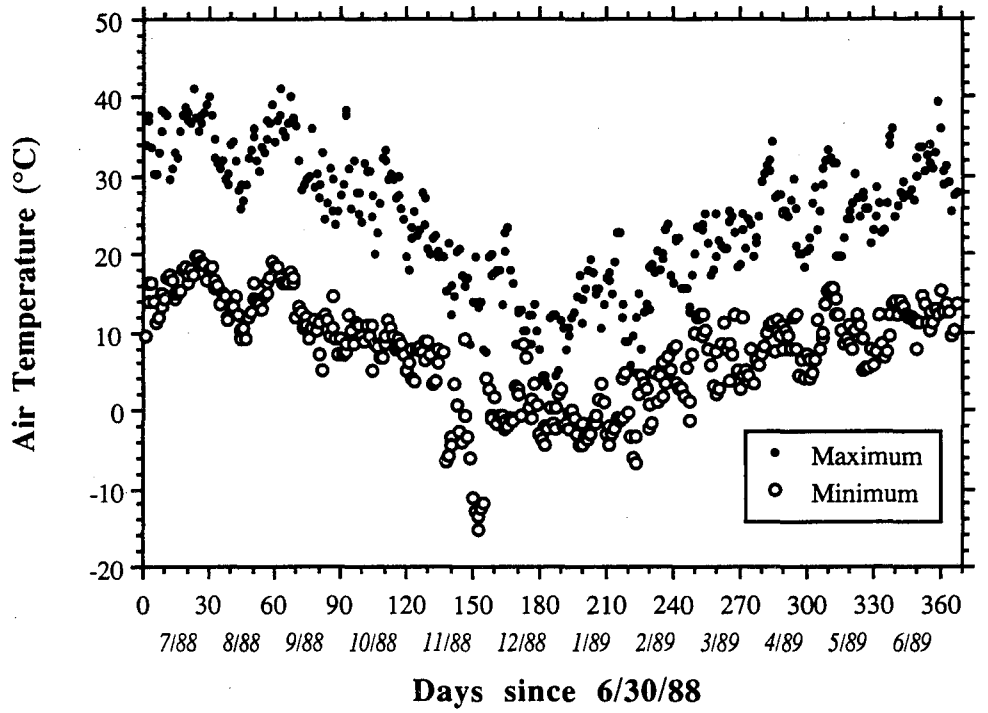

Figure 2.6a Maximum and minimum daily air temperature at Los Banos.

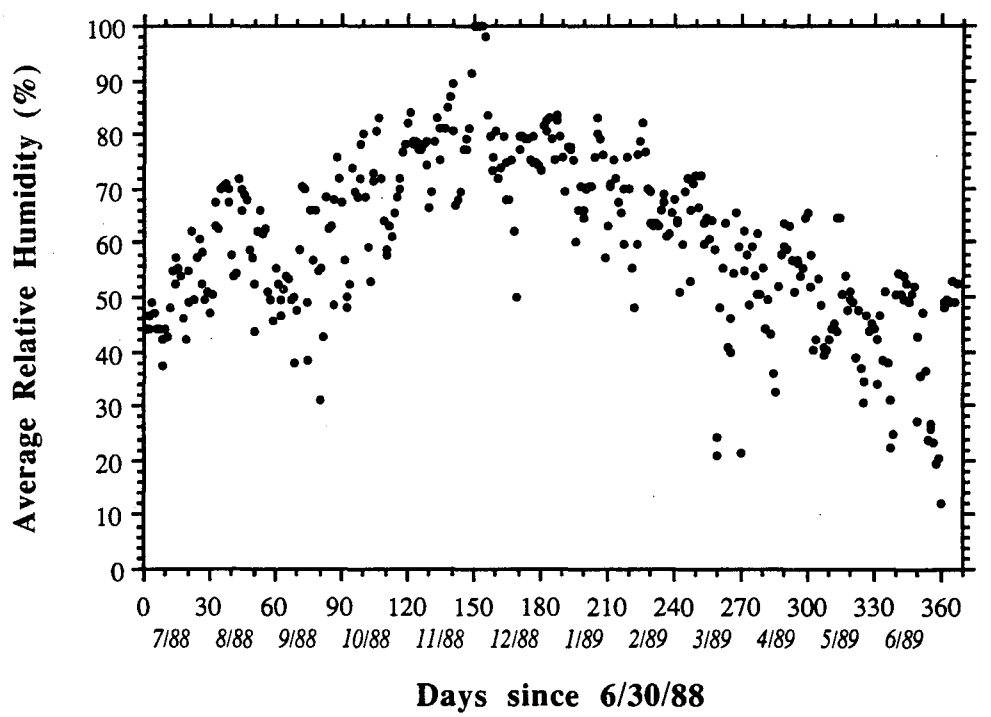

Figure 2.6b Average daily relative humidity at Los Banos.

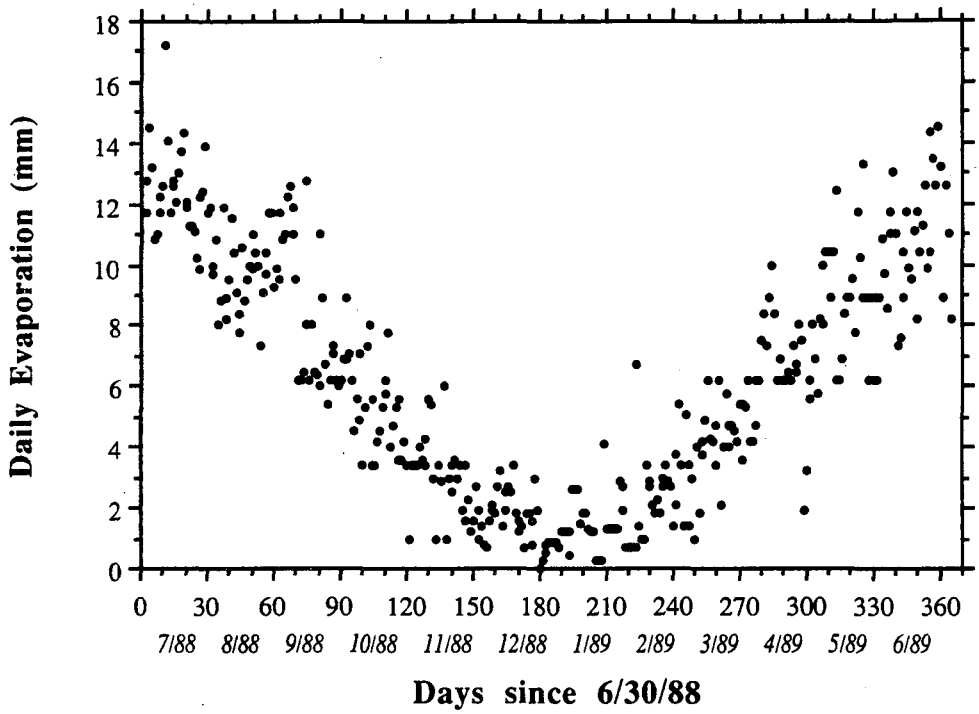

Figure 2.7a Daily pan evaporation at Los Banos Reservoir and Kesterson Reservoir (see text for details).

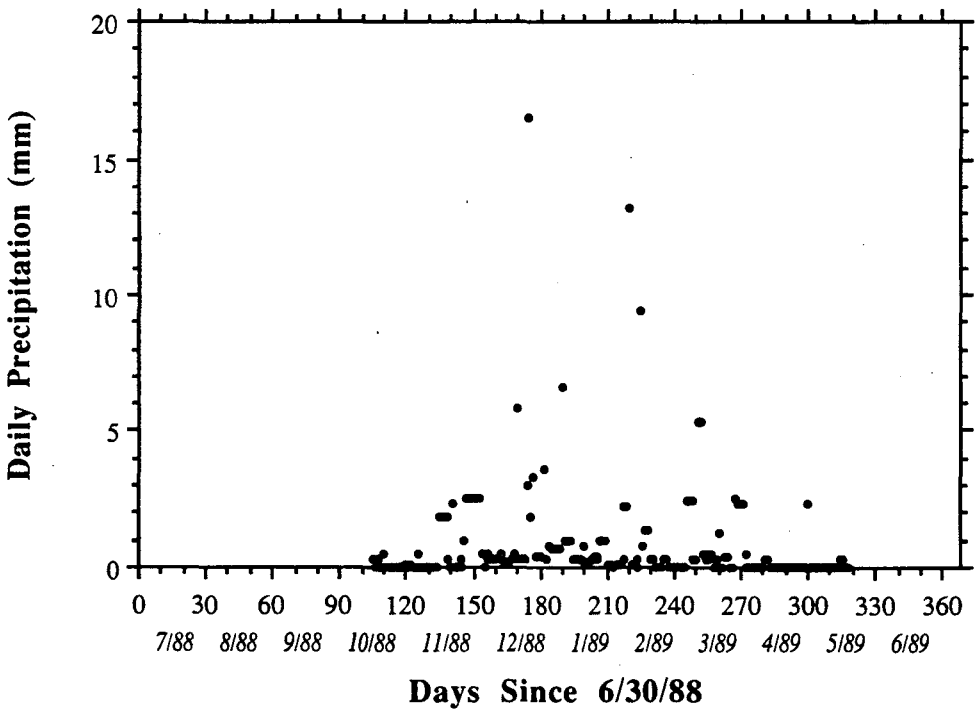

Figure 2.7b Daily precipitation at Kesterson Reservoir.

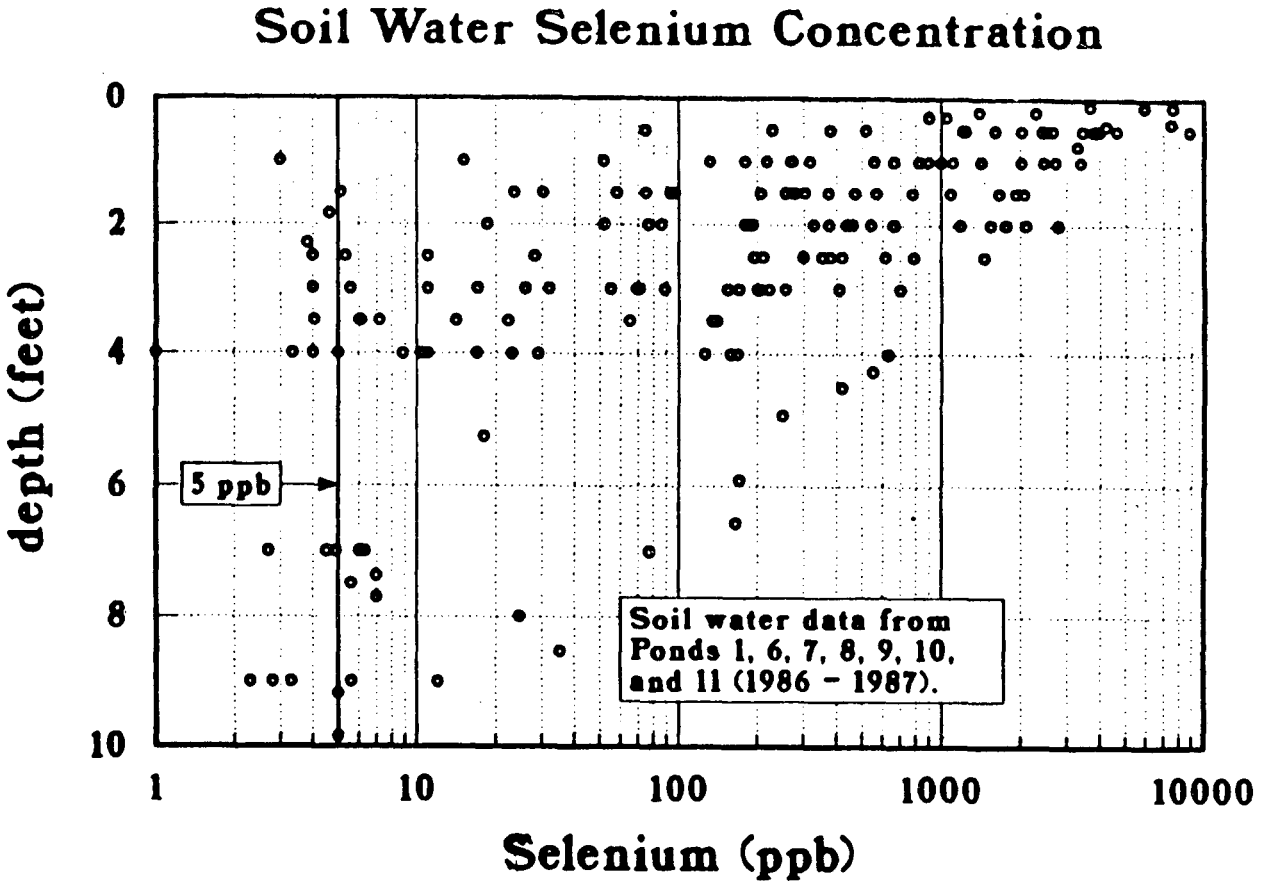

Figure 2.8 Distribution of soil water selenium from monitoring sites in Ponds 1, 6, 7, 8, 9, 10, 11 (from LBL, 1988).

2.2.4 Local Salinity and Selenium Contamination

The distribution of salts and selenium in Kesterson Reservoir soils, soil-water, and groundwater is highly variable and dependent on the specific ecological and geological environment. Certain generalizations may be made, but the actual depth profiles of selenium and salts will be strictly site-specific. In general, two environments may be recognized: (1) in those areas of the reservoir which are, and have been for the last few years, vegetated, most mineral species and selenium, but especially salts will tend to be concentrated in the root zone and, to a lesser degree, at the soil surface, although concentrations of selenium will still be comparably high in the top few centimeters; (2) in areas free of vegetation or with very limited vegetation, both salts and selenium will tend to be concentrated at and near the soil surface. Concentrations of dissolved solids in the top 2 m of soil and in the groundwater are in the range of 10,000 to 50,000 mg/L; concentrations near the soil surface reach the solubility limit of mirabillite ($Na_2SO_4 \cdot 10H_2O$) and have been measured at 15 cm to be as high as 100,000 mg/L. Sodium (Na^+) is the dominant cation and sulfate (SO_4^{2-}) and chloride (Cl^-) are the dominant anions in most parts of the reservoir. Due to their low solubilities, calcite ($CaCO_3$) and gypsum ($CaSO_4$) have precipitated throughout most of the near surface profile (Flexser, 1988; Tokunaga, personal communication, 1988). Selenium, the mobility of which is limited by its complex reduction-oxidation chemistry (see discussion in Section 4.2), is concentrated close to the soil surface. In oxidizing conditions, selenium occurs as selenate (SeO_4^{2-}); when reduced to selenite (SeO_3^{2-}) its mobility is greatly diminished due to strong sorption of the selenite ion onto clay minerals (Elrashidi & others, 1987). Therefore, selenium is fairly mobile in the oxidized environment of the vadose (unsaturated) zone, but is immobilized in the reducing environment of the phreatic (saturated) zone. This leads to a distribution of dissolved selenium as shown in Fig. 2.8. Concentrations of salts and selenium in areas involved in this study are presented and discussed in Chapter 4.

3.0 MEASUREMENT OF BARE SOIL EVAPORATION RATES

3.1 THEORY OF MOISTURE MOVEMENT

The flow of water through porous media is governed by many driving forces, each of which can be related to the gradient of an appropriate potential, where potential is defined as energy per unit mass. Total fluid potential (Φ_t) may be divided into several components:

$$\Phi_t = \Phi_g + \Phi_p + \Phi_o + \ldots \tag{3.1}$$

where Φ_g is the *gravitational potential*, Φ_p is the *pressure potential*, and Φ_o is the *osmotic potential*, all in units of energy per mass (L^2T^{-2}); other components are possible. The gradient of each potential may differ from the others in both direction and magnitude, and in many cases the osmotic potential may be ignored as it will be insignificantly small relative to the other potentials (Hillel, 1980a). The gravitational potential of a body of water, or any other matter, depends on its position relative to a reference plane:

$$\Phi_g = gz \tag{3.2}$$

where g is acceleration due to gravity and z is the elevation relative to a point or plane z_0. Since g may be considered constant in most flow systems, the above expression may be divided by g to give:

$$\phi_g = \frac{\Phi_g}{g} = z \tag{3.3}$$

where ϕ_g will have units of length. This variable is often referred to in hydrogeology and soil physics as the *elevation head.* The elastic compression of a fluid is the source of a pressure potential which is considered positive when greater than atmospheric pressure, zero when equal to atmospheric pressure, and negative when less than atmospheric pressure. It may be defined as the work required to raise water from a reference pressure to a given pressure:

$$\Phi_p = \int_{P_0}^{P} \frac{dP}{\rho} \tag{3.4}$$

where ρ is fluid density (Freeze & Cherry, 1980). This expression may also be divided by g to give a potential in units of length, which under hydrostatic conditions is equivalent to depth below (when positive) or height above (when negative) the groundwater table or the "free-water surface" (Hillel, 1980a):

$$\phi_p = \frac{\Phi_p}{g} = \int_{\psi_0}^{\psi} \frac{\rho g \, d\psi}{\rho g} = \psi \tag{3.5}$$

The term ψ is equivalent to the height of a fluid column and is often referred to as *piezometric* or *pressure head.* The use of the term *head* in soil regimes under negative pressure (suction) is awkward and misleading. Therefore, elevation head and pressure head will be referred to as potentials even though their units are those of length.

The osmotic potential is the result of the change in free energy of the fluid due to the presence of solutes. In dilute solutions, the osmotic pressure may be expressed as follows:

$$\Pi = M_{charge}RT \tag{3.6}$$

where Π is in units pressure [MLT^{-2}], M_{charge} is the molar charge concentration of solute molecules [moles L^{-3}], R is the gas constant [$ML^2T^{-2}moles^{-1}Kelvin^{-1}$], and T is the temperature in Kelvin (Hillel, 1980a). In the consideration of most fluid flow systems, the osmotic potential is neglected, but it is important in the process of vapor diffusion.

While the flow of water is impelled by the above potential gradients, the flow is hindered by the frictional forces generated as water moves past solid particles. The reciprocal of this "resistance" has been lumped into a parameter called *hydraulic conductivity* (K [LT^{-1}]). K is actually a function of both media properties (grain diameter, pore shape and diameter, distribution of grain sizes, sphericity, roundness, and packing of grains) and fluid properties (viscosity, density). Hubbert (1940) derived a physical basis for K based on relationships of forces on a microscopic scale. He was able to define more fundamental components of K:

$$K = \frac{k\rho g}{\mu} \tag{3.7}$$

where g and ρ are as previously defined, μ is the dynamic viscosity of water [$ML^{-1}T^{-1}$], and k is a parameter dependent only on the properties of the medium, called *intrinsic permeability* [L^2]. Under isothermal conditions, the volumetric flow rate of water through porous media (Q), in one dimension, may be described by the following equation:

$$Q = -KA\frac{d\phi_h}{dx} \tag{3.8}$$

where ϕ_h is the total hydraulic potential (=ψ+z), A is the cross-sectional area of flow and $d\phi_h/dx$ is the gradient of hydraulic potential in direction x. This relationship was observed through experiments on saturated sands by Darcy in 1856. In 1907, Buckingham extended this equation to include fluid motion through partially saturated soils, in which case K becomes a function of matric (pressure) potential (Narasimhan, 1982). The more general form of the equation of motion was suggested by Richards (1931):

$$q = - K(\psi) \nabla(\phi_h) \tag{3.9}$$

where q = Q/A and is called *specific flux* [LT^{-1}].

In order to describe transient fluid flow, the above equation needs to be combined with the equation of continuity which states that the rate of inflow into a volume element must be equal to the outflow plus the change in fluid storage:

$$\frac{\delta\theta}{\delta t} = - \nabla \bullet q \tag{3.10}$$

where θ is the volumetric moisture content. When inflow is greater than outflow, $\delta\theta > 0$ and vice versa. Combining the above equation with equation (3.9) gives:

$$\frac{\delta\theta}{\delta t} = \nabla \bullet K(\psi)\nabla(\phi_h) \tag{3.11}$$

The above equation is sometimes referred to as the Richard's Equation. This equation is more appropriately written in terms of mass conservation, where inflow and outflow will be equivalent to $Q_{in}\rho$ and $Q_{out}\rho$, respectively, while the change in storage may be described as follows:

$$M_c \frac{d\psi}{dt} = \frac{d(\rho\theta V)}{d\psi} \frac{d\psi}{dt} \tag{3.12}$$

where M_c is fluid mass capacity [ML^{-1}] and represents a change of fluid mass in a volume element V due to a change in pressure head, ϕ_p (Narasimhan, 1982). The integral form of the combined equation is convenient to use in numerical modelling applications (see Section 5.2):

$$\int_{\Gamma_l} \rho K \vec{\nabla}(\phi_h) \bullet \vec{n} d\Gamma_l = M_c \frac{d\psi}{dt} \tag{3.13}$$

where Γ_l is the surface area of element l, $\bar{n}$ is the unit outward normal vector, and the integral represents the summation of flow into and out of the element l across all surfaces of the element (Narasimhan and Witherspoon, 1977; Narasimhan, 1982).

Under unsaturated conditions, when pores are not completely filled with fluid, fluid motion is slower than under saturated conditions. This is due to the change of permeability with a change in matric potential, often referred to in the vadose zone as suction. As the medium desaturates, fluid occurs in progressively thinner films and finer pores, which leads to greater friction and decreased permeability (Hillel, 1980a). Since large pores tend to desaturate more under the same potential than small pores, the saturation and permeability of a coarse-textured soil will fall more rapidly with a falling matric potential (or rising suction) than those of a fine-textured soil. In effect, while clays have, in general, lower saturated permeabilities than sands, under unsaturated conditions, the reverse is often true. Various empirical and semi-empirical relationships have been derived to predict permeability and saturation of a material over a range of matric potentials. The actual experimental measurement of these properties is tedious, time-consuming, and limited to a

small range of pressure potentials (using conventional methods). A description of one empirical method for deriving soil moisture characteristics based on particle-size distribution may be found in Appendix I. In addition to fluid flow, vapor flow may play a dominant role in water transport in the vadose zone, especially near the soil surface when the saturation is very low.

3.2 IMPORTANT ASPECTS OF BARE SOIL EVAPORATION

The physical process of water evaporation from soil has been studied for many decades; its effects on water and soil management practices have driven most of the research in this field, especially since the second quarter of this century. In 1939, Moore published a paper which described one of the first laboratory experiments designed to study the evaporation of water from a shallow water table. In 1948, Penman derived an expression for calculating potential evaporation rate (E_P) based on a combination of an aerodynamic approach and an energy balance:

$$E_P = \frac{\Delta}{\Delta + \gamma} R_A + \frac{\gamma}{\Delta + \gamma} f(u)(e_A - e_D) \tag{3.14}$$

where Δ is the rate of saturation vapor pressure change with respect to air temperature [$ML^{-1}T^{-2}$degrees $Celsius^{-1}$], γ is the psychrometric constant [$ML^{-1}T^{-2}$degrees $Celsius^{-1}$], R_A is the areal net radiation [LT^{-1}], f(u) is a function of wind velocity u [L^2TM^{-1}], and e_A and e_D are saturation vapor pressures at air and dewpoint temperatures respectively [$ML^{-1}T^{-2}$]. Since Penman, many researchers have derived various expressions describing potential evaporation; most of these expressions are able to predict potential evaporation quite well. However, the evaporation of water from soils is more complex in that it depends not only on meteorological conditions but also on soil properties and moisture content. The force

which drives evaporation at the soil surface is the net solar radiation (Koorevar and others, 1983); drying of the soil surface creates a substantial upward potential gradient. The flow of water towards the soil surface follows the physical processes outlined in the previous section. There are several factors which limit the magnitude of bare soil evaporation. In general, the bare soil evaporation rate will be equal to or less than the potential evaporation rate; the moisture content of soil at the surface as well as physical soil properties are limiting factors in this process. In addition, vapor flow close to the soil surface may become an important flow mechanism under extremely dry conditions (Bresler and others, 1982). While most experimental results have been successfully modelled without accounting for vapor flow (see Appendix II), vapor diffusion is a process which should not be neglected. For example, Gardner and Fireman (1958) found that the evaporation rate from a sandy loam soil decreased from nearly 10 mm/day to less than 0.5 mm/day as a result of a 6 mm thick sand mulch on the soil surface. It was concluded, based on modelling, that water moved through the mulch in the vapor phase. Vapor flow in the vadose zone, under isothermal conditions, has been described by Fick's Law, modified in the following way:

$$J_{S,v} = -(1-S)n\tau_a D_{A,v}\frac{\partial C_{S,v}}{\partial z} \qquad (3.15)$$

where $J_{S,v}$ is a vapor mass flux per unit bulk area [$MT^{-1}L^{-2}$], $D_{A,v}$ is the diffusivity of water vapor in air [L^2T^{-1}], and $\partial C_{S,v}/\partial z$ is the soil gas-phase vapor concentration gradient in direction z [ML^{-4}]; in addition, the flux of Fick's Law is corrected for the limited gas-phase cross-sectional area due to the presence of solid grains (n, porosity) and water ($0 <$ S, saturation, <1), and for the gas-phase tortuosity of the path of diffusion (τ_a, air-filled tortuosity factor, which decreases with increasing tortuosity).

While under field conditions there is no clear division, bare soil evaporation may be divided into two classes: drying of wetted soils and evaporation from a water table. The former process has been described by a great number of researchers. Even though a water table may be present relatively close to the soil surface, evaporation immediately following infiltration will not be very strongly affected by its presence and will depend mostly on external conditions and near-surface soil properties. This process has been studied mostly on short cores in the laboratory (e.g. Staple, 1969; Reynolds & Walker, 1984). Under constant external conditions, three stages of soil drying have been observed (Hillel, 1980b). The initial stage is a constant rate stage during which the soil is still wet enough to transmit water at the same rate as potential evaporation. Therefore, during this stage, bare soil evaporation is *weather-controlled.* The length of this stage will depend on climatic conditions, i.e. on potential evaporation rate itself, and is usually in the range of a few hours to a few days after infiltration. The second, intermediate, stage is one in which the soil evaporation rate slowly declines; the rate is dependent on how fast the soil can transmit water to the soil surface. This stage has been called the *soil-controlled stage.* Depending on the amount of infiltration and soil properties, this stage may last for several days to weeks. The third stage is reached when the soil is too dry for any substantial liquid conduction and subsurface vapor diffusion dominates the evaporative flux. Hillel (1975) noted that in a real system, in which external conditions vary diurnally and seasonally, these three stages may be difficult to distinguish. In addition, in field conditions with a shallow water table, the third stage will rarely be reached since there will be a certain upward flux of water. Fig. 3.1 shows the soil water fluxes on a very small scale, as observed by Jackson and others (1973), after infiltration of 10 cm of water into a loam soil. It is apparent that the flux varies not only in magnitude but also in direction. Therefore, the establishment of distinct stages of drying is unlikely. Since the process of soil drying is transient and highly dependent on several variables which are in turn functions of water potential, analytical solutions can be derived for only the simplest of systems and have usually depended on the

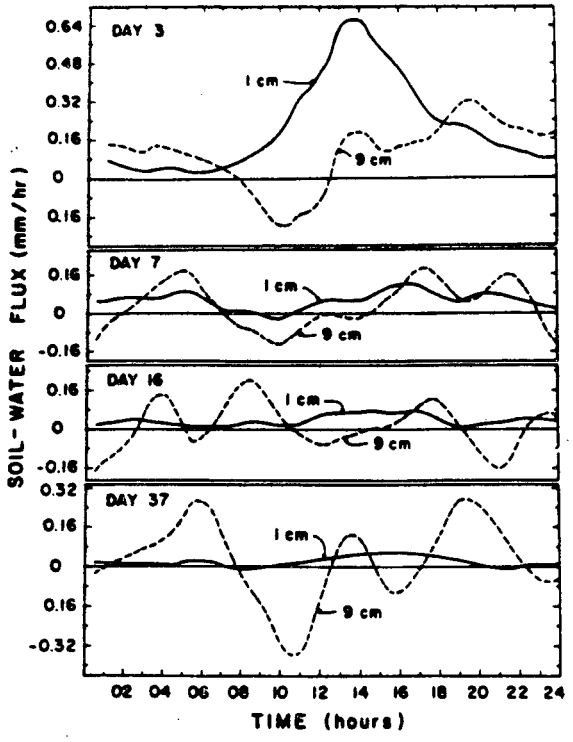

Figure 3.1 Diurnal fluctuations in soil water flux at two depths in a soil, 3, 7, 16, and 37 days after irrigation (from Jackson and others, 1973).

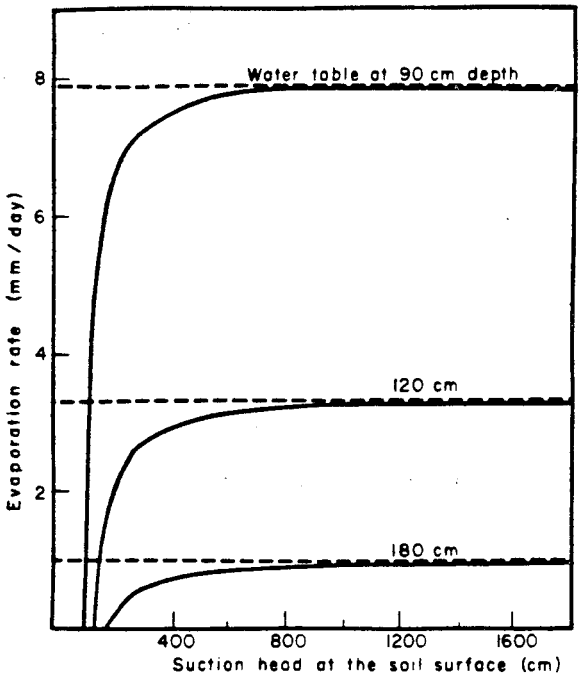

Figure 3.2 Dependence of bare soil evaporation rate on external conditions and the depth to the water table. The soil used in this example is a fine sandy loam (from Hillel, 1980b).

separate treatment of drying stages. Numerical simulations of this transient system have been performed by, among others, Staple (1970, 1971), Hillel (1975, 1976), and Reynolds & Walker (1984). Simulations of three soil systems using the numerical model TRUST are described in Appendix II.

The evaporation of water from shallow water tables has also been studied extensively (Veihmeyer and Brooks, 1954; Gardner, 1958; Gardner and Fireman, 1958; Hadas and Hillel, 1968, 1972; Ripple and others, 1972; Gardner, 1973; Hillel, 1975). Most of these and other such research has been focused on laboratory measurements of steady-state evaporation under generally non-saline conditions. The expected conclusion of such research is that bare soil evaporation decreases with the depth to water table as well as with the increasing coarseness of the sediment. The process of water evaporation from a shallow water table, in a *homogeneous* system, is more easily described analytically, especially when the system is brought to *steady state* in a controlled laboratory environment. An expression was derived by Gardner (1958) for a homogeneous column of soil with a shallow water table:

$$E_{max} = \frac{Aa}{d^n} \tag{3.16}$$

where E_{max} is the maximum evaporation rate from the soil [LT^{-1}], d is the depth to the water table [L], A is a constant dependent on n [L^2T^{-1}], and n and a are dimensionless constants from the following equation:

$$K(\psi) = a(\psi^n + b)^{-1} \tag{3.17}$$

where a, b, and n are emprically derived constants for a given material. The solution of this equation gives results presented in Fig. 3.2. Solutions match results from laboratory experiments with fairly good success, but they are dependent on the homogeneity of the system (see Appendix II). The solution of flow through a heterogeneous system lends itself more to a numerical approach. Such an approach has been taken by a number of researchers (Hillel, 1975; Feddes and others, 1975; Passerat de Sillans and others, 1989). Passerat de Sillans and others used a coupled heat and water transport numerical code which took into account heat and moisture fluxes estimated from meteorological data. The hydraulic and thermal properties of the surface layer of the soil were free parameters used to fit the results of simulation to the first two data points (two days). The model was then run to simulate the evaporation rate on the following four days. As seen in Fig. 3.3, despite the very short run of this experiment, the results are only fair and it appears that the model would substantially overestimate true rates in the future.

More detailed studies of heterogeneous systems have shown the relative impact of soil properties on evaporation rates to increase toward the surface (e.g. Hadas and Hillel, 1972; see also Appendix II). That is, a change in soil properties near the soil surface will have a greater effect on soil evaporation rates than a similar change at depth. Hysteresis has been shown to affect evaporation rates during early stages after infiltration (Bresler and others, 1969); however, in field situations, the spatial variability of soil properties will usually be greater than the variation due to hysteresis effects. An experiment involving infiltration and evaporation has been modelled using the code TRUST, taking into account only the wetting curve; the results of these simulations may be found in Appendix II and show that, at least in the given system, hysteresis effects are minor.

While it is known that the presence of dissolved species in water tends to decrease the evaporation rate due to lowering of the saturation vapor pressure above the water

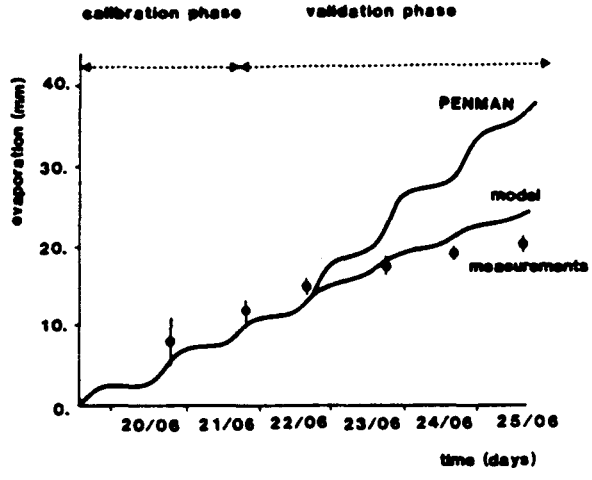

Figure 3.3 Measured and calculated cumulative evaporation based on field data and numerical modelling, respectively. Surface element properties were adjusted so to fit the result of modelling to the first two data points (from Passerat de Silans and others, 1989).

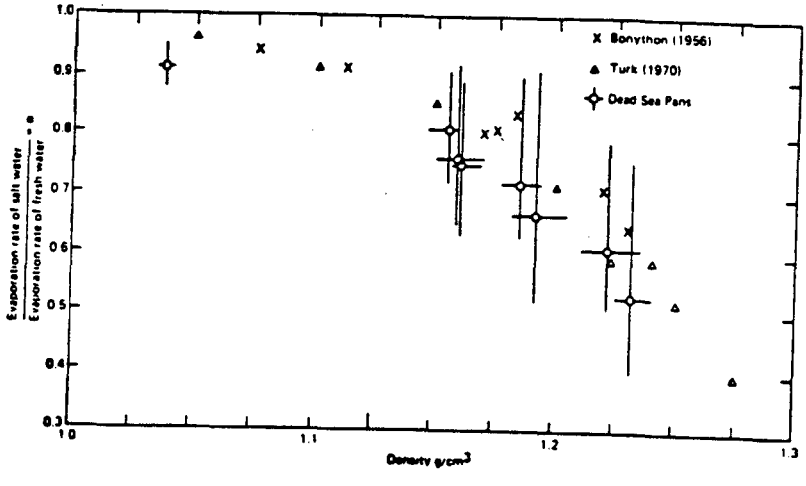

Figure 3.4 Dependence of water evaporation rate on water salinity (here, in terms of water density) (from Salhotra and others, 1985).

surface, there are limited studies of this effect on saline water bodies and even fewer studies of this effect on bare soil evaporation. Salhotra and others (1985) summarized three sets of data (Fig. 3.4) which suggest that salinity (here presented as water density) has a significant effect on evaporation rate. Qayyum and Kemper (1961) studied the effect of mixing NaCl and $CaCl_2$ into the top 10 cm of a 29 cm column on bare soil evaporation rates. They found that a mass concentration of 1.0 % or more of NaCl tended to lower moisture loss from the columns, but the salt distribution in this experiment does not reflect natural conditions since the soil was free of salt in the rest of the profile and thus these results do not apply in general. Finally, the gradient of salt concentrations near the soil surface is usually very steep (see Section 4.4) and may itself drive vapor flow. This aspect of vapor flow is not within the scope of this study and will not be further considered.

3.3 METHODS FOR MEASURING BARE SOIL EVAPORATION

In laboratory experiments, the measurement of a bare soil evaporation rate is straightforward; based on the known rate of water inflow into the system and on changes in the mass of the soil column, such a rate may be continuously and quite accurately monitored. In the field, however, such a measurement is more difficult and subject to greater error than the laboratory measurement. In general, four schemes are available: (1) micrometeorological methods, which involve the calculation of a rate based on measurements of several parameters and using one of a number of available equations (Hillel, 1980b); (2) remote sensing, where evaporation rates are estimated based on radiative and reflective properties of the soil (Hatfield and others, 1983); (3) water balance methods, which require the measurement of soil water flux at a given depth and the changes in water content between that depth and the soil surface (Jackson and others, 1973); and (4) lysimetric methods (van Bavel, 1961; Black and others, 1969; Boast,

1986). Lysimetric methods involve the direct gravimetric measurement of water loss from hydrologically, but not thermally, isolated bodies of soil or sediment. Since such isolation causes changes in boundary conditions, most significantly lower boundary conditions, there is always concern as to whether the rate measured is the same as it would be from a non-isolated body. Additional error may come from disturbance of the soil during construction. To combat these obstacles, large lysimeters have been built; these structures are expensive to build, essentially fixed in space, and must be weighed by a high capacity balance, dedicated to this purpose (Boast, 1986). Recently, Boast and Robertson (1982) suggested a more convenient approach through the use of "micro-lysimeters." The concept is to use small, easily installed, removed, and weighed lysimeters for only a short period of time, during which the boundary conditions are not significantly altered due to the isolation of the soil, that is, only as long as the measured evaporation rate does not deviate from the true evaporation rate. This approach was the one used in the field at Kesterson Reservoir from July 1988 through June 1989. The microlysimeters, which Boast and Robertson tested against large lysimeters, were brass cylinders with an inside diameter of 76 mm, 3 mm thick walls, and a length of 76 mm. The walls were bevelled at the bottom to 0.5 mm in order to facillitate insertion into soil (Fig. 3.5). The bottom of the device was sealed off with a rubber stopper and the entire lysimeter was put into a plastic bag. The lysimeters were placed in a constant evaporativity chamber. Based on several runs, Boast & Robertson concluded that under a variety of external conditions the rates measured by the 76 mm lysimeters did not vary from longer (146 mm) lysimeters until after two days and were less by no more than 10 % after 3.7 days (Fig. 3.6).

In this study, microlysimeters were made out of white PVC, in order to minimize thermal differences between the soil and the inside of the tube. Each cylinder has an inside diameter of approximately 5.1 cm (2 in), a 4 mm (1/6 in) thick wall, and is 10 cm long. The bottom 1.5 to 2.0 cm on the outside of the tube was bevelled to make the edge sharp.

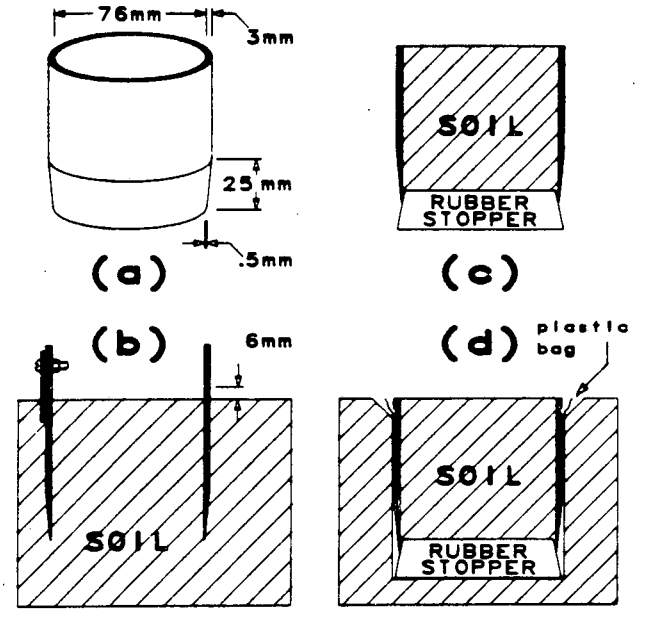

Figure 3.5 Design and procedure for the use of microlysimeter in Boast & Robertson (1982): (a) cylinder design, (b) cylinder pushed into soil, (c) cylinder removed and capped on the bottom prior to weighing, and (d) microlysimeter after being placed back into soil (from Boast & Robertson, 1982).

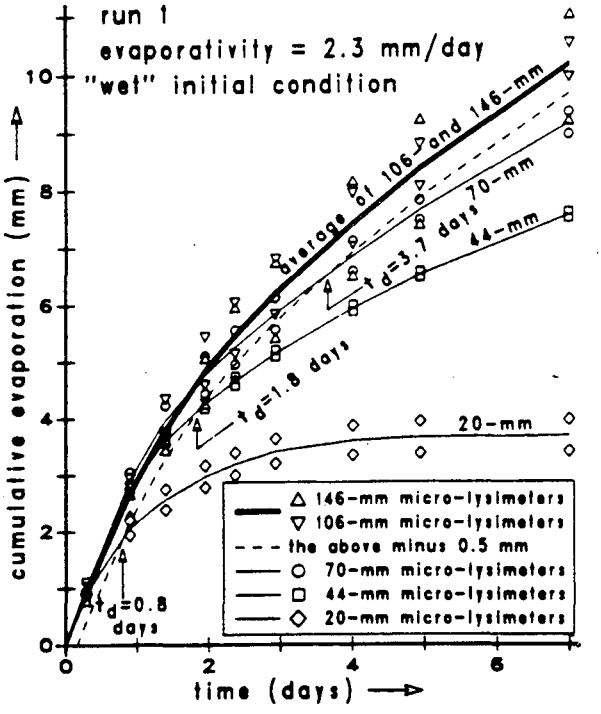

Figure 3.6 Dependence of cumulative evaporation from microlysimeter on time after soil isolation and cylinder length. t_d is the time for each microlysimeter length when the cumulative evaporation deviates by 0.5 mm from actual evaporation (from Boast & Robertson, 1982).

Two sets of eight cylinders were used, each set dedicated to one of the two plots. Except for the first two measurements (7/1/88, 7/29/88) when three to five microlysimeters were used per plot, all other measurements were made using the complete sets. The cylinders were inserted into the soil either by hand (if the soil was moist enough) or by hammering. They were then removed with a set of pliers in such a way as to break off the soil at the bottom of the cylinder from the soil immediately below it. Any soil which was hanging out beyond the bottom of the cylinder was shaved off and the bottom of the cylinder was sealed with a plastic end cap. The end cap was secured to the tube using PVC tape, which also prevented moisture loss through the bottom end. Any soil on the side of the tube was cleaned off. The tubes, with the end cap, PVC tape, and soil were then weighed using a triple beam, 2610 gram capacity Ohaus balance, with a wind shield constructed of wood and plexiglass. After being weighed, the cylinders were placed in unsealed plastic bags and inserted back in the soil so that the tops of the tubes were level with the surrounding soil. After 24 hours, the tubes were removed from the bags, their outside cleaned off, and they were weighed again. Since all boundaries of the tubes were sealed off, except for the top, the change in mass could be due only to loss of water through evaporation or gain of water due to precipitation. Because this study focused on evaporation losses, evaporation rates were measured only during the dry months when no rain fell. The mass of water lost was converted to a volume (assuming density of evaporating water equal to 1.0 g cm^{-3}) and divided by the cross-sectional area of the microlysimeter ($\approx$ 20.26 cm^2). The result is equivalent to a loss of water column; similarly, the flux may be expressed as mass per unit area.

These measurements were made approximately every four weeks, from July 1st until October 25th, 1988, and again from March 17th to June 26th, 1989, with varying frequency. Rates were not measured during the rainy months for three reasons: (1) during rainfall, water would enter the microlysimeter, making it necessary to know the exact mass

of water infiltrating into each cylinder; (2) evaporation of water from a soil is quite rapid immediately following a rainfall event and drops within the next day or so; therefore, a rate measured over a 24 hour period would be a mean value for a range of rates; (3) during a rainfall event of more than a few millimeters, the hydrologic conditions in the tube may become deviant from the surrounding soil due to the presence of a lower boundary at 10 cm. Results of the measurements are described in the following section.

3.4 FIELD DATA, DATA ANALYSIS, AND ERROR ANALYSIS

3.4.1 Bare Soil Evaporation Rates in Plots 8EP and 9BE: Field Data and Analysis

Bare soil evaporation rates measured in the two plots are presented in Fig. 3.7a and 3.7b, for plot 8EP and 9BE, respectively. The error bars in these two diagrams denote one standard deviation on each side of the mean value. The digits in parentheses indicate the number of data points included in the given mean value. With a few exceptions, eight individual microlysimeters were used throughout the study period in each plot. The measurement on 3/17/89 (day 263) in plot 9BE was limited to six cores due to the inadvertant spillage of the other two cores. Overall, values measured in both plots ranged between 0.1 mm/day and 1.5 mm/day. This range is substantially lower than expected based on other studies; however, this was not perceived during the fall season, since the water table in both plots was at a depth of more than 1.5 meters. It was at that time believed that bare soil evaporation rates were being controlled by the overall conductivity of the *soil profile*, which would be a function of the depth of the water table. This conclusion was supported by the apparent correlation between bare soil evaporation rates and the depth to the water table (see Fig. 2.5). In general, this trend is observed when properties of the soil profile control the evaporation rate (cf. Eqn. (3.16)).

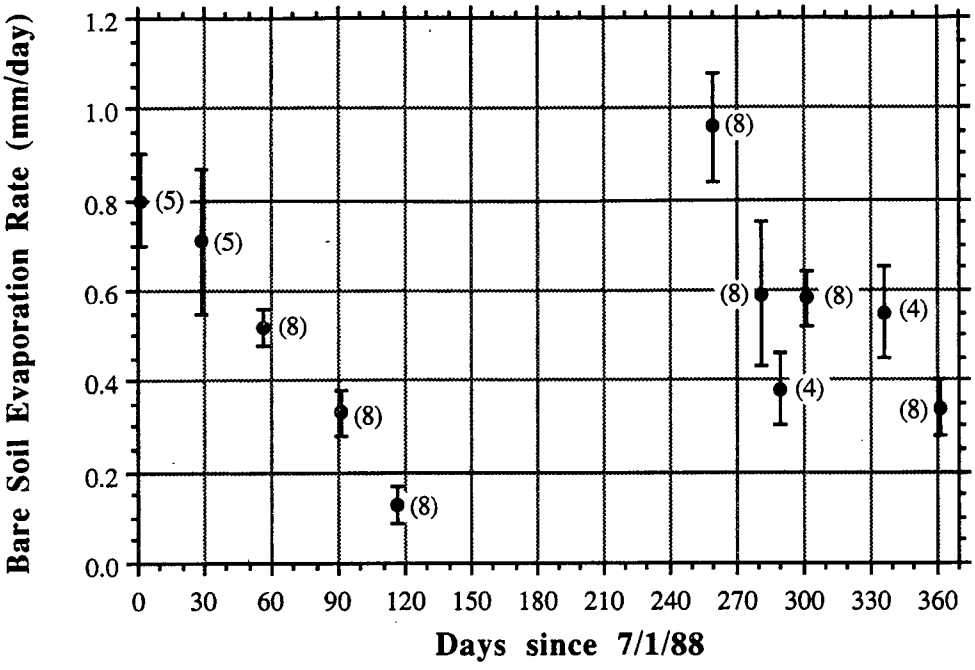

Figure 3.7a Mean field measured bare soil evaporation rates at plot 8EP; error bars represent one standard deviation on each side of the mean. Number of samples in parentheses.

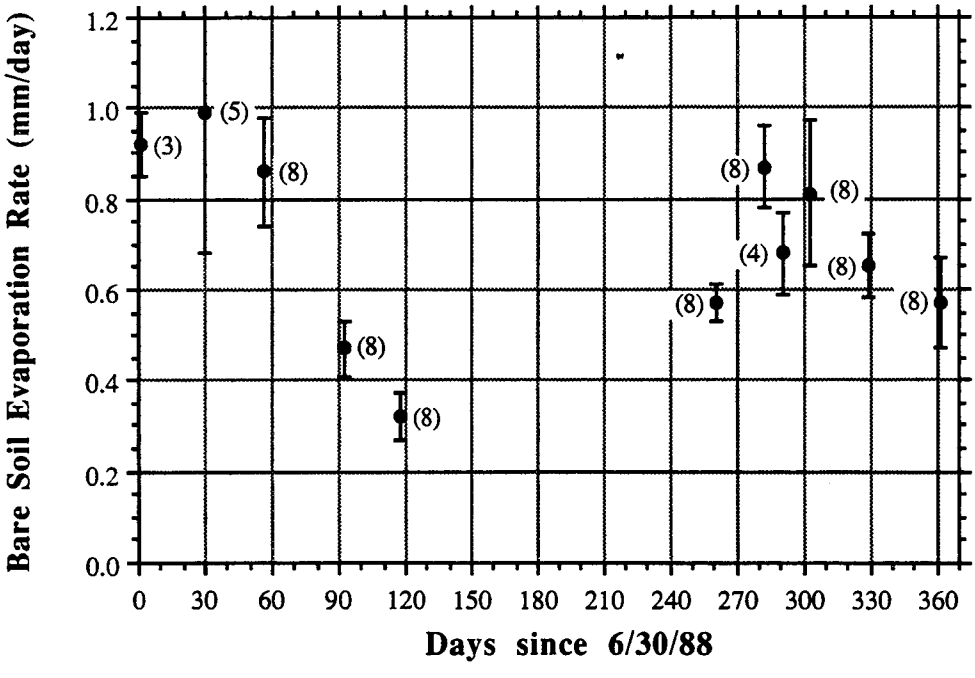

Figure 3.7b Mean field measured bare soil evaporation rates at plot 9BE; error bars represent one standard deviation on each side of the mean. Number of samples in parentheses.

Table 3.1a Bare Soil and Pan Evaporation Data and Calculated Rates: Plot 8EP

Date	Days	Ebs (mm/day)	Mean Ebs (mm/day)	S.D. Ebs (mm/d)	C.V. Ebs (%)	Pan Evap (mm/d)	Grav Moist Content	Ebs calc (mm/day)	Mean Ebs calc (mm/day)	S.D. Ebs calc (mm/day)
7/1/88	1	0.93	0.80	0.10	12.5	12.2	0.193	0.91	0.96	0.10
		0.80					0.185	0.87		
		0.74					0.205	0.97		
		0.86					0.235	1.12		
		0.66					0.202	0.95		
7/29/88	29	0.83	0.71	0.16	22.5	11.7	0.168	0.75	0.71	0.04
		0.48					0.160	0.71		
		0.73					0.161	0.72		
		0.87					0.164	0.73		
		0.64					0.146	0.64		
8/25/88	56	0.51	0.52	0.04	7.7	10.4	0.139	0.54	0.52	0.10
		0.48					0.130	0.51		
		0.58					0.102	0.39		
		0.52					0.103	0.39		
		0.52					0.173	0.69		
		0.47					0.148	0.58		
		0.57					0.142	0.56		
		0.54					0.124	0.48		
9/29/88	91	0.35	0.33	0.05	15.2	8.9	0.115	0.38	0.43	0.05
		0.31					0.125	0.41		
		0.26					0.120	0.40		
		0.40					0.150	0.50		
		0.33					0.128	0.43		
		0.27					0.143	0.48		
		0.37					0.117	0.39		
		0.35					0.144	0.48		

Table 3.1a Bare Soil and Pan Evaporation Data and Calculated Rates: Plot 8EP

Date	Days	Ebs (mm/day)	Mean Ebs (mm/day)	S.D. Ebs (mm/d)	C.V. Ebs (%)	Pan Evap (mm/d)	Grav Moist Content	Ebs calc (mm/day)	Mean Ebs calc (mm/day)	S.D. Ebs calc (mm/day)
10/25/88	117	0.21	0.13	0.04	30.8	3.6	0.155	0.21	0.15	0.03
		0.12					0.128	0.17		
		0.12					0.119	0.16		
		0.12					0.110	0.15		
		0.10					0.093	0.12		
		0.15					0.110	0.15		
		0.10					0.102	0.13		
		0.14					0.110	0.15		
3/17/89	260	0.89	0.96	0.12	12.5	6.2	0.198	0.47	0.50	0.04
		0.95					0.190	0.45		
		0.95					0.221	0.53		
		1.10					0.206	0.50		
		1.00					0.194	0.46		
		0.93					0.232	0.56		
		1.11					0.191	0.46		
		0.75					0.221	0.53		
4/7/89	281	0.67	0.59	0.16	27.1	7.3	0.158	0.44	0.54	0.05
		0.48					0.194	0.55		
		0.68					0.176	0.49		
		0.29					0.198	0.56		
		0.47					0.196	0.55		
		0.61					0.190	0.53		
		0.76					0.217	0.62		
		0.75					0.197	0.55		

Table 3.1a Bare Soil and Pan Evaporation Data and Calculated Rates: Plot 8EP

Date	Days	Ebs (mm/day)	Mean Ebs (mm/day)	S.D. Ebs (mm/d)	C.V. Ebs (%)	Pan Evap (mm/d)	Grav Moist Content	Ebs calc (mm/day)	Mean Ebs calc (mm/day)	S.D. Ebs calc (mm/day)
4/16/89	290	0.46	0.38	0.08	21.1	6.2	0.199	0.48	0.41	0.05
		0.28					0.151	0.35		
		0.37					0.164	0.39		
		0.41					0.179	0.42		
4/28/89	302	0.60	0.58	0.06	10.3	8.0	0.150	0.45	0.50	0.07
		0.54					0.148	0.45		
		0.59					0.163	0.50		
		0.49					0.169	0.52		
		0.53					0.145	0.44		
		0.62					0.202	0.63		
		0.67					0.152	0.46		
		0.61					0.187	0.58		
6/1/89	336	0.51	0.55	0.10	17.5	11.7	0.183	0.82	0.67	0.20
		0.61					0.179	0.80		
		0.64					0.153	0.68		
		0.43					0.091	0.39		
6/26/89	361	0.25	0.34	0.06	17.6	12.6	0.120	0.56	0.61	0.08
		0.28					0.116	0.54		
		0.36					0.150	0.71		
		0.44					0.150	0.72		
		0.30					0.107	0.50		
		0.33					0.130	0.61		
		0.32					0.135	0.64		
		0.40					0.132	0.62		

Table 3.1b Bare Soil and Pan Evaporation Data and Calculated Rates: Plot 9BE

Date	Days	Ebs (mm/day)	Mean Ebs (mm/day)	S.D Ebs (mm/day)	C.V. Ebs (%)	Pan Evap (mm/day)	Grav Moist Content	Ebs calc (mm/day)	Mean Ebs calc (mm/day)	S.D. Ebs calc (mm/day)
6/30/88	1	0.85	0.92	0.07	7.62	12.2	0.344	1.25	1.18	0.10
		0.99					0.277	1.07		
		0.92					0.332	1.22		
7/29/88	30	0.96	0.99	0.31	31.31	11.7	0.242	0.93	0.99	0.04
		1.36					0.259	0.97		
		1.06					0.263	0.99		
		1.05					0.268	1.00		
		0.50					0.287	1.05		
8/25/88	57	1.05	0.86	0.12	13.95	10.4	0.283	0.92	0.86	0.07
		0.79					0.273	0.90		
		0.99					0.284	0.93		
		0.81					0.262	0.87		
		0.82					0.279	0.91		
		0.72					0.229	0.79		
		0.93					0.237	0.81		
		0.73					0.203	0.73		
9/29/88	92	0.49	0.47	0.06	12.77	8.9	0.260	0.74	0.72	0.04
		0.54					0.261	0.75		
		0.49					0.249	0.72		
		0.49					0.229	0.68		
		0.42					0.255	0.73		
		0.49					0.261	0.75		
		0.48					0.259	0.74		
		0.35					0.207	0.63		

Table 3.1b Bare Soil and Pan Evaporation Data and Calculated Rates: Plot 9BE

Date	Days	Ebs (mm/day)	Mean Ebs (mm/day)	S.D Ebs (mm/day)	C.V. Ebs (%)	Pan Evap (mm/day)	Grav Moist Content	Ebs calc (mm/day)	Mean Ebs calc (mm/day)	S.D. Ebs calc (mm/day)
10/25/88	118	0.30	0.32	0.05	15.63	3.6	0.283	0.32	0.32	0.03
		0.35					0.328	0.36		
		0.40					0.257	0.30		
		0.35					0.222	0.27		
		0.25					0.276	0.31		
		0.32					0.284	0.32		
		0.25					0.260	0.30		
		0.32					0.320	0.35		
3/17/89	261	0.59	0.57	0.04	7.02	6.2	0.454	0.78	0.72	0.05
		0.59					0.473	0.80		
		0.60					0.388	0.69		
		0.50					0.395	0.70		
		0.54					0.382	0.69		
		0.59					0.373	0.67		
4/7/89	282	0.75	0.87	0.09	10.34	7.3	0.390	0.82	0.76	0.05
		0.81					0.305	0.69		
		0.88					0.348	0.76		
		0.85					0.349	0.76		
		0.85					0.394	0.83		
		1.07					0.336	0.74		
		0.85					0.375	0.80		
		0.86					0.317	0.71		
4/16/89	291	0.80	0.68	0.09	13.24	6.2	0.332	0.62	0.64	0.02
		0.69					0.353	0.65		
		0.62					0.341	0.63		
		0.62					0.375	0.68		

Table 3.1b Bare Soil and Pan Evaporation Data and Calculated Rates: Plot 9BE

Date	Days	Ebs (mm/day)	Mean Ebs (mm/day)	S.D Ebs (mm/day)	C.V. Ebs (%)	Pan Evap (mm/day)	Grav Moist Content	Ebs calc (mm/day)	Mean Ebs calc (mm/day)	S.D. Ebs calc (mm/day)
4/28/89	303	0.70	0.81	0.16	19.75	8.0	0.354	0.84	0.80	0.05
		0.69					0.292	0.73		
		0.84					0.304	0.75		
		0.75					0.311	0.76		
		0.68					0.379	0.88		
		0.70					0.336	0.81		
		0.96					0.357	0.84		
		1.13					0.345	0.82		
5/24/89	329	0.52	0.65	0.07	10.77	6.2	0.246	0.50	0.54	0.03
		0.60					0.283	0.55		
		0.62					0.250	0.50		
		0.66					0.309	0.59		
		0.68					0.284	0.55		
		0.67					0.286	0.56		
		0.74					0.269	0.53		
		0.74					0.282	0.55		
6/26/89	362	0.41	0.57	0.10	17.54	12.6	0.122	0.61	0.85	0.14
		0.63					0.201	0.87		
		0.65					0.230	0.96		
		0.49					0.210	0.90		
		0.57					0.177	0.79		
		0.54					0.254	1.03		
		0.54					0.149	0.70		
		0.74					0.208	0.90		

Between July 1st and October 25th, 1988, as the water table dropped, measured bare soil evaporation rates dropped from a mean of 0.80 mm/day to a mean of 0.13 mm/day in plot 8EP and from a mean of 0.92 mm/day to 0.32 mm/day in plot 9BE. As the water table dropped, the moisture content of the soil profile declined, which is apparent from potential distributions, as measured using tensiometers (Fig. 3.8) (see Cassell and Klute, 1986 for tensiometer design and installation). At that time, it was believed that since the evaporation rate was mostly a function of the depth to the water table, intermediate rates would decline smoothly between measured points and the measured values could be interpreted as mean rates for the two weeks immediately preceding and two weeks immediately following the date of measurement. The variability of measured values was believed to be most likely related to the spatial variability of soil properties *in the profile*. A more detail description of the data is presented in Table 3.1, and includes the calculated coefficients of variation for each set of measurements. These range from 7.7% to 30.1% for plot 8EP and from 7.0% to 31.3% for plot 9BE for all sets of measurements.

During the spring and early summer of 1989, rates were expected to rise substantially due to the rise of the water table at both plots (see Fig. 2.5). At plot 9BE, the water table was at a depth of 28 cm at its shallowest (day 244), a depth at which almost any soil is expected to be able to transmit water at a rate nearly equivalent to potential evaporation. The increased moisture content throughout the soil profile can be seen through tensiometer data (Fig. 3.9). The fact that bare soil evaporation rates measured at that time were still in the sub-millimeter-per-day range, while pan evaporation was measured in the 2 to 5 mm/day range, indicated that other factors were controlling bare soil evaporation besides the depth to the water table. Further measurements during the season reinforced this suspicion; while the water table was declining at both plots, bare soil evaporation rates measured were erratic, although they did not vary substantially from approximately 0.5 mm/day in plot 8EP and 0.6-0.8 mm/day in plot 9BE. This range of

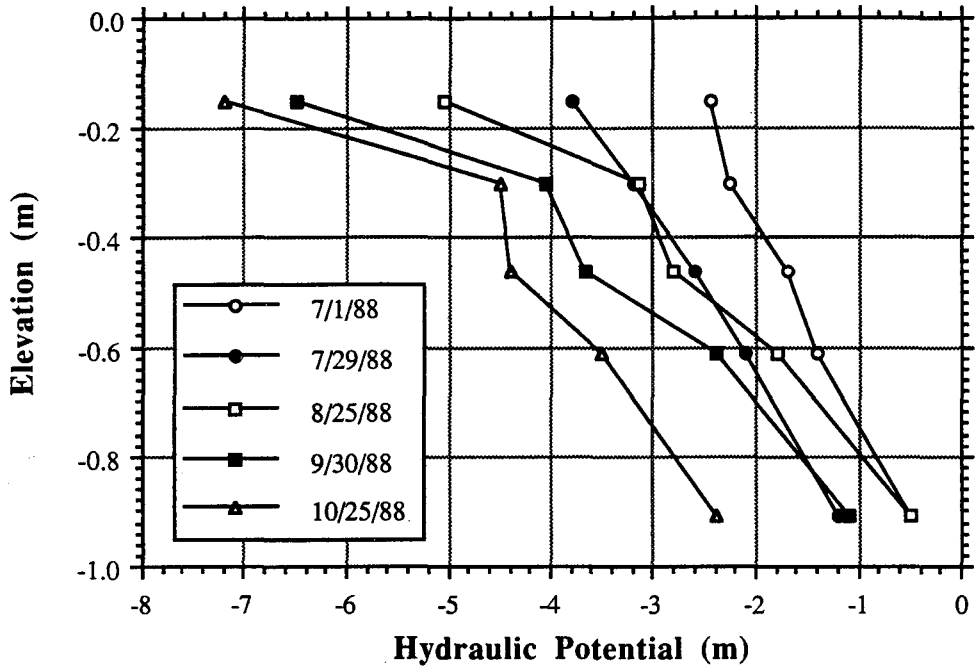

Figure 3.8a Hydraulic potential distribution changes in soil profile of plot 8EP during the summer and fall of 1988.

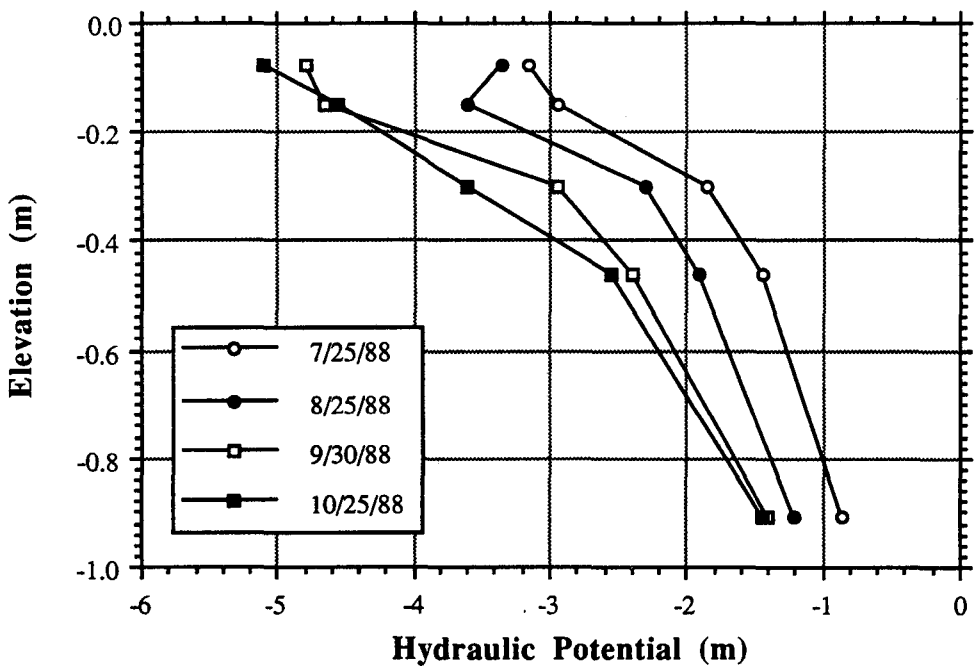

Figure 3.8b Hydraulic potential distribution changes in soil profile of plot 9BE during the fall and summer of 1988.

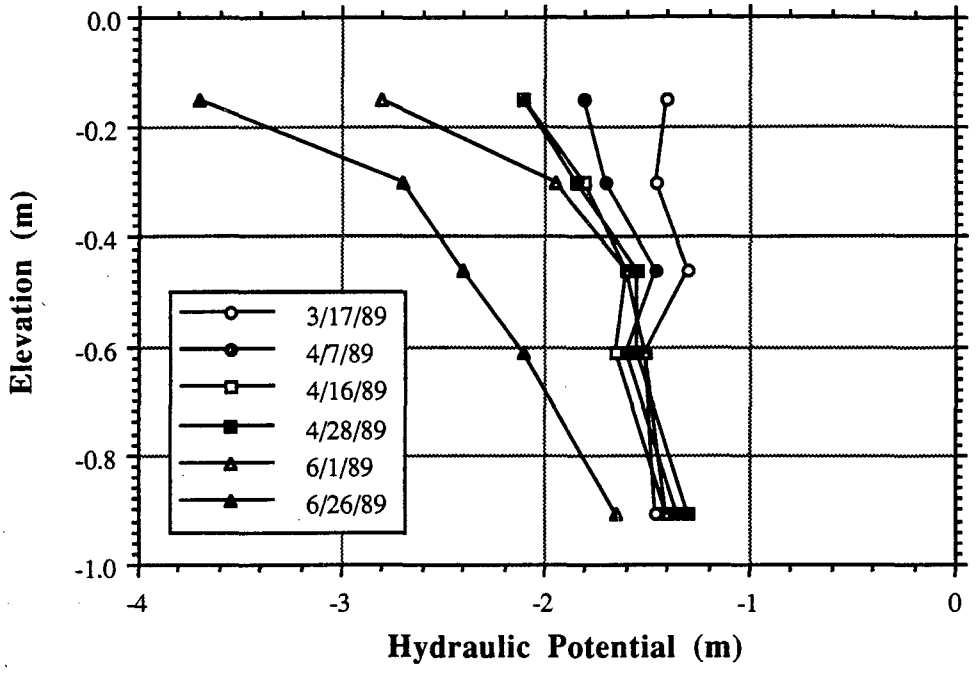

Figure 3.9a Hydraulic potential distribution changes in soil profile of plot 8EP during the spring and summer of 1989.

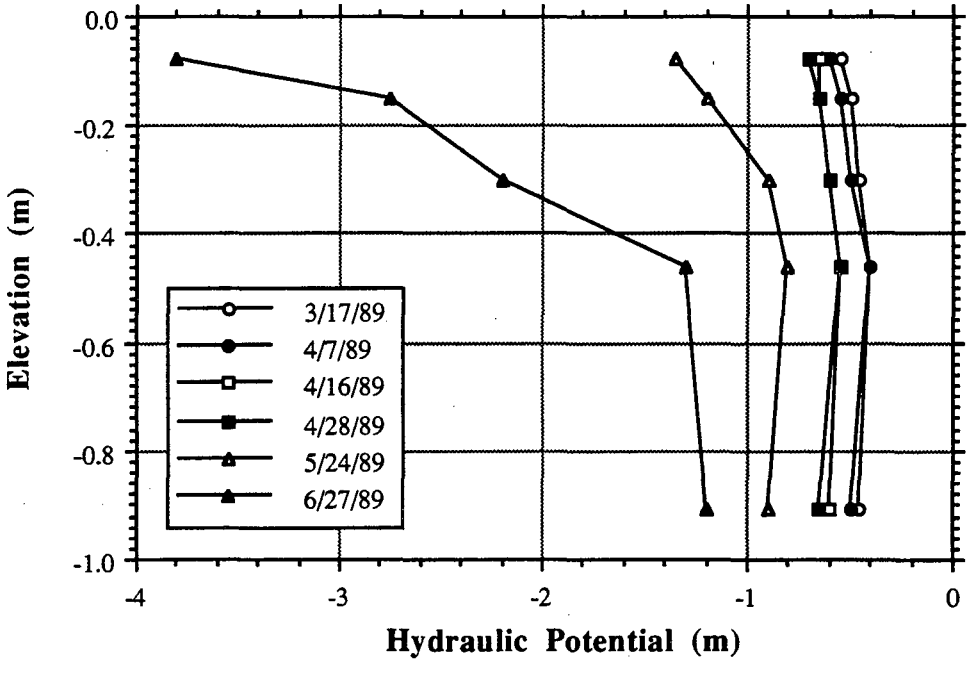

Figure 3.9b Hydraulic potential distribution changes in the soil profile of plot 9BE during the spring and summer of 1989.

rates is similar to that observed from a soil with a surface mulch (Gardner & Fireman, 1958), in which case water vapor diffusion through the high porosity, low bulk density surface layer was found to be the dominant mode of water transport (Fig. 3.10). This suggested that the salt crust present on the soil surface has an effect similar to a surface mulch. The process of vapor diffusion is driven by gradients in vapor concentrations near the soil surface (see Eqn. (3.15)), which means that the lower the external humidity and the higher the temperature, the higher the rate of diffusion. If diffusion is the dominant transport process at these plots, then external (atmospheric) conditions may be controlling soil evaporation. The same atmospheric conditions which control vapor diffusion also control potential evaporation rates. Therefore, there should be a correlation between measured pan evaporation rates and measured bare soil evaporation rates. In addition to the vapor concentration gradient, $J_{S,v}$ of Eqn. (3.15) is also directly proportional to soil gas-phase porosity, tortuosity, and inversely proportional to soil liquid-phase saturation, or moisture content. However, in the given case, a reduction in soil moisture content will lead to an increase in Δz, or the one-dimensional travel distance of water vapor. These relationships are graphically presented in Fig. 3.11. Also, while vapor diffusion may be dominant near the soil surface, water movement below the top 2-3 cm is certain to be dominated by liquid flow; therefore, a lower moisture content will cause a decrease in unsaturated soil conductivity which will hinder the transport of water towards the soil surface. The vapor concentration (or humidity) in a soil is directly related to matric and osmotic potentials (Koorevar and others, 1983). Table 3.2 shows the relationship between matric head and soil humidity (here osmotic effects due to solute concentrations are ignored).

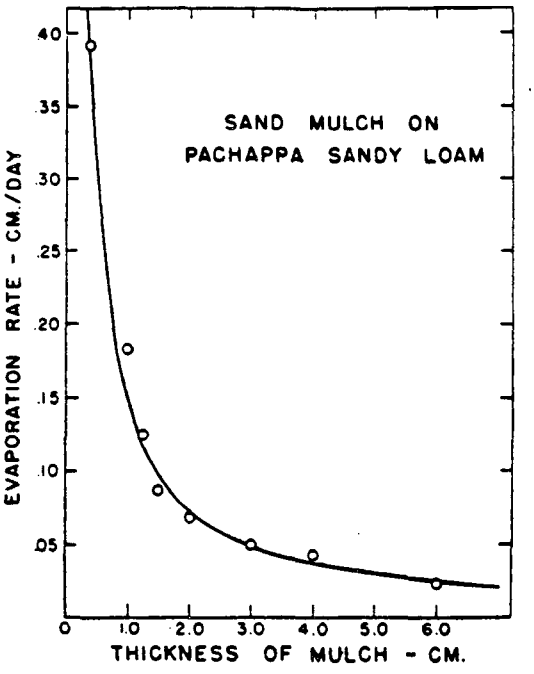

Figure 3.10 Dependence of bare soil evaporation rate on the thickness of a surface sand mulch on a 100 cm column of Pachappa sandy loam (from Gardner & Fireman, 1958).

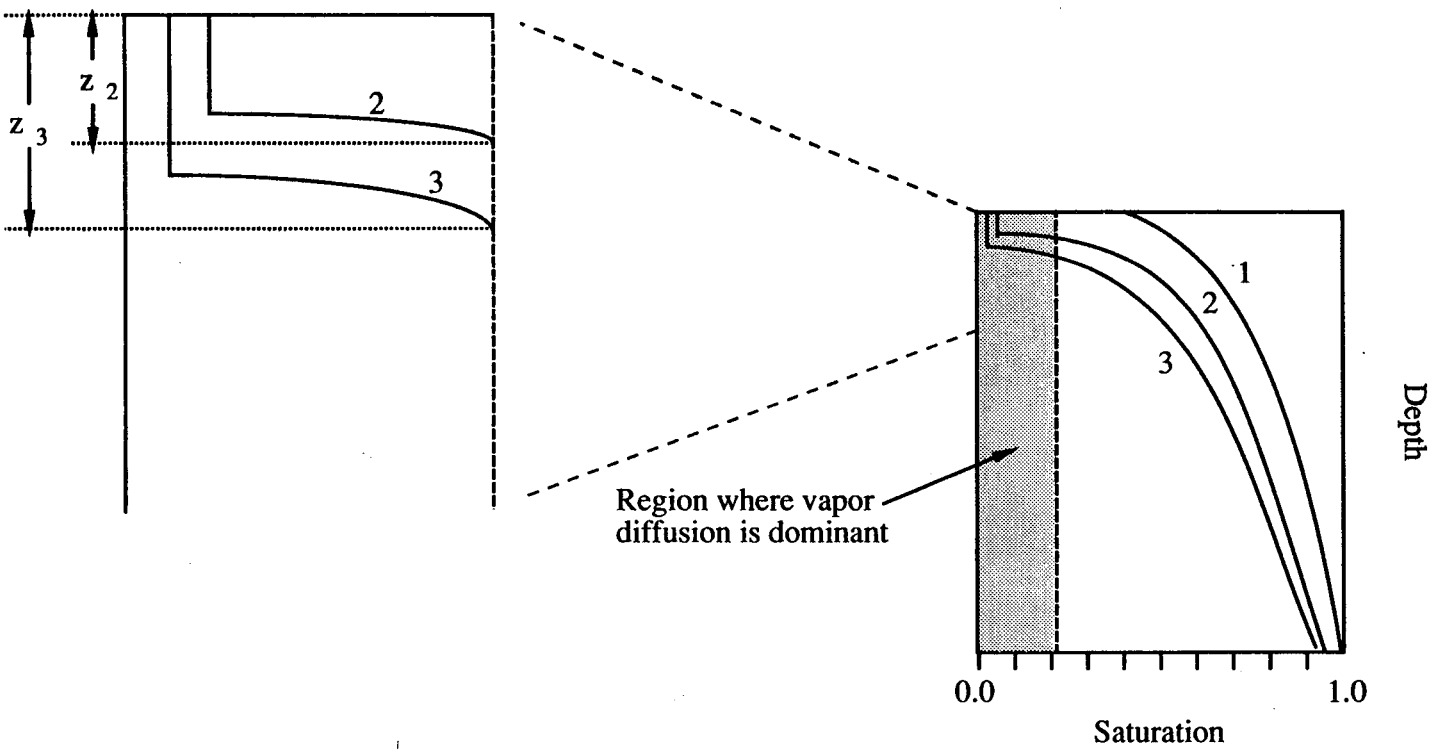

Figure 3.11 Conceptual representation of the dependance of vapor diffusion on soil saturation.

Table 3.2 The Relationship Between Soil Humidity and Matric Potential (adapted from Koorevar and others, 1983).

Matric potential (m)	Soil Relative Humidity (%)
-0.01	100.00
-0.10	100.00
-1.0	99.99
-10	99.93
-10^2	99.3
-10^3	92.8
-3.2×10^3	78.9
-10^4	47.2
-3.2×10^4	9.3
-10^5	0.06

At a matric head of -3,200 m, soil humidity is 78.9%, whereas at a matric head of -10,000 m, soil humidity drops to 47.2%. This drop reduces the vapor concentration difference between the soil and the atmosphere which, in the given case, would lead to a reduction in vapor flow. On the other hand, the change in saturation associated with such a decline in matric potential would be fairly minor (5 to 15% for most soils). Therefore, it is likely that a decrease in moisture content of near-surface soils will result in a decrease in bare soil evaporation rates. The correlation between bare soil evaporation and pan evaporation should be a positive one: both increase with increasing temperature and decreasing humidity.

In order to test the above dependences, bare soil evaporation rate (E_{bs}) data was fit to the following equation:

$$E_{bs} = C\, E_{pan}\, \theta^{b}_{grav,9} \qquad (3.18)$$

where E_{pan} is the measured pan evaporation rate [LT^{-1}], $\theta_{grav,9}$ is gravimetric moisture content of the top 9 cm of soil [MM^{-1}], and C and b are dimensionless constants, essentially dependent on soil characteristics, but without any particular significance attached to either one. This form of equation was chosen because of its simplicity and its potentially physical meaning. The exponent on the moisture content term will define the relative significance of the two variables. For each plot, two data points were chosen for which E_{bs}, E_{pan}, and $\theta_{grav,9}$ differed; for both plots, the data from 7/29/88 and 8/25/88 were chosen. Eqn. (3.18) was then solved for C and b for each plot. For plot 8EP, C was found to be equal to 0.44 and b to be equal to 1.08; the same values for plot 9BE were found to be 0.224 and 0.732, respectively. The values of the constant b indicate that external conditions and moisture content are equally important in determining bare soil evaporation. E_{pan} and $\theta_{grav,9}$ data for each sample date was used to calculate a bare soil evaporation rate ($E_{bs,calc}$). The results of this calculation are compared with the actual measurements in Fig. 3.12. (The lines which join points in this graph are only for the purpose of differentiation between the two data sets and do not indicate the expected trends between data points.) With a few exceptions, the fit is satisfactory; the point on day 263 was not expected to be fitted well due to the fact that the measurement may have been affected by a rainfall event of 1.3 mm on the previous day. Therefore, the rate measured on that day would be expected to be somewhat elevated. This effect, however, was not observed in plot 9BE, possibly due to more rapid infiltration of water into the higher porosity surface soil there, although this explanation is probably not satisfactory. The last two data points from each plot do not fit very well either, due possibly to a fairly rapid

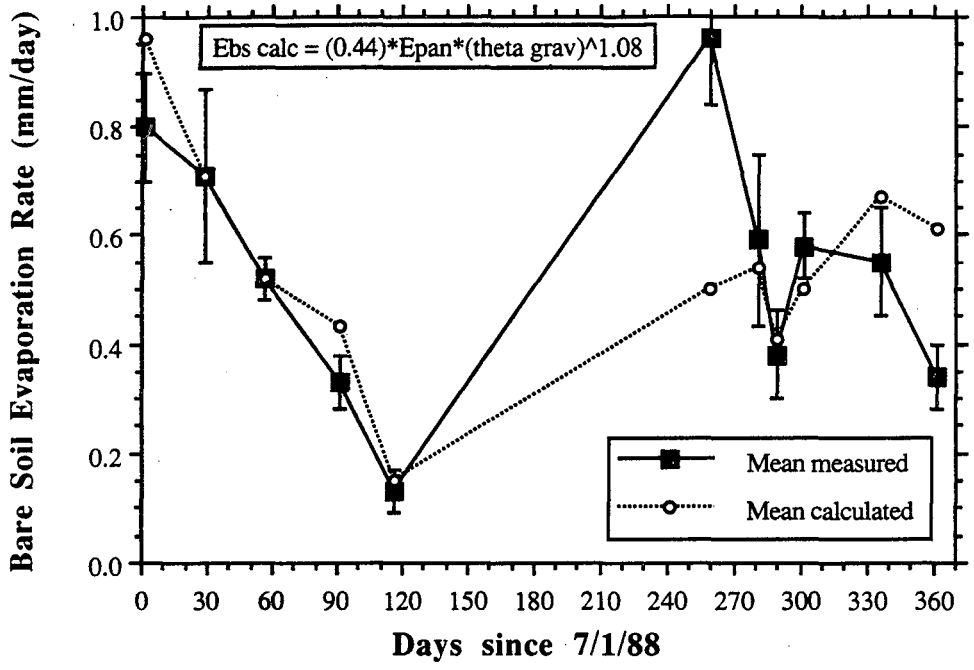

Figure 3.12a Measured and calculated bare soil evaporation rates for plot 8EP; error bars represent one standard deviation on each side of the measured mean.

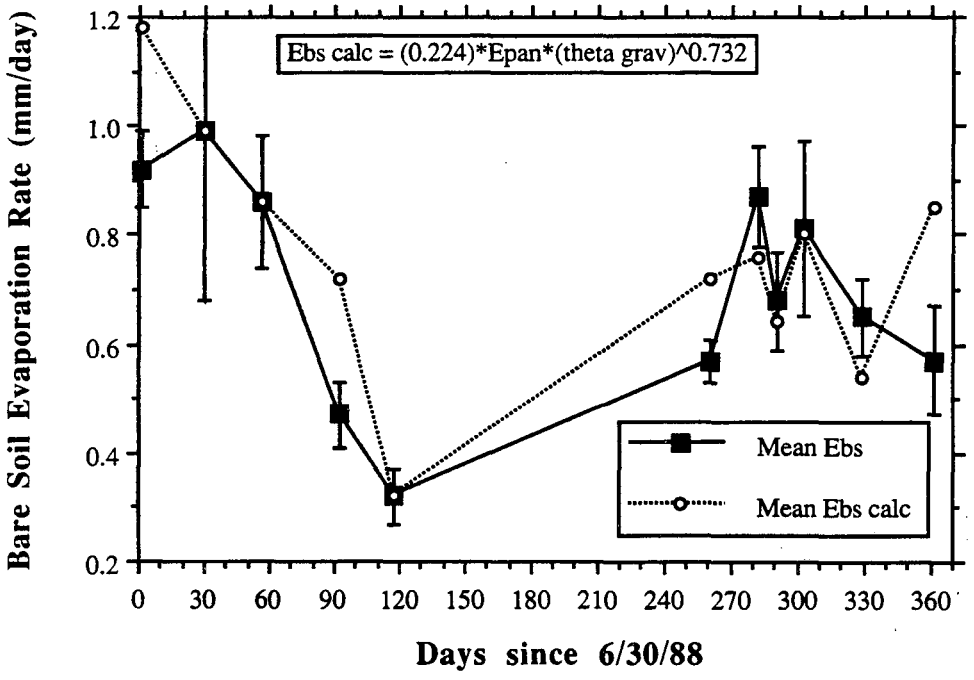

Figure 3.12b Measured and calculated bare soil evaporation rates at plot 9BE; error bars represent one standard deviation on each side of the measured mean.

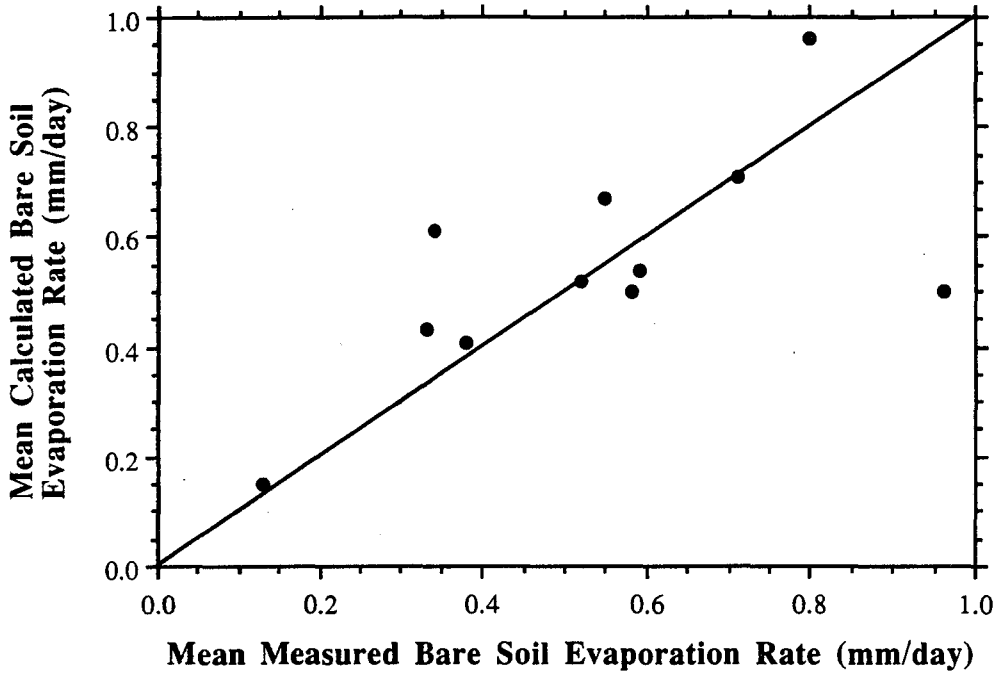

Figure 3.13a Calculated vs. measured bare soil evaporation rates at plot 8EP.

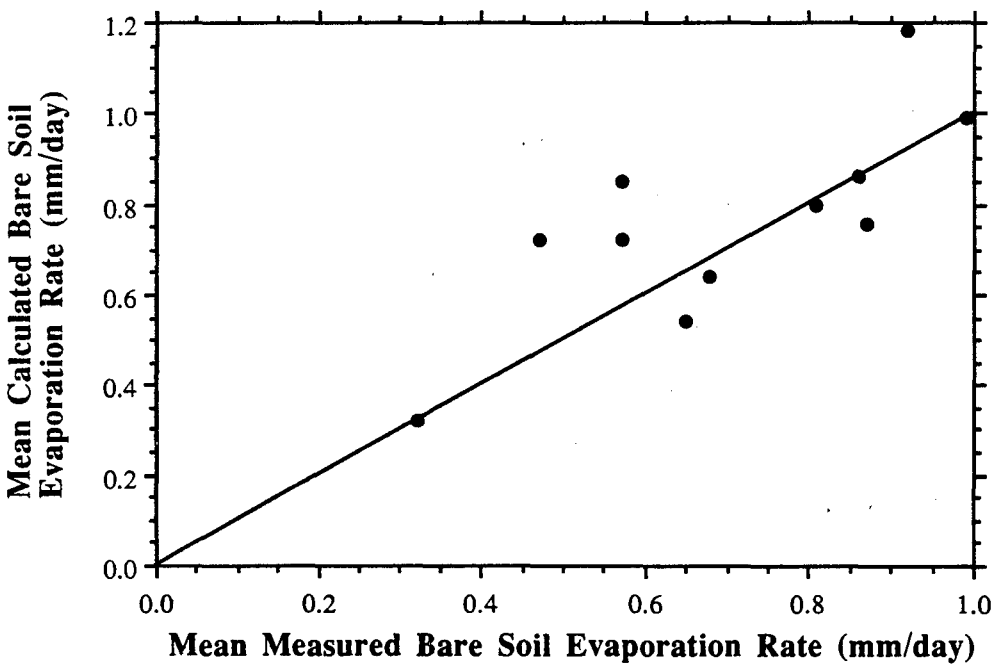

Figure 3.13b Calculated vs. measured bare soil evaporation rates at plot 9BE.

drying of surface soil during this period. A comparison of gravimetric moisture content of soil from both plots between 7/1/88 and 6/26/89 (Table 3.1), shows a substantial net drying of the soil over an annual cycle, clearly demonstrating the transient state of the soil profile in both plots, as a result of the presence of excess water, a remnant from when the ponds were flooded. This should result in lower soil evaporation rates over the next annual cycle; indeed, this trend is seen in data from both plots. However, the calculated values are higher than the measured values in May and June of 1989, suggesting, perhaps, that soil properties of the top 9 cm interval have changed somewhat since the beginning of the twelve month cycle and are no longer described by the above calculated constants, C and b. The correlation between $E_{bs,calc}$ and E_{bs} is presented in Fig. 3.13. The line in these plots designates a slope of 1.

A few points need to be made about this analysis. (1) It is not intended to serve as a predictive tool, but rather as a test of the supposition that soil moisture content and atmospheric conditions are the chief factors controlling bare soil evaporation; as such, this has been shown, although the system is clearly more complicated than this analysis allows for. (2) Bare soil evaporation is affected not only by bulk moisture content, but also by the *distribution* of moisture within the 9 cm interval; this is not taken into account in the above analysis. (3) Pan evaporation rates were estimated based on rates measured in Los Banos (see Section 2.2.3) and slight variations may be expected to occur, even within the Reservoir; unfortunately, due to an initial ignorance about the processes involved, pan evaporation rates were not measured within the test plots themselves, as it was assumed that bare soil evaporation was controlled by the soil profile and not external conditions. Therefore, the data may have been fit more successfully if pan rates were measured within the test plots.

The significance of vapor diffusion in this process is more quantitatively demonstrated using a numerical model. The results of numerical modelling of the system in plot 8EP, using the code TRUST are presented in Chapter V.

While the above approach should not be used for quantitative prediction of evaporation rates in the future, it may be used to estimate an average seasonal rate for the two drying seasons in question. This may be done by linearly interpolating $\theta_{grav,9}$ between measured values and using pan evaporation rates measured on each day of the two periods. When this is done, the patterns of evaporation shown in Fig. 3.14 are calculated. The average rates are presented in Table 3.3 below.

Table 3.3 Calculated Average Seasonal Rates of Bare Soil Evaporation for Plots 8EP and 9BE, Compared With Average Seasonal Pan Evaporation Rates.

Season	Total Pan Evaporation (mm)	Total Bare Soil Evap, P8EP (mm)	Total Bare Soil Evap, P9BE (mm)	Avg E_{pan} (mm/day)	Avg E_{bs} at 8EP (mm/day)	Avg E_{bs} at 9BE (mm/day)
Summer & Fall 1988	1071.4	60.8	92.0	9.08	0.52	0.78
Spring & Summer 1989	836.4	47.9	75.5	8.20	0.47	0.74

Since it is known that this approach overestimates bare soil evaporation during the second season, the average bare soil evaporation rates calculated for that season should be

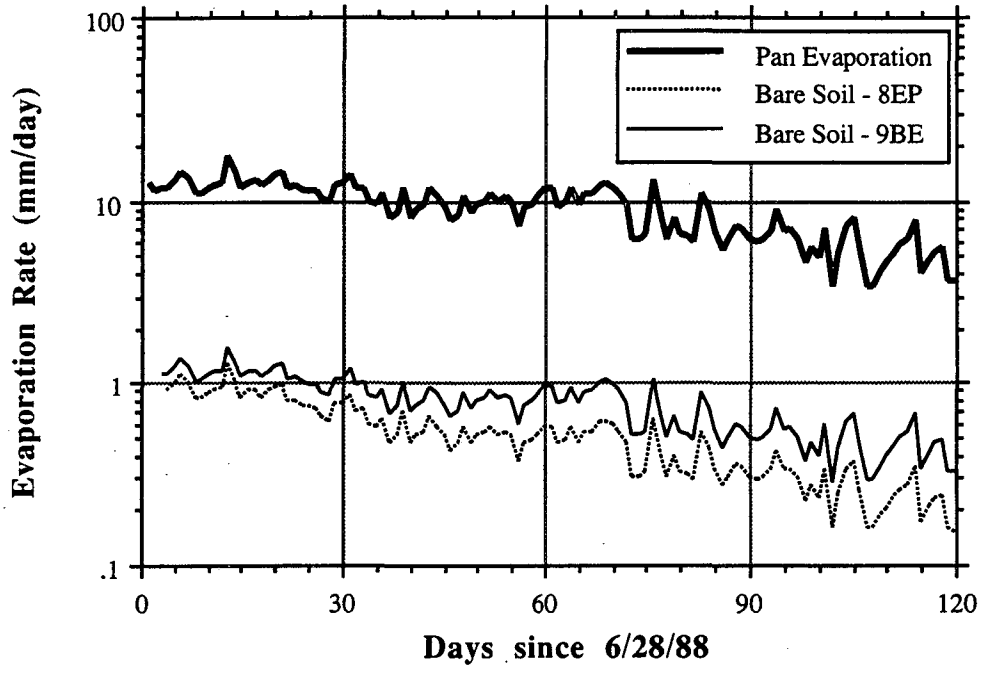

Figure 3.14a Seasonal trends in bare soil evaporation as calculated based on pan evaporation data; summer & fall, 1988.

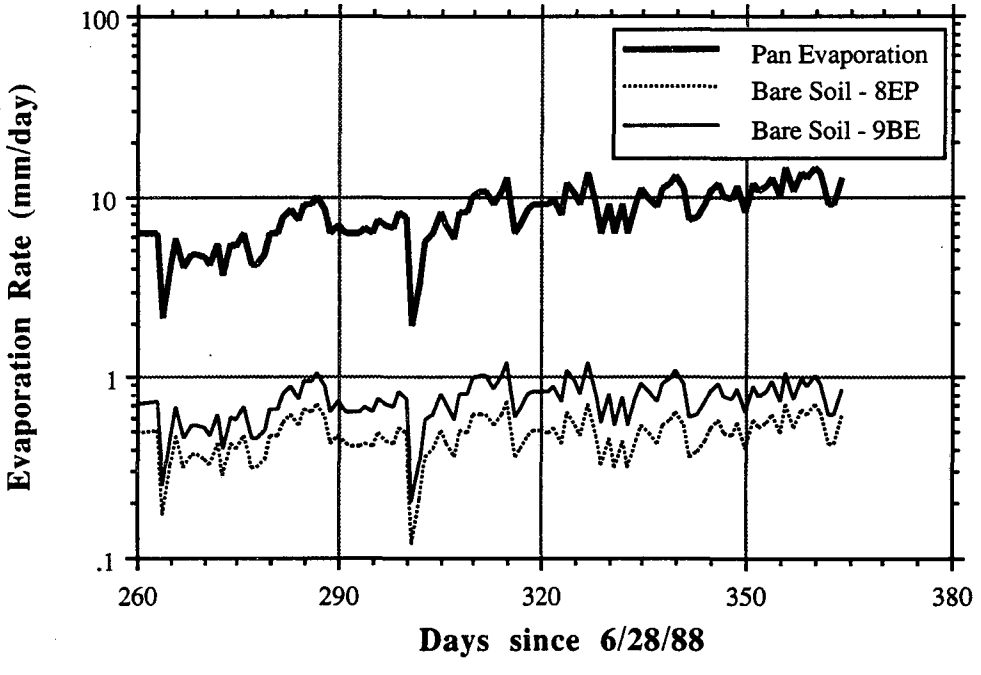

Figure 3.14b Seasonal trends in bare soil evaporation as calculated based on pan evaporation data; spring & summer, 1989.

considered to be upper limits on the actual rates. Rates calculated for the first season should be fairly accurate.

3.4.2 Errors Involved in Bare Soil Evaporation Rate Measurement

The method used for making these measurements is described in Section 3.3. There are several potential sources of error involved. (1) Evaporation rates are based on mass differences of soil cores, which are measured in the field using a 2610 gram capacity balance. This balance nominally has a precision of 0.1 g; however, it is possible to interpolate between 0.1 g marks. In the field, masses were recorded down to 0.01 g, although it is more reasonable to assume a precision of 0.02 g, based on the reproducibility of individual measurements. On particularly windy days, the precision of the balance may go to as much as 0.05 g. For the purpose of this analysis, 0.05 g will be assumed to be the precision of the balance. Since rates are based on *differences* in mass, the error, due to the random nature of the uncertainty, is equal to the square root of the sums of the squares of the uncertainty for each measurement (Taylor, 1982). Therefore, the total error in the difference of these masses is equal to: $((0.05)^2 + (0.05)^2)^{0.5} = 0.07$ g. (2) The mass difference is then converted to volume through division by water density (1.00 gcm^{-3}) and the error becomes equal to 0.07 cm^3. The mass difference is then divided by the cross-sectional area of the microlysimeter. This introduces somewhat more error, in that the radius of the microlysimeter is equal to 2.54 ± 0.05 cm, which gives an area of 20.26 ± 0.79 cm^2. After dividing water volume by cross-sectional area, the total error becomes equal to the square root of the sum of the original fractional uncertainties; therefore, the *fractional* error becomes: $((0.07/1)^2 + (0.79/20.26)^2)^{0.5} = 0.08$ or 8% for a sample which lost 1 g of water during the measurement period. This is approximately an average value; for the lowest mass difference observed (0.20 g, 0.10 mm/day) the fractional error is 35% and for the greatest mass difference observed (2.73 g, 1.36 mm/day), the fractional error is

4.7 %. This gives an average precision of 0.04 mm/day to the bare soil evaporation rate measurement.

There are also small errors associated with the measurement of $\theta_{grav,9}$. The method for measuring gravimetric moisture content is described in Section 4.3.2. The precision of the method is dependent on the precision of the laboratory balance, which is 0.01 g. Therefore, for a soil sample of 50.00 g which contains 10.00 g of water (θ_{grav} = 0.250), the fractional error would be equal to 0.1%, which, in general, is insignificant. There are errors associated with the selection of a subsample for θ_{grav} determination; if a soil sample is not thoroughly homogenized, the given subsample may not be representative of the larger sample. There will always be intrasample variability, but it may be considered insignificant, especially if the subsample is sufficiently large (e.g. 10 - 20% of the total sample). The results of measurement of both E_{bs} and θ_{grav} are dependent on the spatial variability of soil within each plot. This is unavoidable, and is one of the two main reasons why as large a number of samples needs to be taken as possible. The other reason for a large sample set is the possibility of core disturbance by wind and animals. Wind tends to displace dry soil and salt crust; it may be assumed that, on average, approximately the same mass of soil will blow into as out of a given microlysimeter. However, it is possible that the net mass change will not be zero. Installing a number of microlysimeters greatly increases the chances of the average rate measured not being affected by saltation. The presence of jackrabbits and coyotes at Kesterson Reservoir raises the possibility of core disturbance by animals. On one occasion, a microlysimeter which was not part of this study was urinated on by a coyote and thereby became worthless for that particular measurement. Physical disturbances by jackrabbits would most likely have an effect similar to saltation. Neither the wind nor animal disturbances can be quantified. Finally, there is yet another source of unquantifiable error, that of the human variety.

4.0 MEASUREMENT OF CHEMICAL CHANGES IN NEAR-SURFACE SOILS

Changes in soil and soil water chemistry often serve as an indication of a water flux. While direct measurements of evaporation using microlysimeters are very useful in determining rates over short periods of time, constant monitoring would be required to measure an average flux for a longer period of time. Whereas measuring of chemical changes in the near surface sediments is subject to a slew of errors, and its precision is greatly limited by spatial variability of concentrations and soil properties, it may be used effectively to monitor long-term changes in species concentrations, from which an average evaporative flux may be discerned.

4.1 THEORY OF SOLUTE TRANSPORT

In order to arrive at a mathematical description of the solute transport process, a number of models have been derived; statistical geometric models, which use parameters based on physical properties of the medium, water, and solute have been most popular due to their physical basis (Gillham & Cherry, 1982). In general, solute transport is considered to be the result of two processes: *advection* and *diffusion*. Advection refers to the transport of dissolved chemical species with the bulk motion of water:

$$J_{adv} = qC \tag{4.1}$$

where J_{adv} [$ML^{-2}T^{-1}$] is the mass of solute flowing across a unit cross-sectional area of medium per unit time, q [LT^{-1}] is specific flux, and C [ML^{-3}] is the concentration of solute in solution. Due to the macroscopic and microscopic heterogeneities in porous media,

which lead to a range of pore sizes and potential path shapes and sizes, the bulk flow of water is effectively an average quantity. Therefore, some percentage of solute will flow faster than this bulk flow and some percentage will flow slower. This mechanical mixing results in the dispersion of a solute front often observed in field situations. Along with mechanical mixing, molecular diffusion also tends to cause the dispersion of a solute front. Diffusion is a net flux of solute from high to low concentrations due to Brownian motion along a concentration gradient (Gillham & Cherry, 1982). According to Fick's Law,

$$J_w = - D_0 \nabla C \tag{4.2}$$

where J_w [$ML^{-2}T^{-1}$] is a mass flux of solute per unit area in pure water, D_0 [L^2T^{-1}] is a diffusion coefficient, and ∇C [ML^{-4}] is a concentration gradient. In porous media, this flux (J_{diff}) will also be dependant on the limited cross-sectional area of flow due to the presence of solid grains (porosity, n), the relative saturation of pores (saturation, S), and the non-linearity or tortuosity of the flow path (tortuosity factor, τ):

$$J_{diff} = - D_0 (n S \tau^A) \nabla C \tag{4.3}$$

It has been observed that under unsaturated conditions, the exponent A is greater than one, which reflects the increased tortuosity due to desaturation (Porter and others, 1960; Barraclough & Tinker, 1981). The magnitude of A has been found to be dependant on moisture content. While not being a diffusion process, dispersion due to mechanical mixing has been described as one:

$$J_m = - D_m \nabla C \tag{4.4}$$

where J_m [$ML^{-2}T^{-1}$] is the mass flux due to mechanical dispersion, D_m [L^2T^{-1}] is the mechanical dispersion coefficient. Since the form of equations (4.3) and (4.4) is the same, the two have often been combined into a single equation:

$$J_{hd} = - D_{hd} \nabla C \qquad (4.5)$$

where J_{hd} is the mass flux due to *hydrodynamic dispersion*, and $D_{hd} = D_{diff} + D_m$.

Transport in the aqueous phase is impeded by *adsorption* of species onto solid matter. Adsorption is a complicated process which has often been over-simplified for the purpose of solute transport modelling. Cation exchange is the primary mechanism for adsorption in porous media. It is driven by a charge imbalance on the surfaces of minerals; layer-type aluminosillicates exhibit negative surface charge due to ionic substitutions (Sposito, 1984) and are most significant in the sorption process, although species may be adsorbed onto other minerals as well. The charge on any mineral surface is dependant on pH and the process of adsorption is kinetically limited. Laboratory measurements of adsorption in batch systems have resulted in the derivation of equilibrium partitioning coefficients, usually denoted by K_d, which is the ratio of the mass concentration of species "residing" on the solid to the mass concentration of the same species in solution. The process of adsorption is not treated in great detail in this study.

Solute transport is affected by chemical reactions between dissolved and precipitated species and within the solution. The understanding of precipitation and dissolution of salts in the near-surface soil system is required for the estimation of water fluxes based on chemical changes. The likely chemical behavior of species present in the soil system of plots 8EP and 9BE is discussed in the following section.

4.2 SPECIES MOBILITY AND REACTIVITY

4.2.1 Major Ions

Soil water in both plots is dominated by the presence of sodium, calcium, magnesium, sulfate, and chloride. Potassium and bicarbonate are present in substantially lower concentrations. In general, $Na^+ > Ca^{2+} \geq Mg^{2+} > K^+$, and $SO_4^{2-} \geq Cl^- > HCO_3^-$. Mobility of these ions is limited to a certain extent by their solubilities. Table 4.1 presents information about equilibrium solubility products and solubilities of minerals which have either been found or are likely to precipitate at Kesterson Reservoir.

Table 4.1. Solubility Product Constants and Solubilities of Minerals Present or Likely to be Present at Kesterson Reservoir.

Mineral Name	Mineral Formula	pK at 25°C	Solubility at 25°C pH 7 (mg/L)
Calcite	$CaCO_3$	8.41	100†
Epsomite	$MgSO_4 \cdot 7H_2O$	1.88	267,000
Gypsum	$CaSO_4 \cdot 2H_20$	4.58	2100
Halite	NaCl	-1.57	360,000
Magnesite	$MgCO_3$	7.83	10*
Mirabillite	$Na_2SO_4 \cdot 10H_2O$	1.23	280,000
Sylvite	KCl	-0.90	210,000

pK data from Lindsay, 1979; solubility data from Seidell, 1958, except as noted by *.

† Partial pressure of $CO_2 = 10^{-3}$ bar.

* Magnesite solubility calculated from pK value.

As is apparent from this table, the solubilities of calcium, sulfate, and magnesium are strongly limited by their low solubilities relative to gypsum, calcite, and magnesite. In most near-surface soils at Kesterson Reservoir, concentrations of these ions exceed the listed solubility values; calcite and gypsum have been found to be present throughout most profiles investigated (Flexser, 1988; Tokunaga, personal communication, 1988). On the other hand, the very high solubilities of sulfate minerals and halite, allow for equally high concentrations of sodium and chloride; under most field conditions, the concentrations of these two species do not exceed their solubilities, except at the soil surface, or within millimeters of the surface, where water evaporation is taking place. It is important to note that solubilities of minerals are dependant on the ionic strength and temperature of the solution. In general, the solubilities of the above minerals will increase with ionic strength, although their relative mobilities will not change significantly. Of the two most soluble species, sodium mobility is potentially further limited by its sorption through cation exchange. Chloride mobility may be altered in the other direction, i.e. increased through *negative adsorption*, or anion exclusion, when, due to the negative charge on the surface of clay particles, it is repelled away from the solid surface, with the resultant apparent increase in concentration in the bulk solution (Sposito, 1982). This may lead to an overestimate of water flow; since this effect is very minor in solutions with a chloride concentration of approximately 1000 mg/L or more (Van De Pol and others, 1977), anion exclusion is most likely not significant in view of the substantially higher chloride concentrations in the field. Due to its high solubility and mobility, chloride has been used routinely as a tracer for fluid flow (e.g. MacFarlane and others, 1983). Although all major ions were analyzed for as part of this study, only chloride was used to quantitatively analyze water flow.

4.2.2. Selenium

Part of the rationale for measuring and estimating evaporation rates is to be able to understand selenium fluxes near the soil surface. The difficulty of making estimates based on changes in selenium concentration is in part a result of the complex, reduction/oxidation-controlled chemistry of selenium. The many transformations which selenium undergoes in the soil system lead to a greatly decreased mobility; furthermore, the fact that selenium speciation is strongly kinetically controlled makes the quantitative analysis of selenium concentration changes so much more difficult.

The redox speciation of Se is shown in the Eh-pH diagram of Fig. 4.1. The solubility and mobility of selenium in a soil system depend on the redox state of the element. In general, the oxidized forms of selenium are more mobile than the reduced forms. In an aqueous environment, the tetravalent selenite ion, SeO_3^{2-}, the hexavalent selenate ion, SeO_4^{2-}, and elemental selenium, Se^0, are the most common selenium species. Elemental selenium is highly insoluble in water and its dissolution kinetics are extremely slow (McNeal & Balistrieri, 1989). It is usually found in soils as a result of selenide (Se^{2-}) oxidation or chemical and/or biological reduction from selenite. Selenite is usually found in mildly oxidizing environments; its salts are moderately soluble, but its mobility is most hindered by its strong affinity for sorption onto iron oxides (Balistrieri & Chao, 1987) and clay particles (Bar-Yosef & Meek, 1987). Selenate is found in oxidizing environments; its salts are highly soluble and it adsorbs only weakly. In general, the solubility of selenium salts will be comparable to the equivalent sulfate salts (e.g. Na_2SeO_4 (Na_2SO_4) - high solubility; $CaSeO_4$ ($CaSO_4$) - low solubility). Water which was brought into Kesterson Reservoir contained mostly selenate and some selenite (Weres and others, 1985). As water percolated through pond bottoms, much of the selenate and selenite became reduced to

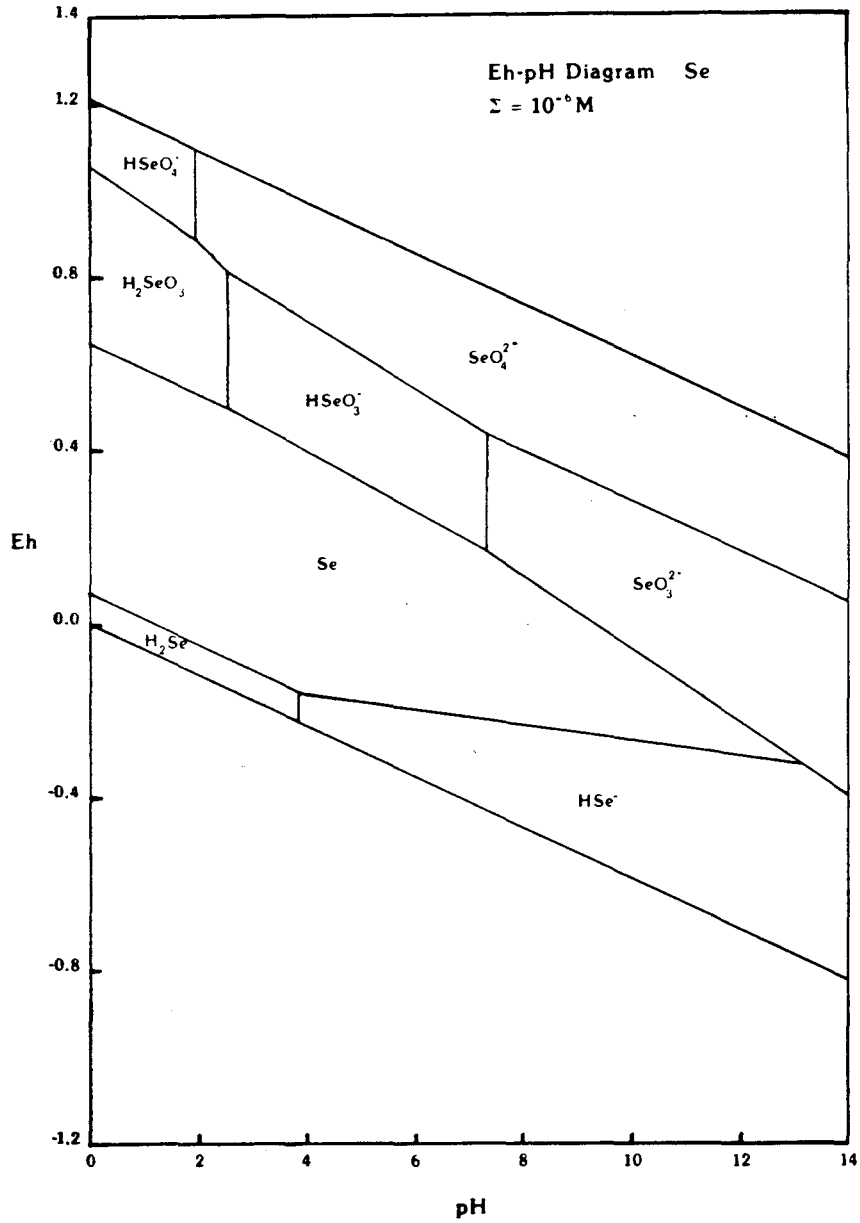

Figure 4.1 Eh-pH diagram for the Se-H_2O system (from McNeal & Balistrieri, 1989).

elemental selenium, which currently comprises a large percentage of the total selenium inventory in Kesterson soils. Besides changing redox states, selenium has been found to be volatile; losses of selenium through volatilization have been observed at Kesterson Reservoir, but have not yet been adequately quantified (Frankenberger & Karlson, 1988). In addition, a yet undetermined fraction of the selenium inventory exists in organic forms, the solubility of which is not known. In the top 9 cm of soil at the two plots of interest, water soluble selenium comprises between 4% and 20% of the total selenium (see Section 4.4.2). In consideration of these factors and the spatial variability of selenium near the soil surface, apparent changes in selenium concentrations cannot be used to estimate near-surface water fluxes.

4.3 FIELD AND LABORATORY METHODS FOR SAMPLE COLLECTION, PREPARATION, AND ANALYSIS

4.3.1 Procedures for sample collection

Four types of samples were collected as part of this study: (1) surface (9 cm) soil cores, (2) soil profiles, (3) soil water, and (4) groundwater. The first type of samples was collected using the same technique as described in Section 3.3; in fact, the same soil cores which were used to measure bare soil evaporation rates were used as soil samples. Through the use of the same set of coring devices in each sampling period, a uniformity of sample size was maintained. Soil variability is known to interfere with comparisons of temporal changes in soil salinity (Rhoades, 1978, 1984). Therefore, all samples were collected from small areas within each plot; this reduced the spatial variability which obscures trends (see Fig. 4.2 for plot diagrams). After the microlysimeters were weighed for the second time, the top of each cylinder was covered with 2.7 mil-thick plastic and

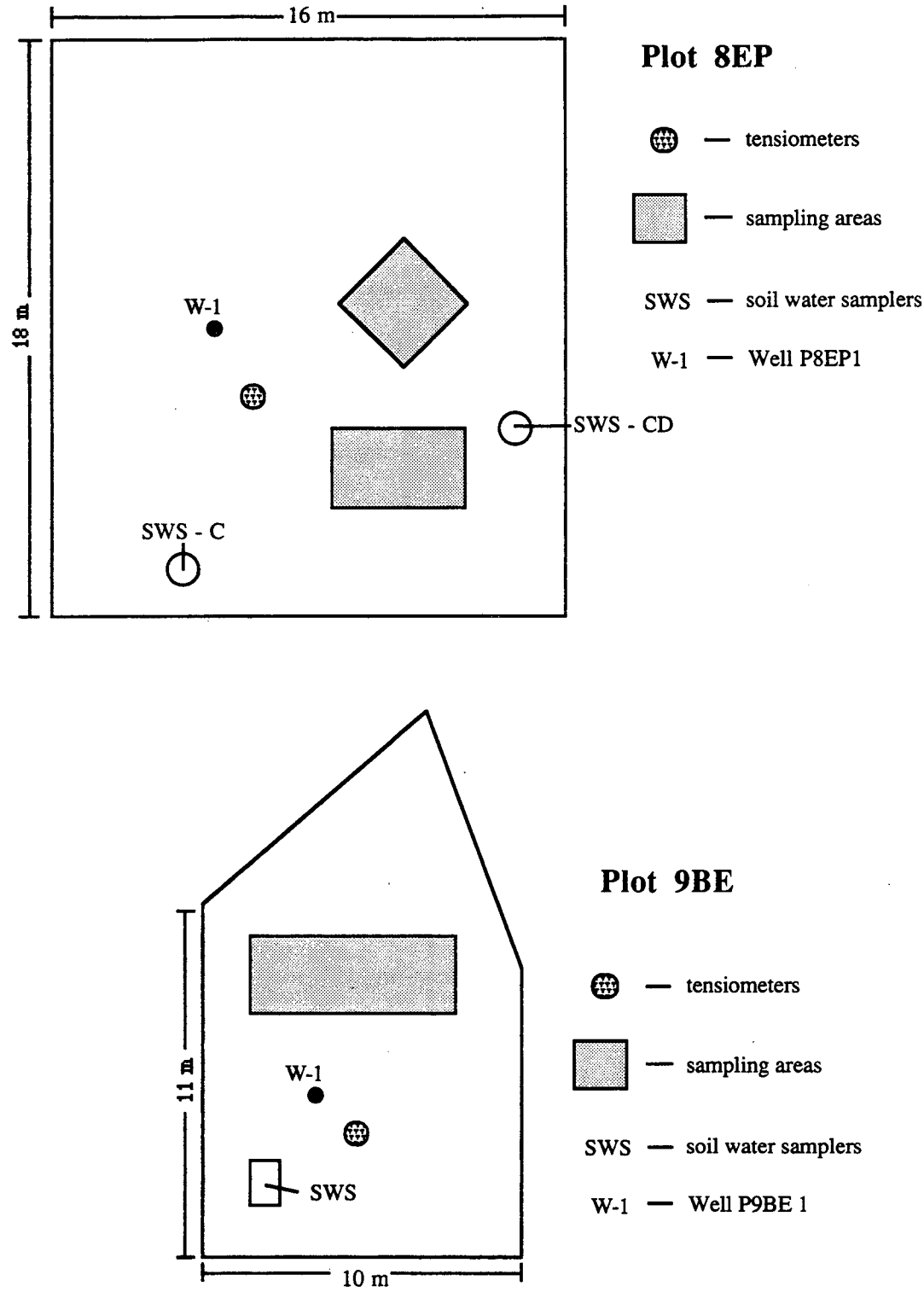

Figure 4.2 Approximate layouts of plots 8EP and 9BE.

secured with PVC tape to avoid spillage of soil and loss of moisture. The cores were then transported in a vertical position back to the laboratory.

Soil profile samples were collected using a manually operated auger. An auger head with a diameter of 5 cm (2 in) was used to core down to the desired depth. The sample interval depended on depth: near the soil surface, 5 cm depth intervals were sampled; deeper than 30 cm, 10 cm intervals were sampled. The top 10 cm of a profile was sampled using a PVC tube, which was sealed in the field and cut up in the laboratory into the following intervals: 0.0 to 0.5 cm, 0.5 to 2.5 cm, 2.5 to 5.0 cm, 5.0 to 7.5 cm, and 7.5 to 10.0 cm. For each interval below 10 cm, soil was removed from the auger head; the outside of the augered core was removed and only the uncontaminated center portion of each core was sampled. If the soil was unconsolidated, the entire contents of each auger head were collected. The auger head was cleaned between intervals. Soil samples were placed into heavy duty, resealable plastic freezer bags (2.7 mils wall thickness) and transported to the laboratory.

Soil water was collected through ceramic cup soil water samplers. Several sets of samplers in plot 8EP had been installed in December 1987 by T. Tokunaga, with cups at the following depths: 0.15 cm, 0.30 cm, 0.46 cm, and, 0.61 cm. Samplers in plot 9BE were installed in late September, 1988 at the following depths: 0.15 cm, 0.30 cm, 0.45 cm, 0.60 cm, 0.90 cm, 1.20 cm. Each sampler consists of a 5.1 cm (2 in) diameter PVC tube, a 5 cm long porous ceramic cup at the bottom end, a rubber stopper at the top end, and a rubber tube passing through a hole in the stopper. A sampler is installed with the center of the ceramic cup at the desired sampling depth. In plot 9BE, holes were drilled using a hand auger, the samplers were placed into them, and the holes were then backfilled using native soil from the appropriate depth intervals. In order to collect a soil water sample, the top of the tube was sealed with the rubber stopper, and a vacuum was applied through the rubber

tubing which was subsequently tightly clamped. The vacuum applied has to be high enough to create a potential inside the tube lower than that in the soil surrounding the cup. When this condition is fulfilled, water will enter the tube through the ceramic cup. Depending on the vacuum applied and the moisture content of the soil, hours to days are required to collect a sample large enough for analysis. In general, any sample greater than 10 ml was collected, although such as small sample may not be representative of the surrounding soil water. Water was removed from the sampler using a syringe and Tygon tubing. At each sampling, the entire contents of the sampler were removed. Samples were collected in 60 ml or 120 ml plastic bottles with plastic screw-caps. The rubber stopper was then placed back into the tube and the tubing was clamped to prevent evaporation and insect intrusion.

Groundwater was sampled from three wells: P8EPW-1, in plot 8EP; KR103, approximately 100 m west of plot 8EP, and P9BEW-1, in plot 9BE. Well KR103 was installed by the Bureau of Reclamation; its depth is 305 cm and it is screened over the bottom 140 cm. The other two wells were installed in July of 1988. P8EPW-1 was hand augered down to a depth of 240 cm and a 5.1 cm (2 in) diameter PVC casing, screened over the bottom 61 cm (2 ft) was installed. P9BEW-1 was hand-augered to a depth of 220 cm and a similar casing was installed. Both wells were backfilled with bentonite clay. The depth of the water table in each well was periodically measured, the volume of water in the well casing was estimated, and then three times that volume of water was removed before sampling approximately 120 ml of water. A hand vacuum pump was used to lift water to the surface.

4.3.2 Methods for Sample Preparation

Once in the laboratory, the cores containing the surface soil samples were weighed and measured. The soil was then carefully extracted from the tube and homogenized, i.e. chopped up and thoroughly mixed. Homogenization was carried out in a metal bowl; soil was chopped until it passed a 4.75 mm-mesh sieve. In order to prevent significant drying of the sample, this procedure was performed as rapidly as possible. After the soil was homogenized, a subsample of known mass (usually between 10 and 50 g) was placed into an open stainless steel container and put into a 105°C oven. The subsample was allowed to dry for approximately 24 hours. The remainder of the sample was placed into a plastic bag and stored in a humidified chamber. After subsequent weighing, the gravimetric moisture content of the soil (mass of water per mass of solid) was calculated. Another subsample of known mass (on the order of 10 to 20 g) was then used to prepare a 10:1 water to soil extract. If one is interested in determining the actual concentrations of solutes in pore water, lower ratio extracts are more commonly used (Rhoades, 1984) (from saturation paste extracts to 5:1 extracts); higher ratios, however, are more suitable for monitoring relative changes in solute concentrations rather than absolute concentrations in soil water (Carpena and others, 1968; Rhoades, 1984). 10:1 extracts will also come closer to dissolving most salts in a soil; if a salt is always saturated in a soil, the actual composition of pore water will not change over time. However, the total mass of salts in the soil will increase. It is this mass which was of interest in this study. The subsample was placed into a clean and dry, 250 ml, glass beaker and an appropriate mass of water was added. A magnetic stirring bar was placed in the beaker and the top of the beaker was covered tightly with aluminum foil to prevent spillage of water and soil during the stirring process. The beaker, with the soil, water, and stirring bar, were placed onto a magnetic stirrer. The stirring speed was adjusted high enough so as to keep the soil suspended and moving at all times, and yet not so high as to cause the soil/water suspension to hit the aluminum foil

covering the beaker. The stirring process went on for 2 hours. Subsequently, the suspension was poured into a 250 ml plastic bottle which was then sealed with a screw-cap. This suspension was centrifuged at between 3000 and 6000 revolutions per minute for 5 to 20 minutes, depending on the texture of the soil. The supernatant liquid was then poured off and filtered through a 0.45 μm filter in preparation for chemical analysis. The final liquid was placed in 60 ml or 120 ml plastic bottles with screw-caps. The remainder of each soil sample was stored in a plastic bag in a humidified chamber.

The samples from soil profiles were treated in a similar manner, except that their volume was not measured; otherwise, the extract procedure was identical.

Soil water and groundwater samples were filtered through a 0.45 μm filter. When the concentrations of major ions or selenium were expected to be high, or when there was only a small volume of sample available, the sample was diluted 2 to 5 times. The electrical conductivity (EC) of each water sample was measured before other analyses were performed.

4.3.3 Analytical Procedures

Three analytical methods were used for the analysis of water samples. Sodium, calcium, magnesium, sulfate, and boron were analyzed for using an Inductively Coupled Plasma Spectrophotometer (ICP) produced by Applied Research Laboratories. The ICP method of analysis is most useful in the parts-per-million range and is well suited for the above species; however, boron concentrations were usually 10 ppm or less and the quality of boron analyses is at this point questionable. For this reason, the results of these analyses will not be presented.

Potassium and selenium were analyzed for using atomic absorption spectroscopy (AAS) coupled with a hydride generator. Potassium and selenite were determined directly. AAS cannot be used to determine selenate directly; therefore, the water sample is reduced using a combination of 5 ml of the sample, 5 ml of 12N HCl, and 0.2 ml of 2% ammonium persulfate. This solution is then heated in a boiling water bath for 10 minutes and subsequently analyzed for selenite using hydride generator AAS. This second analysis will give "total" selenium in the form of selenite. The difference between this "total" concentration and the original selenite concentration is equal to the selenate concentration. However, some organic selenium compounds, e.g. selenoaminoacids, will be oxidized and their concentration will be read as part of the "total" concentration. Therefore, even though standard selenite and selenate solutions analyzed using this method may give very good results, interference of organic selenium and organic matter in field samples may increase analysis error. The ICP and AAS analyses were performed by personnel in LBL's Earth Science Division Analytical Chemistry laboratory.

Chloride was analyzed for using Mohr titration, as described by Flaschka and others (1969). A known quantity of sample (1 to 10 ml) is titrated with silver nitrate at a concentration comparable to the expected concentration of the chloride ion. Chromate ion is used as an indicator. The solubility of silver chromate is considerably greater than that of silver chloride. When all the chloride precipitates as silver chloride, silver chromate forms and imparts a rusty red-brown color to the solution, which indicates the endpoint. There are no true "interferences" in this method, except for the simultaneous titration of other halides, most notably bromide, in the solution. However, since in the field setting, bromide is not expected to be present in concentrations within an order of magnitude of chloride concentrations, this effect is ignored. In general, for analyses of extracts from soils deeper in the profile than 10 cm, it was possible to accurately calculate chloride concentrations based on a charge balance of concentrations of the other ions. However, for

extracts from near surface soils, the error propagated from the other analyses made this calculation highly inaccurate.

4.4 CHANGES IN SPECIES CONCENTRATIONS IN THE UPPER 9 CM OF THE SOIL PROFILE

Before changes in near surface concentrations may be discussed, the recent history of plots 8EP and 9BE must be taken into account, along with the distribution of species in the vadose zone of those two plots. With a few exceptions, results of chemical analyses of soil extracts were normalized to the mass of soil, not to the original mass or volume of pore water because during the extraction process previously precipitated salts are dissolved; therefore, the normalization to water volume would give unrealistically high concentrations of most species, especially those species which have limited solubility, such as calcium and sulfate. While normalizing to solid mass will also give meaningless results for low solubility species, as they will not be completely dissolved out during the extraction process, the resultant concentration is independent of moisture content which changes with time.

4.4.1 Distribution of Species in the Vadose Zone

Both plots are located in ponds which were periodically flooded with agricultural drainage water; the height of water column which infiltrated into either profile is very difficult to estimate, although the amounts were certainly different for either of the two plots. In fact, plot 9BE was flooded during the winter of 1987/88 through May of 1988, while plot 8EP was only periodically flooded during the winter of 1986/87, both mostly due to Pond 7 overflow. The vadose zone of plot 9BE is texturally much coarser than that

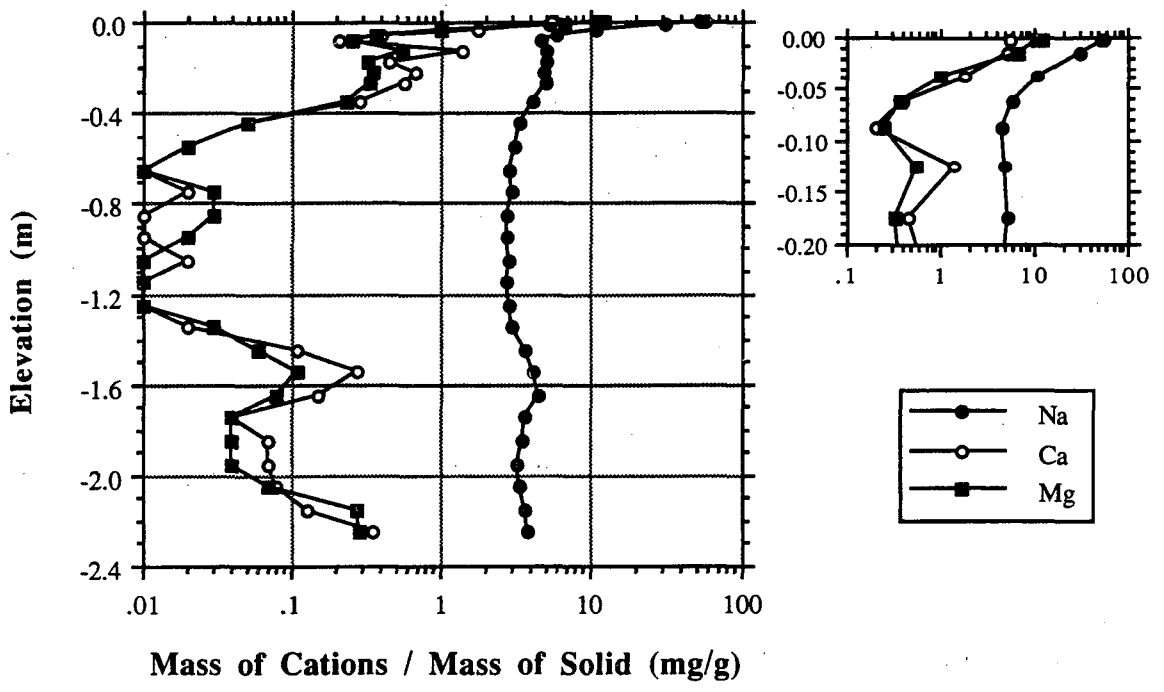

Figure 4.3a Distribution of sodium, calcium, and magnesium in vadose zone of plot 8EP, 7/21/88. Close-up view shown in inset graph.

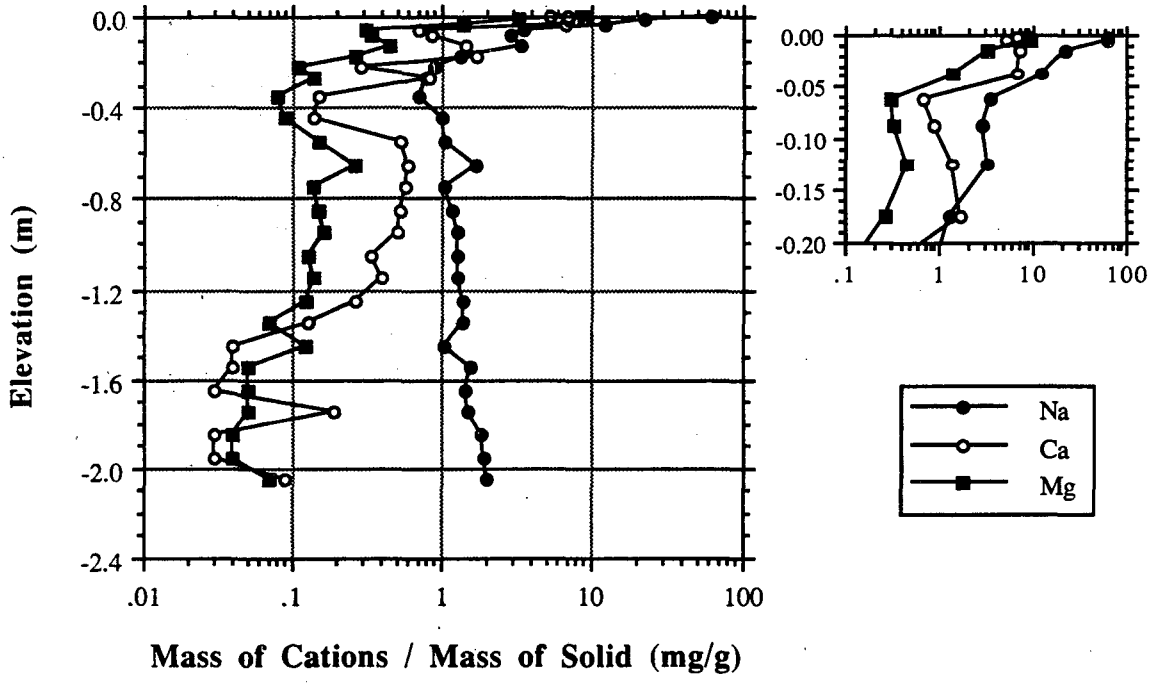

Figure 4.3b Distribution of sodium, calcium, and magnesium in vadose zone of plot 9BE, 7/25/88. Close-up view shown in inset graph.

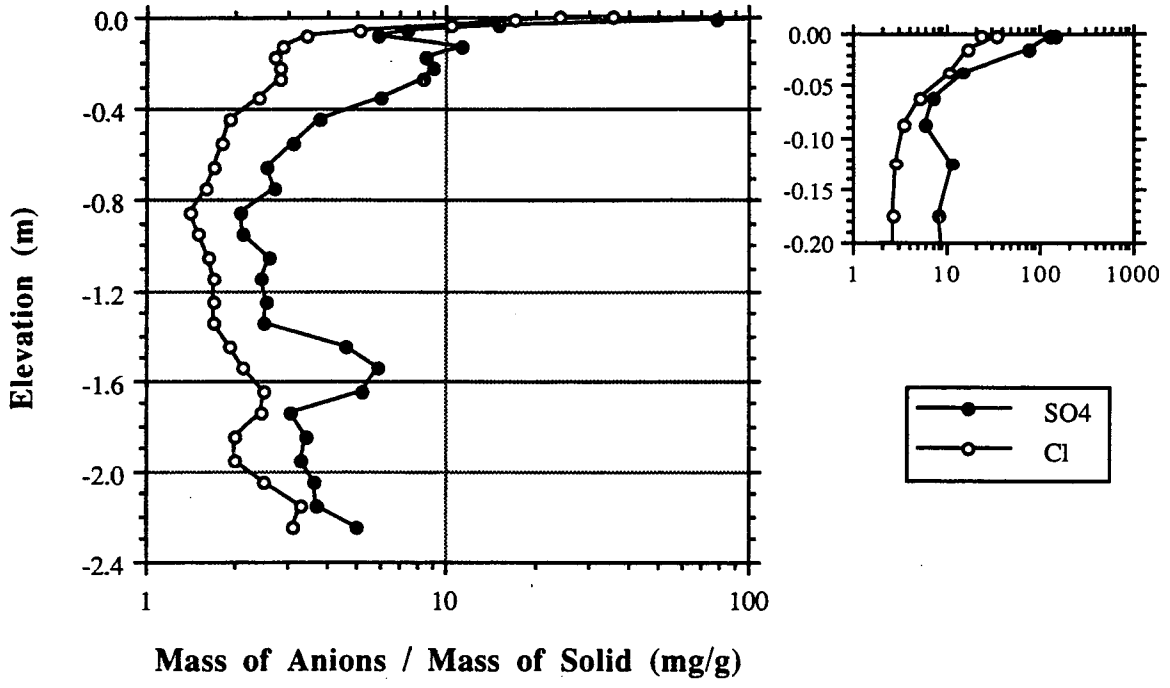

Figure 4.4a Distribution of sulfate and chloride in vadose zone of plot 8EP, 7/21/88. Close-up view shown in inset graph.

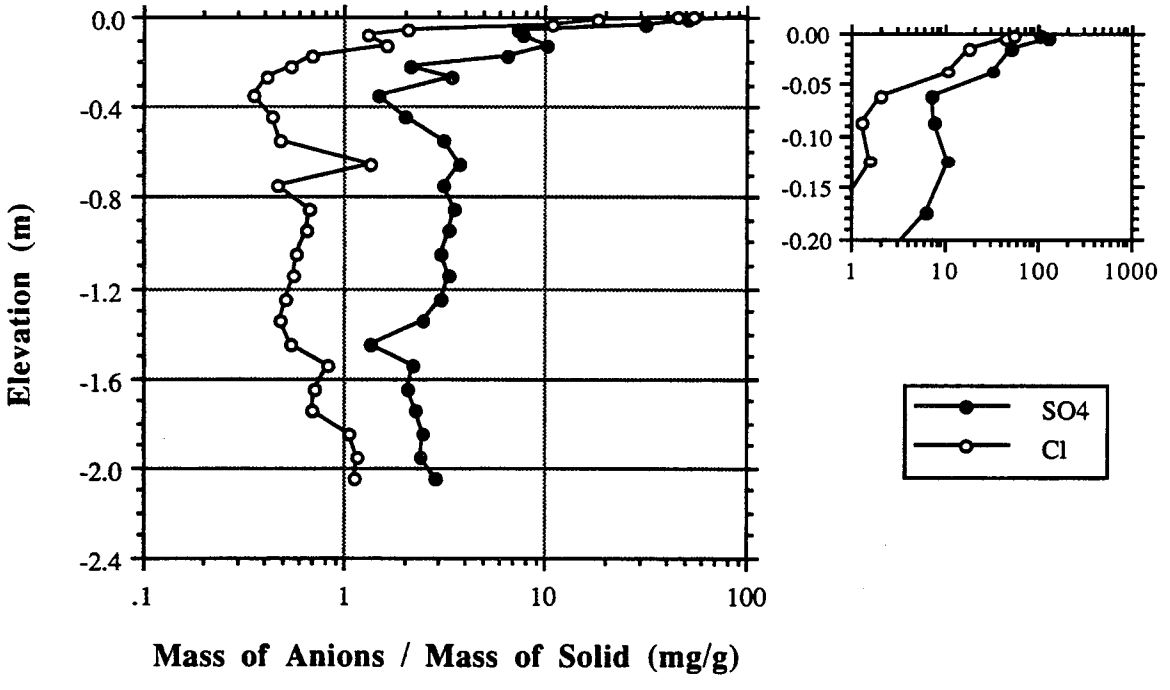

Figure 4.4b Distribution of sulfate and chloride in vadose zone of plot 9BE, 7/25/88. Close-up view shown in inset graph.

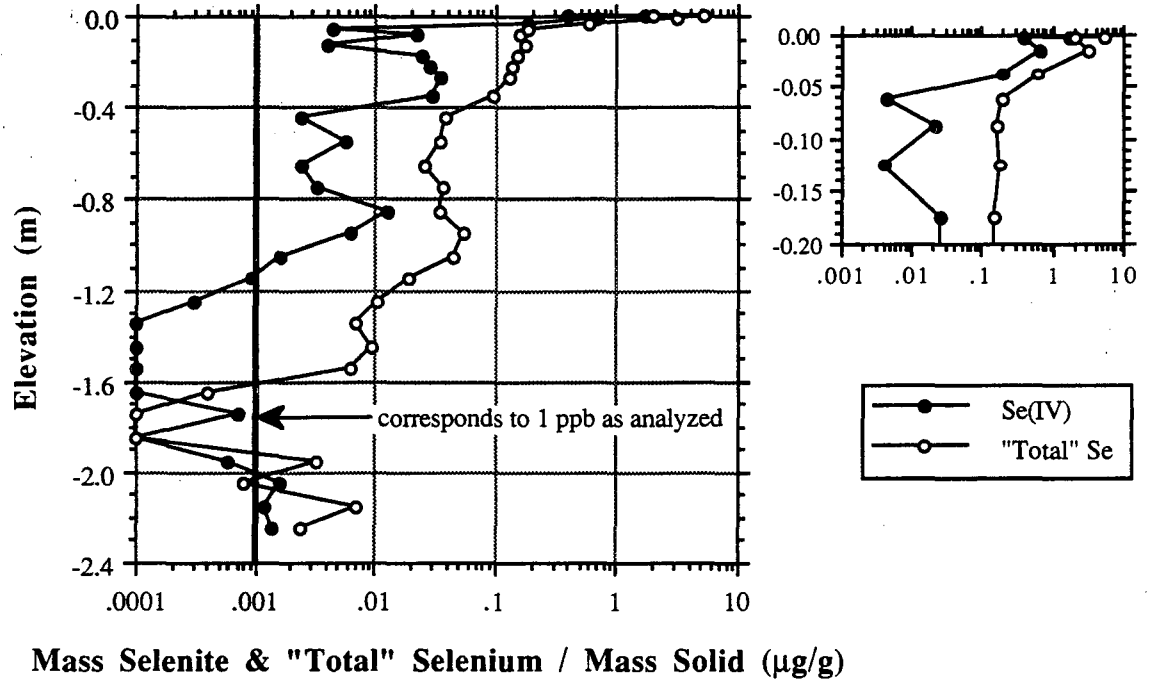

Figure 4.5a Distribution of selenite and "total" selenium in vadose zone of plot 8EP, 7/21/88. Close-up view shown in inset graph.

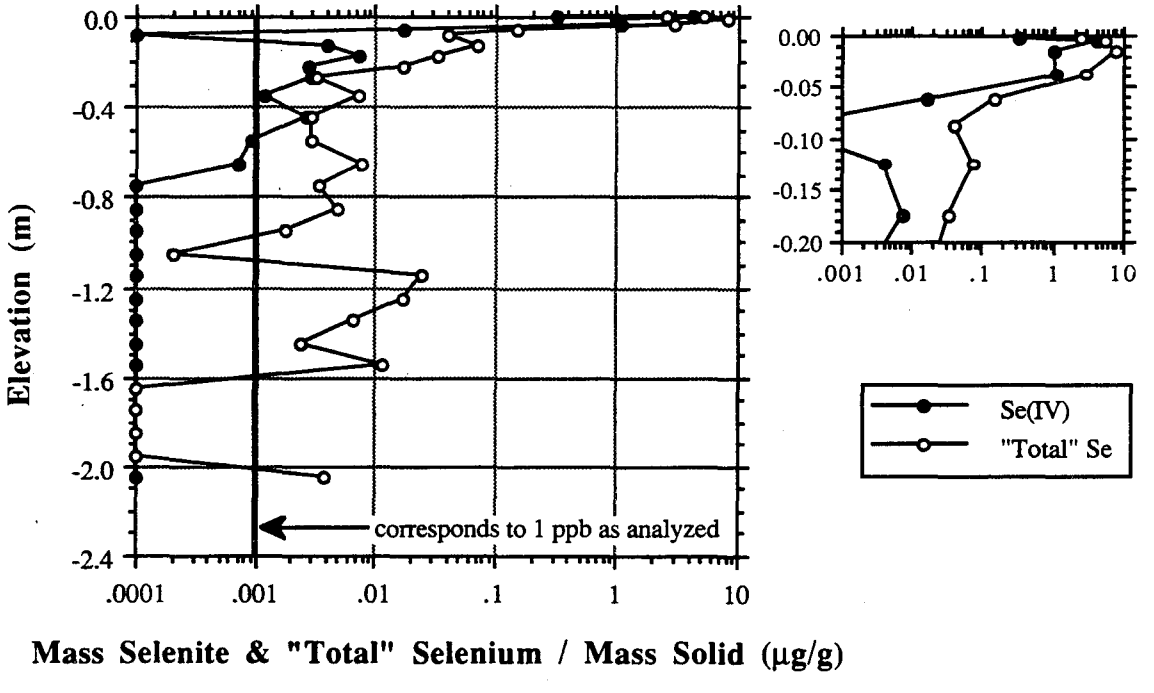

Figure 4.5b Distribution of selenite and "total" selenium in vadose zone of plot 9BE, 7/25/88. Close-up view shown in inset.

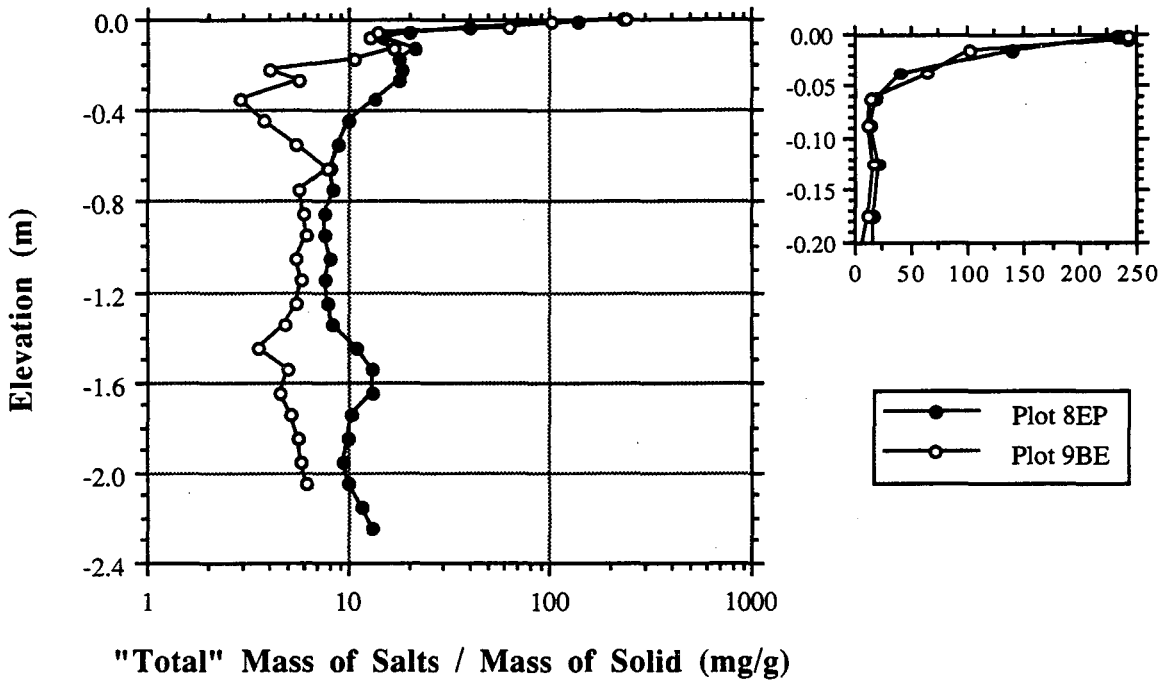

Figure 4.6a Distribution of "total" salts in vadose zone of plot 8EP (7/21/88) and 9BE (7/25/88). Close-up view shown in inset graph.

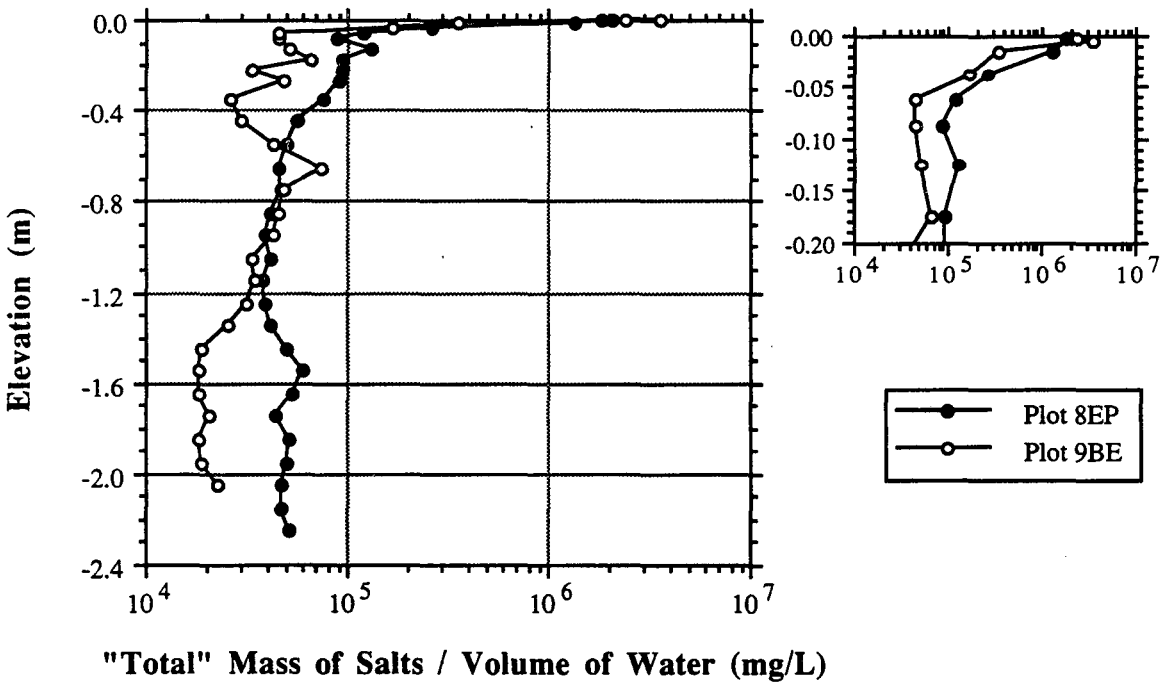

Figure 4.6b Distribution of "total" mass of salts in vadose zone of plots 8EP (7/21/88) and 9BE (7/25/88). Concentrations normalized to field water content.

of 8EP (see Fig. 2.3). This would suggest that when flooded, water would move vertically at a higher velocity than at plot 8EP and would lead to a more rapid flushing out of salts from the soil profile. This was indeed found to be the case (Figs. 4.3-4.6). Profile distributions of all species are found to be strongly skewed toward the surface, although the concentrations of all species, except Ca^{2+} and Mg^{2+}, are higher throughout the profile of plot 8EP than 9BE. Within a few centimeters of the surface, concentrations of all species are comparable in the two plots. As seen in Fig. 4.6b, the near surface concentrations, when normalized to field moisture content, are absurdly high (>10^6 ppm), suggesting that a high proportion of salts in this interval was precipitated in the field.

4.4.2 Qualitative Analysis of Time-Trend Data

Samples of the top 9 cm of soil were collected from both plots on a monthly basis. The relative changes in salt concentrations are indicative of near-surface water fluxes. Each point in Figures 4.7 - 4.17 represents the result of analysis of an extract from one 9 cm core of soil. The spread of data points on any given day reflects the spatial variability within each plot; as mentioned before, despite sampling within a relatively small area (4 to 5 m^2), the spatial variability was rather large, especially in plot 9BE (see following paragraphs). In general, changes in species concentrations are more difficult to discern from data from plot 9BE. Nevertheless, three cycles of drying, wetting, and drying, resulting in corresponding increases, decreases, and increases in salt concentrations are observed at both plots. In reality, there are only two periods: one of drying and salinization during the late spring, summer, and early fall, and another of wetting and desalinization during late fall, winter, and early spring months. In Figures 4.7 - 4.17 the summer and early fall months are represented by data from day 1 through approximately day 120; the wet period took place from approximately day 120 until day 240. Following day 240, increases in salt concentrations were due to evaporation during late spring and early

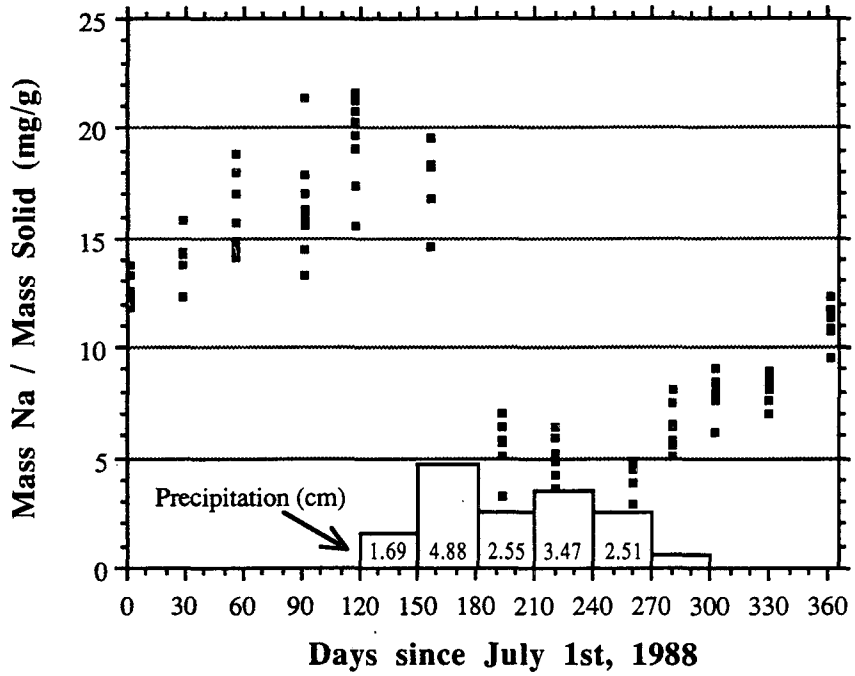

Figure 4.7a Changes in sodium concentration in the top 9 cm of soil in plot 8EP: July 1988 - June 1989. Precipitation in cm shown in boxes on time axis.

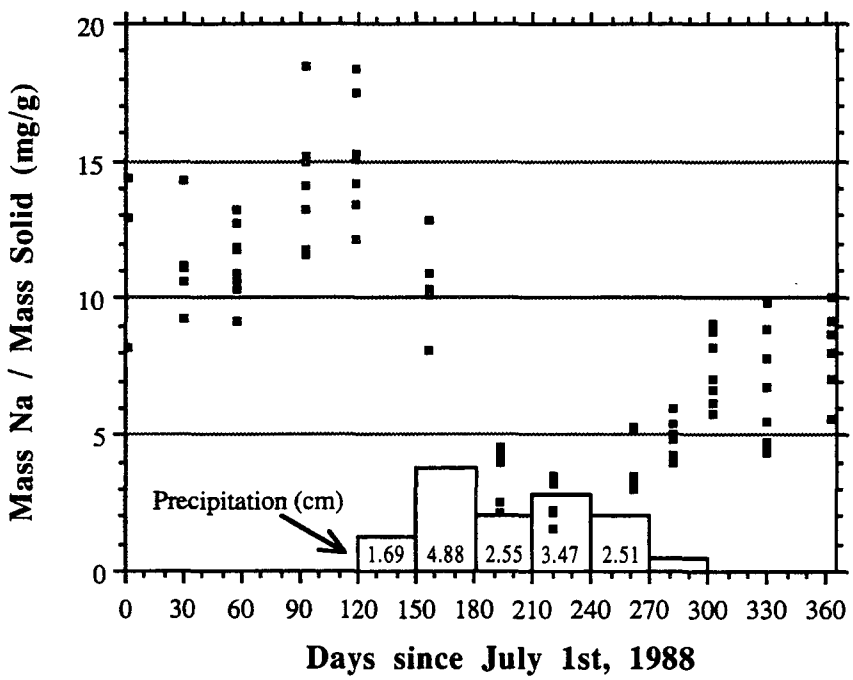

Figure 4.7b Changes in sodium concentration in the top 9 cm of soil in plot 9BE: July 1988 - June 1989. Precipitation in cm shown in boxes on time axis.

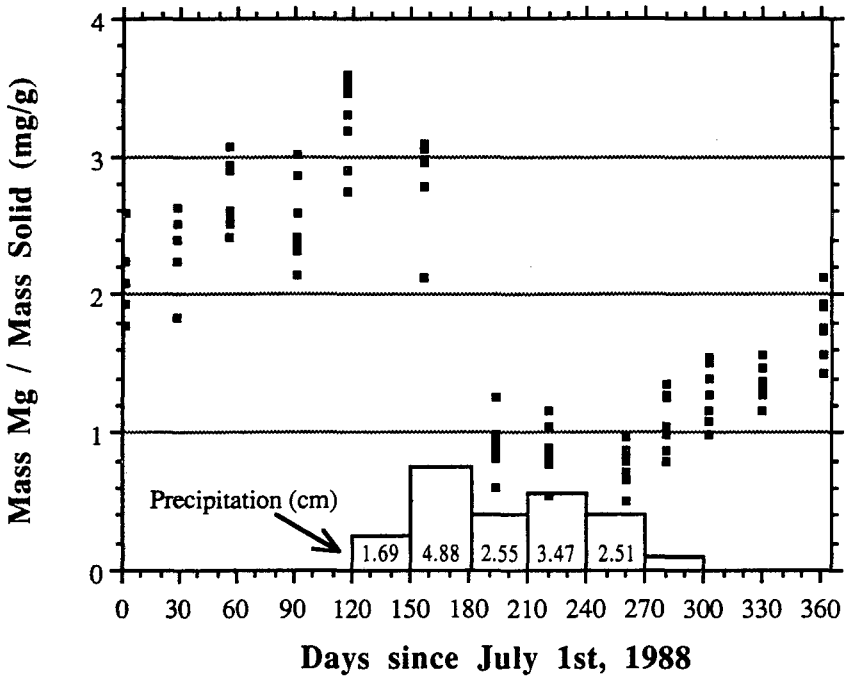

Figure 4.8a Changes in magnesium concentration in the top 9 cm of soil in plot 8EP: July 1988 - June 1989. Precipitation in cm shown in boxes on time axis.

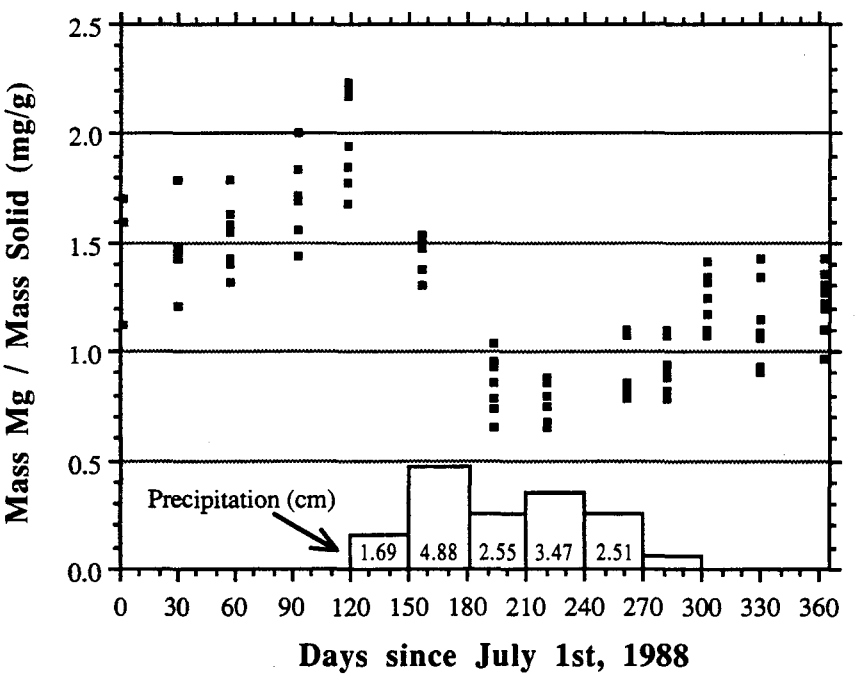

Figure 4.8b Changes in magnesium concentration in the top 9 cm of soil in plot 9BE: July 1988 - June 1989. Precipitation in cm shown in boxes on time axis.

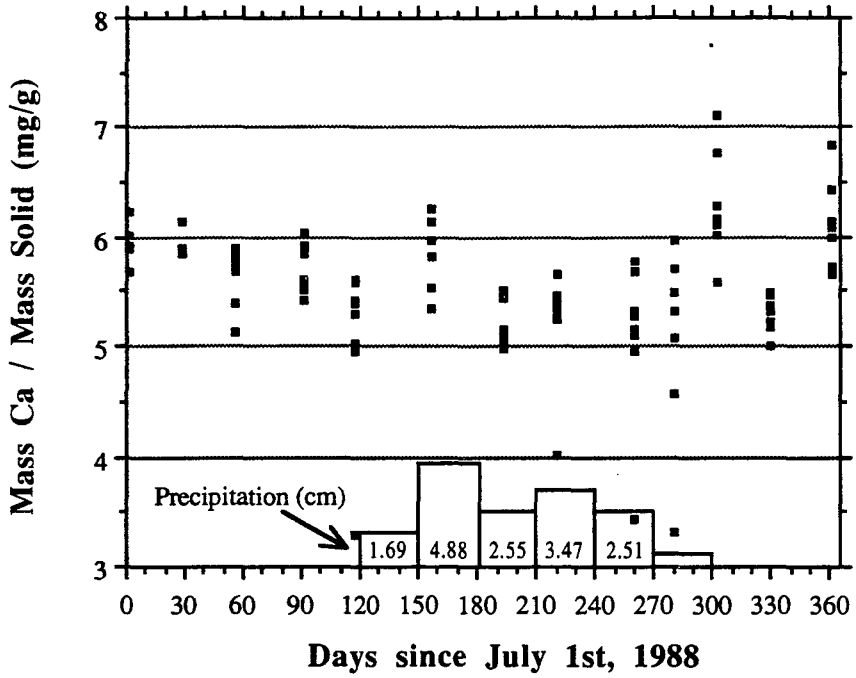

Figure 4.9a Changes in calcium concentration in the top 9 cm of soil in plot 8EP: July 1988 - June 1989. Precipitation in cm shown in boxes on time axis.

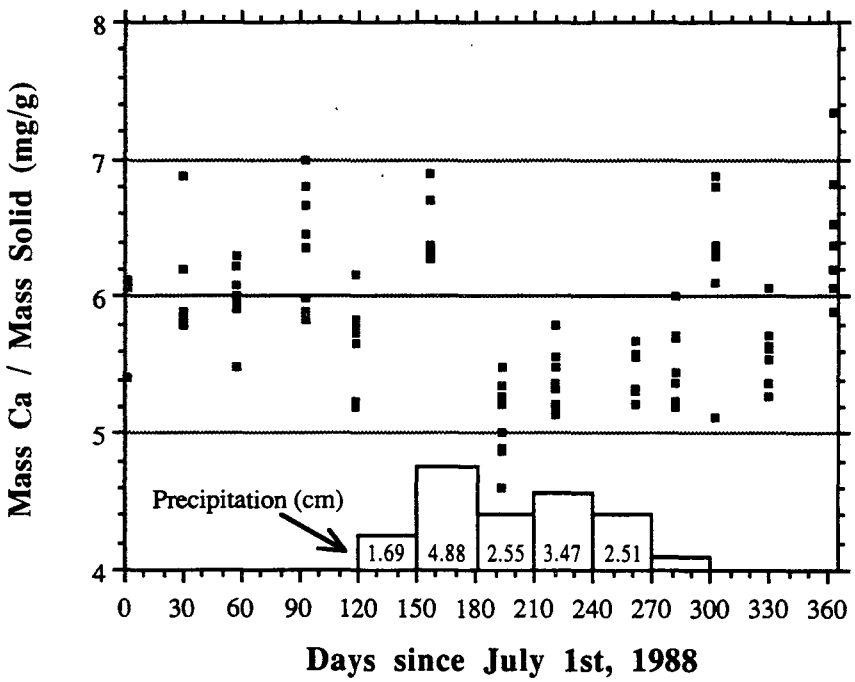

Figure 4.9b Changes in calcium concentration in the top 9 cm of soil in plot 9BE: July 1988 - June 1989. Precipitation in cm shown in boxes on time axis.

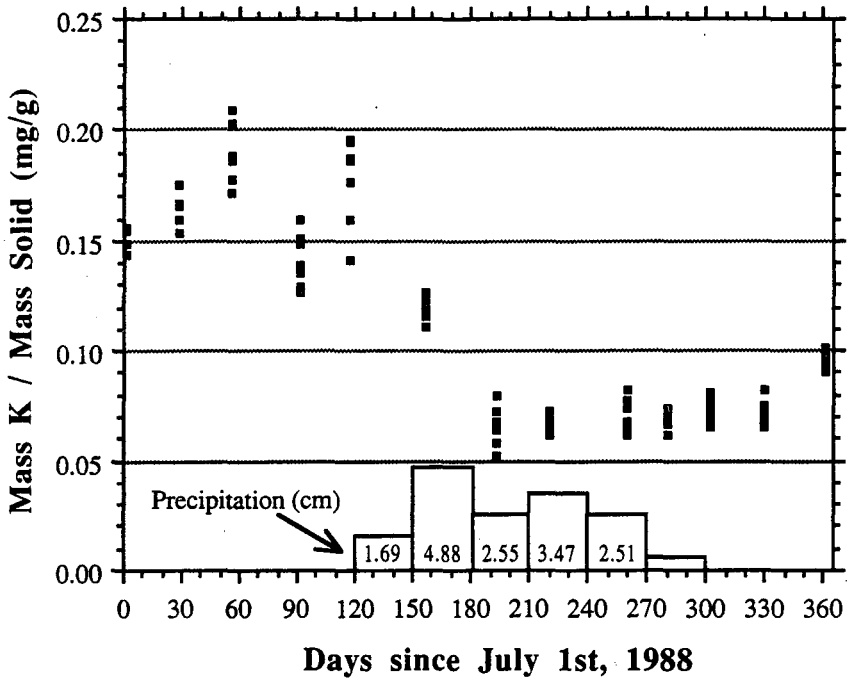

Figure 4.10a Changes in potassium concentration in the top 9 cm of soil in plot 8EP: July 1988 - June 1989. Precipitation in cm shown in boxes on time axis.

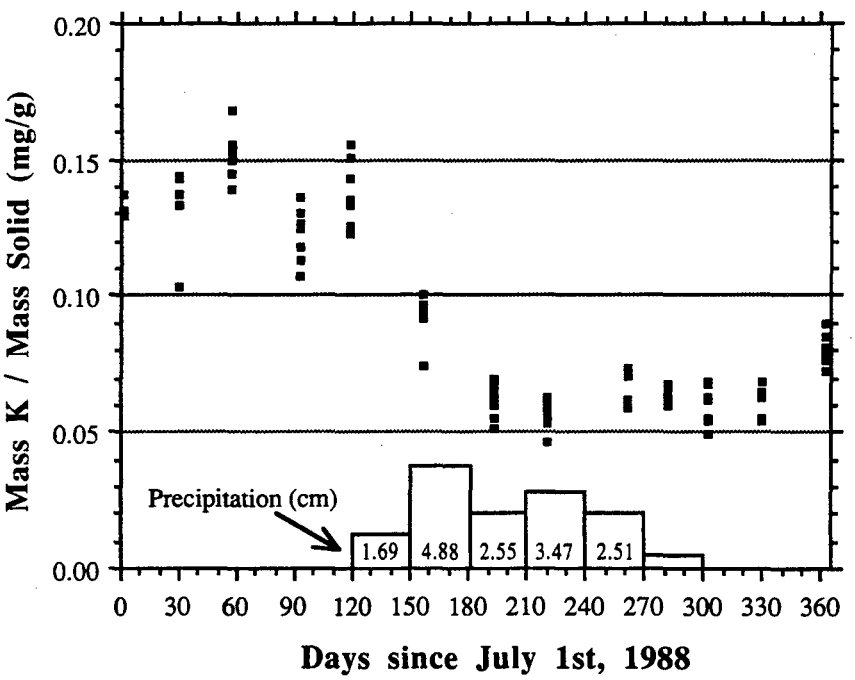

Figure 4.10b Changes in potassium concentration in the top 9 cm of soil in plot 9BE: July 1988 - June 1989. Precipitation in cm shown in boxes on time axis.

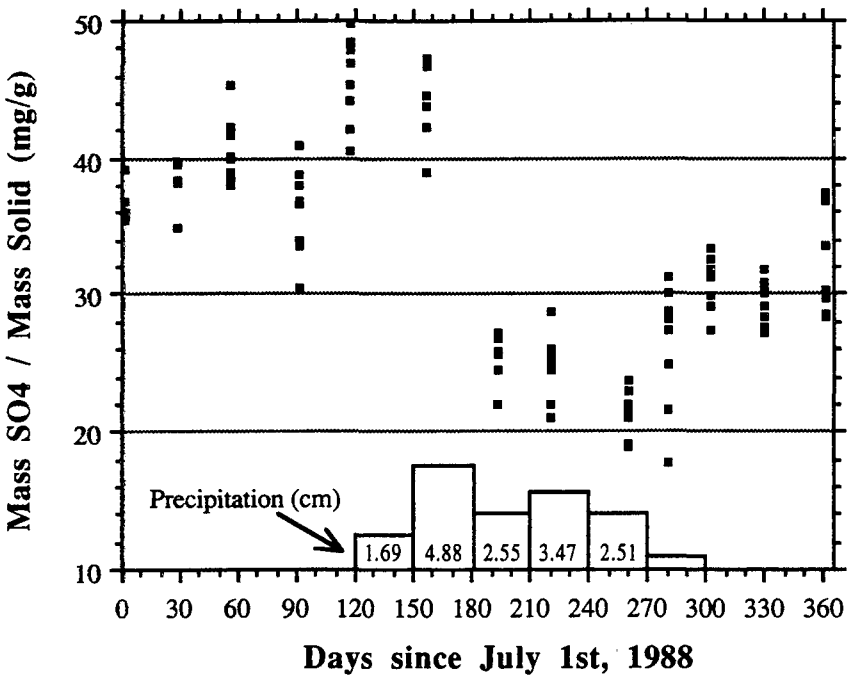

Figure 4.11a Changes in sulfate concentration in the top 9 cm of soil in plot 8EP: July 1988 - June 1989. Precipitation in cm shown in boxes on time axis.

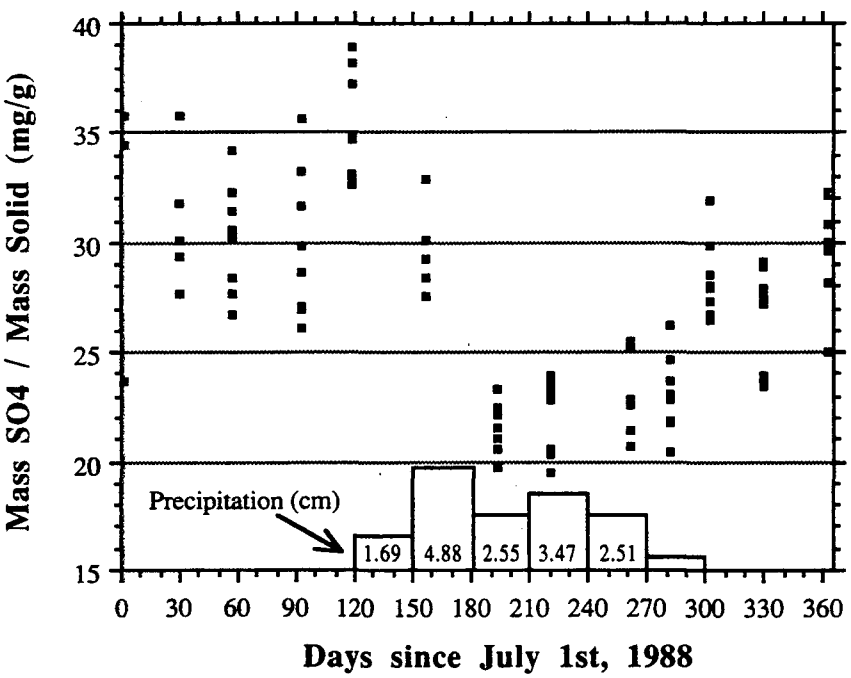

Figure 4.11b Changes in sulfate concentration in the top 9 cm of soil in plot 9BE: July 1988 - June 1989. Precipitation in cm shown in boxes on time axis.

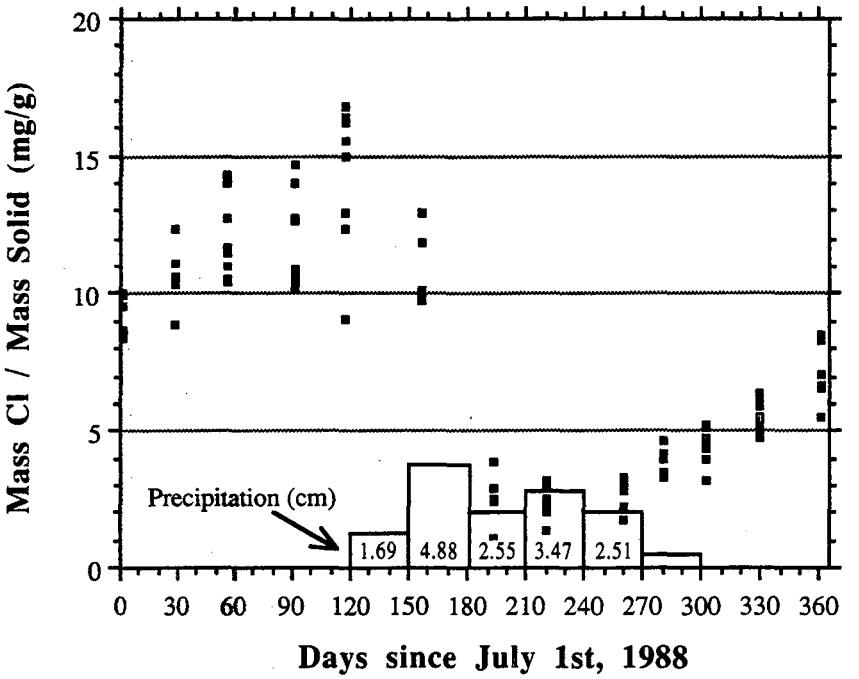

Figure 4.12a Changes in chloride concentration in the top 9 cm of soil in plot 8EP: July 1988 - June 1989. Precipitation in cm shown in boxes on time axis.

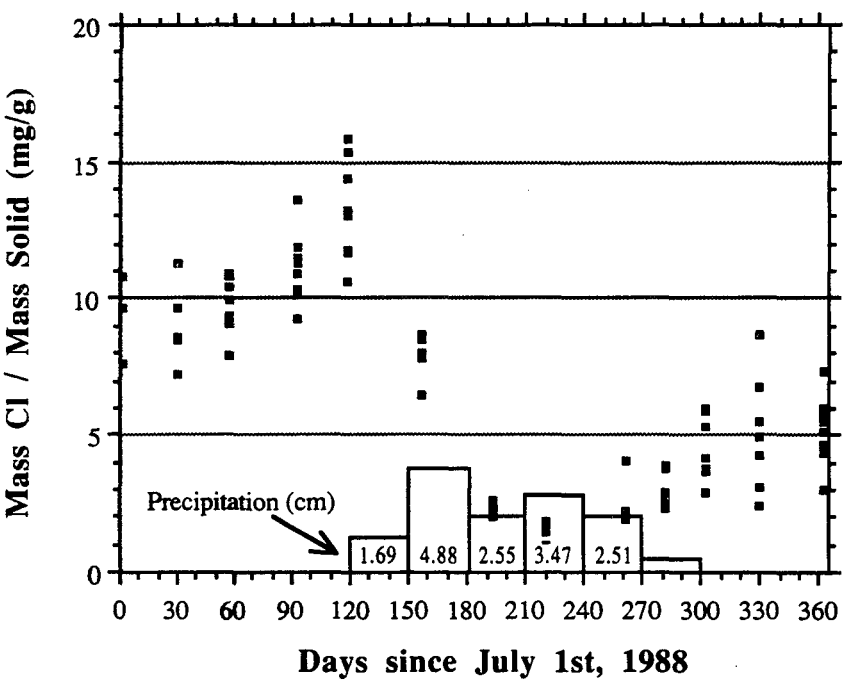

Figure 4.12b Changes in chloride concentration in the top 9 cm of soil in plot 9BE: July 1988 - June 1989. Precipitation in cm shown in boxes on time axis.

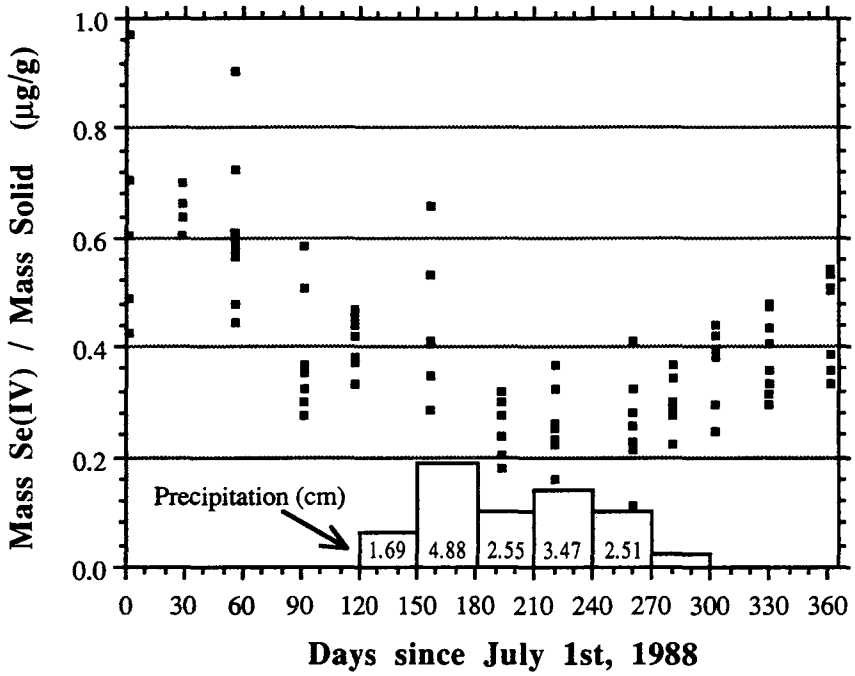

Figure 4.13a Changes in selenite concentration in the top 9 cm of soil in plot 8EP: July 1988 - June 1989. Precipitation in cm shown in boxes on time axis.

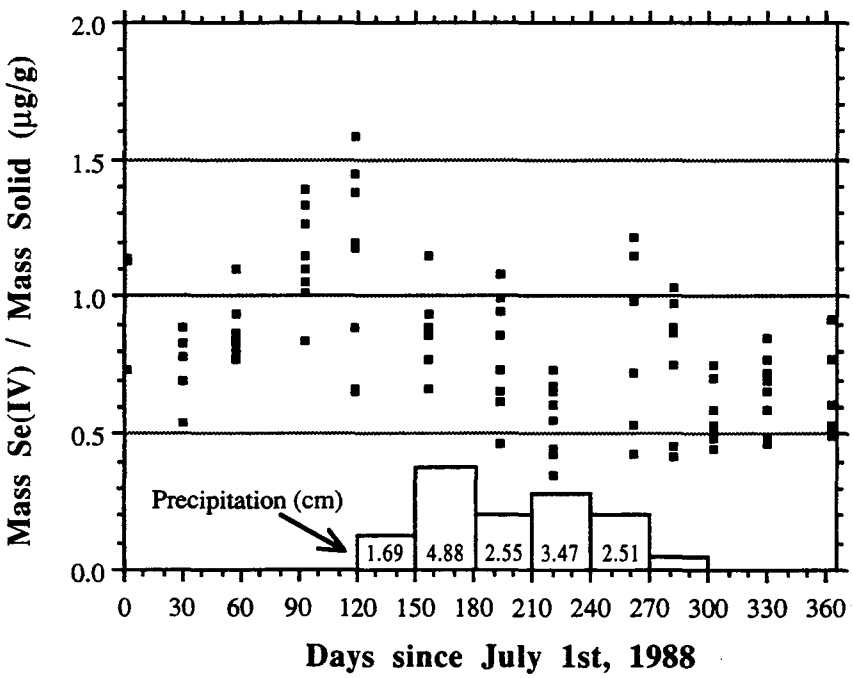

Figure 4.13b Changes in selenite concentration in the top 9 cm of soil in plot 9BE: July 1988 - June 1989. Precipitation in cm shown in boxes on time axis.

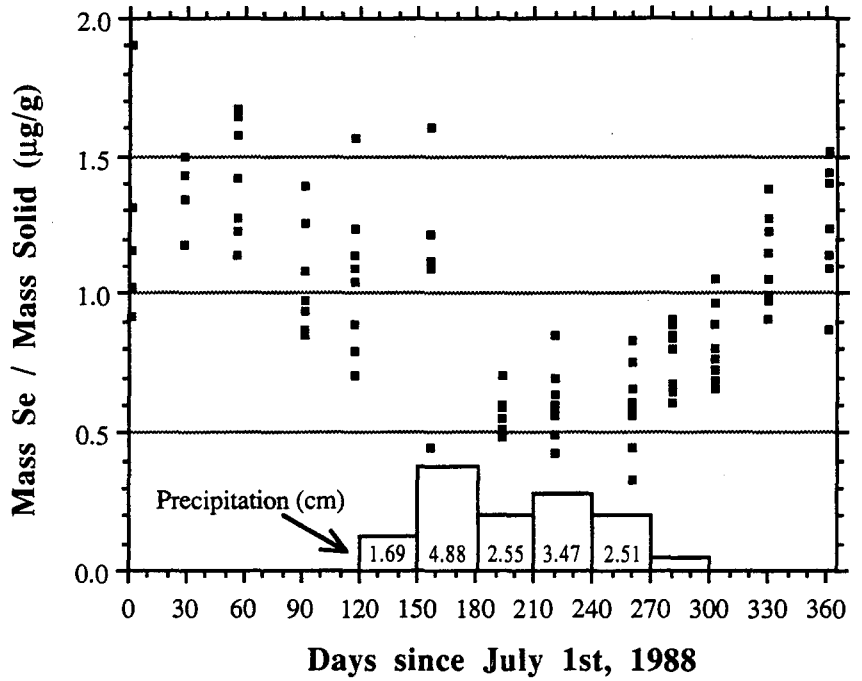

Figure 4.14a Changes in water-extractable selenium concentration in the top 9 cm of soil in plot 8EP: July 1988 - June 1989. Precipitation in cm shown in boxes on time axis.

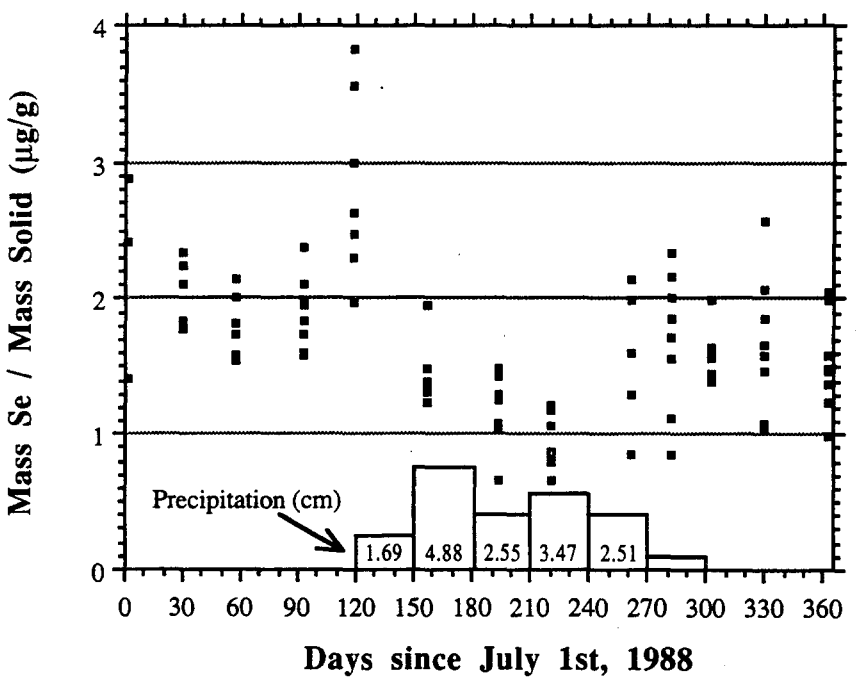

Figure 4.14b Changes in water-extractable selenium concentration in the top 9 cm of soil in plot 9BE: July 1988 - June 1989. Precipitation in cm shown in boxes on time axis.

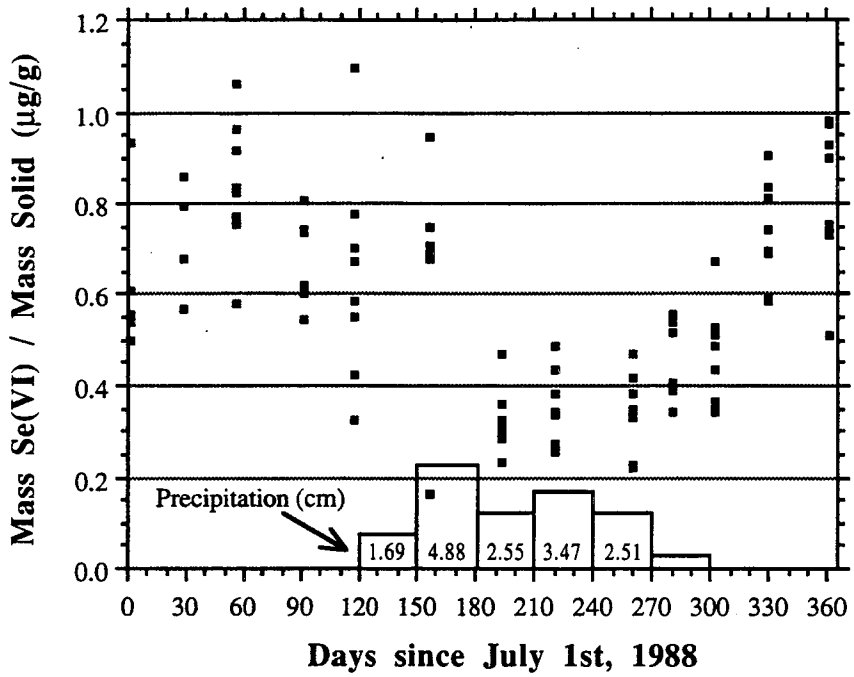

Figure 4.15a Changes in selenate concentration in the top 9 cm of soil in plot 8EP: July 1988 - June 1989. Precipitation in cm shown in boxes on time axis.

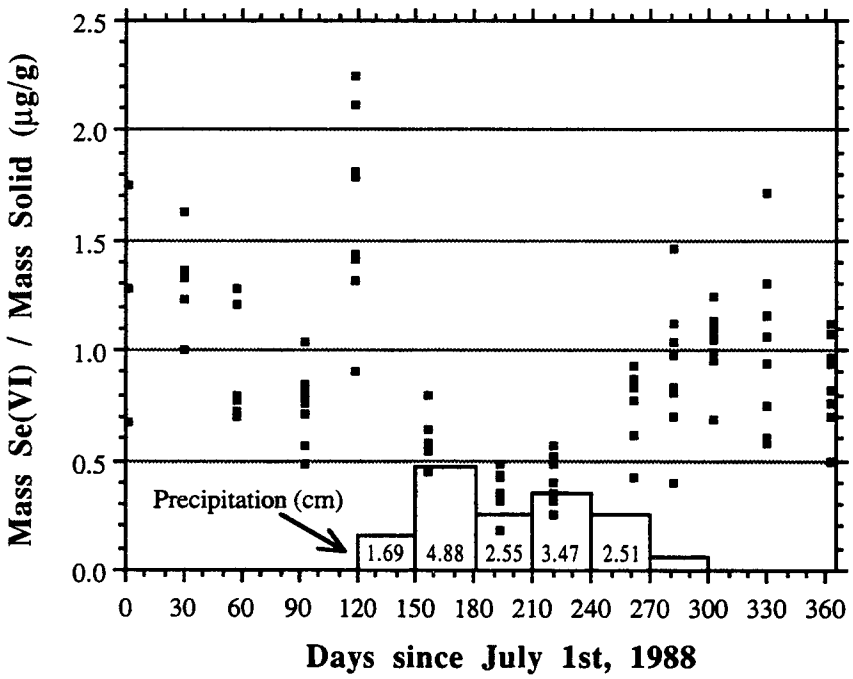

Figure 4.15b Changes in selenate concentration in the top 9 cm of soil in plot 9BE: July 1988 - June 1989. Precipitation in cm shown in boxes on time axis.

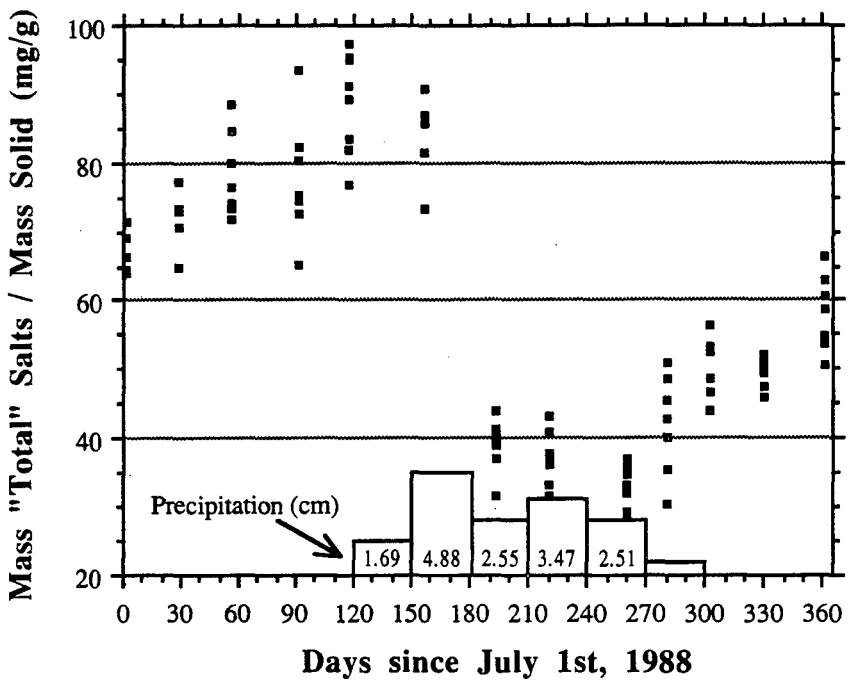

Figure 4.16a Changes in "total" salt concentration in the top 9 cm of soil in plot 8EP: July 1988 - June 1989. Precipitation in cm shown in boxes on time axis.

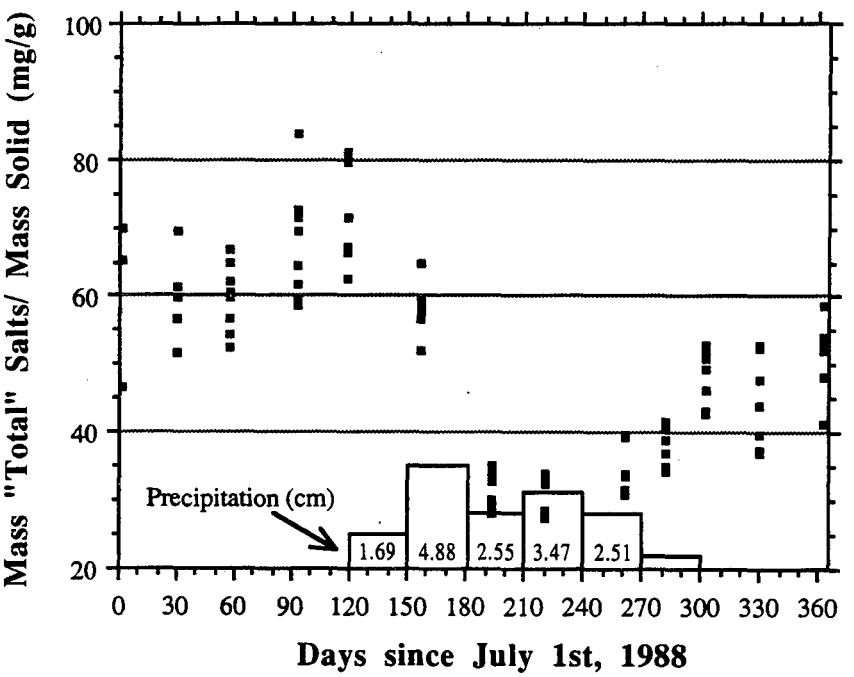

Figure 4.16b Changes in "total" salt concentration in the top 9 cm of soil in plot 9BE: July 1988 - June 1989. Precipitation in cm shown in boxes on time axis.

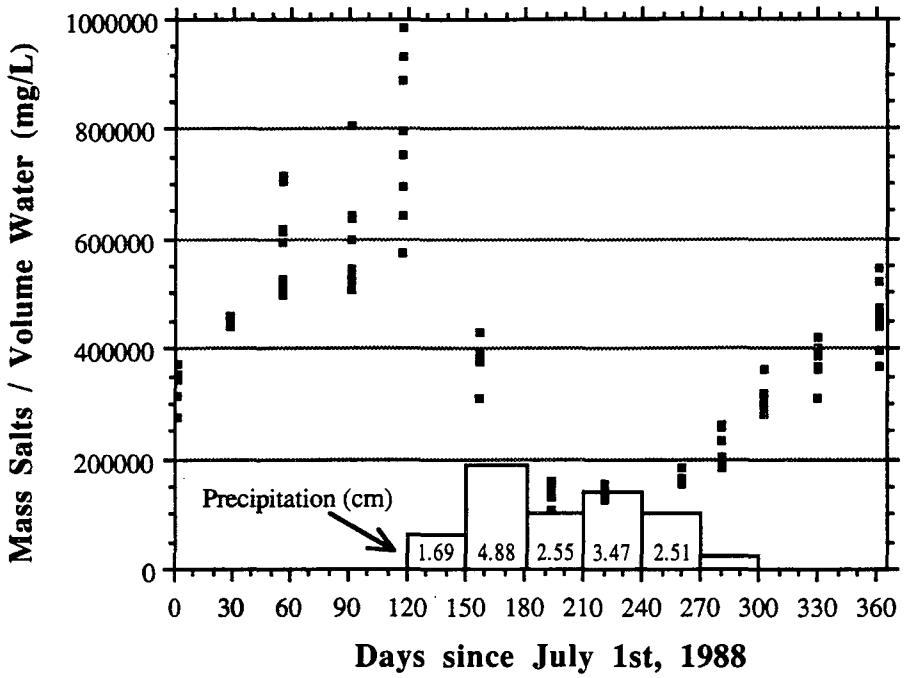

Figure 4.17a Changes in "total" salt concentration in the top 9 cm of soil in plot 8EP: July 1988 - June 1989. Precipitation in cm shown in boxes on time axis.

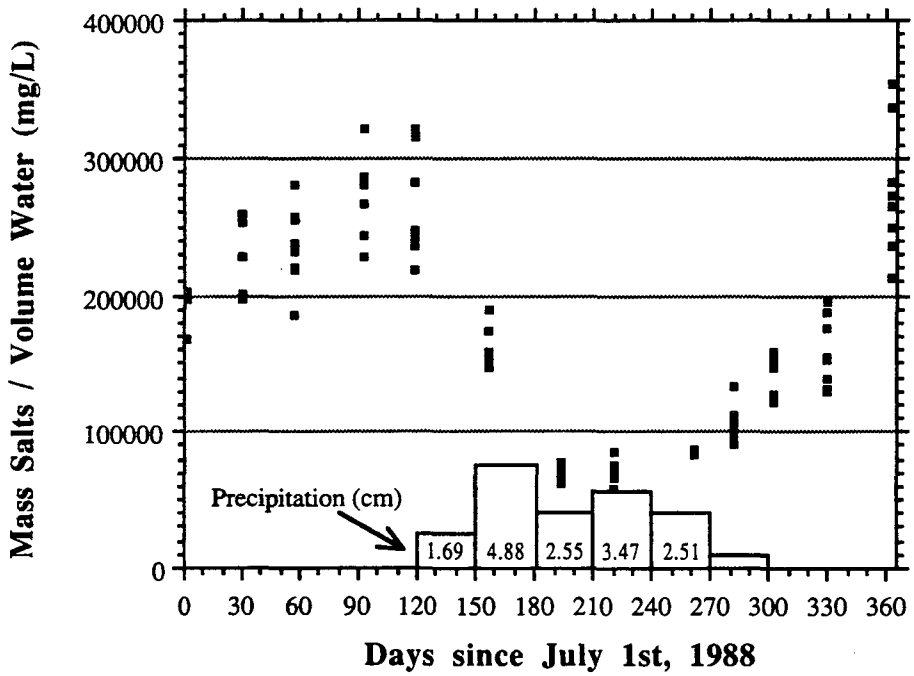

Figure 4.17b Changes in "total" salt concentration in the top 9 cm of soil in plot 9BE: July 1988 - June 1989. Precipitation in cm shown in boxes on time axis.

summer months (see Figures 2.6 & 2.7 for weather patterns during the study term).

Concentrations of the most mobile species (Na^+, Cl^-) changed most dramatically with time. During the first drying period (July - October, 1988), the mean sodium concentration in the top 9 cm increased from 12.73 mg/g (C.V.[1]= 6.3%) to 19.47 mg/g (C.V. = 10.7%) in plot 8EP and from 11.85 mg/g (C.V. = 27.3%) to 15.54 mg/g (C.V. = 14.9%) in plot 9BE (Fig. 4.7). The mean chloride concentration rose from 9.33 mg/g (C.V. = 7.8%) to 14.30 mg/g (C.V. = 18.5%) in plot 8EP and from 9.38 mg/g (C.V. = 17.3%) to 13.23 mg/g (C.V. = 14.0%) in plot 9BE (Fig. 4.12). On the other hand, calcium concentrations did not change significantly. This confirms that gypsum did not dissolve out completely during the extraction process, and that relative changes in calcium cannot be gauged using this procedure. Based on this, sulfate also cannot be used as a tracer since an unknown fraction of it remains undissolved in gypsum. A combination of concentrations of all cations and anions results in a "total" salt concentration; this is obviously not a true "total" since the extract solution is saturated with respect to gypsum. However, on the whole, it may give a better idea of overall soil salinity changes (Fig. 4.16). The mean "total" salts concentration increased from 67.11 mg/g (C.V. = 4.5%) to 88.66 mg/g (C.V. = 8.3%) in plot 8EP during the first drying period, and from 60.59 mg/g (C.V. = 20.2%) to 72.40 mg/g (C.V. = 9.7%) in plot 9BE during the same period. No clear trends emerge from the distribution of selenium data during the summer and fall of 1988 (Figs. 4.13 - 4.15). This is probably in large part due to the much greater spatial variability of selenium than major ions. An apparent decrease in selenite concentrations in plot 8EP may be due to oxidation of selenite to selenate, but the data is not conclusive. Since selenite is mostly found adsorbed onto solid matter in the soil, changes in *selenate*

---

[1] Coefficient of Variation (C.V.) = Standard Deviation (S.D.) divided by Mean of data set times 100.

concentrations are more indicative of soluble selenium behavior (Fig. 4.15). In neither plot, however, did selenate concentrations change along any discernable trend.

With the onset of the rainy season in late October, salts which had been accumulating near the soil surface were beginning to get flushed down deeper into the soil profile by infiltrating rainwater. This effect is quite apparent in the rather sudden decrease in concentrations of all species, except calcium, after day 150. A greater decrease in concentrations in plot 9BE between days 120 and 150 is consistent with the higher flow rates expected in the coarser-textured sediments of that plot. During the rainy season, the mean concentration of sodium in plot 8EP declined from a high of 19.47 mg/g at the end of the summer to 5.05 mg/g (C.V. = 17.2%) on day 220. The corresponding decrease in plot 9BE was from 15.54 mg/g to 2.84 mg/g (C.V. = 25.7). Similar decreases were observed in chloride concentrations (Fig. 4.12). Coincident with these declines, were decreases in selenate concentrations at both plots (Fig. 4.15). While still obscured by spatial variability, the range of selenate concentrations during this period was between 0.0 and 0.5 μg/g which was lower than at any time before; even though it is certain that some selenate was being flushed out of the surface 9 cm of soil during this period, these data do not positively confirm this. However, data from soil-water samplers and extracts from soil profiles in both plots also support this notion. Changes in EC and concentrations of chloride and selenate in in-situ soil-water of plots 8EP and 9BE are shown in Figures 4.18 through 4.23. Following rainfall events of early winter, significant pulses of salts and selenium were observed moving through the soil profile. These changes are much more easily discernable in plot 9BE where sediment texture is coarse and front infiltration potentially more rapid. As seen in Figures 4.19 and 4.23, concentrations of both salts and selenate rose most sharply at a depth of 15 cm and progressively less with depth. Such a pattern of increase is due to the flushing out of species from the top few centimeters of soil. This pattern is confirmed by data from extracts made of soil in profile at both plots. A

number of samples were taken down to a depth of 60 cm in plot 8EP and 50 cm in plot 9BE on March 31st, 1989. The concentrations of chloride and selenate in extracts of these samples are compared with their concentrations in July of 1988 in Figures 4.24 - 4.25. Multiple points at the same depth on the same date indicate duplicate, triplicate, or quadruplicate samples. The depletion of chloride in the top 5 to 10 cm of the soil profile and its elevation below that interval are apparent in both plots and while decreases in selenate concentrations are not as evident near the soil surface, probably due to spatial variability, its increase at depth is more distinct. While detection of a selenate decrease in surface samples is impeded by spatial variability of selenium concentrations, data from soil-water samplers and soil extracts in profile leave little doubt that selenate was being flushed out along with chloride and other salts.

In the months following most of the season's rainfall events, concentrations of species in the top 9 cm of the soil profile slowly increased in response to evaporatively induced water flow toward the surface. Between day 220 and day 361, the mean concentration of sodium in plot 8EP ascended from a low of 5.05 mg/g to 11.10 mg/g (C.V. = 7.6%); the corresponding increase in plot 9BE was from 2.84 mg/g to 8.24 mg/g (C.V. = 16.6%) (Fig. 4.7). The mean chloride concentration rose from 2.35 mg/g to 7.09 mg/g (C.V. = 13.3%) in plot 8EP and from 1.12 mg/g to 5.21 mg/g (C.V. = 24.6%) in plot 9BE (Fig. 4.12). Similar increases were observed in total salts concentrations (Fig. 4.16). Unlike during the summer and fall of 1988, increases in selenate concentrations were easily discernable during the late spring and summer of 1989 and resulted in selenate concentrations ranging from 0.5 to 1.0 μg/g at plot 8EP and 0.5 to 1.5 μg/g in plot 9BE. Redistribution of salts and selenate in the soil profile was observed through soil-water samplers (Figs. 4.18 -4.23). Due to the limited data from plot 8EP during this period (sampler failure), this redistribution is not very evident; however, concentrations of major ions in shallow samplers were beginning to decline on day 240. This decrease is

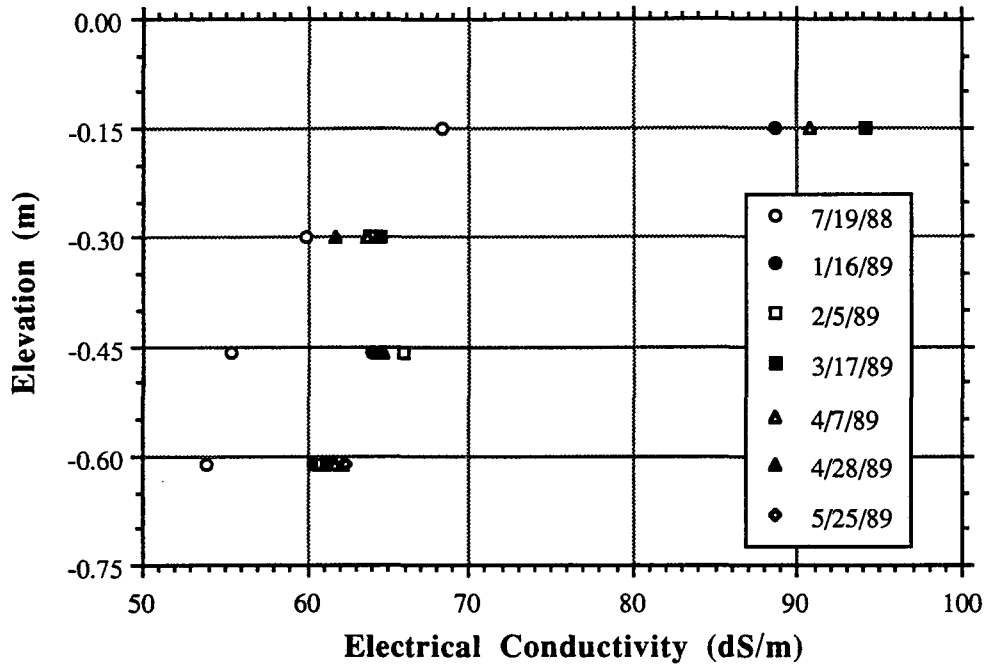

Figure 4.18a Changes in EC in soil-water at four depths in plot 8EP: profile view (7/19/88 - 5/25/89).

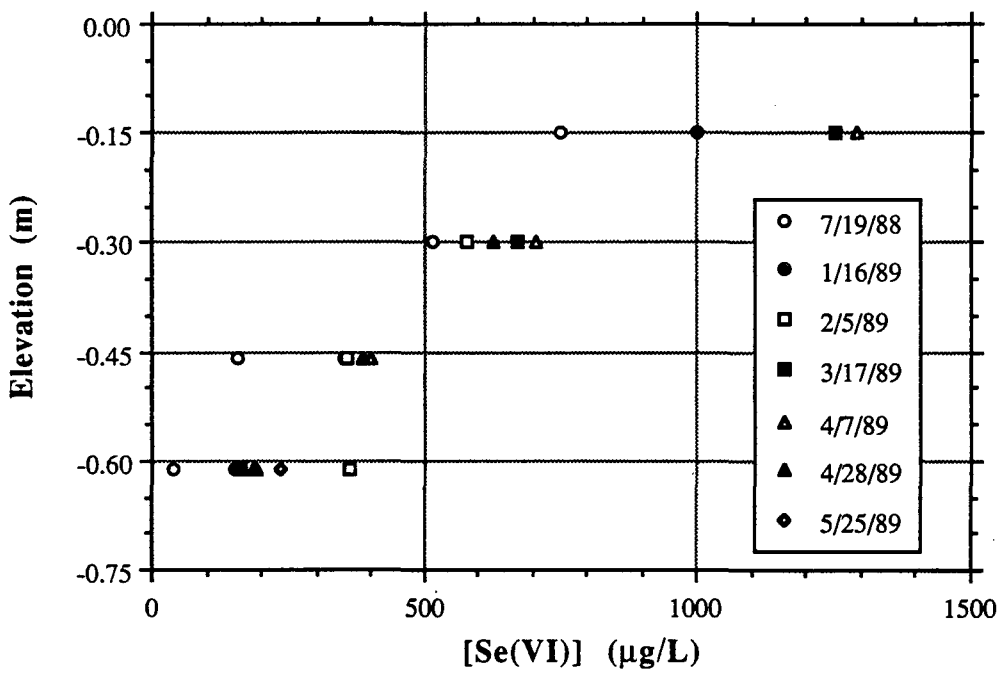

Figure 4.18b Changes in selenate in soil-water at four depths in plot 8EP: profile view (7/19/88 - 5/25/89).

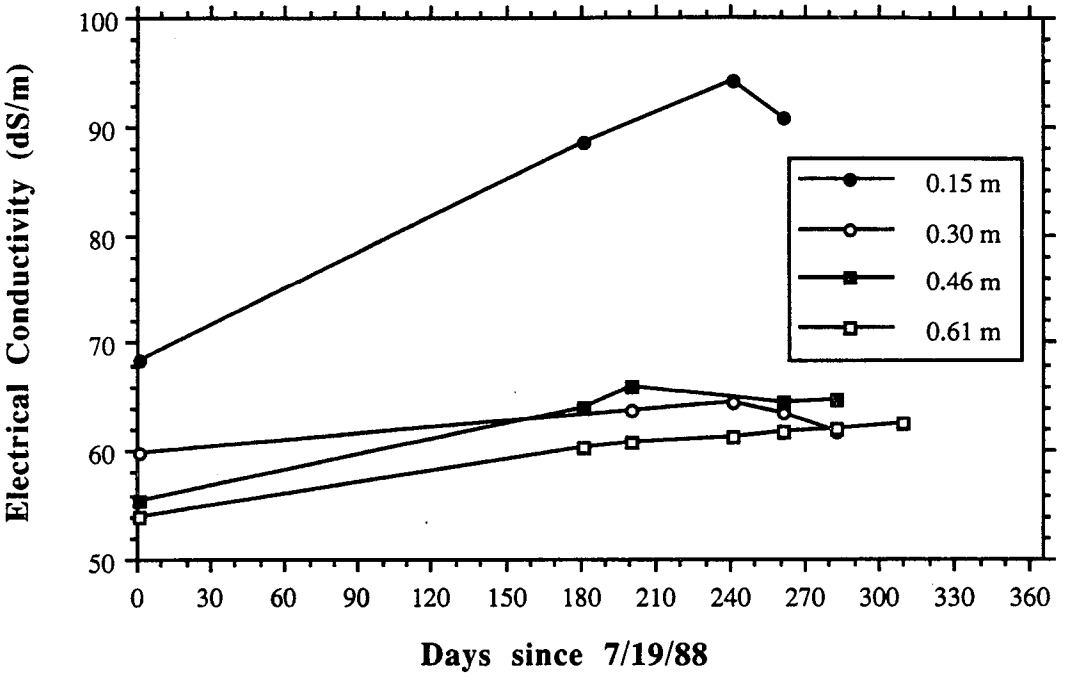

Figure 4.19a Changes in EC in soil-water at four depths in plot 8EP (7/19/88 through 5/25/89).

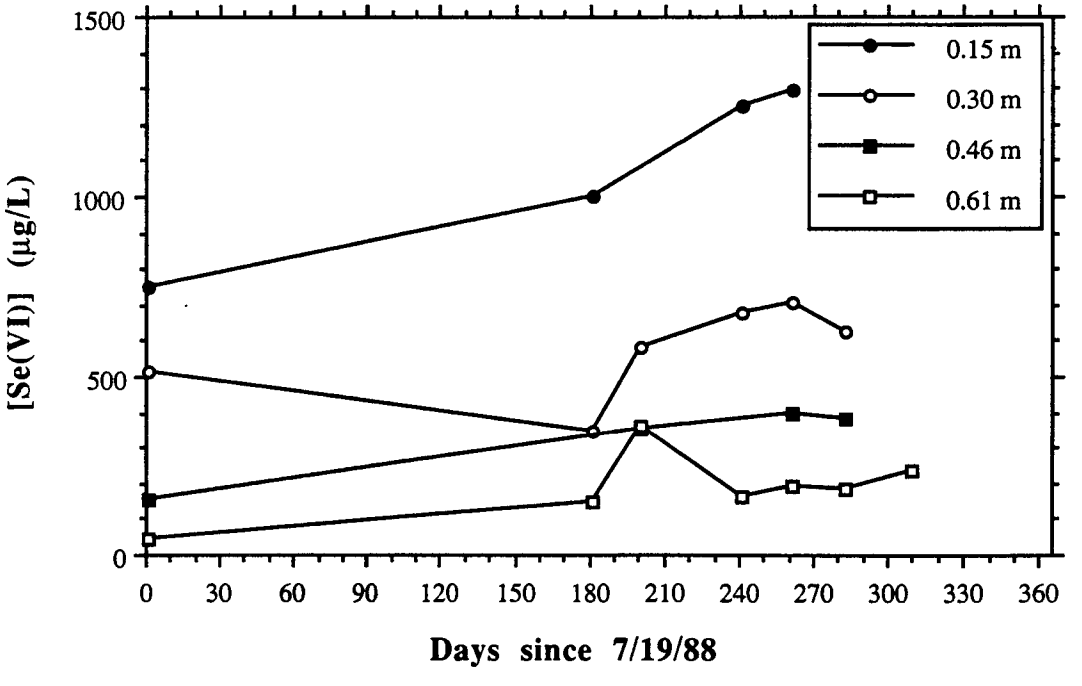

Figure 4.19b Changes in selenate concentrations in soil-water at four depths in plot 8EP (7/19/88 through 5/25/89).

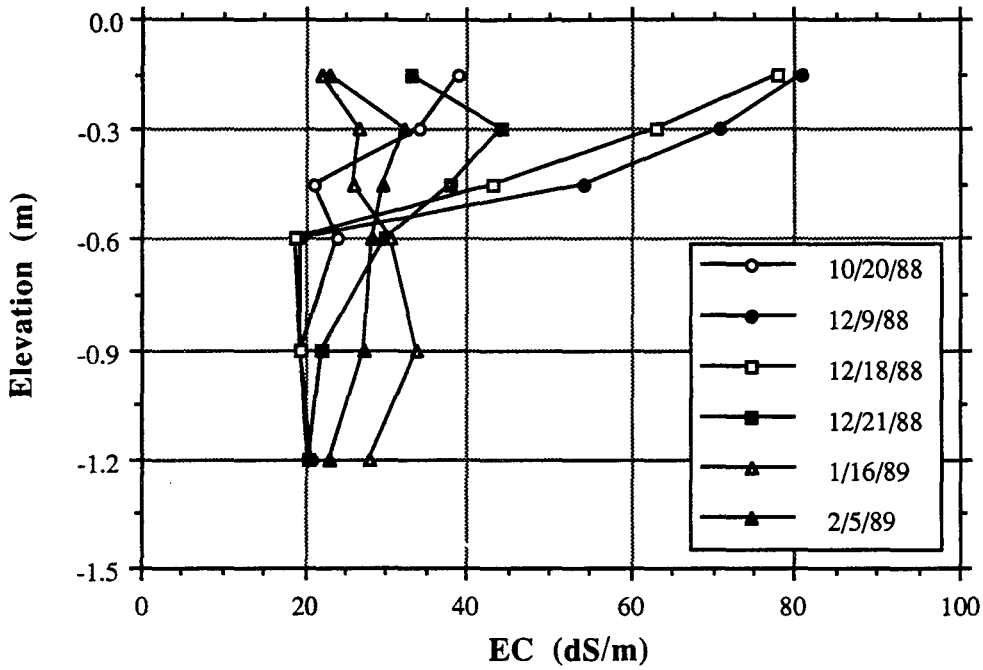

Figure 4.20a Changes in EC in soil-water at six depths in plot 9BE: profile view (10/20/88 - 2/5/89).

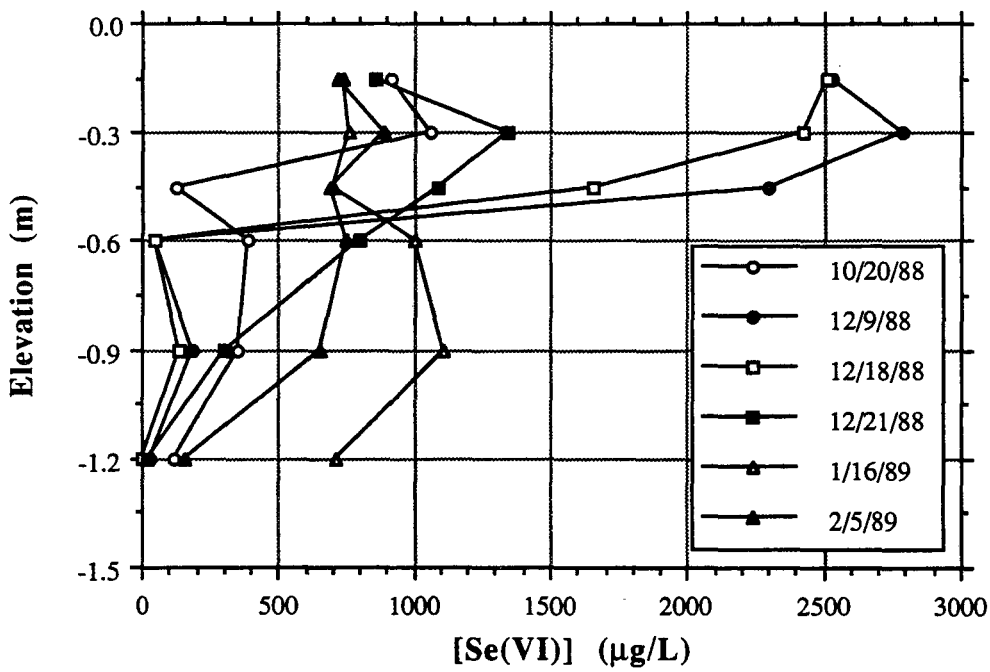

Figure 4.20b Changes in selenate concentrations in soil-water at six depths in plot 9BE: profile view (10/20/88 - 2/5/89).

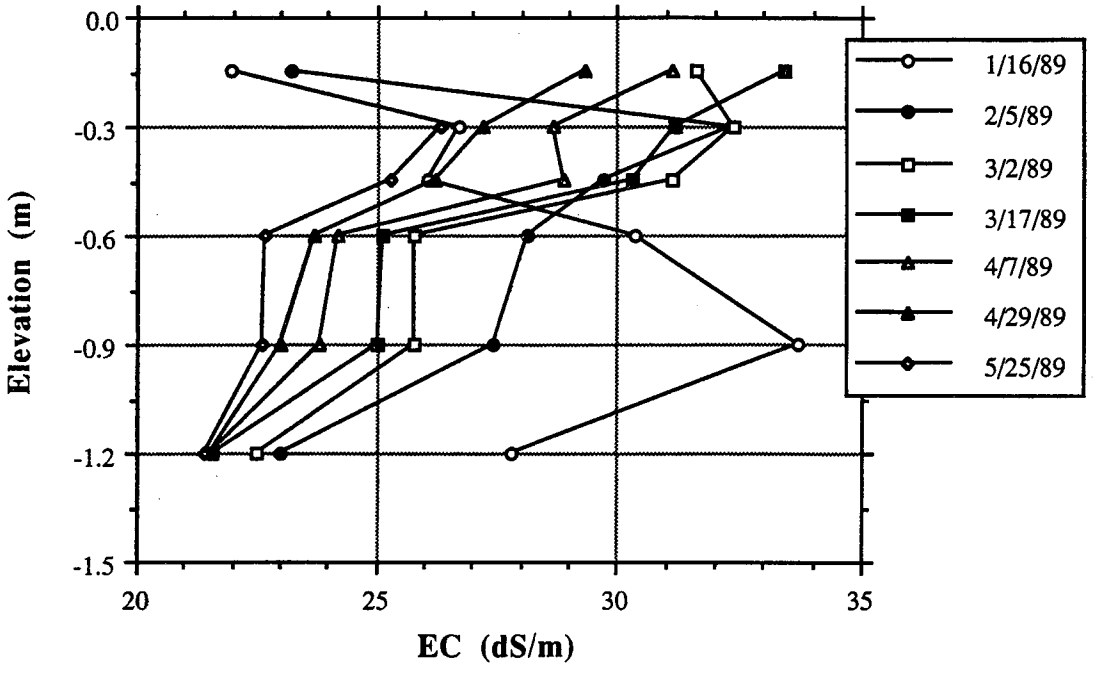

Figure 4.21a Changes in EC in soil-water at six depths in plot 9BE: profile view (1/16/89 - 5/25/89).

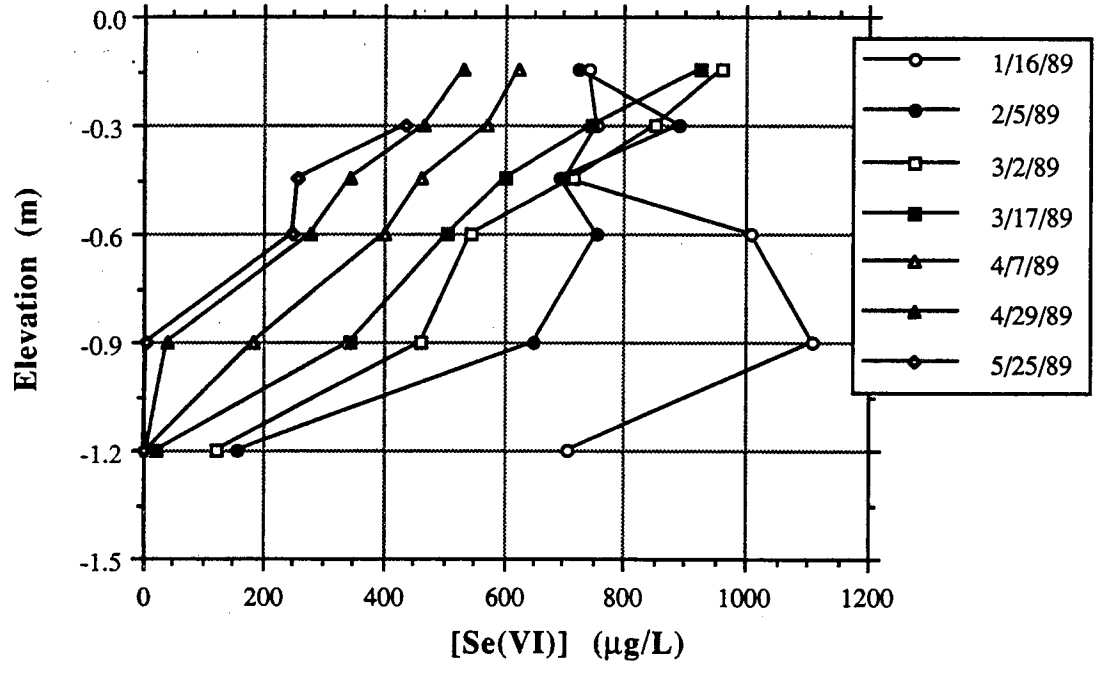

Figure 4.21b Changes in selenate concentrations in soil-water at six depths in plot 9BE: profile view (1/16/89 - 5/25/89).

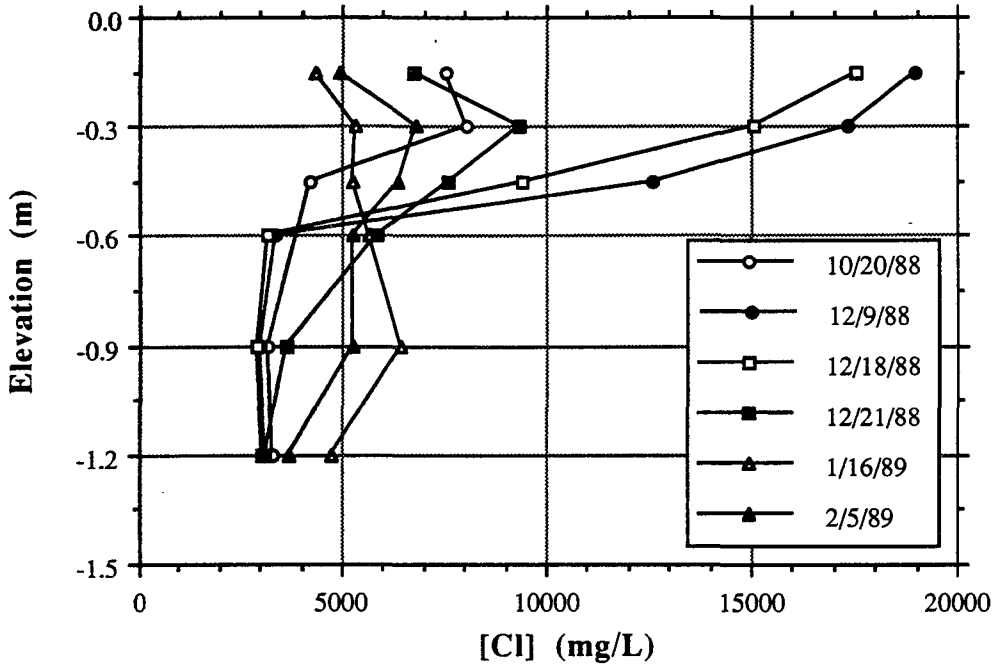

Figure 4.22a Changes in chloride concentrations in soil-water at six depths in plot 9BE: profile view (10/20/88 - 2/5/89).

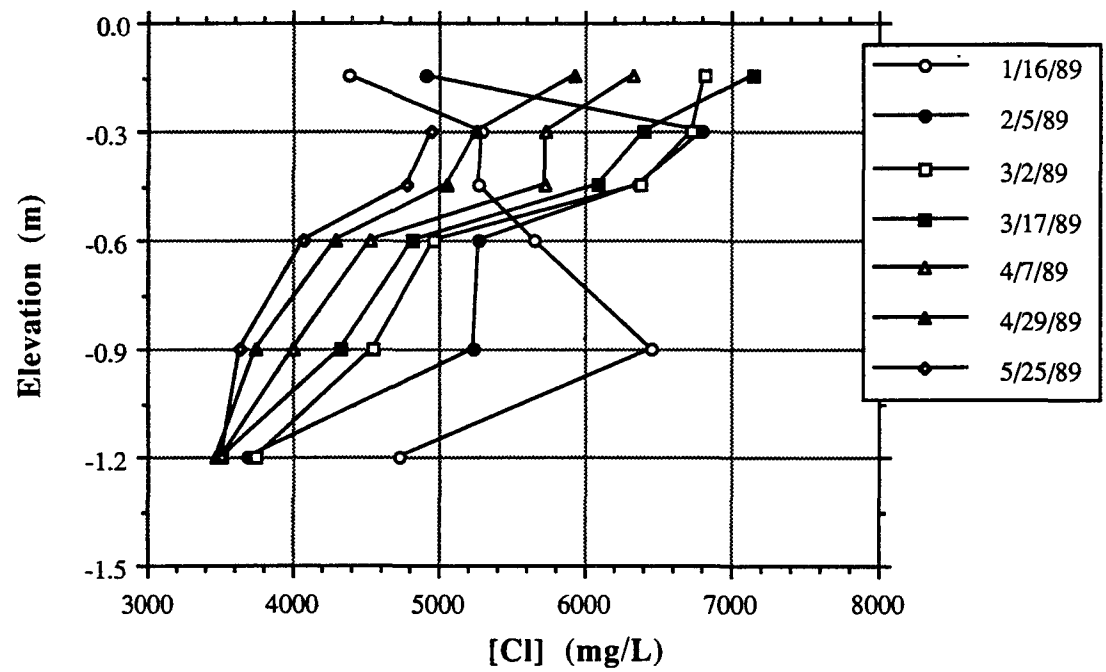

Figure 4.22b Changes in chloride concentrations in soil-water at six depths in plot 9BE (1/16/89 - 5/25/89).

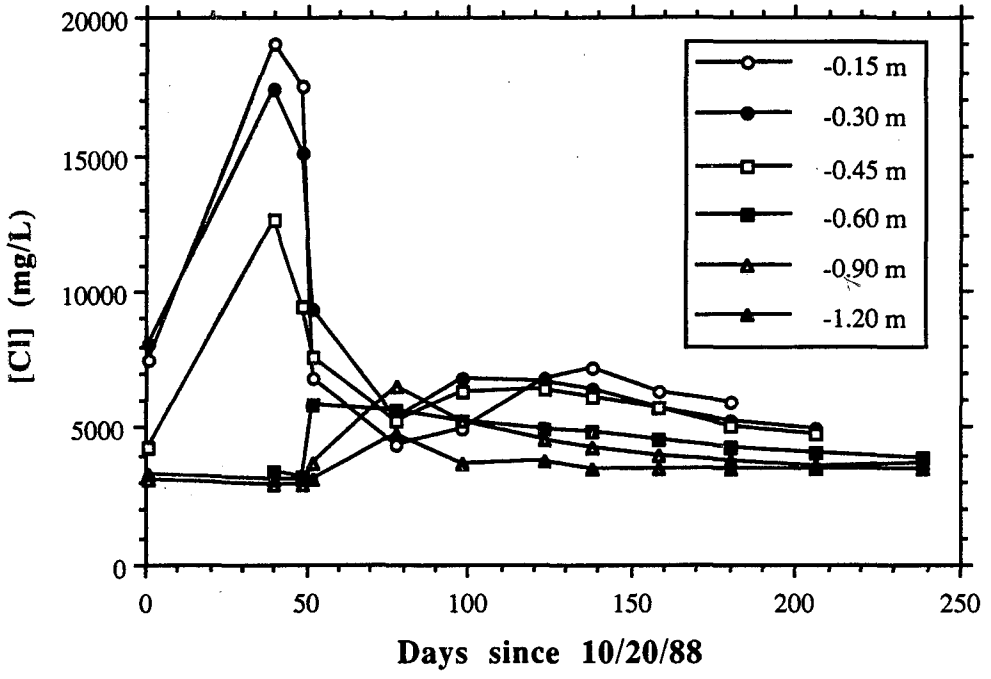

Figure 4.23a Changes in chloride concentrations in soil-water at six depths in plot 9BE (10/20/88 - 5/25/89).

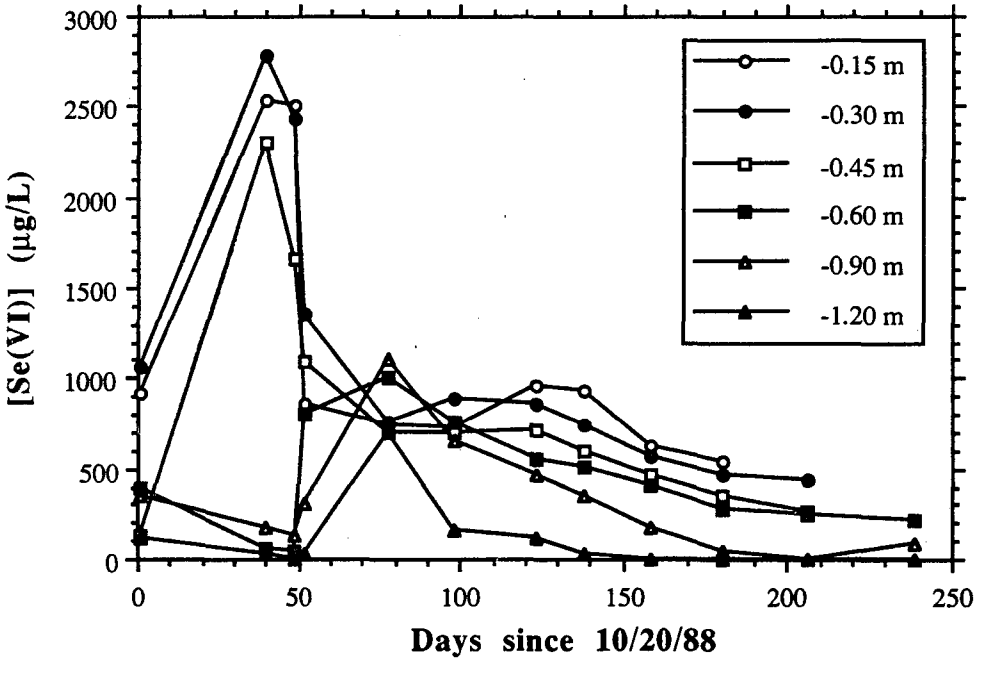

Figure 4.23b Changes in selenate concentrations in soil-water at six depths in plot 9BE (10/20/88 - 5/25/89).

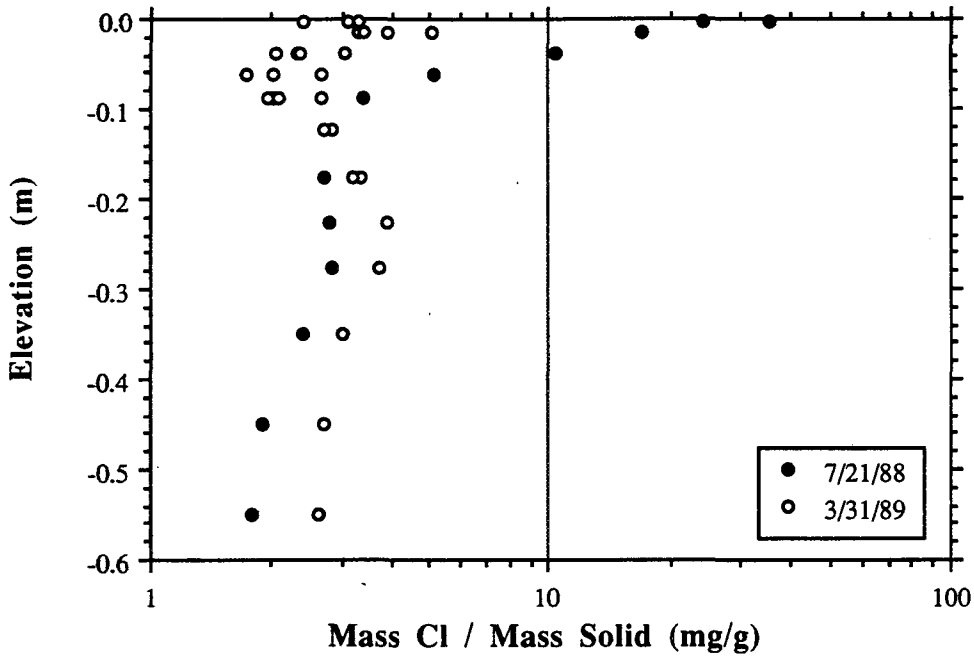

Figure 4.24a Changes in chloride distribution in the soil profile of plot 8EP.

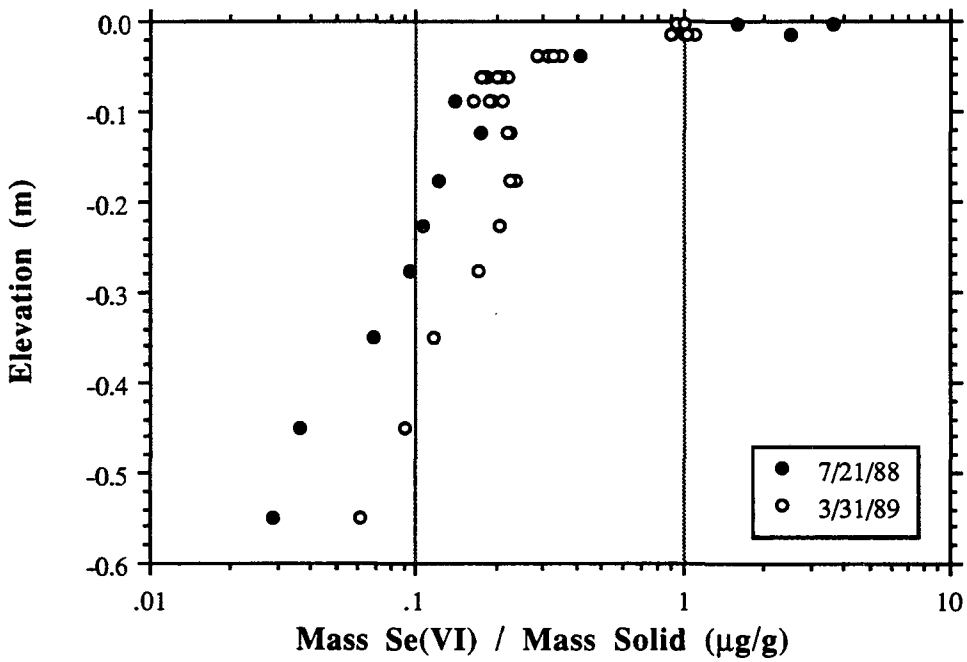

Figure 4.24b Changes in selenate distribution in the soil profile of plot 8EP.

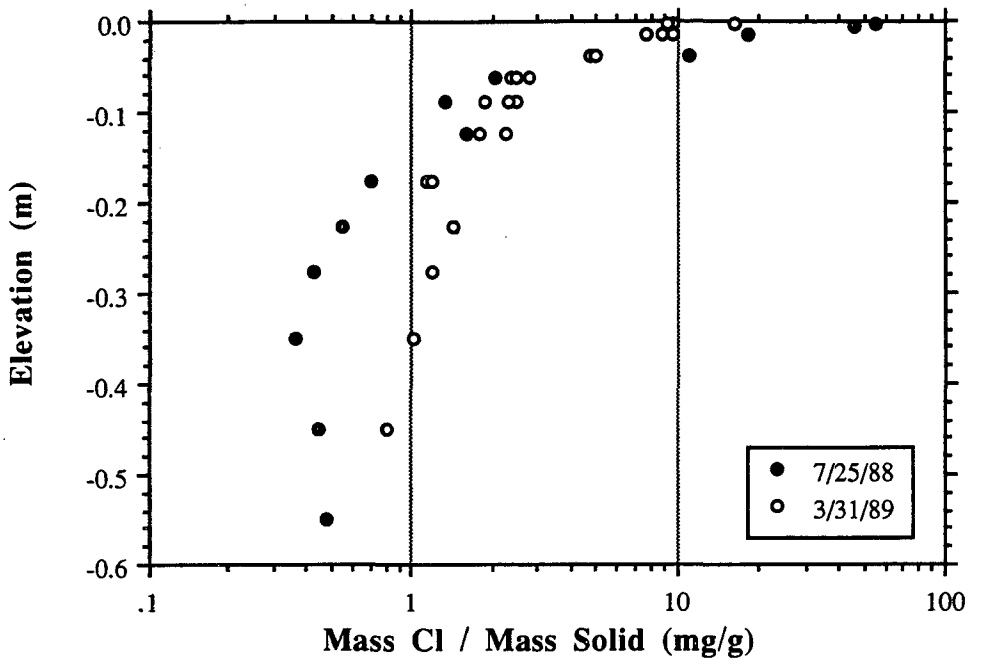

Figure 4.25a Changes in chloride distribution in the soil profile of plot 9BE.

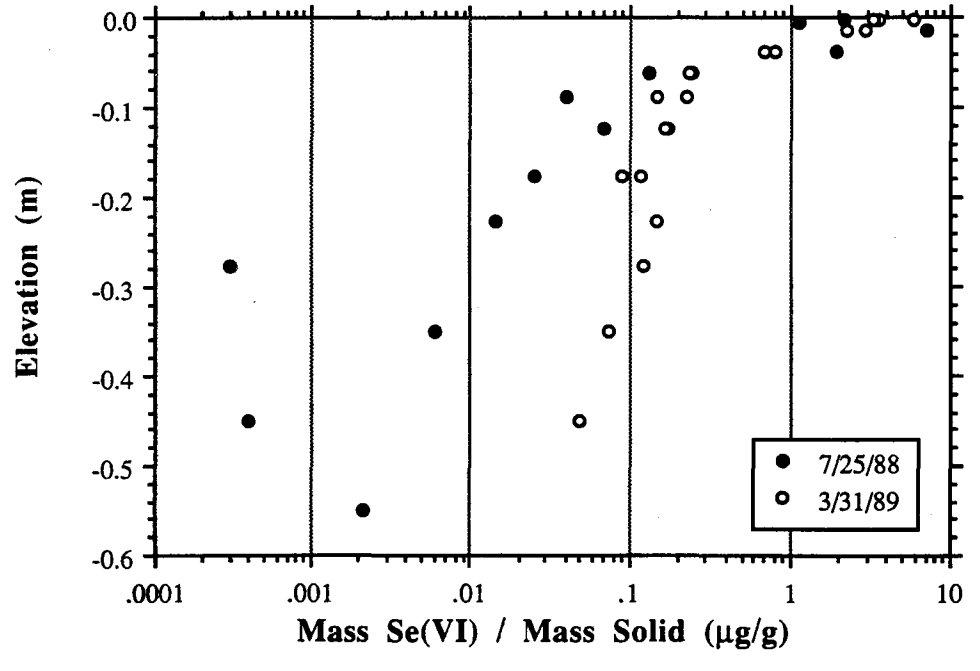

Figure 4.25b Changes in selenate distribution in the soil profile of plot 9BE.

unambiguous in soil-water of plot 9BE (Figs. 4.21, 4.22b, and 4.23). Such a pattern is indicative of the movement of water toward the soil surface; by 5/25/89, the distribution of chloride in the profile of plot 9BE was very similar to the distribution before the onset of the rainy season. Selenate concentrations, however, seem to have declined from their pre-winter levels.

The year encompassed by this study was a particularly dry one (total precipitation = 162 mm, compared with an average of 1982/84 and 1985/88 precipitation of 279 mm). Nevertheless, a net decrease in the near surface concentrations of both salts and selenate was observed. This decrease, while slight, is indicative of a system in transition. Due to the unnatural accumulation of salts and selenium at and near the soil surface as a result of ponding and subsequent evaporation, the redistribution of species in the next few years will most likely result in a net decrease, albeit small, of salt concentrations at the soil surface. This may or may not be true for soluble selenium, depending on the rate of oxidation of the insoluble fraction, although an increase of soluble selenium due to evaporative concentration seems unlikely. According to the results of XRF analyses of four soil samples from each plot (Table 4.2), water-extractable selenium comprises between 3.8% and 20.1% of total selenium in the top 9 cm of soil.

The inventory of potentially oxidizable selenium is substantial, especially in plot 9BE and may be even greater in certain other parts of Kesterson Reservoir. The rate of selenium oxidation will play an important role in determining soluble selenium concentrations. Trends of soluble selenium redistribution will depend very strongly on rainfall patterns in the years to come.

Table 4.2 Concentrations of Water-Extractable Selenium vs. Total Selenium by XRF analysis

Plot and Sample Name	Date collected	Total Se as analyzed by XRF (µg/g)	Water-extractable Se (µg/g)	% of water-extractable Se
Plot 8EP ML1E	10/25/88	7.8	1.6	20.1
Plot 8EP ML8E	10/25/88	4.6	0.7	15.3
Plot 8EP Surf1D	2/5/89	5.9	0.4	7.1
Plot 8EP Surf4D	2/5/89	8.0	0.9	10.7
Plot 9BE ML3E	10/25/88	26.5	3.8	14.4
Plot 9BE ML6E	10/25/88	16.5	2.0	12.0
Plot 9BE Surf4D	2/5/89	17.2	0.7	3.8
Plot 9BE Surf6D	2/5/89	22.9	1.2	5.3

4.5 QUANTITATIVE ANALYSIS OF CHLORIDE ACCUMULATION: CALCULATION OF SEASONAL EVAPORATION RATES

The qualitative analysis of data presented in the previous section helped delineate two fairly distinct stages in the annual cycle of wetting and drying of the surface soils at Kesterson Reservoir. In order to quantitatively describe the evaporative concentration of species near the soil surface and thereby estimate seasonal evaporation rates, a non-reactive, high solubility, high concentration species must be used. Satisfying these criteria, chloride will serve as a tracer in this analysis.

4.5.1 Approach

Bare soil evaporation rates may be estimated based on increases in chloride concentrations in the top 9 cm of soil (or any top interval for that matter), changes in the moisture content of that interval, and the chloride concentration gradient along which chloride diffusion takes place. The first two variables can and have been measured in the field over the period of this study and have been presented in previous sections. Unfortunately, the magnitude of chloride diffusion in the soil must be estimated and involves substantial error due to the unknown relationship between tortuosity and saturation in Kesterson sediments, especially in surface soils. Figure 4.26 displays the water and chloride fluxes (q_w and J_{Cl} respectively) into and out of the surface 9 cm of soil.

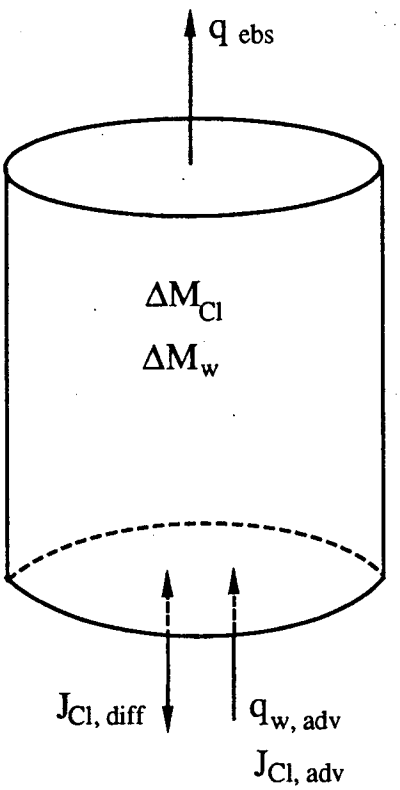

Figure 4.26 Water and chloride fluxes into and out of the top 9 cm of soil.

Water mass balance requires that the mass of water entering the element be equal to the mass of water leaving the element plus any mass of water accumulated within the element:

$$q_{w,\,adv}\,\rho_w A\Delta t = q_{w,\,ebs}\,\rho_w A\Delta t + \Delta M_w \tag{4.6}$$

where $q_{w,adv}$ is the advective flux of water from below the element [LT^{-1}], $q_{w,ebs}$ is the evaporative flux of water out of the top of the element [LT^{-1}], ρ_w is the density of water [ML^{-3}], A is the cross-sectional area of the element, Δt is the time increment, and ΔM_w is the change in the mass of water within the element. M_w may be expressed as the product of gravimetric moisture content and the mass of solid within the element:

$$\Delta M_w = \Delta\theta_{grav} M_{solid} \tag{4.7}$$

Equation (4.6) can then be rewritten as:

$$q_{w,\,adv} = q_{w,\,ebs} + \Delta\theta_{grav}\frac{M_{solid}}{\rho_w A\Delta t} \tag{4.8}$$

A similar mass balance expression may be set up for chloride:

$$J_{Cl,\,adv} A\Delta t + J_{Cl,\,diff} A\Delta t = \Delta M_{Cl} \tag{4.9}$$

where $J_{Cl,adv}$ is the advective flux of chloride into the element [$ML^{-2}T^{-1}$], $J_{Cl,diff}$ is the diffusive flux of chloride into or out of the element [$ML^{-2}T^{-1}$], and ΔM_{Cl} is the net change in chloride mass within the element. The advective flux of chloride may be expressed as follows:

$$J_{Cl,\,adv} = q_{w,\,adv}\, C_{Cl,\,lb} \tag{4.10}$$

where $C_{Cl,lb}$ is the concentration of chloride per volume of soil solution at the lower boundary of the element. The diffusive flux of chloride may be described in the following way:

$$J_{Cl,\,diff} = -\,[D_0 nS\tau]\frac{\Delta C_{Cl}}{\Delta z} \tag{4.11}$$

where D_0 is the diffusivity of the chloride ion in water [L^2T^{-1}], n is porosity, S is relative saturation, τ is a tortuosity factor, and $\Delta C_{Cl}/\Delta z$ is the chloride soil solution concentration gradient [ML^{-4}]. Combining equations (4.9) through (4.11):

$$q_{w,\,adv}\, C_{Cl,\,lb} - [D_0 nS\tau]\frac{\Delta C_{Cl}}{\Delta z} = \frac{M_{Cl}}{A\Delta t} \tag{4.12}$$

Solving for $q_{w,adv}$, one obtains:

$$q_{w,\,adv} = \left(\frac{\Delta M_{Cl}}{A\Delta t} + [D_0 nS\tau]\frac{\Delta C_{Cl}}{\Delta z}\right)\frac{1}{C_{Cl,\,lb}} \tag{4.13}$$

substituting the above expression for $q_{w,adv}$ in equation (4.8) and rearanging to solve for $q_{w,ebs}$:

$$q_{w,\,ebs} = \frac{\Delta M_{Cl}}{C_{Cl,\,lb} A\Delta t} + \frac{1}{C_{Cl,\,lb}}[D_0 nS\tau]\frac{\Delta C_{Cl}}{\Delta z} - \Delta\theta_{grav}\frac{M_{solid}}{\rho_w A\Delta t} \tag{4.14}$$

The first term on the right hand side of equation (4.14) represents the component of bare soil evaporation which results from an upward movement of water from a lower soil

interval, without resulting in changes in moisture content. The second term is the correction for diffusion of chloride; the third term is the additional evaporation which causes net drying of the soil interval. As mentioned before, terms 1 and 3 can be calculated with greater accuracy than term 2; this is due to the fact that the tortuosity factor, τ, is not a constant under desaturating conditions. Research conducted over the last two to three decades has shown that the tortuosity of flow path increases significantly with decreasing moisture content, as a result of water film thinning in the porous medium. The proportion of water-filled pores which are connected to a continuous pore network gradually declines along with moisture content (Pinner & Nye, 1982). This results in the lowering of the diffusivity of species in porous media and a reduction in diffusive flux under a given concentration gradient. This effect has been characterized by using "impedence factors" in place of tortuosity factors (Porter and others, 1960; Barraclough and Tinker, 1981, 1982). In general, it has been found that the impedence factor is an approximately linear function of volumetric moisture content (θ_{vol}); the slope of this function varies from soil to soil and has also been found to be dependent on the compaction of a given soil (Fig. 4.27). It appears that the linear nature of this function breaks down as θ_{vol} falls below 0.1 or so. Unfortunately, the slope of this function for soil in plots 8EP and 9BE is not known. However, certain assumptions may be made based on the bulk density of these near-surface soils and their textural compositions. For example, the surface 9 cm of soil at plot 8EP is texturally characterized as a clay loam to loam with a bulk density of 1.31 g cm^{-3} (C.V. = 4.3%, n = 96). Therefore, it is texturally similar to the sandy clay loam and the loam of Fig. 4.27a. On the other hand, the surface 9 cm of the soil at plot 9BE is a clay loam to silty clay loam with a bulk density of 0.96 g cm^{-3} (C.V. = 7.1%, n = 94), which makes it most similar to the clay and silty clay loam of Fig. 4.27a. The impedence factor for the two Kesterson soils was assumed equal to the impedence factor for the above mentioned soils from Fig. 4.27a (Barraclough and Tinker, 1981). Quite obviously, such comparisons must be made with extreme caution: the impedence factor of any given soil

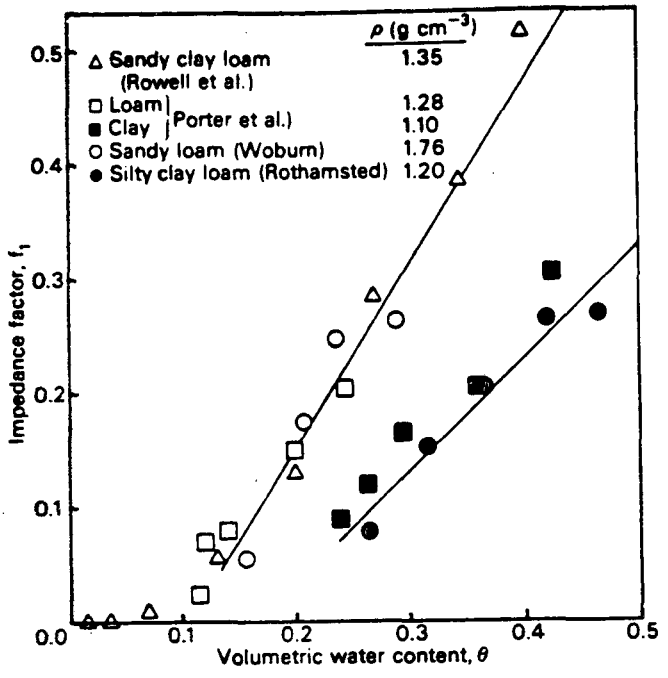

Figure 4.27a Impedence factor, f_1, as a function of volumetric water content in five different soils, each soil at a constant bulk density (from Barraclough & Tinker, 1981).

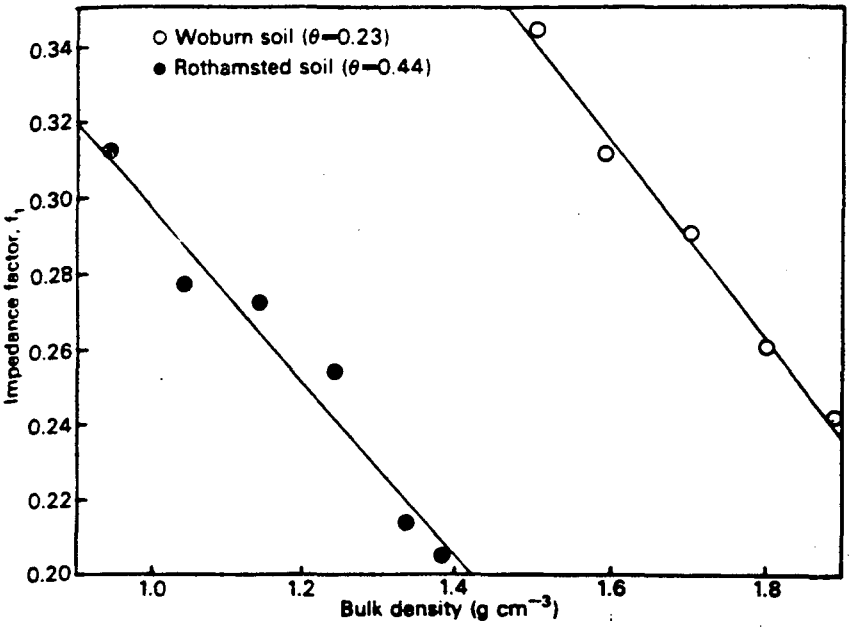

Figure 4.27b Impedance factor, f_1, as a function of bulk density at a constant volumetric water content.

depends on other properties, such as structure and organic matter content. Thus, diffusivities calculated using these functions must be interpreted as highly approximate.

4.5.2 Results

Table 4.3 summarizes the calculations involved in solving equation (4.14) for both plots and for two seasons for each plot. In general, the concentration of chloride at the lower boundary of the surface soil element is not known exactly; however, based on profile samples, the concentration at a 15 cm depth will be only slightly lower than at a 10 cm depth (see Figs.4.4, 4.24, 4.25). Therefore, chloride concentrations as measured in the 15 cm soil water samplers are used for this calculation. Due to very low soil pressure potentials during the summer and fall of 1988, it was possible to collect only one sample in each plot from the 15 cm sampler. The concentration of chloride in this sample is used for the entire season. In the spring and early summer of 1989, it was possible to collect samples in plot 9BE until late May, and in plot 8EP until late April. For the remainder of this season, concentrations were extrapolated from previous trends. Δz for the calculation of term 2 was taken as 10 cm - approximately the distance from the middle of the near-surface interval to the 15 cm sampler. $q_{w,evap}$, as calculated with or without term 2, is within the range of bare soil evaporation rates measured in the field using microlysimeters. This is an encouraging result, considering the spatial variability of parameters involved. All measured values used in the calculation of Table 4.3 are mean values of samples collected on the given day in each plot, with the exception of the mass of solid which is an average of all measurements within each season; this was done to avoid error due to small differences in solid mass, although this averaging did not make a significant difference in seasonal averages. The effect of spatial variability is apparent in the monthly values of $q_{w,evap}$ calculated using this approach. For example, in plot 8EP, during the fall season, $q_{w,evap}$ between 8/25/88 and 9/29/88 was calculated to be 0.19 mm/day (0.01 mm/day if

Table 4.3a Calculation of Bare Soil Evaporation Based on Chloride Fluxes and Changes in Moisture Content: Plot 8EP

Plot 8EP

Date	Days	Bulk Density (g/cm3)	Mean [Cl] at 5 cm (g/m3)	Mass of Solid (g)	Theta Grav	Theta Vol	Δt (days)	[Cl] at 15 cm (g/m3)	ΔM Cl (g)	Effective Diffusivity (m2/s)	Term 1 (mm/day)	Term 2 (mm/day)	Term 3 (mm/day)	*q evap w/o diff (mm/day)*	*q evap w/diff (mm/day)*
7/1/88	1	1.38	46200	249.6	0.204	0.282		15000							
7/29/88	29	1.34	66500	249.6	0.160	0.214	28	15000	0.38	1.1E-10	0.39	0.27	-0.19	0.59	0.86
8/25/88	56	1.31	91800	249.6	0.133	0.174	27	15000	0.27	5.7E-11	0.41	0.21	-0.12	0.54	0.75
9/29/88	91	1.34	93900	249.6	0.130	0.174	35	15000	0.06	4.0E-11	0.00	0.18	-0.01	0.01	0.19
10/25/88	117	1.38	127400	249.6	0.116	0.160	26	15000	0.69	3.5E-11	0.72	0.19	-0.07	0.78	0.98
Average Seasonal Rates >>>>											0.35	0.21	-0.09	0.45	0.66
3/17/89	1	1.35	13500	235.3	0.207	0.279		23700							
4/7/89	22	1.29	19600	235.3	0.191	0.246	21	22000	0.20	1.3E-10	0.23	-0.03	-0.09	0.31	0.28
4/28/89	43	1.27	27500	235.3	0.165	0.210	21	19500	0.15	9.1E-11	0.21	0.01	-0.14	0.35	0.36
5/24/89	70	1.21	41500	235.3	0.133	0.161	27	17000	0.19	4.9E-11	0.24	0.04	-0.14	0.37	0.41
6/26/89	102	1.25	54600	235.3	0.130	0.163	32	15000	0.39	3.1E-11	0.35	0.05	-0.01	0.37	0.42
Average Seasonal Rates >>>>											0.27	0.02	-0.09	0.36	0.38

Table 4.3b Calculation of Bare Soil Evaporation Based on Chloride Fluxes and Changes in Moisture Content: Plot 9BE

Plot 9BE

Date	Days	Bulk Density (g/cm3)	Mean [Cl] at 5 cm (g/m3)	Mass of Solid (g)	Theta Grav	Theta Vol	Δt (days)	[Cl] at 15 cm (g/m3)	ΔM Cl (g)	Effective Diffusivity (m2/s)	Term 1 (mm/day)	Term 2 (mm/day)	Term 3 (mm/day)	*q evap w/o diff (mm/day)*	*q evap w/diff (mm/day)*
6/30/88	1	1.05	29400	178.8	0.318	0.334		6000							
7/29/88	30	1.05	34400	178.8	0.264	0.277	29	6000	-0.16	8.3E-11	-0.46	0.31	-0.16	-0.30	0.01
8/25/88	57	0.99	38400	178.8	0.256	0.253	27	6000	0.22	5.1E-11	0.68	0.22	-0.03	0.70	0.92
9/29/88	92	0.89	45000	178.8	0.248	0.221	35	6000	0.25	3.2E-11	0.59	0.16	-0.02	0.61	0.78
10/25/88	118	0.91	48000	178.8	0.279	0.254	26	6000	0.38	3.2E-11	1.19	0.19	0.11	1.09	1.27
Average Seasonal Rates >>>>											0.48	0.22	-0.03	0.51	0.73
3/17/89	1	0.85	6600	172.5	0.411	0.349		7150							
4/7/89	22	0.91	8000	172.5	0.352	0.320	21	6320	0.01	1.1E-10	0.05	0.01	-0.24	0.29	0.30
4/28/89	43	0.94	12900	172.5	0.335	0.315	21	5920	0.26	9.4E-11	0.99	0.06	-0.07	1.06	1.11
5/24/89	70	0.95	17500	172.5	0.276	0.262	27	5600	0.09	6.8E-11	0.30	0.10	-0.19	0.48	0.57
6/26/89	102	1.01	27500	172.5	0.194	0.196	32	5300	0.06	2.7E-11	0.17	0.07	-0.22	0.39	0.47
Average Seasonal Rates >>>>											0.35	0.06	-0.18	0.53	0.59

diffusion is neglected). However, direct measurements during this period found the rates to average at 0.46 mm/day (S.D. = 0.17). On the other hand, the rate calculated over the following month, 9/29/88 to 10/25/88 was 0.98 mm/day (0.78 mm/day if diffusion neglected), while rates measured directly fell to 0.23 mm/day (S.D. = 0.11). Over the entire season though, the average calculated rates are quite close to directly measured rates. Average seasonal bare soil evaporation rates during the summer and fall of 1988 were calculated as 0.66 mm/day (0.45 mm/day without diffusion) and 0.73 mm/day (0.51 mm/day without diffusion) for plots 8EP and 9BE respectively. During the spring and summer of 1989, the rates were computed to be 0.38 mm/day (0.36 mm/day without diffusion) and 0.59 mm/day (0.53 mm/day without diffusion) for plots 8EP and 9BE respectively (compare with Table 3.3).

4.5.3 Analysis of trend signifcance and errors involved

Due to the relatively high frequency of sampling and spatial variability, it may be expected that changes in the mean concentrations of chloride observed from month to month may not be significant. A *t*-test was used to determine whether differences between mean chloride concentrations were significant. Table 4.4 summarizes the results.

Differences over each season as a whole are significant at the 1% confidence level. The results of the above test suggest that evaporation rates calculated in Table 4.3 should not be trusted at the monthly interval, especially during the summer and fall (1988) season; instead, only seasonal averages should be considered dependable.

It is important to know the cumulative error involved in the flux calculation. This problem will be treated separately for each of the three main terms of Eqn. (4.14), since

they have different amounts of unresolved uncertainty (Table 4.5). Cumulative error was calculated as the square root of the sum of the squares of individual errors (Taylor, 1982).

Table 4.4 Results of *t*-test Performed to Test the Significance of Monthly and Seasonal Chloride Concentration Changes.

Date	Mean [Cl]	Standard Deviation [Cl]	Number of Samples	Significant at 1% error?	Significant at 5% error?
Plot 8EP					
7/1/88	9.33	0.73	5		
7/29/88	10.67	1.25	5	No	Yes
8/25/88	12.03	1.50	8	No	No
9/29/88	12.03	1.73	8	No	No
10/25/88	14.30	2.64	8	No	Yes
3/17/89	2.80	0.53	8	Yes	Yes
4/7/89	3.73	0.49	8	Yes	Yes
4/28/89	4.51	0.65	8	Yes	Yes
5/24/89	5.51	0.58	8	Yes	Yes
6/26/89	7.09	0.94	8	Yes	Yes
Plot 9BE					
6/30/88	9.38	1.62	3		
7/29/88	8.47	1.12	5	No	No
8/25/88	9.71	1.02	8	No	Yes
9/29/88	11.12	1.33	8	No	Yes
10/25/88	13.23	1.85	8	Yes	Yes
3/17/89	2.75	1.00	6	Yes	Yes
4/7/89	2.83	0.63	8	No	No
4/28/89	4.32	1.25	8	Yes	Yes
5/24/89	4.85	2.11	8	No	No
6/26/89	5.21	1.28	8	No	No

Table 4.5 Uncertainties Involved in the Estimation of Water Fluxes Based on Changes in Chloride Concentrations and Moisture Content.

Term	Variable	Error	Cumulative Error
1	Δ Mass of Cl	2.8%	
1,2	[Cl] at 15 cm	(2%)	
1,3	Cross-Sectional Area	3.9%	
1,3	Δt	0	
2	Diffusivity in water	?*	
2	Average Porosity	1.8%	
2	Average Saturation	2.1%	
2	Impedence(Tortuosity)	~50%**	
2	Δ [Cl]	(2.8%)	
2	Δ z	(0)	
3	$\Delta \theta_{grav}$	0.1%	
3	Mass of Solid	0.05%	
3	Density of Water	0	
1	>>>	>>>	5.2%
2	>>>	>>>	~50%
3	>>>	>>>	3.9%

* The error associated with chloride diffusivity in water is dificult to estimate, due to its temperature dependence; however, it will be no greater than the error associated with the impedence (tortuosity) term.

** This "error" is roughly estimated based on the data in Barraclough & Tinker (1981) and Pinner & Nye (1982) and is due to the fact that the relationship between impedence factor and volumetric water content for Kesterson soils is not known.

Note: all other error values are based only on errors involved in the measurement of a variable for an average soil or water sample and do not take into account spatial variability. For values in parentheses, the calculated error is probably negligible compared with uncertainties in the way these variables are defined.

It is quite clear from the above error analysis that Term 2 needs to be treated separately since the uncertainty associated with that term is one order of magnitude greater than for the other two terms. The combined error for terms 1 and 3 results in an uncertainty of approximately 0.02 mm/day for both plots, for both seasons. The uncertainty in Term 2 is at least 0.11 mm/day for both plots during the first season and at least 0.01 mm/day and 0.03 mm/day during the second season for plot 8EP and 9BE, respectively.

5.0 NUMERICAL ANALYSIS

The low rates of bare soil evaporation measured in plots 8EP and 9BE are suggestive of a process dominated by vapor diffusion. This proposition appears to be supported by the analysis presented in Section 3.4. The variation in bare soil evaporation rates was moderately well explained based on two variables which would likely control vapor diffusion: external atmospheric conditions and moisture content. A potentially more quantitative, or at least more physically based, analysis may be made through a numerical simulation of the process, with and without vapor diffusion. Such simulations have been performed using the computer program TRUST, which is described in Section 5.2.1.

5.1 PAST EFFORTS IN NUMERICAL MODELING OF EVAPORATION FROM SOIL

As mentioned in Section 3.2, most laboratory studies of bare soil evaporation have been focused on homogeneous, non-saline porous media. Thus, numerical modeling of those experiments has also been limited to this fairly simple system. Some of the first attempts at *analytical* modeling of such systems under steady-state conditions came from Gardner (Gardner, 1958; Gardner and Fireman, 1958). Through a number of laboratory experiments and modeling, the significance of vapor flow under extremely dry conditions in the presence of a surface mulch was appreciated. When a soil profile is heterogeneous and boundary conditions vary, numerical solutions are far easier to obtain than analytical ones. The difficulty of the solution process increases with increasing soil dryness, in part due to the exceptionally steep potential gradients near the soil surface. The presence of very low potentials in the system demands a good understanding of relationships between saturation and conductivity at those low potentials, both of which are extremely difficult to

determine. The drier the system, the more important the above understanding becomes. Therefore, such extreme situations have usually been avoided and systems in which vapor flow is significant have not been routinely modelled. In addition, until recently (e.g. Passerat de Silans and others, 1989; to a lesser degree, van Bavel and Hillel, 1976), numerical simulations of bare soil evaporation have been limited to a single phase, isothermal approach.

In general, two distinct input parameters are not only most important in such modeling, but are also most difficult to determine: moisture properties of the porous medium and the upper boundary condition. When soil moisture properties (desaturation curve, conductivity curve) have been well characterized and potential evaporation is kept constant, simulation results have been reasonably good (e.g. Bresler and others, 1969; Staple, 1970, 1971). Commonly, simulations are made for soil systems immediately after or shortly after infiltration of water (as in following a rainfall event or irrigation). In such cases, bare soil evaporation rates are relatively high; simulations are usually carried out to a few hours or a few days after such an event. Simulations of bare soil evaporation over periods of more than 50 days (Nimah and Hanks, 1973) are not common in the literature.

The more pressing problem has been the treatment of the upper boundary condition. In general, two types of approaches have been used. In one, a steady Neumann (constant flow = potential evaporation) condition is applied until the saturation of the surface node falls below an air-dry (residual) saturation; thereafter, the boundary condition is changed to a steady Dirichlet (constant potential) boundary where the potential of the surface node is kept at the value corresponding to residual saturation (Hanks and others, 1969; Staple, 1971). In the other one, bare soil evaporation is calculated using the bulk aerodynamic, or Dalton-type, equation:

$$q_{bs} = C\,F(u)\,(e_s - e_a) \qquad (5.1)$$

where C is a constant which embodies the complex parameter of resistance, F(u) is a function of wind speed, u (dimensions of CF(u) are $[L^2TM^{-1}]$), e_s is the vapor pressure at the soil surface, and e_a is the vapor pressure of the ambient air. In order to calculate e_s, the temperature and relative humidity of the surface element must be known; in an isothermal model, humidity may be calculated from the pressure potential (see Table 3.2).

Staple (1971, 1972) found that while both approaches slightly overestimate actual evaporation rates, the second approach is more accurate in that it continuously corrects for humidity changes in the surface element. When there is no maximum rate assigned, as there is in the first approach, the bare soil evaporation rate may be slightly over-estimated during the early stages of drying; this, however, is not a problem a few hours after soil wetting. In the long run, the two methods gave similar results. Staple's experiments have been simulated using the code TRUST: the results may be found in Appendix II. In general, TRUST was found to be able to simulate the system quite well. In addition, it was found that results are significantly improved with a reduction in the size of the surface element: Staple used a near-surface nodal spacing of either 0.75-cm or 0.188-cm, both of which are too coarse. Similar mesh-size dependences were found by Dane and Mathis (1981), who used nodal spacings as small as 0.00118 cm. Therefore, a zero-volume surface node was used in simulations of bare soil evaporation at Kesterson Reservoir. Refinement of the mesh more than a few centimeters below the soil surface has a negligible effect.

The minimum surface potential of approach 1 may be determined based on ambient atmospheric conditions (Neumann and others, 1975):

$$\psi_S = (RT/Mg) \ln(h) \qquad (5.2)$$

where ψ_S is the pressure potential at the soil surface, R is the universal gas constant, T is absolute temperature, M is the molecular weight of water, g is acceleration due to gravity, and h is relative air humidity. An assumption is made that ambient atmospheric conditions correspond to conditions at the soil surface: this, in general, is not true, but in most cases is a fair approximation, especially when averaged over a daily cycle. This boundary condition was also used to simulate Staple's experiment, without imposing a maximum evaporation rate equal to pan evaporation. Results of these simulations are in Appendix II and are satisfactory, especially in the later stages.

Hillel (1975) simulated bare soil evaporation under diurnally fluctuating external conditions and found that under cyclic conditions, total evaporation tends to be somewhat lower than under steady external conditions. This may be the result of nighttime moisture resorption, and the fact that the soil system is always slightly thermally out of synch with the atmosphere. Bare soil evaporation has also been studied numerically in relation to plant root water uptake (e.g. Nimah and Hanks, 1973; Feddes and others, 1975).

5.2 NUMERICAL ANALYSIS

5.2.1 Numerical Model TRUST

Numerical simulations were performed using the code TRUST, a program for transient and steady state fluid flow in 1-D, 2-D, or 3-D, saturated or unsaturated, deformable media, under isothermal conditions (Narasimhan and others, 1978). The

program can handle heterogeneous media, anisotropic systems, and non-linear boundary conditions. The algorithm is based on the Integral Finite Difference Method (IFDM) (Narasimhan and Witherspoon, 1976), which is a generalization of the finite difference method. In the IFDM, the flow region may be divided into arbitrarily shaped volume elements: in contrast to the finite difference method, in the IFDM one need not specify a global coordinate system. The conservation equation for the IFDM was described in Section 3.1 (Eqn. 3.13). For a given volume element l, which is in contact with neighboring elements m = 1,2, ..., M, Eqn. (3.13) may be discretized as follows:

$$\sum_{m=1}^{M} U_{lm}[(z_m - z_l) + (\bar{\psi}_m - \bar{\psi}_l)] = M_{c,l}\frac{\Delta\psi_l}{\Delta t} \tag{5.3}$$

where z is equal to the elevation of a node, $\bar{\psi}$ is a time averaged pressure potential over the interval Δt, and U_{lm} is the *conductance* of the interface between volume elements l and m and is defined as follows:

$$U_{lm} = \frac{\rho \bar{K}_{lm} \Delta\Gamma_{lm}}{D_{lm}} \tag{5.4}$$

where $\bar{K}_{lm}$ is the mean hydraulic conductivity at the interface, $\Delta\Gamma_{lm}$ is the surface area shared by the two elements, and D_{lm} is the distance between nodal points l and m. A matrix of equations of the format of Eqn (5.3) is solved by one of the several methods available within the code; since problems in this study are one-dimensional, an efficient tridiagonal solver which employs LU decomposition was used (Johnson and Riess, 1977).

5.2.2 Calculation of Internodal Conductances: the Problem of $\bar{K}_{lm}$ Averaging

The use of discretized equations requires the spatial averaging of several parameters. Hydraulic conductivity is one of them and its proper evaluation has been a topic often considered in the literature. In a case in which the conductivity in each of the two neighboring elements is constant, and changes in a stepwise fashion at the interface, a harmonic mean of conductivities is needed to preserve the continuity of flow (Edwards, 1972; Narasimhan, 1975):

$$\bar{K}_{lm} = \frac{K_l K_m (d_{l,m} + d_{m,l})}{K_l d_{m,l} + K_m d_{l,m}} \tag{5.5}$$

However, under transient conditions, where permeability changes as function of pressure potential and time, the use of a harmonic mean may lead to extreme errors (Haverkamp and Vauclin, 1979; Schnabel and Richie, 1984). This problem is especially acute in situations where very steep potential gradients are present, for example in infiltration and evaporation problems. In addition to the harmonic mean, a number of averaging techniques have been evaluated: arithmetic mean, geometric mean, upstream weighted conductance, and the integrated mean (Narasimhan, 1982b; Schnabel and Richie, 1984). Schnabel and Richie found all techniques to satisfactorily simulate infiltration into three different soils, with the exception of the harmonic mean. A comparison of the harmonic and arithmetic mean in a simulation of infiltration was made using TRUST and confirmed the inadequacy of the harmonic mean (see Appendix II). Nevertheless, there is no strong physical argument for the use any of the tested averages. Since the arithmetic mean was found to work well in the simulation of Staple's (1971) experiment, both for infiltration and evaporation, it was used for all simulations of bare soil evaporation at Kesterson Reservoir.

5.2.3 Determination of Conductivity and Saturation Curves for Kesterson Soils

Based on studies by, among others, Hadas and Hillel (1972) and results of simulations using TRUST (see Appendix II), one may conclude that hydraulic properties of soils at depth in the soil profile have very little impact on bare soil evaporation. On the other hand, the hydraulic properties of the surface 5 to 10 cm play a crucial role in the determination of a surface flux. This is at the same time a boon and a bane. For one, the hydraulic properties of material from deeper than 10 or 20 cm could be more easily determined: the saturation of this soil remains quite high year-around (approximately 75% to 100%), which means that the pertinent part of both the saturation and conductivity curves could be determined in the laboratory. On the other hand, the hydraulic properties of near-surface soils are more difficult to determine, for two reasons: (1) soil in the top 5 cm of the profile has a high organic matter content and it is not very well compacted, as a result of which it is very difficult to sample this soil interval while preserving its original structure, and (2) the potentials which are present in this interval in the field are so low (thousands of meters of suction) that their determination in the laboratory would require an amount of effort and time which is beyond the scope of this research. Factors which may often lead to the overestimation of saturated hydraulic conductivity, as pointed out by Tokunaga (1988), such as flow between sample and permeameter walls, and bulk volume changes, are very likely to occur when such measurements are done in near-surface material. Finally, the presence of a salt crust in the top 2 to 3 cm of the soil profile leads to further doubts as to whether hydraulic properties of this soil could be determined in the laboratory.

Since properties of deeper soils do not play a very important role in limiting the evaporation rate, they may be estimated by using semi-empirical equational representations of saturation and conductivity curves without introducing significant error into the

evaporation rate calculation. The expressions which were used for this purpose are ones derived by Campbell (1974, 1985) based on particle-size distribution; they are presented in Appendix I. The expressions require the knowledge of sand (>50μm, ≤2mm), silt (<50μm, >2μm), and clay (<2μm) fractions, dry bulk density of the soil, and the saturated conductivity. Saturated conductivities were measured in the field using a Guelph Permeameter (Reynolds and Elrick, 1985). This method provides data on relatively undisturbed, in-situ soil under unsaturated conditions.

The code TRUST is a single-phase program. In order to indirectly simulate vapor flow, it may be modified by incorporating a "vapor conductivity" into the fluid conductivity. Fluid flow is driven by potential gradients. Under isothermal conditions, humidity gradients in the soil drive vapor flow. Since soil humidity may be calculated from pressure potential (see Table 3.2), a pseudo-two-phase flow may be simulated. The goal is therefore to express a "vapor conductivity" in a form compatible with that used in the simulation of liquid flow. Isothermal vapor flow in one dimension may be described by Fick's law:

$$J_{A,v} = -D_{A,v}\frac{\partial C_{A,v}}{\partial z} \tag{5.6}$$

where $J_{A,v}$ is a mass flux [$ML^{-2}T^{-1}$], $D_{A,v}$ is the diffusivity of water vapor in air [L^2T^{-1}], $C_{A,v}$ is the mass concentration of water vapor in air [ML^{-3}], and $\partial C_{A,v}/\partial z$ [ML^{-4}], is the concentration gradient along the direction of flow, x. In soil, diffusivity will be reduced due to the limited cross-sectional area for flow and increased path tortuosity, and a vapor diffusivity in soil, $D_{S,v}$, may be defined as:

$$D_{S,v} = D_{A,v}\,(1-S)\,n\,\tau_a \tag{5.7}$$

where S, n, and τ_a are liquid saturation, porosity, and air-filled tortuosity factor, respectively. Eqn. (5.6) then becomes:

$$J_{S,v} = -D_{S,v}\frac{\partial C_{S,v}}{\partial z} \tag{5.8}$$

where $C_{S,v}$ is a mass concentration of water vapor in soil air [ML^{-3}]. Dividing the above expression by ρ_w, water density, results in a vapor specific flux, $q_{S,v}$ [LT^{-1}]:

$$q_{S,v} = -D_{S,v}\frac{1}{\rho_w}\frac{\partial C_{S,v}}{\partial z} \tag{5.9}$$

Under isothermal conditions, water vapor concentration, $C_{S,v}$ is equal to the product of a saturation vapor concentration at the given temperature, C_0, and soil relative humidity, h_S. Thus, Eqn. (5.9) becomes:

$$q_{S,v} = -D_{S,v}\frac{1}{\rho_w}C_0\frac{\partial h_S}{\partial z} \tag{5.10}$$

The dependence of soil humidity on water potential is known to be (after Feddes and others, 1974):

$$h_S = \exp\left[\phi_t\frac{Mg}{RT}\right] \tag{5.11}$$

where under very low pressure potentials, potentials other than the pressure potential become negligable, and the following is approximately true:

$$h_S = \exp\left[\psi \frac{Mg}{RT}\right] \tag{5.12}$$

the spatial gradient of humidity may be better represented as follows:

$$\frac{\partial h_S}{\partial z} = \frac{\partial h_S}{\partial \psi}\frac{\partial \psi}{\partial z} \tag{5.13}$$

in order to separate the dependence of soil humidity on pressure potential. Substituting the right hand side of Eqn. (5.13) into Eqn. (5.10) gives:

$$q_{S,v} = -\frac{D_{S,v} C_0}{\rho_w}\left(\frac{\partial h_S}{\partial \psi}\right)\left(\frac{\partial \psi}{\partial z}\right) \tag{5.14}$$

Taking the derivative of h_S with respect to ψ (Eqn. (5.12)) gives the result:

$$\frac{\partial h_S}{\partial \psi} = \frac{\partial}{\partial \psi}\left(\exp\left[\psi \frac{Mg}{RT}\right]\right) = h_S \frac{Mg}{RT} \tag{5.15}$$

Substituting Eqn. (5.15) into Eqn. (5.14),

$$q_{S,v} = -\left\{\frac{D_{S,v} C_0}{\rho_w} h_S \frac{Mg}{RT}\right\}\left(\frac{\partial \psi}{\partial z}\right) \tag{5.16}$$

which is of the desired form, where the bracketed expression is equivalent in dimension to a conductivity [LT^{-1}], and will from here on be defined as a *vapor conductivity*, K_v. A similar result was arrived at by Campbell (1985). Since vapor flux and liquid flux are additive, so are the respective conductivities. Therefore, a total conductivity curve may be calculated. The relative magnitudes of the two conductivities and the total conductivity are

illustrated in Figs. 5.8 and 5.9. Vapor conductivity does not play an important role at suctions of less than a thousand meters and therefore will only be significant in the upper few centimeters. Results of numerical modeling showed that in the given system, only in the top 1cm are pressure potentials low enough for vapor flow to have a significant effect. The result of adding vapor conductivity to liquid conductivity is the presence of a total conductivity "plateau" at pressure heads on the order of thousands to tens of thousands of meters: this is exactly the range of surface potentials created by typical ranges of air humidity and temperatures.

5.2.4 Input Parameters for Numerical Simulation

Input parameters for numerical simulations of one-dimensional flow in plot 8EP were based on both field and laboratory measurements. Particle-size distribution, a parameter necessary to the calculation of conductivity and desaturation curves, as described in Appendix I, was determined using the hydrometer method of Day (1965); the results of this procedure for both plots are presented in Fig. 2.3. Below a depth of 30 cm, 10 cm depth intervals of soil were homogenized for this purpose. Between 10 and 30 cm, 5 cm intervals were used. Soil from the top 10 cm of plot 9BE was analyzed as a single interval. This was done since the top 2-5 cm of that soil is highly organic, a factor which may interfere in the analysis. The same interval from plot 8EP was analyzed as both a single sample and two subsamples: 0-4 cm and 4-9 cm. The results did not differ significantly between these two approaches. The results in Fig. 2.3 are based on a single soil sample per interval, in each plot, except for the surface 10 cm, for which five samples from each plot were analyzed. Particle-size distributions for each of the surface samples in plot 8EP are shown in Fig. 5.1.

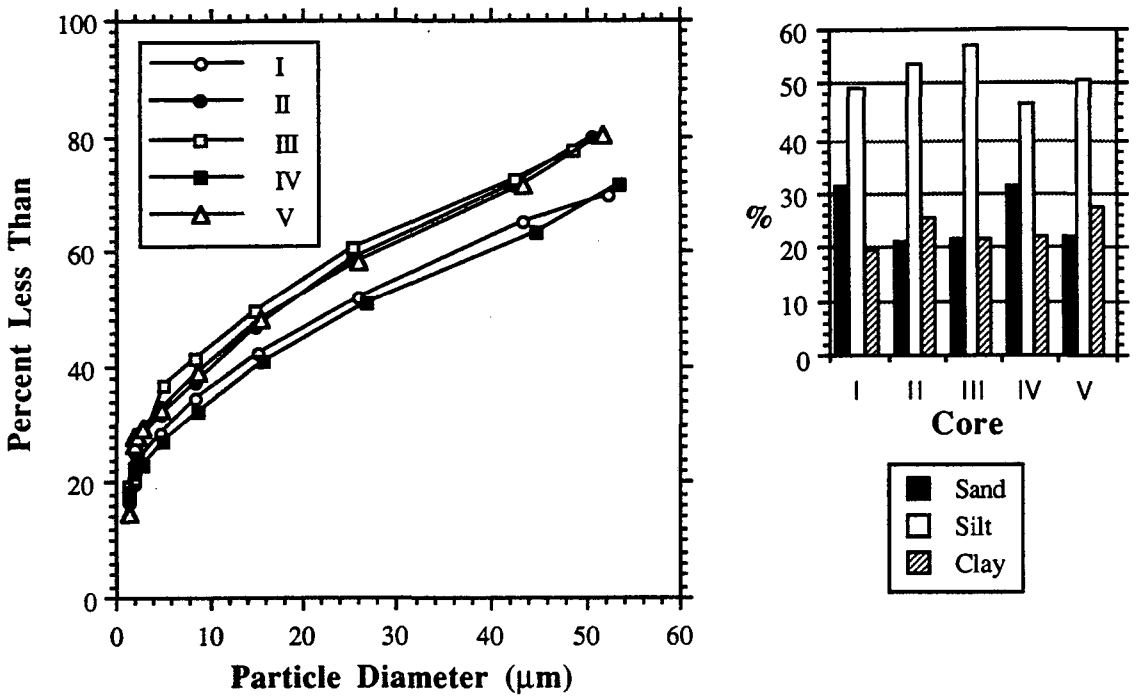

Figure 5.1a Particle-size distribution in five near-surface soil cores (I-V) from plot 8EP: 0 to 4 cm depth.

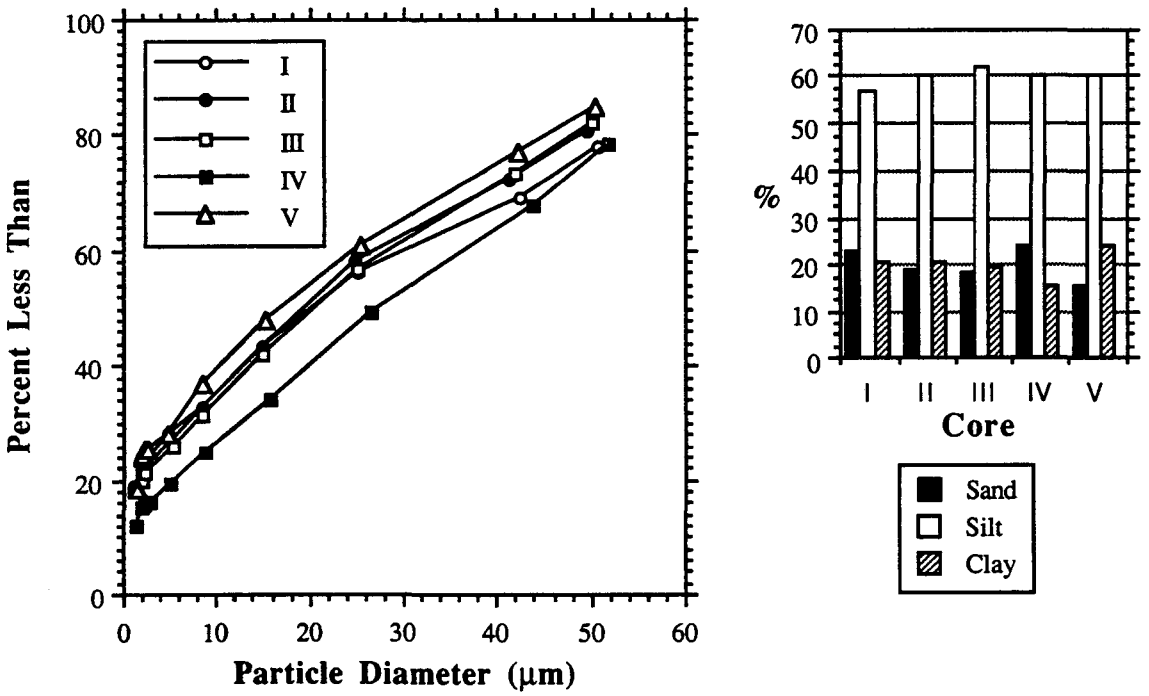

Figure 5.1b Particle-size distribution in five near-surface soil cores (I-V) from plot 8EP: 4 to 9 cm depth.

Dry bulk density was measured for samples between 0 and 20 cm depth. Below that interval, it was difficult to obtain an undamaged core which could be used for a volume measurement; however, the dry bulk density of most unconsolidated loam soils will fall between 1.60 and 1.80 gcm^{-3}, depending on the relative clay content and compaction. This is seen in the fairly rapid increase in bulk density from the loose surface soil to soil at 20 cm depth (Table 5.1). Therefore, the bulk density for all of the soil intervals below 10 cm is assumed to be 1.65 gcm^{-3}, except for a few more clayey intervals (ρ_{bulk} = 1.60 gcm^{-3}) and a few sandier intervals (ρ_{bulk} = 1.75 gcm^{-3}).

Table 5.1 Measured Bulk Densities for Near-Surface Soil at Plot 8EP

Soil Interval	Number of samples	Mean Bulk Density (g cm^{-3})	Std. Deviation (g cm^{-3})
0.0 - 2.5 cm	4	0.73	0.10
2.5 - 5.0 cm	4	1.45	0.08
5.0 - 7.5 cm	5	1.63	0.10
7.5 - 10.0 cm	5	1.60	0.15
10.0 - 15.0 cm	2	1.60	0.04
15.0.- 20.0 cm	1	1.68	–

Saturated conductivities were measured using a Guelph Permeameter (Reynolds and Elrick, 1985). The results for plot 8EP are presented in Fig. 5.2. Measurements were not made below 1.7 m due to the limitation of the tool and the presence of the groundwater table at 1.85 m at the time of measurement. The saturated conductivity of the surface material (2.5 cm) was a free parameter, which was used to fit the simulated evaporation rate to the first data point. When a combined liquid and vapor conductivity was used, this

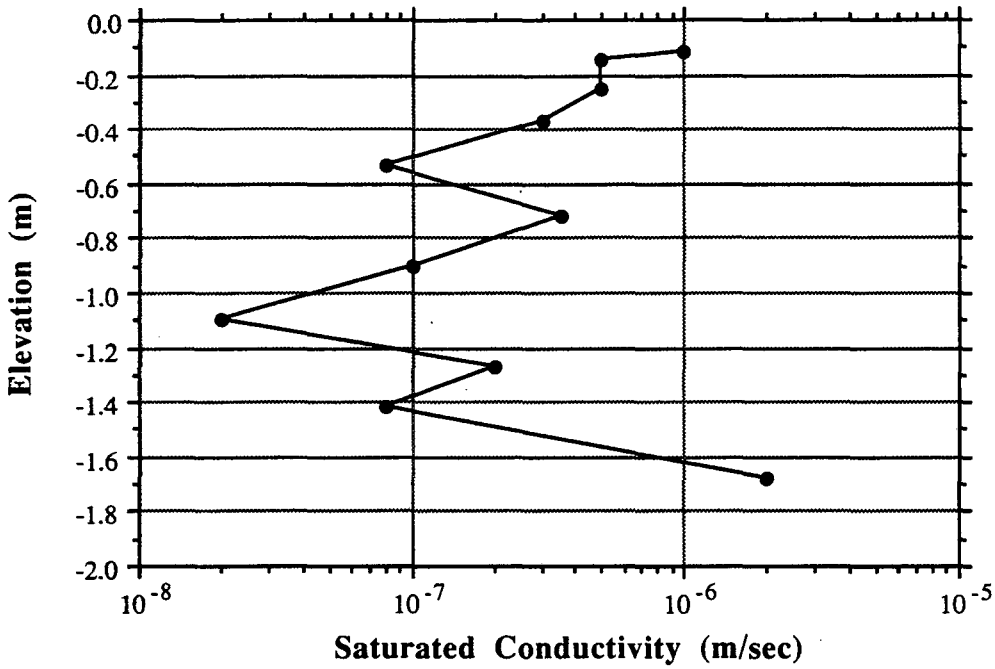

Figure 5.2 Saturated conductivity in plot 8EP profile, as measured using a Guelph Permeameter.

saturated conductivity was determined to be 6.37×10^{-6} ms^{-1} (saturated permeability = 6.5×10^{-13} m^2). When only a liquid conductivity was used, K_{sat} was determined to be 1.23×10^{-5} ms^{-1} ($k_{sat} = 1.25 \times 10^{-12}$ m^2). Once these were calibrated, they were used for the remainder of the simulations.

Based on experience gained in modeling evaporatively driven flow of experiments by Staple (1969, 1971) and Hadas and Hillel (1968, 1972), a mesh with very fine near-surface nodal spacing was designed to be used in the simulation of flow through plot 8EP soil (Fig. 5.3). The mesh was also designed in such a way as to separate sediment of differing texture and hydraulic properties. All properties used in the simulations are summarized in Table 5.2. Also listed there are parameters, calculated from particle-size distribution and bulk density, necessary for the calculation of saturation and conductivity curves based on the approach of Campbell (1974, 1985) (see Appendix I for derivations). The final expressions are as follows:

$$\psi = \psi_{air} (S)^{-b} \tag{5.17}$$

and,

$$K(\psi) = K_{sat}\left(\frac{\psi}{\psi_{air}}\right)^{-(2+3/b)} \tag{5.18}$$

where ψ_{air} is an air-entry pressure based on particle-size distribution and bulk density, S is liquid saturation, and b is a parameter based on particle-size distribution.

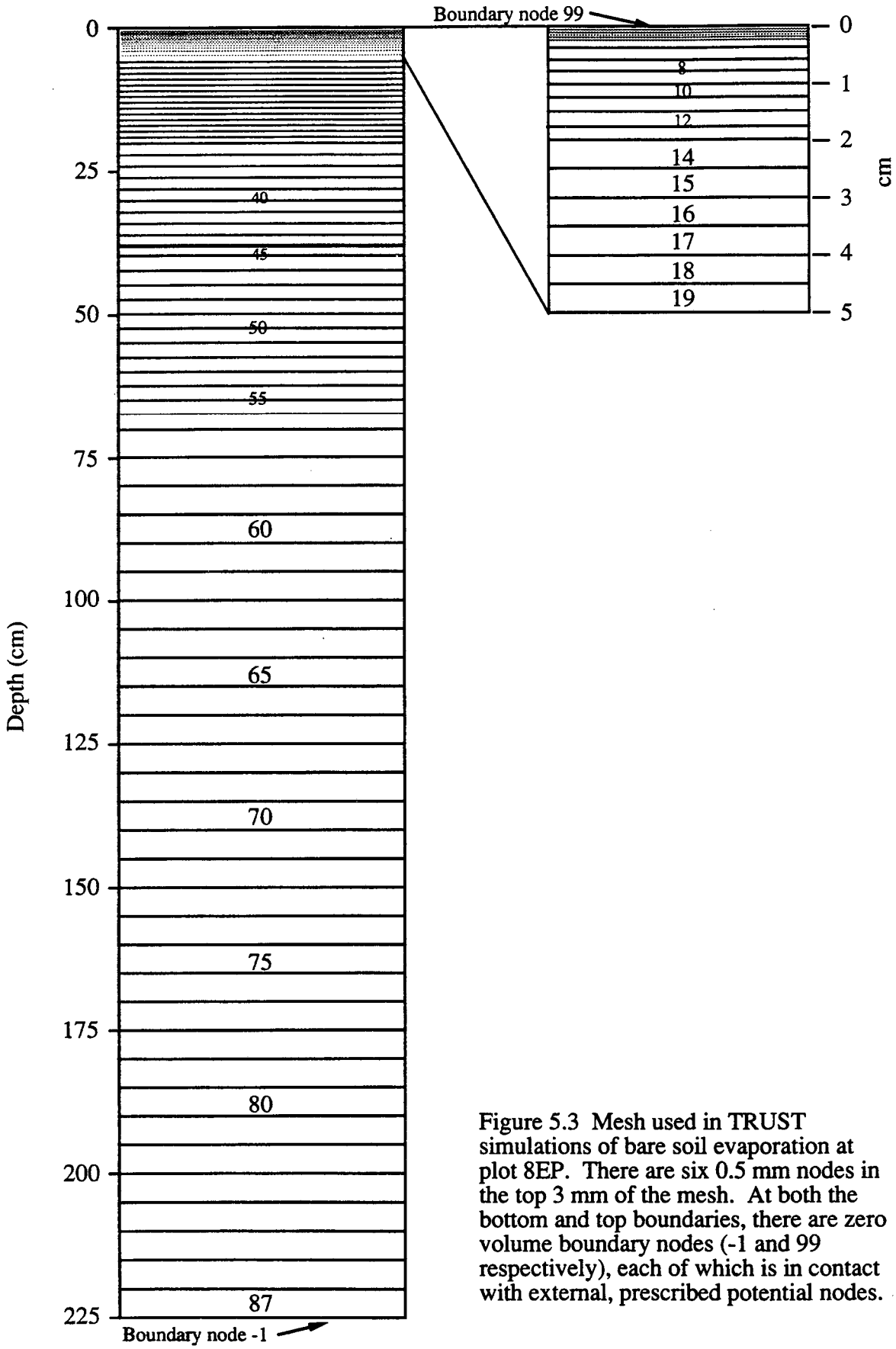

Figure 5.3 Mesh used in TRUST simulations of bare soil evaporation at plot 8EP. There are six 0.5 mm nodes in the top 3 mm of the mesh. At both the bottom and top boundaries, there are zero volume boundary nodes (-1 and 99 respectively), each of which is in contact with external, prescribed potential nodes.

Table 5.2 Input Data for TRUST Simulation of Bare Soil Evaporation at Plot 8EP

Material #	Interval (m)	Sand %	Silt %	Clay %	b	ρ_{bulk} (g/cm3)	ψ_{air} (m)	K_{sat} (m/sec)
1	0.000-0.025	19.5	52.5	28.0	8.9563	0.75	-0.013	6.37E-06
2	0.025-0.050	19.5	52.5	28.0	8.9563	1.40	-0.533	1.47E-06
3	0.05-0.10	19.5	52.5	28.0	8.9563	1.63	-1.329	9.80E-07
4	0.1-0.2	17.5	59.5	23.0	8.3262	1.65	-1.236	5.00E-07
5	0.2-0.3	17.0	61.5	21.5	8.1382	1.65	-1.182	5.00E-07
6	0.3-0.4	25.0	57.0	18.0	7.1984	1.65	-0.829	3.04E-07
7	0.4-0.5	22.0	57.5	20.5	7.7058	1.65	-0.990	9.80E-08
8	0.5-0.6	23.0	53.0	24.0	8.1629	1.65	-1.107	8.43E-08
9	0.6-0.7	22.5	51.0	26.5	8.5624	1.65	-1.240	9.80E-08
10	0.7-1.0	17.0	55.5	27.5	9.0335	1.60	-1.248	1.96E-07
11	1.0-1.2	18.5	57.0	24.5	8.487	1.65	-1.276	6.27E-08
12	1.2-1.4	19.0	59.0	22.0	8.0896	1.65	-1.140	9.80E-08
13	1.4-1.5	17.5	55.0	27.5	9.0016	1.65	-1.482	8.00E-08
14	1.5-1.6	21.0	59.0	20.0	7.6885	1.65	-0.997	1.08E-07
15	1.6-1.7	14.5	64.0	21.5	8.3013	1.65	-1.270	9.80E-08
16	1.7-1.8	16.5	57.5	26.0	8.8373	1.65	-1.435	9.80E-08
17	1.8-1.9	30.0	38.5	31.5	9.0009	1.60	-1.044	9.80E-08
18	1.9-2.0	41.5	30.5	28.0	8.0702	1.60	-0.702	1.96E-07
19	2.0-2.1	64.0	19.0	17.0	5.4582	1.75	-0.374	7.84E-07
20	2.1-2.2	69.5	16.5	14.0	4.7178	1.75	-0.278	9.80E-07
21	2.2-2.3	74.5	15.5	10.0	3.858	1.75	-0.200	1.96E-06

The lower boundary was kept at a constant potential, corresponding to the depth of the water table. The upper boundary condition was treated in a way similar to method (1) in Section 5.1, except that only the Dirichlet condition was used, whereby a potential calculated from Eqn. (5.2) was used as an external potential. In those simulations which

took into account diurnal fluctuations in humidity and temperature, variations in external potential were an input parameter. Humidity and temperature data for the calculation of the external potential were obtained from a Los Banos weather station (CIMIS System Station No. 56).

Two different sets of initial conditions were used. While Campbell's expression for unsaturated conductivity has been examined by several authors (e.g. Schuh and others, 1984; Saxton and others, 1986; Schuh and Bauder, 1986) and is in general regarded as acceptable, the equation for the saturation curve, has not been scrutinized. Therefore, its reliability must be strongly questioned and a transient simulation which would encompass the entire seasonal cycle was not performed. While being an approximation, a steady-state simulation was considered less ambiguous. For the purpose of a steady-state simulation, the initial conditions were chosen to be a fully saturated soil profile and an upper boundary condition equal to the average potential for the day of interest. When inflow through the lower boundary was equal to the evaporation at the upper boundary, the system was considered to be at steady-state. In order to test whether diurnal fluctuations in the external potential affect the average daily evaporation rate, a series of 24-hour, transient simulations was performed, where the initial conditions were set equal to the final conditions of the steady state runs.

5.2.5 Simulation Results and Some Sensitivity Analyses

Bare soil evaporation rates were simulated for each day on which they were measured in the field. There were, in total, eleven such days, five during the late summer and early fall of 1988 and six during the late spring and early summer of 1989. As illustrated in Fig. 5.3, the mesh consisted of 87 volume elements plus two zero-volume boundary nodes. Element size ranged from 5 cm to 0.5 mm, with size decreasing toward

the soil surface. It took 20 to 30 days in order for the system to come to steady-state; the program was taking 60 second time-steps, and the run time on a CDC 8650 was between 25 and 35 minutes CPU. Simulations which used the final conditions of the steady-state runs and ran for the 24-hour period of the field measurement, used only 1 to 2 minutes CPU, while also taking 60 second time steps. It was found that the results of the steady-state/transient modeling (with the exception of one point) were between 2% and 5% less than those of the steady-state simulations, a difference not significant compared with the error involved in bare soil evaporation rate measurement. For the comparison of diffusive vs. non-diffusive evaporation, the steady-state/transient approach was used. As mentioned before, the saturated conductivity of the top material (2.5 cm) was an adjustable parameter, fixed to allow for an exact fit of the first data point. This was done for both the diffusive and the non-diffusive case.

Results of simulations using both approaches are shown in Fig. 5.4. Lines joining both the data points and the simulation results are only for the purpose of differentiation and do not indicate between-point trends. Neither approach was able to satisfactorily simulate field-measured rates. However, the simulations which took into account vapor diffusion (Fig. 5.4b), gave results which, while not always correct in magnitude, followed trends in rates somewhat more closely. In general, in the non-diffusive case, the answer was almost not at all sensitive to variations in surface potential, but instead was highly dependant on the depth to the water table. This was to be expected and is in accord with the concept of a profile-controlled evaporation rate. It needs to be pointed out that the data point on day 261 was collected within 24 hours of a rainfall event and cannot be expected to be well simulated without the application of an appropriate amount of water in the simulation, which was not done (see Section 3.4).

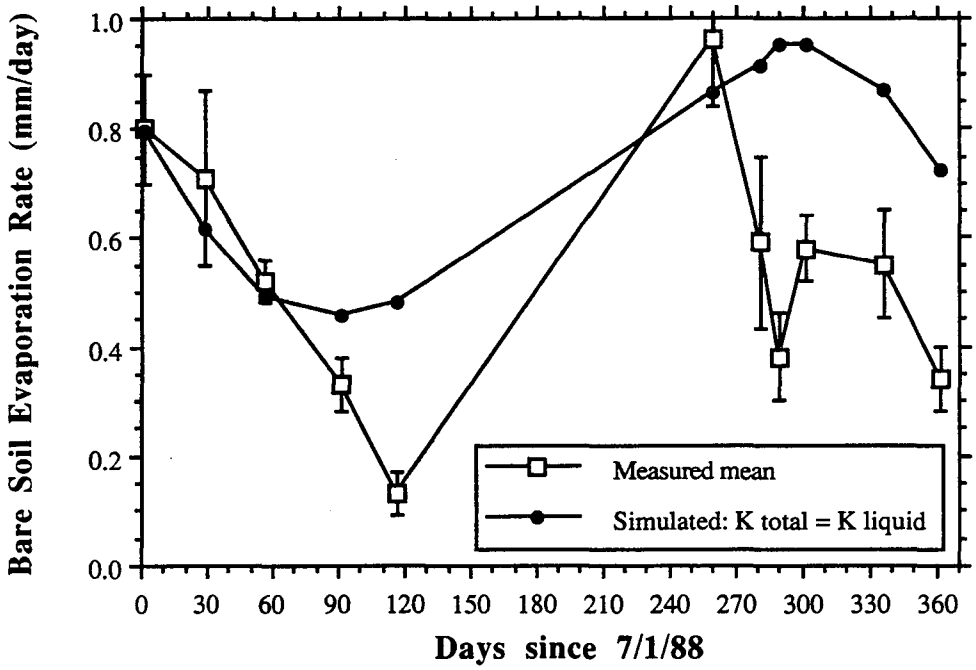

Figure 5.4a Numerically simulated bare soil evaporation rates at plot 8EP compared with actual measured rates; vapor diffusion not taken into account.

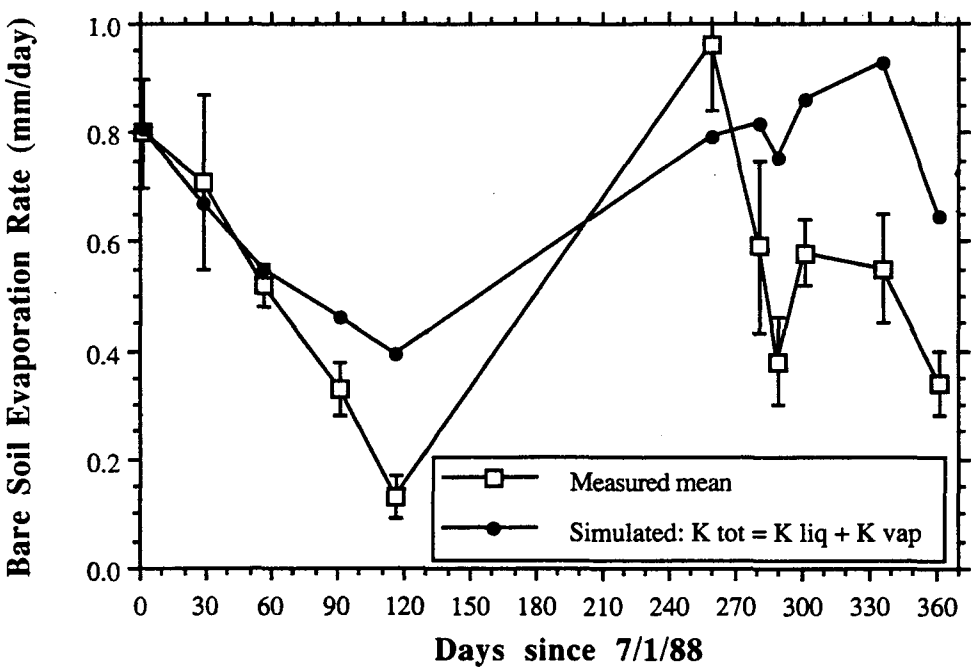

Figure 5.4b Numerically simulated bare soil evaporation rates at plot 8EP compared with actual measured rates; vapor diffusion taken into account.

Due to the coincidence of a falling water table and increasing (progressively less negative) surface potentials during the summer and fall of 1988, the non-diffusive approach gives deceptively good results. In general, the problem of separating the effects of the above two factors, and a third, the drying of the soil surface, renders this analysis somewhat ambiguous. Because of the small improvement in simulation results when vapor diffusion is taken into account, it remains uncertain what fraction of the evaporative flux may be attributed to a diffusive flux.

While this numerical analysis was not meant to serve as a predictive tool, it may be prudent to consider reasons for the mediocrity of simulation results. Sensitivity analyses may shed light on the limitations of these simulations. The greatest unknown and at the same time probably the most significant variables are the hydrologic properties of near-surface soil. This is confirmed by comparing the sensitivity of the evaporation rate to changes in conductivity at depth and near the surface. Reducing the saturated conductivities, and therefore, according to Eqn. (5.18), all unsaturated conductivities, of *all* soil intervals below 2.5 cm by one-half resulted in a decline in bare soil evaporation of only 6% (at a depth to water table of 1.80 m). A reduction by one order of magnitude, resulted in an evaporation rate decline of only 31%. On the other hand, a reduction of the conductivity of the surface 2.5 cm of soil by one-half resulted in an evaporation rate decline of 42% (see Fig. 5.5a); a reduction by one order of magnitude, however, resulted in a rate decline of 50% and from the shape of the curve in Fig. 5.5a it appears that rate will not decline much further. This is due to the dominance of vapor diffusion and the vapor conductivity term which was not varied in this simulation and underscores the fact that at the lower limit, bare soil evaporation rate is governed by vapor diffusion.

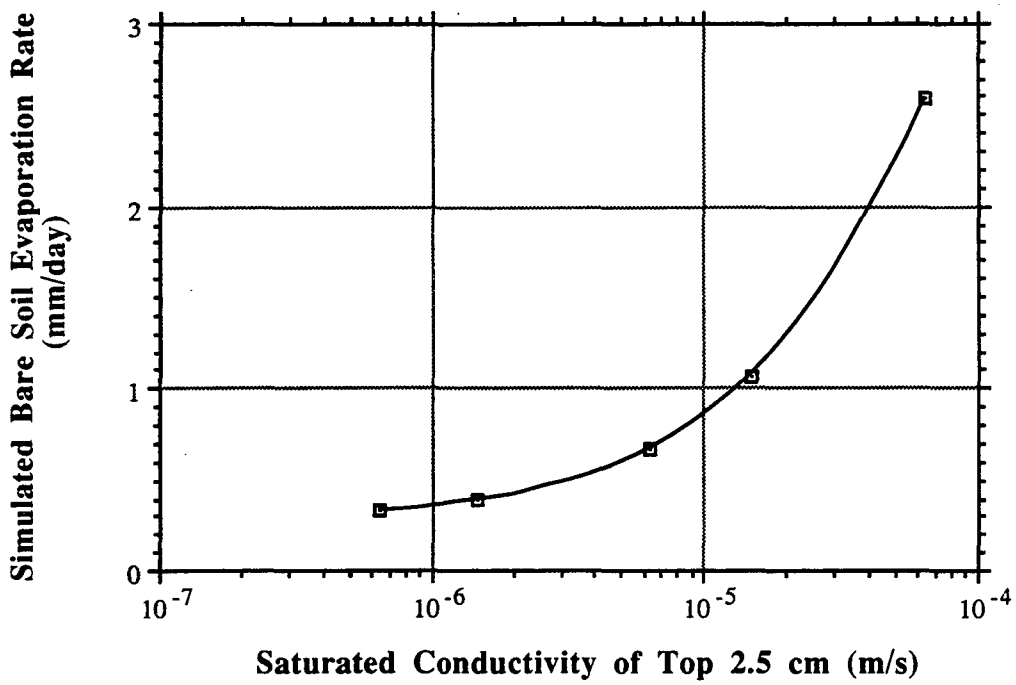

Figure 5.5a Dependence of simulated bare soil evaporation rate on the saturated conductivity of the top 2.5 cm of soil at plot 8EP.

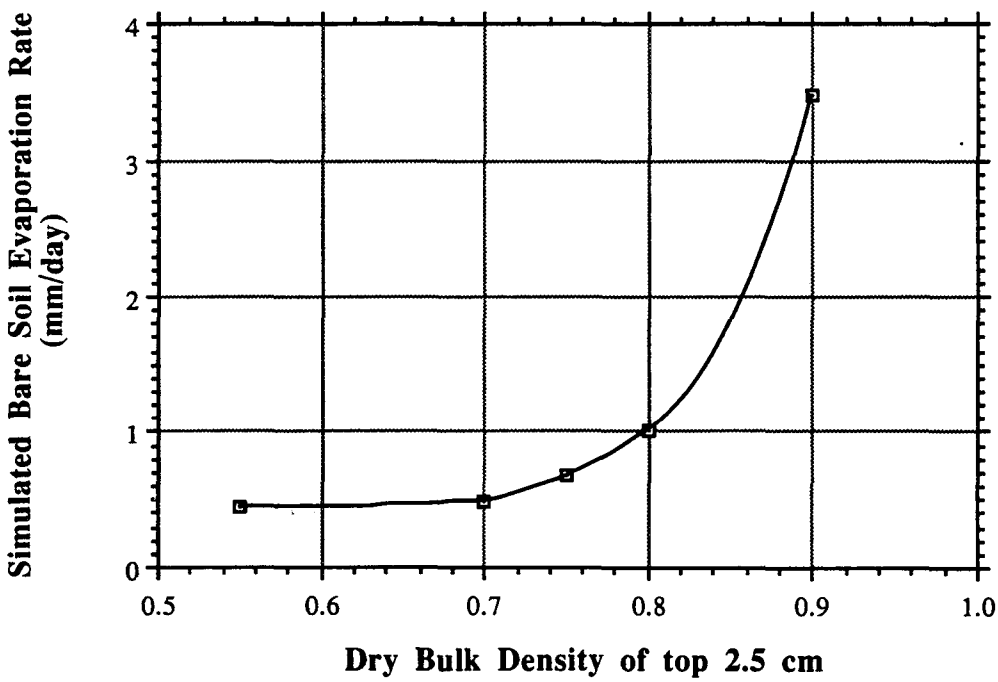

Figure 5.5b Dependence of simulated bare soil evaporation rate on the dry bulk density of the top 2.5 cm of soil at plot 8EP.

Along with the magnitude of the conductivity curve of the near-surface soil, the shape of that curve, along with the shape of the saturation curve are unknown. Since both curves are based on, in these simulations, particle-size distribution and bulk density, changing either or both of those variables will result in a change in the shape of each curve. Fig. 5.5b presents the results of varying the bulk density (and porosity) of the top 2.5 cm of soil. As in the case of varying the saturated conductivity (Fig. 5.5a), the evaporation rate plateaus at about 0.4 mm/day at a bulk density below 0.70 gcm^{-3}, but becomes quite high at a bulk density of 0.90 gcm^{-3}. Based on measurements in four cores, the mean dry bulk density of this soil interval in plot 8EP is 0.73 gcm^{-3} (S.D. = 0.10 gcm^{-3}). Therefore, a bulk density of 0.90 gcm^{-3} is quite unlikely, as is one of 0.55 gcm^{-3}. In the most likely range of bulk density, evaporation rates vary by approximately 0.6 mm/day. The bulk density of 0.75 gcm^{-3} and the two extreme bulk densities were used to simulate evaporation rates on all eleven days (Figure 5.6a,b). As expected, the difference between the results of simulations employing bulk densities of 0.55 and 0.75 gcm^{-3}, was relatively small, while all rates were approximately four to five times higher when a bulk density of 0.90 gcm^{-3} was used. It appears that, not unlike the non-diffusive simulations of Fig. 5.4a, the rates modeled using the highest bulk density are not very sensitive to external potential changes and more or less reflect changes in depth to the water table. The effects of changing the bulk density on the shape of the desaturation curve are presented in Fig. 5.7a. If vapor diffusion were not taken into account, the total conductivity curve would change as shown in Fig. 5.7b. However, both the liquid conductivity, and to a smaller extent, the vapor conductivity, change with bulk density. This results in a varying influence of vapor conductivity on total conductivity (Fig. 5.8a,b; Fig. 5.9a). When liquid conductivity is increased (e.g., when bulk density goes from 0.75 to 0.90 gcm^{-3}), the range of the total conductivity plateau is decreased, resulting in a decreased significance of vapor

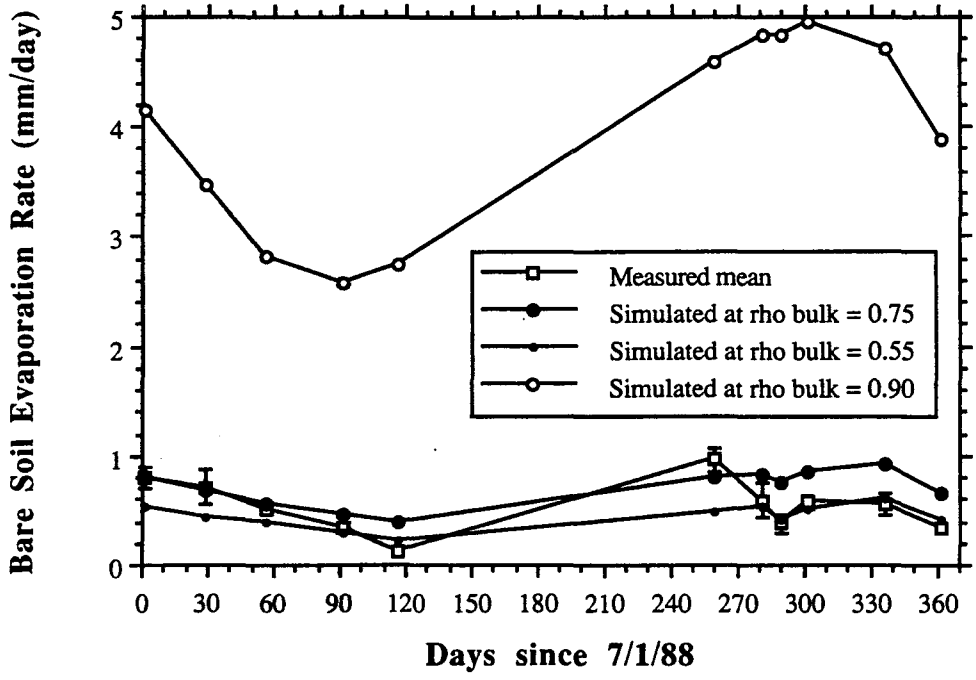

Figure 5.6a Numerically simulated bare soil evaporation rates at plot 8EP at three different dry bulk densities of the top 2.5 cm of soil, compared with measured rates; vapor diffusion taken into account.

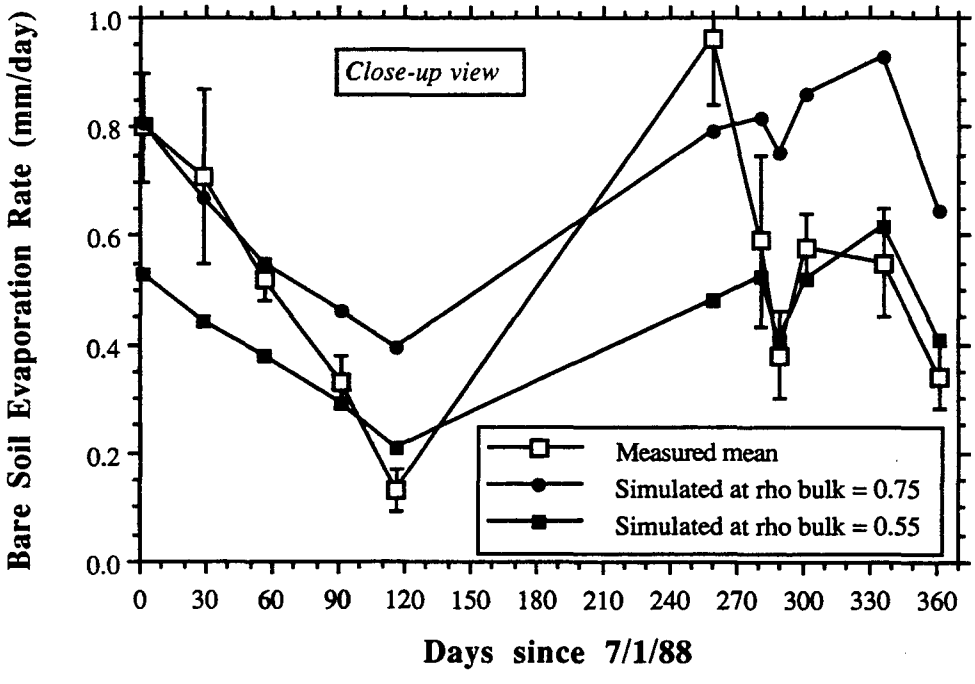

Figure 5.6b Numerically simulated bare soil evaporation rates at plot 8EP at two different dry bulk densities of the top 2.5 cm of soil, compared with measured rates; vapor diffusion taken into account.

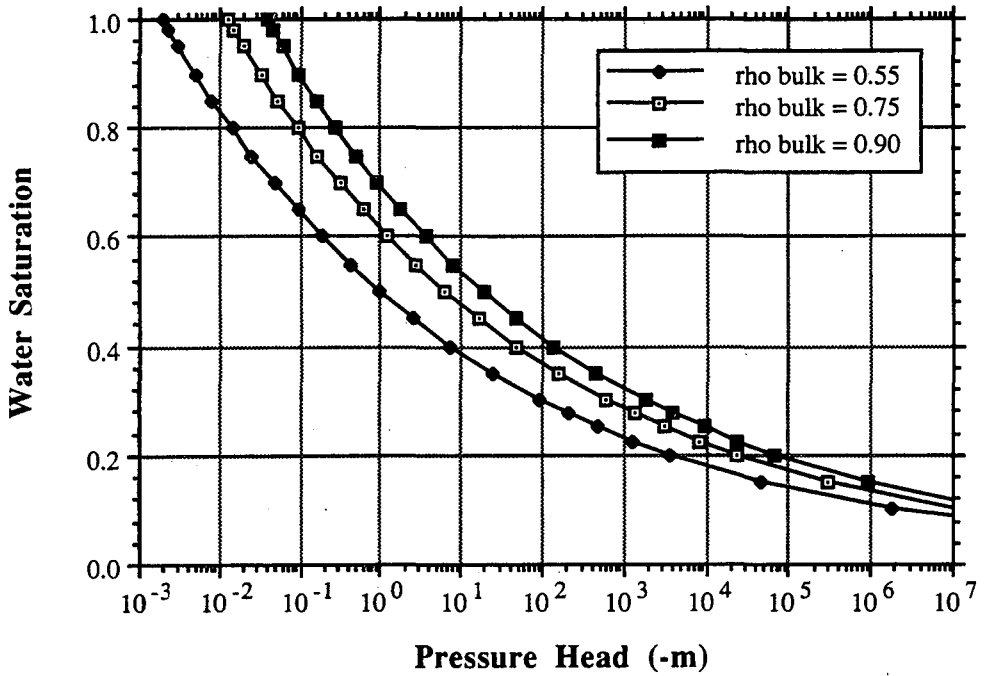

Figure 5.7a Dependence of the shape of the saturation curve on bulk density (material #1).

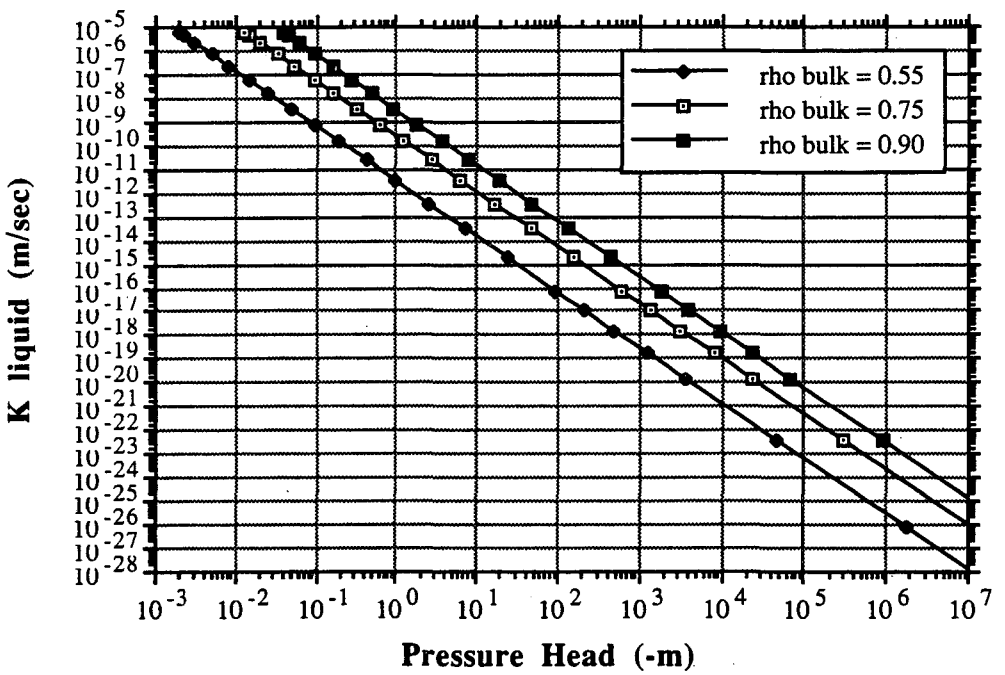

Figure 5.7b Dependence of the shape of the conductivity curve on bulk density (material #1).

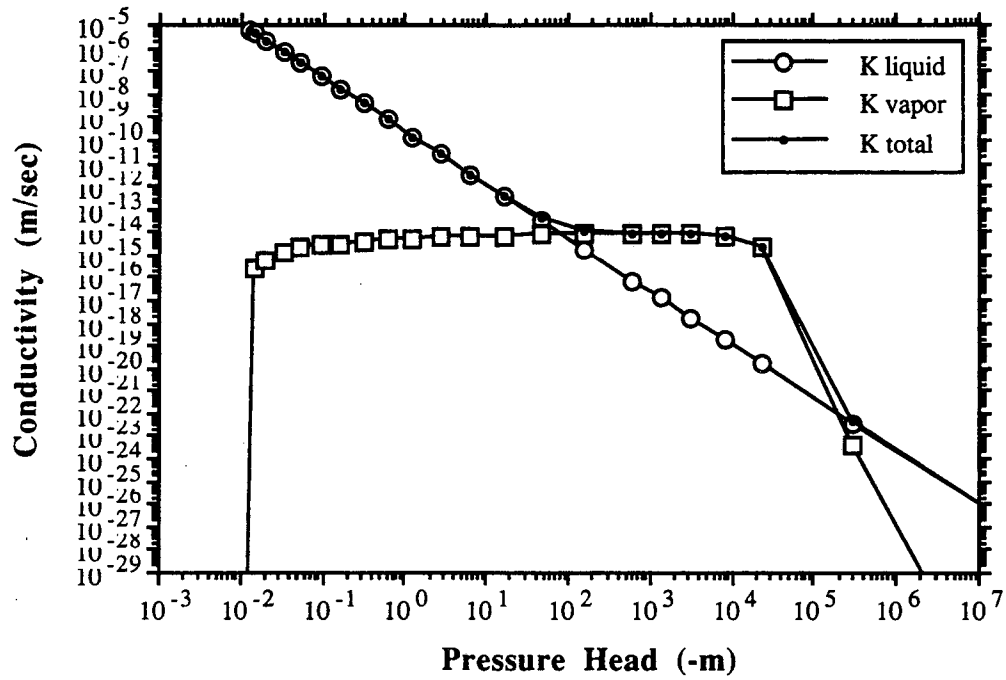

Figure 5.8a Liquid, vapor, and total conductivity curves at a bulk density of 0.75 g/cm3 (material #1).

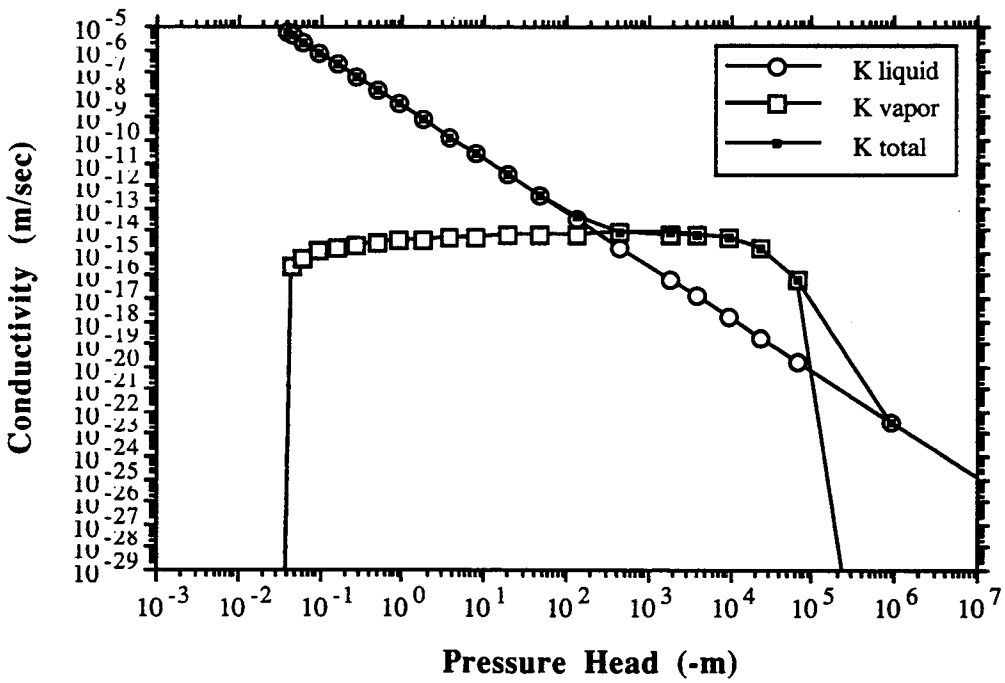

Figure 5.8b Liquid, vapor, and total conductivity curves at a bulk density of 0.90 g/cm3 (material #1).

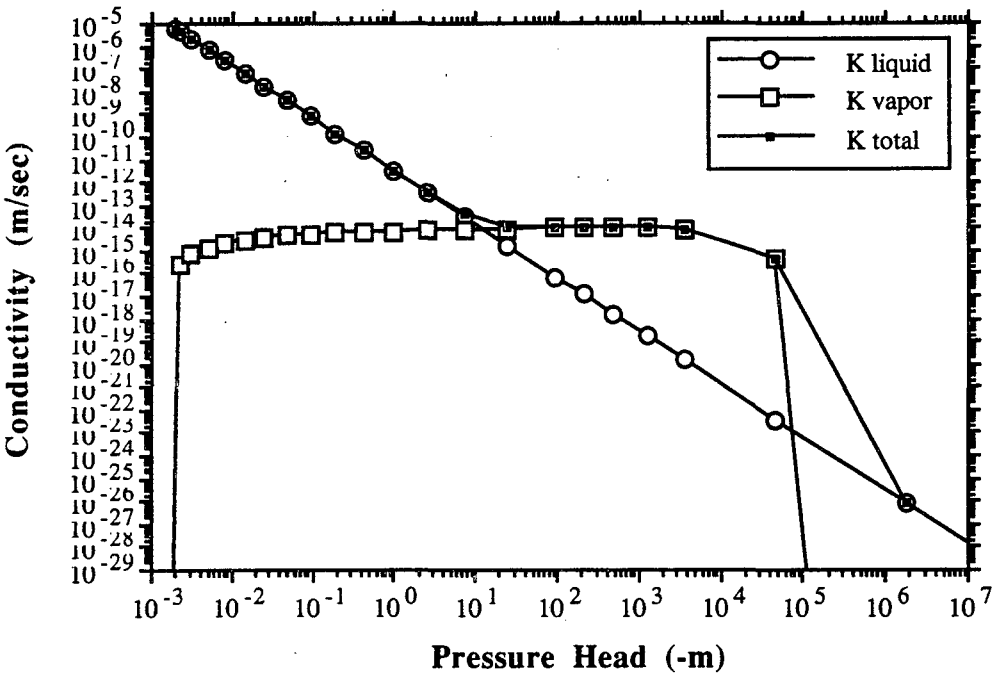

Figure 5.9a Liquid, vapor, and total conductivity curves at a bulk density of 0.55 g/cm3 (material #1).

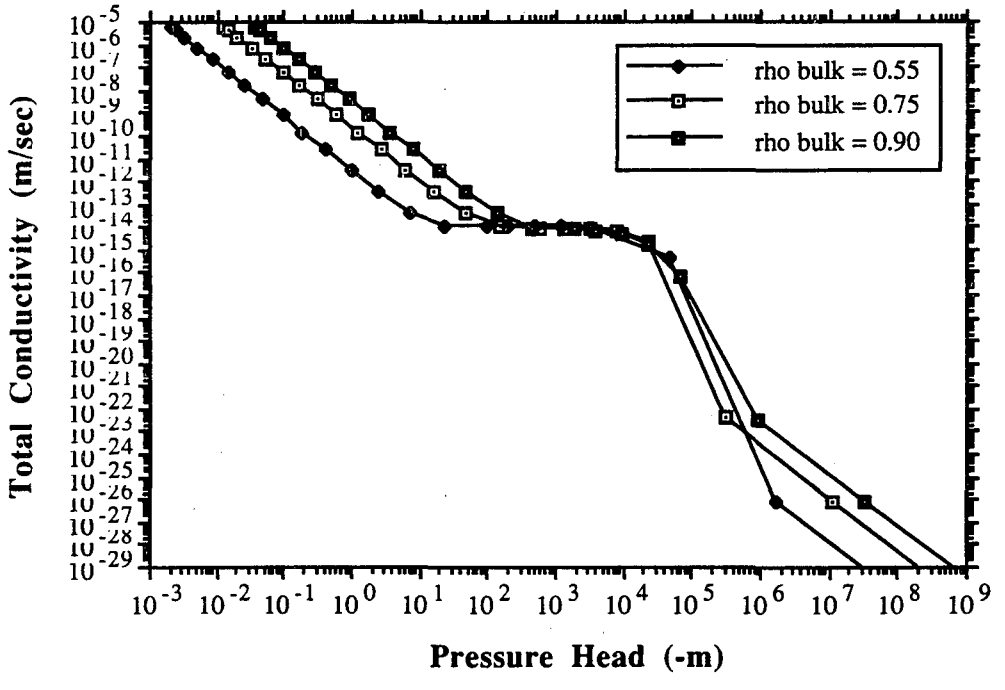

Figure 5.9b Total conductivity curves at three different bulk densities (material #1).

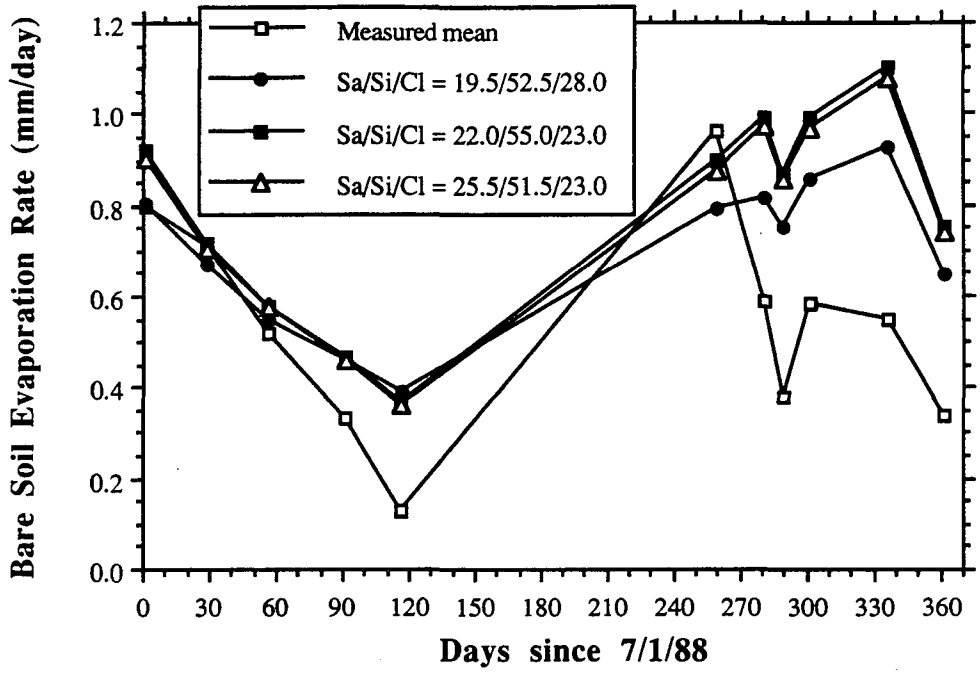

Figure 5.10a Numerically simulated bare soil evaporation rates at plot 8EP at 3 different particle-size distributions in the top 2.5 cm of soil, compared with measured rates; vapor diffusion taken into account.

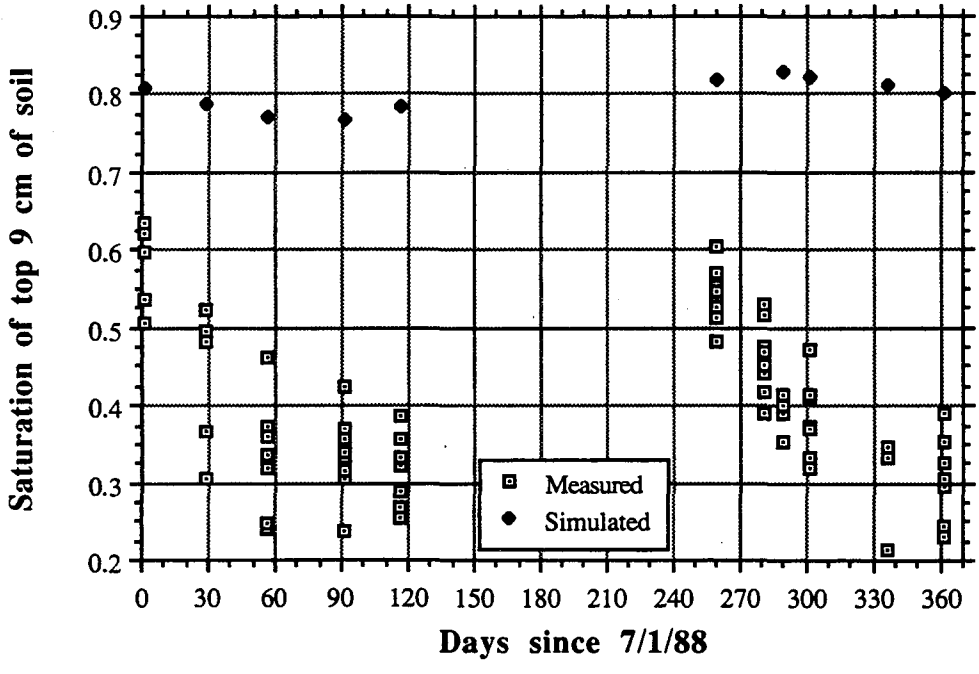

Figure 5.10b Measured and simulated saturation of the top 9 cm of soil in plot 8EP.

conductivity in controling bare soil evaporation. The dependence of total conductivity on bulk density is shown in Fig. 5.9b.

There is a certain range of possible particle-size distributions in the upper soil interval, and the sensitivity of the simulation to this factor was evaluated. The surface textural composition used in all prior simulations was 19.5% sand, 52.5% silt, and 28% clay. Two other compositions were then used, which spanned the range of likely compositions: 22% sand, 55% silt, 23% clay, and, 25.5% sand, 51.5% silt, and 23% clay. The results of these simulations are shown in Fig. 5.10a and indicate very little variation in the predicted rates. The fact that the curves are offset is not critical, since the first point of the original set of simulations was matched to the measured value while the other two sets were not fitted.

Finally, one has to consider the limitations of the expressions used for deriving the conductivity and saturation curves (Eqns. (5.17) and (5.18). These equations have not been tested against actual curves for a soil containing a saline crust. The range of curve shapes which they predict is limited and may not include a realistic shape or magnitude for this material. In fact, at least the saturation curves for materials 1 and 2 and probably 3 are incorrect, as can be seen from the very poor simulation of liquid saturation in the top 9 cm of soil (Fig. 5.10b). Field data indicate a progressive net drying of this interval, while simulations predict small moisture decreases caused by the lowering of the water table; this reinforces the need for a fully transient simulation, but one in which material properties are much better defined. In theory, it is possible to "design" a set of curves for this material in order to match more precisely the results of direct measurements. This, however, was not within the scope of this study and may constitute some future endeavor.

6.0 CONCLUSIONS

Results of direct, physical measurements of bare soil evaporation rates as well as calculations of average rates based on chemical changes in near-surface soil, indicate that the process of bare soil evaporation is very slow at both plots 8EP and 9BE. Directly measured rates in plot 8EP ranged from 0.13 mm/day (S.D. = 0.04) to 0.96 mm/day (S.D. = 0.12); in plot 9BE these rates ranged from 0.32 mm/day (S.D. = 0.05) to 0.99 mm/day (S.D. = 0.31). Based on two data points from each plot, an equation of the following form:

$$E_{bs} = C\, E_{pot}\, \theta^{b}_{grav,9} \qquad (3.18)$$

was fit to solve for a bare soil evaporation rate dependent only on potential evaporation (E_{pot}) and the moisture content of the top 9 cm of soil ($\theta^{b}_{grav,9}$). Overall, the fit was satisfactory and Eqn. (3.18) was used to predict bare soil evaporation rates for both plots over the two seasons when rates were measured. This calculation gave average rates for the summer/fall 1988 season of 0.52 and 0.78 mm/day for plots 8EP and 9BE, respectively, and 0.47 and 0.74 mm/day for the two plots during the spring/summer 1989 season (see Table 3.3). Changes in chemistry were used in the quantitative analysis of soil evaporation rates. By taking into account changes in chloride concentration in the top 9 cm of soil, concentration gradients in soil water, and the net drying out of the 9 cm interval, average seasonal bare soil evaporation rates were estimated for both plots (see Table 4.3). The rates for the first season, for plots 8EP and 9BE, respectively, were between 0.45 and 0.66 mm/day and between 0.51 and 0.73 mm/day, depending on whether chloride diffusion in soil water was taken into account or not. For the second season, the rates were between 0.36 and 0.38 mm/day and between 0.53 and 0.59 mm/day, for plots 8EP and

9BE respectively. These values agree well with those obtained through an extrapolation of directly measured data, although they are somewhat lower during the spring/summer 1989 season. This is probably due to the fact that Eqn. (3.18) overestimates bare soil evaporation rates during the last two months of that season. The reasons for this overestimation are discussed in Section 3.4.1.

The above data support several conclusions. Firstly, either approach was satisfactory in estimating bare soil evaporation rates. While the direct approach is very useful in determining actual rates and their field variability, the indirect approach is probably more effective in calculating average seasonal rates. Used in tandem, these two methods not only provide more information but may also be used to test one anothers accuracy. Since rates measured by both methods agree, one may put more faith in the results.

Secondly, in agreement with the qualitative changes in chloride and selenium concentrations near the soil surface, moisture fluxes due to the low rates of bare soil evaporation are not likely to cause a substantial increase in either salt or selenium concentrations over the next few years. This conclusion is strongly dependent on site-specific properties of the soil surface and soil profile and may not be arbitrarily applicable at other locations at Kesterson Reservoir. It is also dependent on future weather and revegetation patterns. Considering the redistribution of salts and selenium during the twelve months of this study, it is possible that there may be a net decrease of salt concentrations during wetter years. The fate of selenium is controlled by the kinetics of its oxidation reactions and volatilization. However, it may be said with some certainty that over an annual cycle, selenium concentrations are not likely to increase *due to an evaporative flux.*

Thirdly, the results of the quantitative analysis of Section 3.4.1 and numerical modeling of Chapter 5, suggest the importance of external conditions and soil surface conditions in controlling the magnitude of soil evaporation rates in these particular settings. Vapor diffusion may be an important component of this flux. It is likely that the presence of salt and a salt crust near and at the soil surface, has an effect similar to a mulch in limiting bare soil evaporation. This suggests that salt-laden soils may come to a pseudo-steady-state condition (over an annual cycle) under which the further accumulation of salts near the soil surface is limited by the presence of the salts themselves. The unremarkable results of numerical simulations suggest that a better understanding of hydraulic properties of near-surface soils may shed light on the evaporation process from a playa-like environment.

In applying these results to Kesterson Reservoir as a whole, the following conclusions may be made:

- In areas of the Reservoir which are in a similar setting to plots 8EP or 9BE, i.e., highly saline, highly seleniferous, covered by a salt crust, unvegetated or only sparsely vegetated, and not filled with non-native soil, similarly low bare soil evaporation rates may be expected. Those areas which have higher salt concentrations are not likely to become more vegetated very rapidly, thus salt and selenium distributions in the soil profile are not likely to change significantly over the next few years. Areas with lower salt concentrations are likely to become revegetated, which will cause the redistribution of salts and soluble selenium towards the root zone.

- In vegetated areas of the Reservoir, which have not been filled with non-native soil, further increases in salt and selenium concentrations in the root zone are likely; this conclusion is supported by field data collected by T.K. Tokunaga (personal

communication, 1989). Significant evaporative concentration of species near the soil surface is not expected.

- In areas of the Reservoir which have been filled by non-native soil from the Delta-Mendota Canal, movement of salts and selenium into the non-native material is to be expected. Due to the enormous variability in physical properties of this material, it is difficult to estimate the length of time necessary for a reconcentration of species near the surface of the fill sediment. However, due to the relatively non-saline character of this material, bare soil evaporation rates are likely to be limited mostly by profile properties and the distance to the groundwater table.

Finally, all of the above findings may be useful in choosing an appropriate management strategy for Kesterson Reservoir. These data illustrate the inevitability of salt and soluble selenium concentration near the soil surface under unvegetated conditions. They also provide estimates of salt and selenium response to rainfall which may be extended to the likely response to irrigation. The fact that surface concentrations of soluble selenium and salts remained low during the winter due to very sparse precipitation, may suggest that even infrequent irrigation may be sufficient to keep soluble and potentially more biologically available selenium below the soil surface. Furthermore, the physical management of the soil surface may also be designed to minimize salt and selenium accumulation, for example by periodic mulching, which would tend to reduce bare soil evaporation rates in areas not covered by a surface salt crust.

6.1 SUGGESTIONS FOR IMPROVEMENTS IN FIELD AND LABORATORY METHODS.

A number of improvements in field methods could lead to a better understanding of the system. Due to the fairly low evaporative fluxes, changes in salts and selenium concentrations near the soil surface occur very slowly. Therefore, more infrequent, but more intensive sampling may yield better results. Unfortunately, plots from which surface soil is sampled for this type of analysis must be small to overcome spatial variability, but a reduced sampling frequency (e.g. every two months instead of monthly) would allow for an increased sample set within the same plot (e.g. sixteen vs. eight samples.) In order to gain a better understanding of salt and selenium distribution, the top 10 or 15 cm of soil should be divided into smaller intervals (1 to 2 cm), since the greatest changes in concentration occur in this interval. A laboratory method for extracting soil water without dissolving precipitated salts or desorbing adsorbed selenium would be useful in determining the exact concentrations of species moving into the top interval. A higher precision field balance with a better wind-shield could improve the accuracy and precision of the bare soil evaporation rate measurement. Finally, a laboratory column experiment in which external atmospheric conditions could be controlled to mimic changes in field atmospheric conditions would allow for precise and continuous measurements of moisture, salt, and selenium fluxes.

APPENDIX I: DERIVATION OF SATURATION AND CONDUCTIVITY CURVES FROM PARTICLE-SIZE DISTRIBUTION AND BULK DENSITY

Due to the difficulty in the direct laboratory measurement of soil hydraulic properties, researchers have found it necessary to put much effort into the derivation of expressions for the prediction of saturation and conductivity under negative pressure potentials based on soil textural data (e.g. Brooks and Corey, 1964; Campbell, 1974; Clapp and Hornberger, 1978; Gupta and Larson, 1979; Arya and Paris, 1981; Schuh and others, 1984; Schuh and Bauder, 1986). Several of these attempts are summarized by Saxton and others (1986). Most of these studies involved the derivation of linear regression equations of the following form:

$$\theta = a \times \text{sand}(\%) + b \times \text{silt}(\%) + c \times \text{clay}(\%) + d \times \text{organic matter}(\%) + e \times \rho_{bulk}\ (\text{g cm}^{-3}) \quad \text{(AI.1)}$$

where a, b, c, d, and are regression coefficients which vary with pressure potential (Gupta and Larson, 1979). The success of such expressions is usually limited to the soil types on which they were based. Gardner and others (1970) proposed an empirical relationship of the form

$$\psi = a\,\theta^{-b} \quad \text{(AI.2)}$$

Campbell (1974) suggested the potential applicability of an equation of a similar form, which takes into account air entry potential (ψ_{air}) and saturated water content (θ_S):

$$\psi = \psi_{air}\left(\frac{\theta}{\theta_S}\right)^{-b} \qquad \text{or} \qquad \psi = \psi_{air}(S)^{-b} \tag{AI.3}$$

where S is liquid saturation. Campbell (1985) further developed the above expression, and went on to calculate both the air-entry pressure and the exponent b based on particle-size distribution and soil bulk density. Campbell made the following assumptions: (1) $\phi_{p,air}$ becomes more negative with decreasing mean pore diameter, (2) b increases with increasing standard deviation of pore size, and (3) pore size and particle size are correlated. Based on these assumptions and fitting of Eqn. (AI.3) to the data of Hall and others (1977) and Bache and others (1981), the following relationships were derived for soils at a bulk density of 1.3 gcm^{-3}:

$$\psi_{air,std} = -0.5\ d_g^{-0.5} \tag{AI.4}$$

$$b = -2\ \psi_{air,std} + 0.2\ \sigma_g \tag{AI.5}$$

where d_g is the geometric mean particle diameter and σ_g is the geometric standard deviation (from a textural classification developed by Shirazi and Boersma (1984) based on the assumption that particle-size distribution is approximately log-normal):

$$d_g = \exp\left[\ \sum m_i \ln (d_i)\ \right] \tag{AI.6}$$

$$\sigma_g = \exp\left[\ \sum m_i (\ln (d_i))^2 - (\ln (d_g))^2\ \right]^{0.5} \tag{AI.7}$$

where m_i is the mass fraction of each textural class i and d_i is the arithmetic mean diameter of class i. $\psi_{air,std}$ is the air-entry pressure at a bulk density of 1.3 g cm^{-3}. In order to account for variations in bulk density, an empirical correction was derived:

$$\psi_{air} = \psi_{air,std} (\rho_{bulk}/1.3)^{0.67b} \qquad \text{(AI.8)}$$

from which the air-entry pressure required for Eqn. (AI.3) is obtained.

Macroscopic models for saturated and unsaturated conductivity have been proposed by, among others, Childs and Collis-George (1950) and Childs (1969). These methods rely on the knowledge of the saturation curve in order to calculate unsaturated conductivities. Childs (1969) derived the following equation for hydraulic conductivity based on pore-size and pore-size distribution:

$$K = M \int_0^R \int_0^R r^2 F(r)dr \, F(r)dr \qquad \text{(AI.9)}$$

where K is conductivity, r is the pore radius, M is a constant, R is the radius of the largest water-filled pore, and F(r) is the pore-size distribution function, such that:

$$n = \int_0^\infty F(r)dr \qquad \text{(AI.10)}$$

where n is total porosity. Campbell (1974) combined Eqn. (AI.3) with the capillary rise equation:

$$\psi = -\frac{2\gamma}{r} \qquad \text{(AI.11)}$$

where γ is surface tension, which gives:

$$r = -\left(\frac{2\gamma}{\psi}\right)\left(\frac{\theta}{\theta_S}\right)^b \qquad \text{(AI.12)}$$

Through the assumption of cyllindrical pore geometry, $F(r)dr = d\theta$; substituting this and Eqn. (AI.12) into Eqn. (AI.9) and integrating between limits of θ equivalent to limits of r, gives:

$$K = M' \, \theta^{2b+2} \qquad \text{(AI.13)}$$

where M' is the sum of M and other constants and can be calculated at a known pair of K and θ, for example, saturated conductivity and the corresponding, saturated, moisture content, θ_S:

$$M' = K_{sat} / \theta_S^{2b+2} \qquad \text{(AI.14)}$$

and Eqn. (AI.13) becomes:

$$K = K_{sat}\left(\frac{\theta}{\theta_S}\right)^{2b+2} \qquad \text{(AI.15)}$$

Combining the above equation with Eqn. (AI.3) gives a pressure potential dependence of conductivity:

$$K(\psi) = K_{sat}\left(\frac{\psi}{\psi_{air}}\right)^{-(2+2/b)} \qquad \text{(AI.16)}$$

Based on an empirical fit of several soil samples, and justified as the result of "pore interaction" (Jackson, 1972; Campbell, 1974, 1985), the exponent of the potential ratio in the above equation has been modified to give the final result of:

$$K(\psi) = K_{sat}\left(\frac{\psi}{\psi_{air}}\right)^{-(2+3/b)} \qquad \text{(AI.17)}$$

which is also presented in Section 5.2.4 as Eqn. (5.17). The above expression has been compared with other expressions in its ability to predict unsaturated conductivity of various materials (e.g. Campbell 1974; Schuh and others, 1984) and results have mostly been favorable.

APPENDIX II: SIMULATIONS OF INFILTRATION AND EVAPORATION EXPERIMENTS: PROGRAM VALIDATION.

Before the modelling of processes in the unsaturated zone at Kesterson Reservoir was performed, the code TRUST was used to model controlled laboratory experiments, in order to validate its ability to simulate fluid flow problems involving very steep potential gradients and especially problems in which evaporation from the soil surface is a dominant flux. For this purpose, a set of infiltration and evaporation laboratory experiments performed by Staple (1969; 1971) and evaporation experiments from a shallow water table by Hadas and Hillel (1968; 1972) were modelled.

Staple (1969) performed infiltration experiments using three soils, among which was Rideau clay, which was later used for an evaporation experiment. Infiltration and redistribution experiments were performed in brass cylinders 6.25 cm in diameter and 24 to 35 cm in height. Soil was air-dried, passed through a 2 mm sieve, mixed, and mechanically packed to the required density (1.19 gcm^{-3}). Saturation and conductivity curves for the materials were measured using a number of approaches, depending on the pressure potential range. Hysteresis in the conductivity curve was not measured, and while it was measured for the saturation curve, only the wetting part of that curve was used in TRUST simulations; the soil hydraulic properties are shown in Fig. AII.1. Multiple columns under identical conditions were set up, so that a subset could be sectioned at chosen time intervals for moisture content analysis. 3.81 cm (1.5 in) of water was applied to the top of each column of Rideau Clay and allowed to infiltrate; the tops of the columns were covered to prevent evaporation while allowing for air pressure equilibrium with the atmosphere. The moisture distribution in the soil profile after 5 minutes, 1 hour, and 1 day are shown in Fig. AII.2.

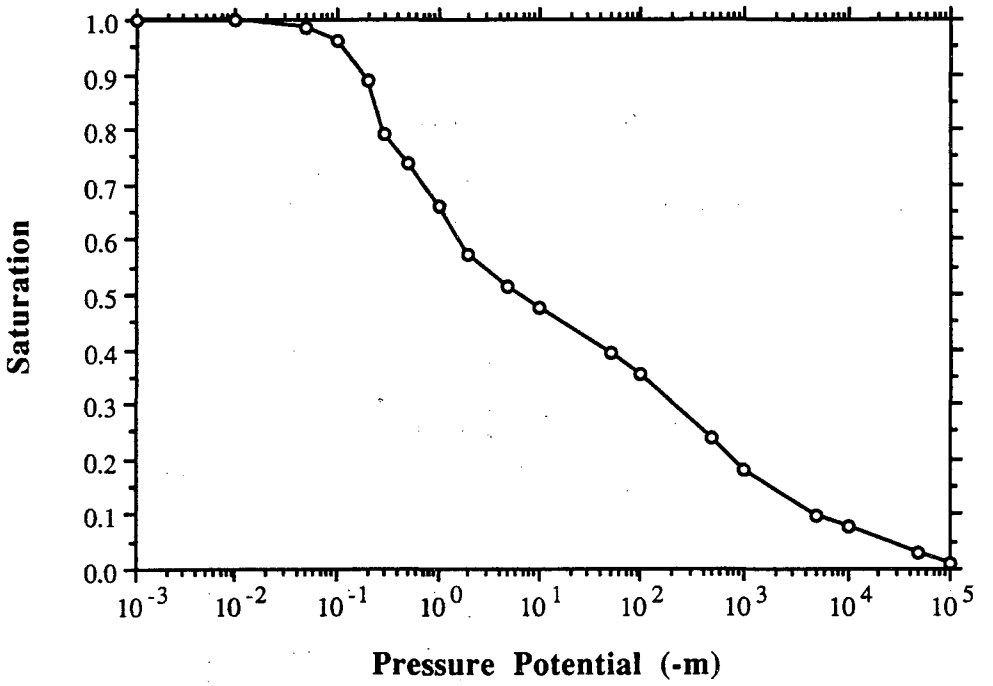

Figure AII.1a Saturation curve for Rideau clay as measured by Staple (1969).

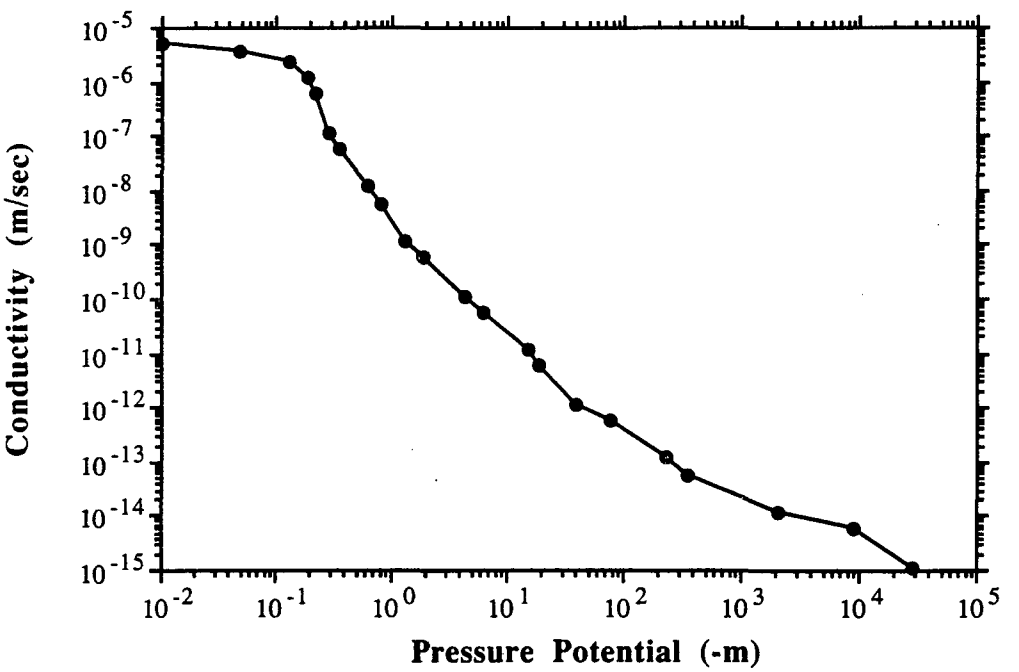

Figure AII.1b Conductivity curve for Rideau clay as measured by Staple (1969).

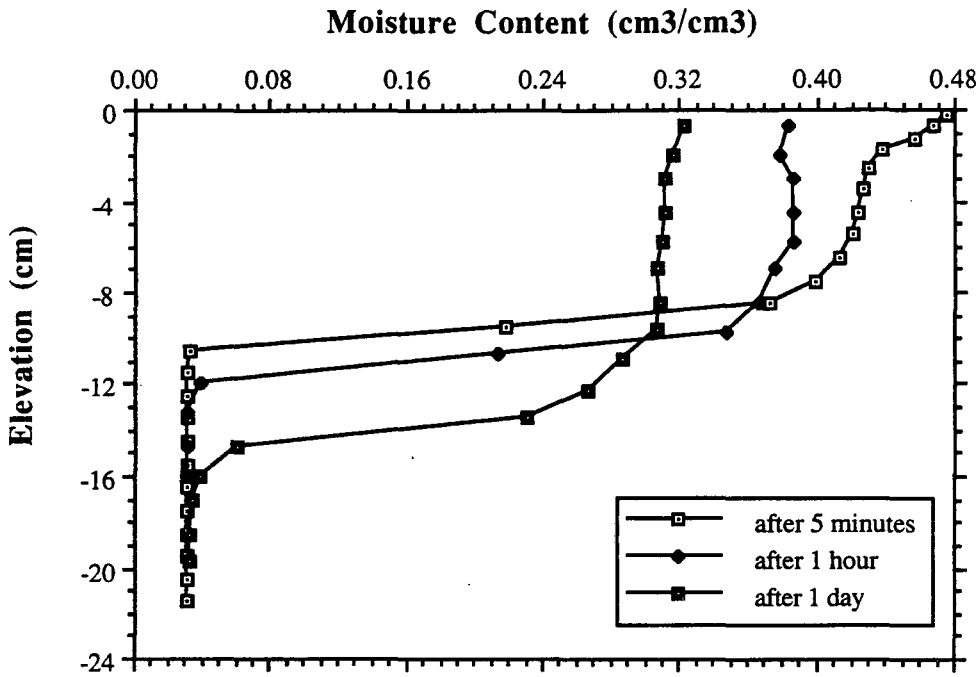

Figure AII.2 Soil moisture redistribution profiles for Rideau Clay after infiltration of 3.81 cm (1.5 in) of water.

In order to simulate the system, a 1-D mesh was set up (Fig. AII.3); the mesh was designed down to a depth of 22 cm so as to assure that the lower boundary condition (no flow) would not affect the flow regime. The upper boundary was also designated as a no flow boundary. Initial conditions were set equal to the 5 minute moisture distribution, shown in Fig. AII.2. The program was then run for 24 hours. At first, a harmonic mean was used to average unsaturated conductivities (see discussion in Section 5.2.2); as found in other studies, this approach was inadequate due to the extremely high potential gradients present during redistribution of an infiltrating front. Therefore, an arithmetic mean was used and this approach gave much better results (Fig. AII.5). In Fig. AII.4, the complete results of this simulation may be found. Due to the rapidity of the infiltration process, 1 second time steps were used, although it was found that using 10 second time steps did not alter the results significantly. The slight inaccuracy of the simulation just above the infiltrating front after 1 day are most likely due to the fact that hysteresis was not taken into account. Overall, the simulation was considered successful.

The same soil properties were used in the simulation of infiltration, redistribution, and evaporation in another experiment by Staple (1971), in which 2.5 cm (1 inch) of water was added to uniformly packed columns of air-dry Rideau clay. The columns were 6.5 cm in diameter and 15 cm in height. Laboratory procedures similar to those in the infiltration/redistribution experiment were used. After infiltration was completed, the soil columns were subjected to a constant potential evaporativity for 31 hours; subsets of cylinders were sectioned after 0, 4, 24, and 31 hours of evaporation in order to determine the soil moisture profile (Fig. AII.4; note: 31 hour results were not given by Staple).

In order to simulate this system and test its sensitivity to mesh dimensions and boundary conditions, three different meshes and two different upper boundary conditions

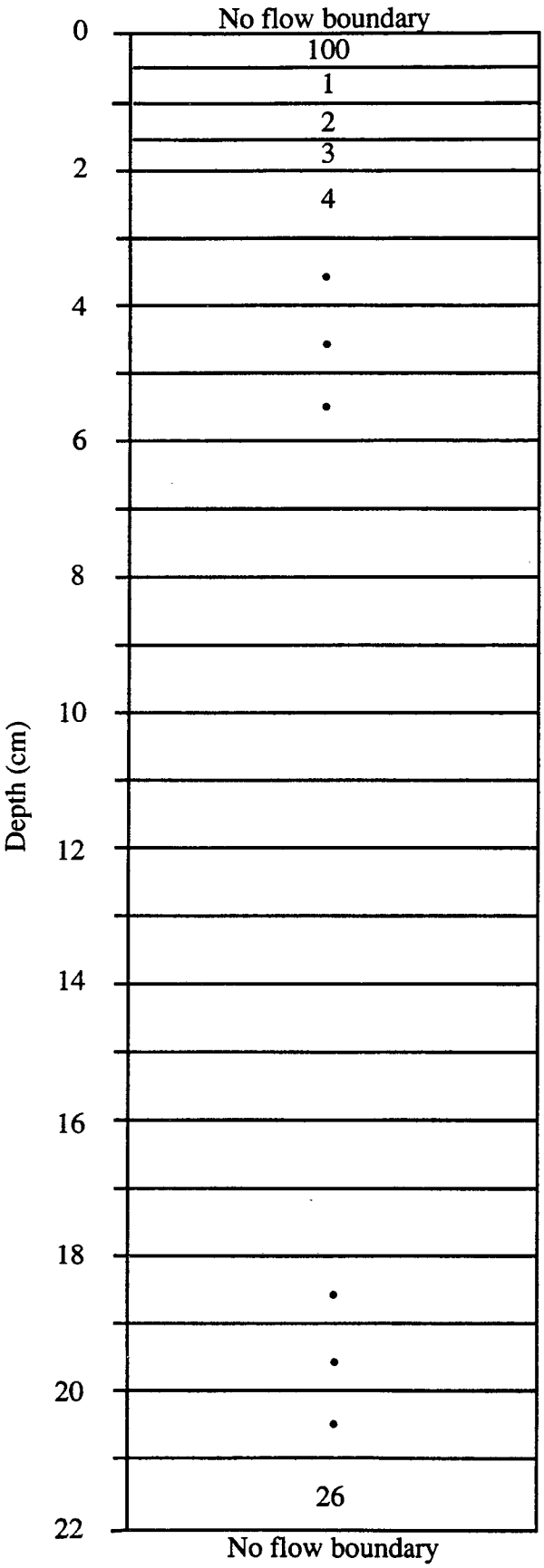

Figure AII.3 1-D mesh for the numerical simulation of redistribution experiment by Staple (1969).

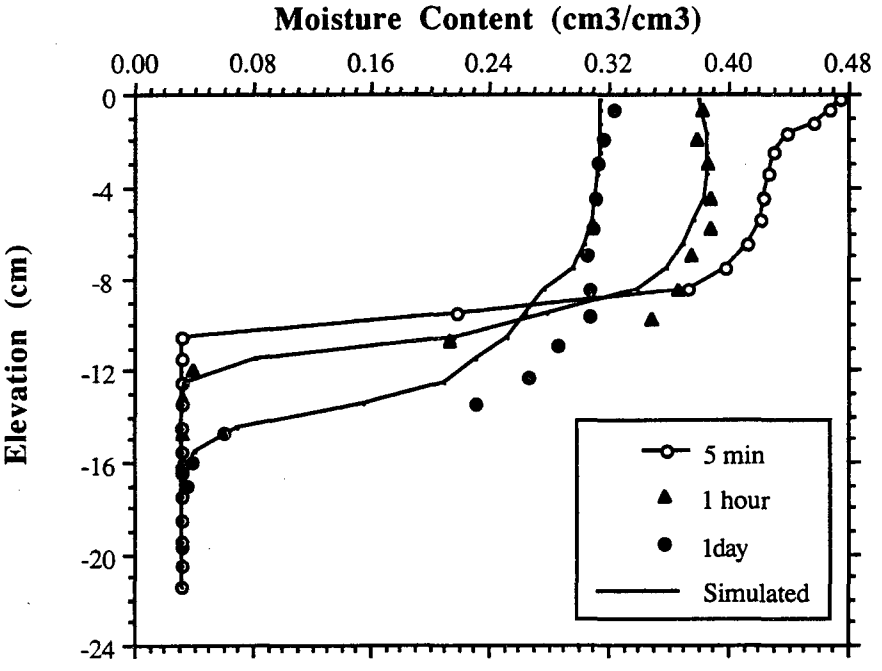

Figure AII.4 Soil moisture redistribution profiles for Rideau Clay after 3.81 cm (1.5 in) of infiltration: actual data (symbols) and simulation results (lines), using arithmetic mean for averaging conductivity.

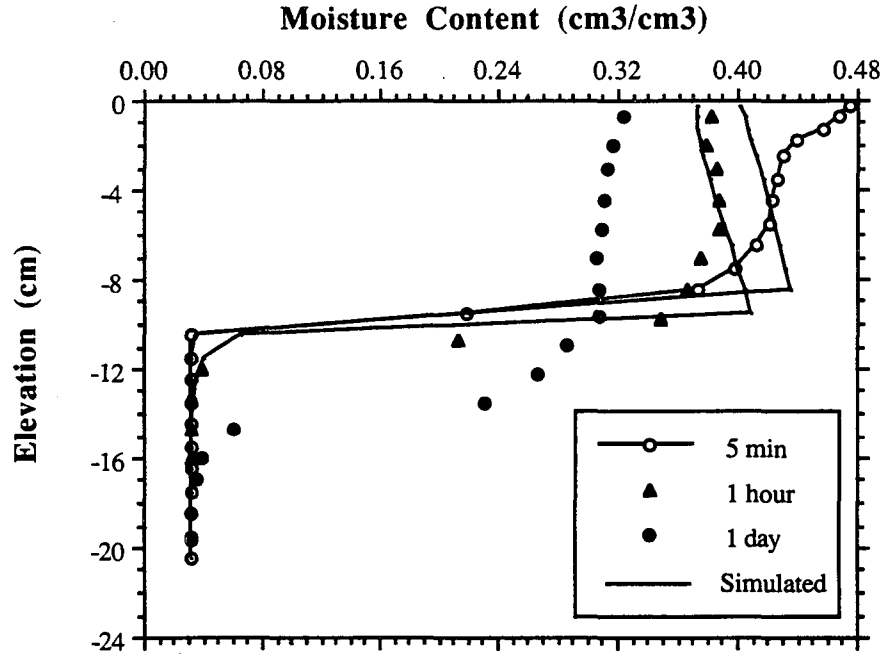

Figure AII.5 Soil moisture redistribution profiles for Rideau Clay after 3.81 cm (1.5 in) of infiltration: actual data (symbols) and simulated results (lines) using harmonic mean for averaging conductivity.

were used; all other parameters were the same as in the infiltration/redistribution experiment. In the "coarse" mesh, thetop element was 2.5 mm thick; in the "medium" mesh, the top element was 1.0 mm thick; in the "fine" mesh, the top element was 0.5 mm thick (see Figs. AII.6,7,8). The first set of simulations was performed with the upper boundary controlled by a sink term equal to or less than potential evaporation. Bare soil evaporation remained equal to potential evaporation as long as the moisture content of the surface element did not fall below an air-dry value as given by Staple (1971) to be 0.03 cm^3cm^{-3}. This value is equivalent to a pressure potential of -13,450 m. The numerical code was modified so that the pressure potential in the surface element was checked after each time step and if it fell below the minimum potential, the evaporation rate would be cut down by 0.1% until the resulting potential was equal to or higher than the minimum potential. The results of these simulations are presented in Figs. AII.9a,b,10a. As can be seen from these figures, all three meshes gave results closely simulating laboratory data; however, mesh refinement near the soil surface markedly improved moisture distribution in the top 3 cm after 31 hours (Fig. 10b). The inaccuracies in the fit at the infiltrating front after 4 hours are again probably due to only the wetting curve being used in the simulation.

Besides its ability to predict moisture distributions, TRUST needed to be able to simulate bare soil evaporation rates. Fig. AII.11 shows the measured cumulative evaporation from the soil core over the 31 hours of the experiment. It also shows the results of simulations using the three different meshes (potential evaporation is designated by a dashed line). The significance of mesh refinement is apparent from this figure; using the coarse mesh resulted in serious overestimation of the evaporation rate.

The medium mesh was used to test the sensitivity of the system to the minimum potential prescribed to the surface element. The data, presented in Figure AII.12, suggest that at early stages of drying the system is not very sensitive to this parameter.

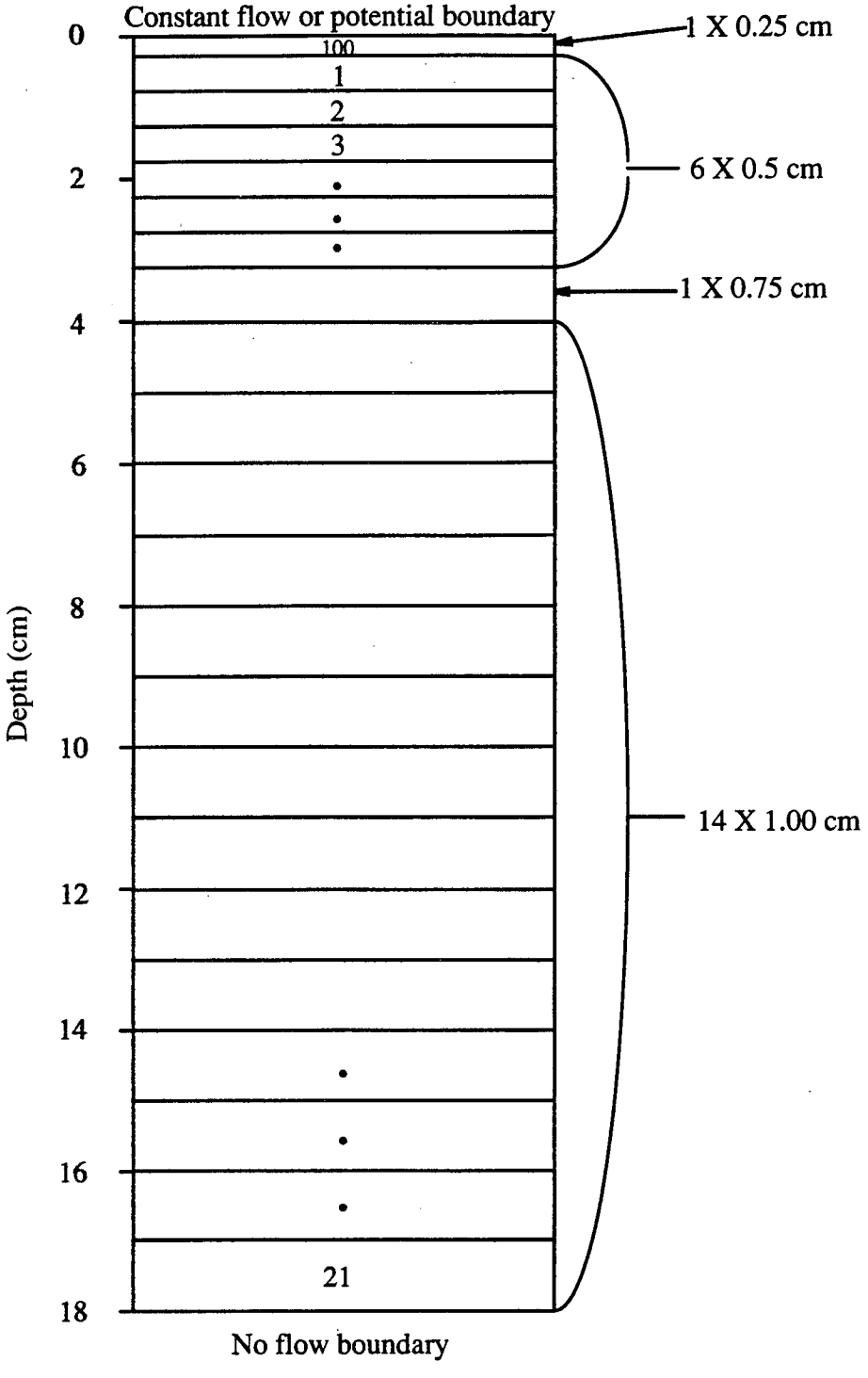

Figure AII.6 "Coarse" 1-D mesh for the numerical simulation of redistribution/evaporation experiment by Staple (1971). Both a constant potential and sink boundary conditions at the soil surface were used in the simulations.

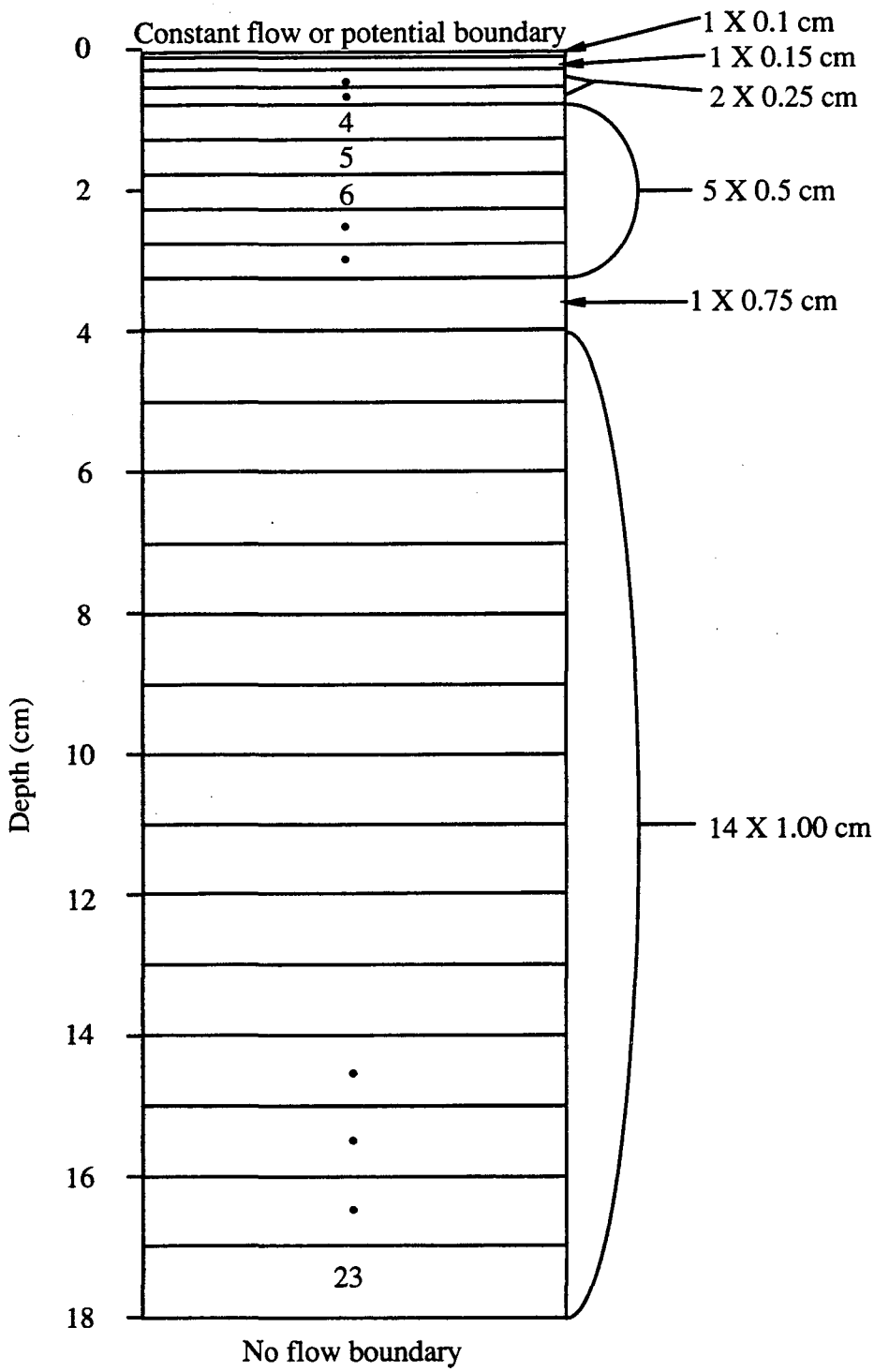

Figure AII.7 "Medium" 1-D mesh for the numerical simulation of redistribution/evaporation experiment by Staple (1971). Both a constant potential and sink boundary conditions at the soil surface were used in the simulations.

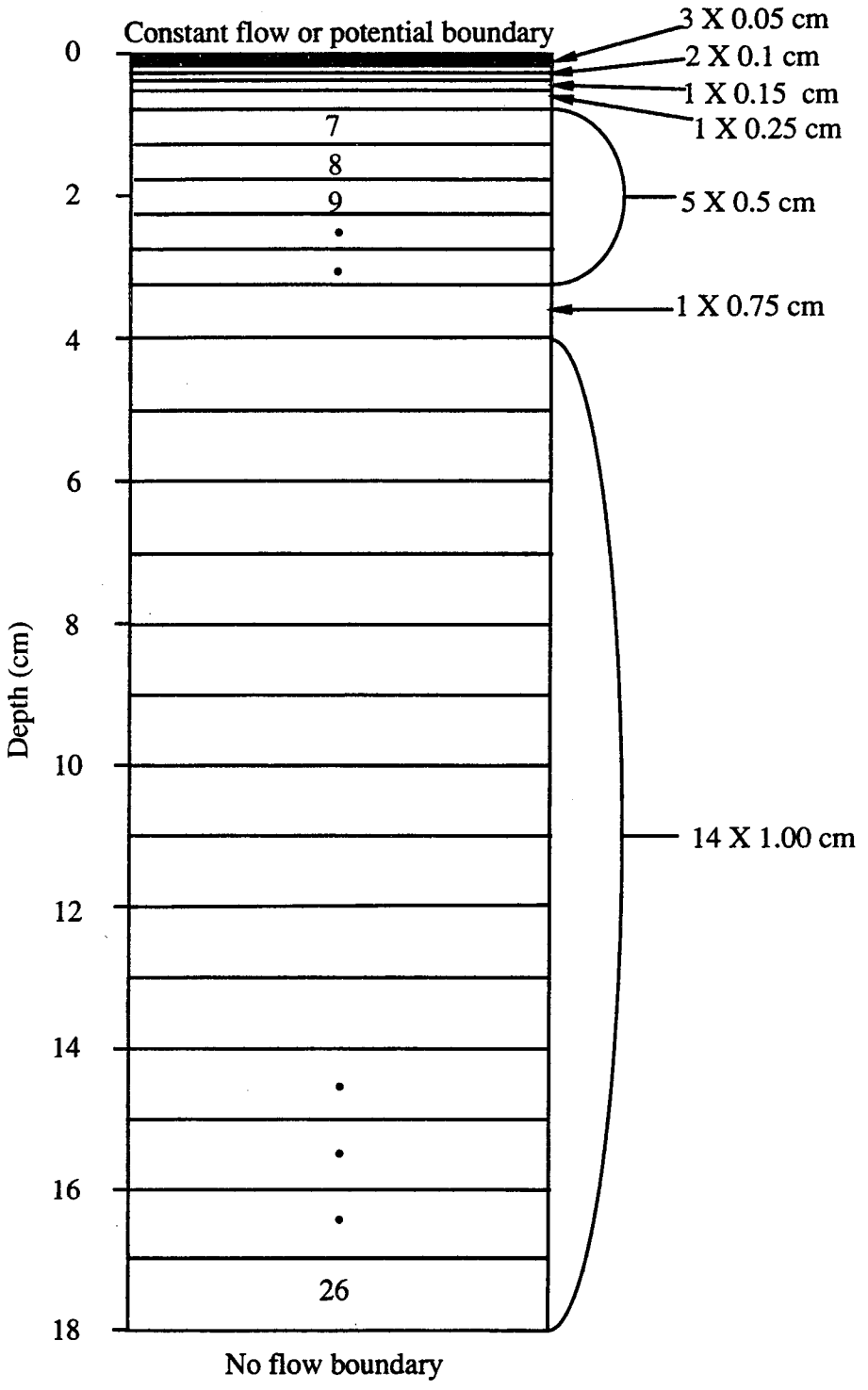

Figure AII.8 "Fine" 1-D mesh for the numerical simulation of redistribution/evaporation experiment by Staple (1971). Both a constant potential and sink boundary conditions at the soil surface were used in the simulations.

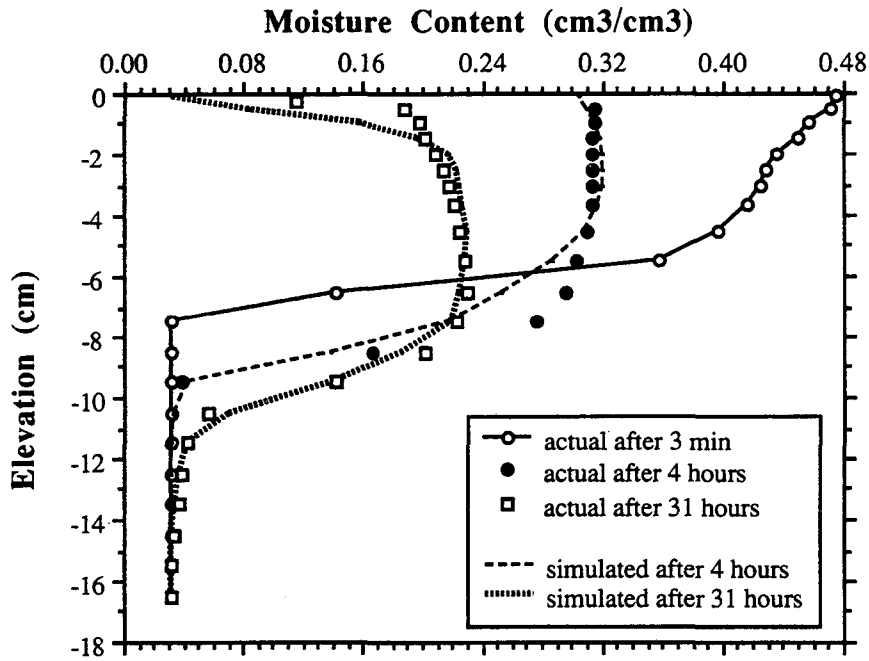

Figure AII.9a Soil moisture distribution profiles during evaporation: actual data and simulated results. Potential evaporation = 9mm/day. Coarse mesh.

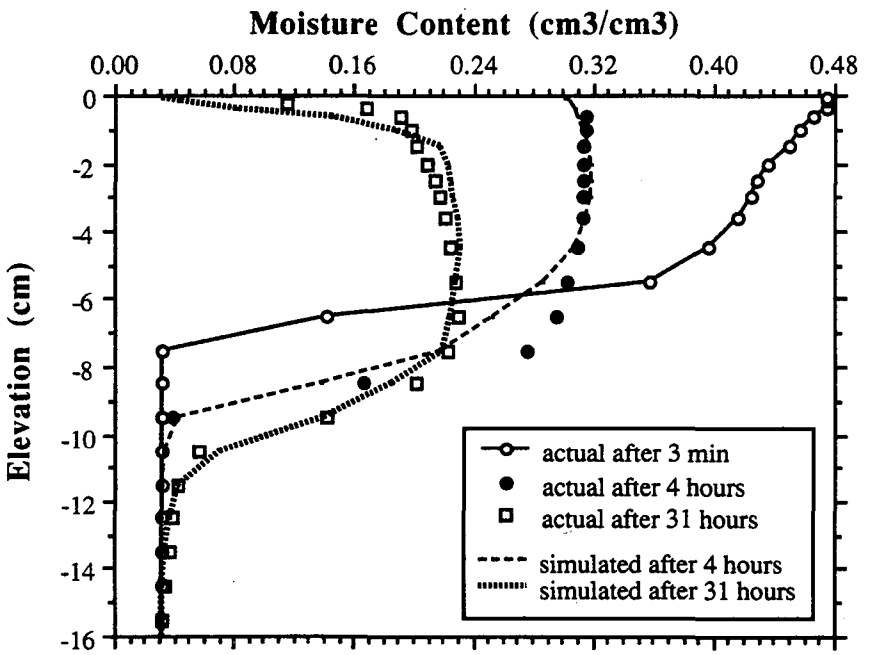

Figure AII.9b Soil moisture distribution profiles during evaporation: actual data and simulated results. Potential Evaporation = 9 mm/day. Medium mesh.

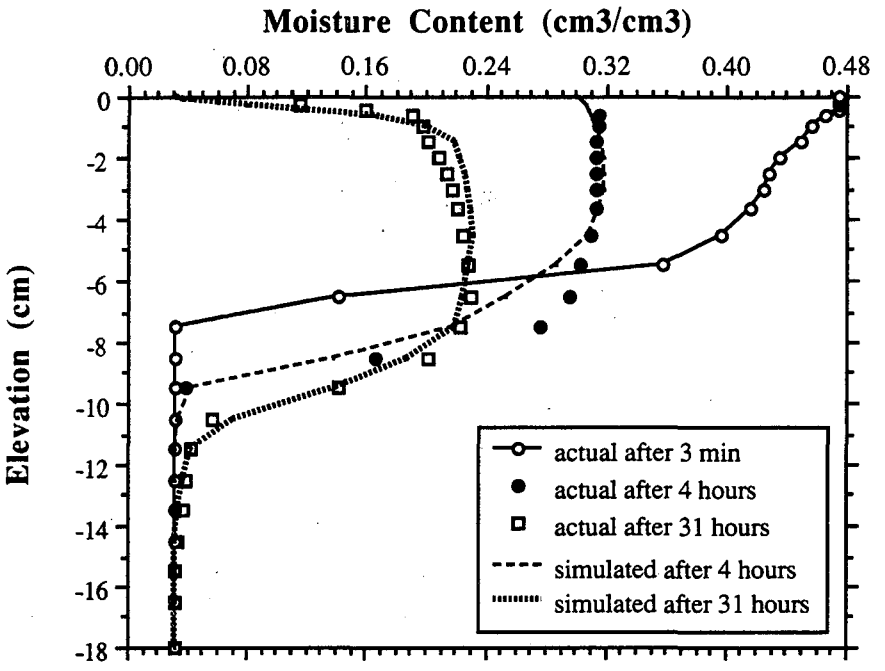

Figure AII.10a Soil moisture distribution profiles during evaporation: actual data and simulated results. Potential Evaporation = 9mm/day. Fine mesh.

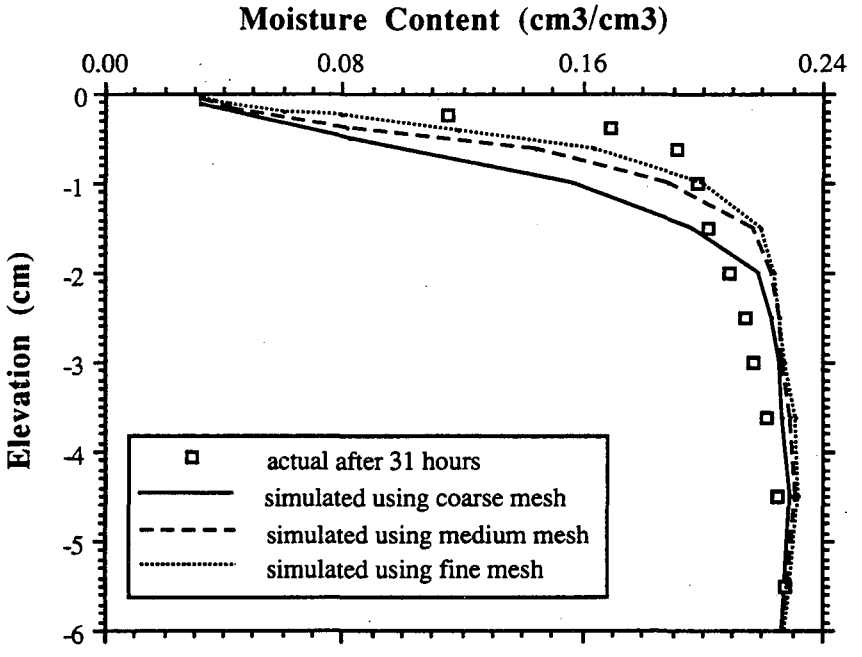

Figure AII.10b Close-up view of soil moisture distribution after 31 hours: Comparison of results using 3 different meshes.

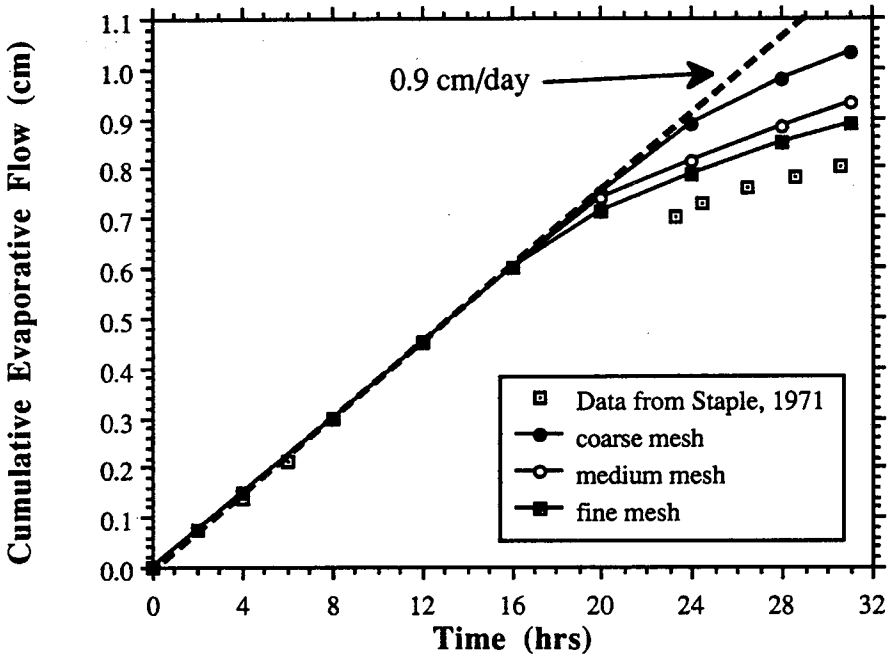

Figure AII.11 Total water loss due to evaporation with time. Sink in top node = 0.9 cm/day or less. External potential in simulations was set at -13,450 m. Comparison of three meshes.

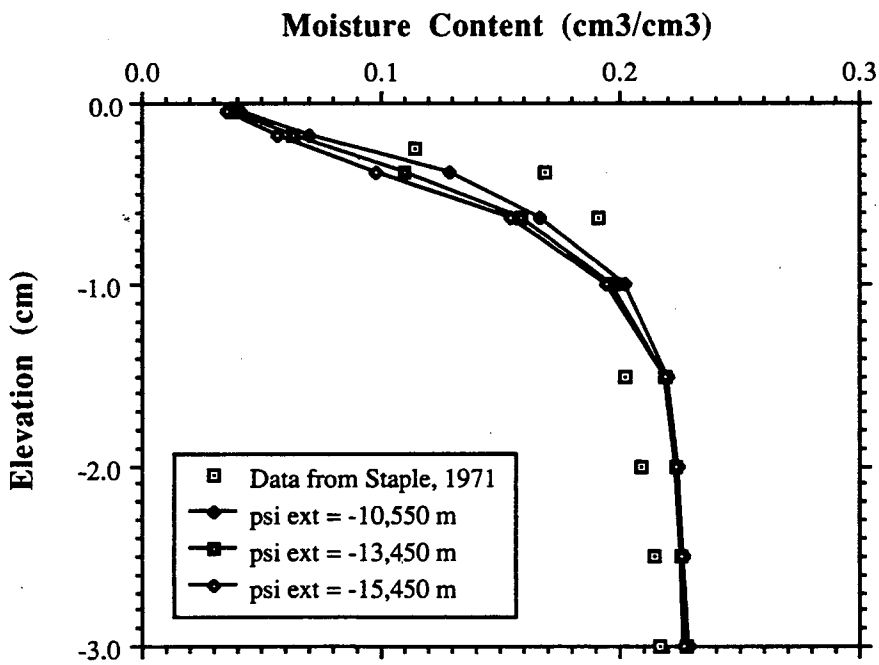

Figure AII.12 Close-up view of soil moisture distribution after 31 hours: comparison of results using 3 different external potentials ("medium" mesh).

The second approach to the upper boundary condition was to prescribe a constant external potential throughout the simulation and not limit the evaporation rate. A zero-volume boundary node was set up above the top node and the medium and fine meshes were used. A comparison of the results using these two meshes shows that the system is still mesh-sensitive but probably less sensitive than it was when the first boundary condition was used (Fig. AII.13a,b). An important observation to make is that the simulated evaporation rate during the first 16 to 20 hours exceeded the potential evaporation rate; after one day, though, the differences between actual and simulated rates were equal to or less than those found using the sink boundary condition.

The above simulations showed TRUST's ability to simulate a fairly complex wetting and drying system. However, simulation of evaporation from a water table, while being a simpler problem, also required some validation. Unfortunately, experimental data which would include soil properties, ambient atmospheric conditions, potential evaporation rates, measured bare soil evaporation rates, and steady-state evaporation from a water table could not be found. All of the above, except the saturation curve were described by Hadas and Hillel (1968; 1972) for Gilat Loess. Since bulk density of this material was given, a particle-size distribution typical of a loess was used to estimate a desaturation curve using the approach of Campbell (1974, 1985) as outlined in Appendix I. Similarly, the conductivity curve was estimated based on an average loess textural composition (silty loam) and compared with the curve given by Hadas and Hillel (1972) which was a fitted curve based on an unspecified number of data points (Fig. AII.14). The calculated curve was considered to be adequate and was used in the simulations (both Case A and Case B were used). In the experiment, Gilat loess was packed into tubes, 5 cm in diameter, and 70 and 120 cm long; the dry bulk density of the soil was 1.45 ± 0.03 g cm^{-3}. A constant water level was maintained at the bottom of each column and the flow into each column was

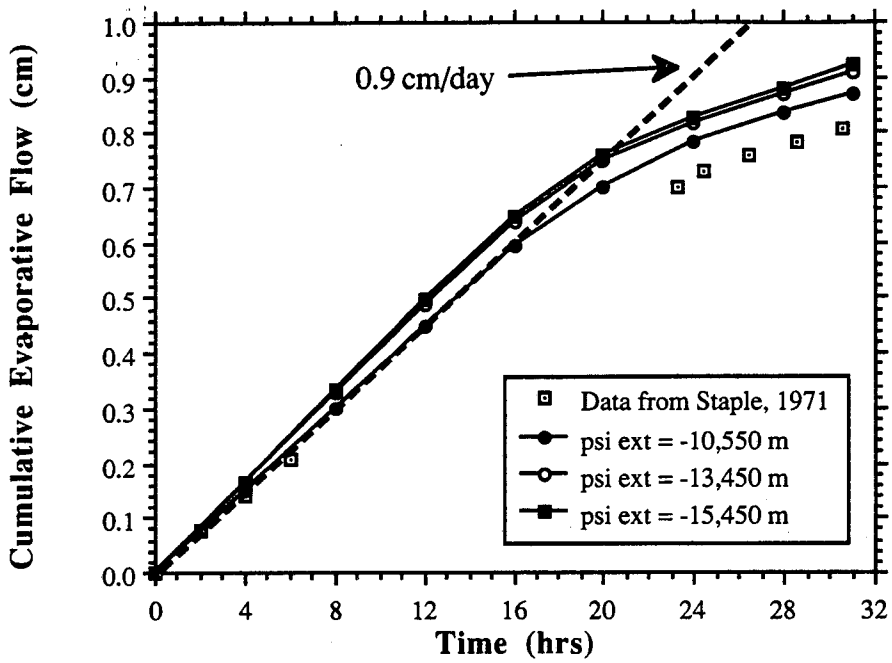

Figure AII.13a Total water loss due to evaporation with time. No sink: rate controlled by external potential. Each curve shows results of simulation with different external potential. Medium mesh.

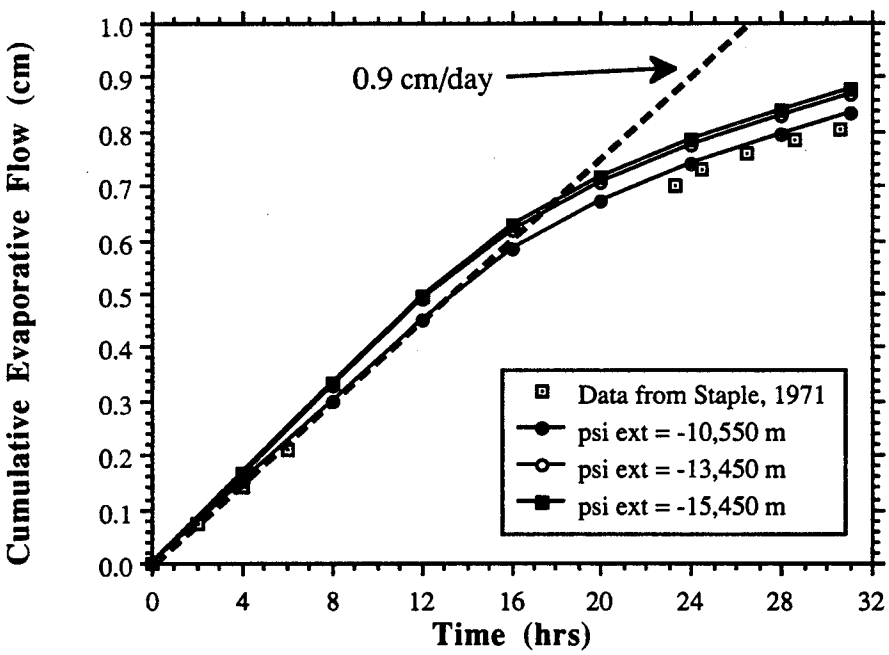

Figure AII.13b Total water loss due to evaporation with time. No sink; rate controlled by external potential. Each curve shows results of simulation with different external potential. Fine mesh.

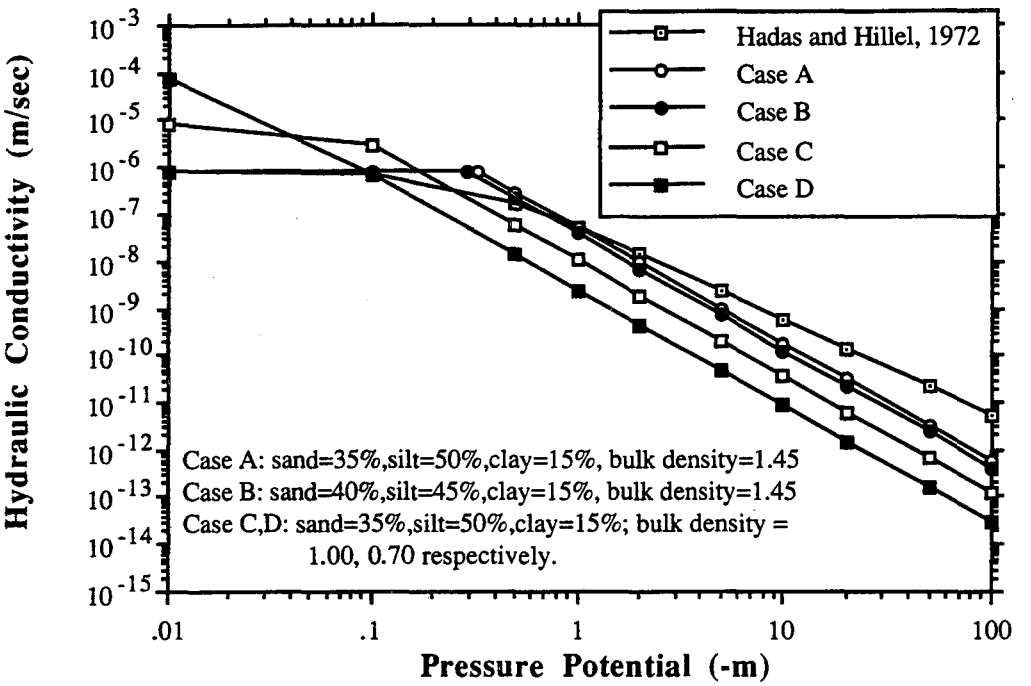

Figure AII.14 Conductivity curves for Gilat Loess as given by Hadas and Hillel, 1972, and as calculated from typical silty loam composition (A, B). Also, curves resulting from reduction of bulk density.

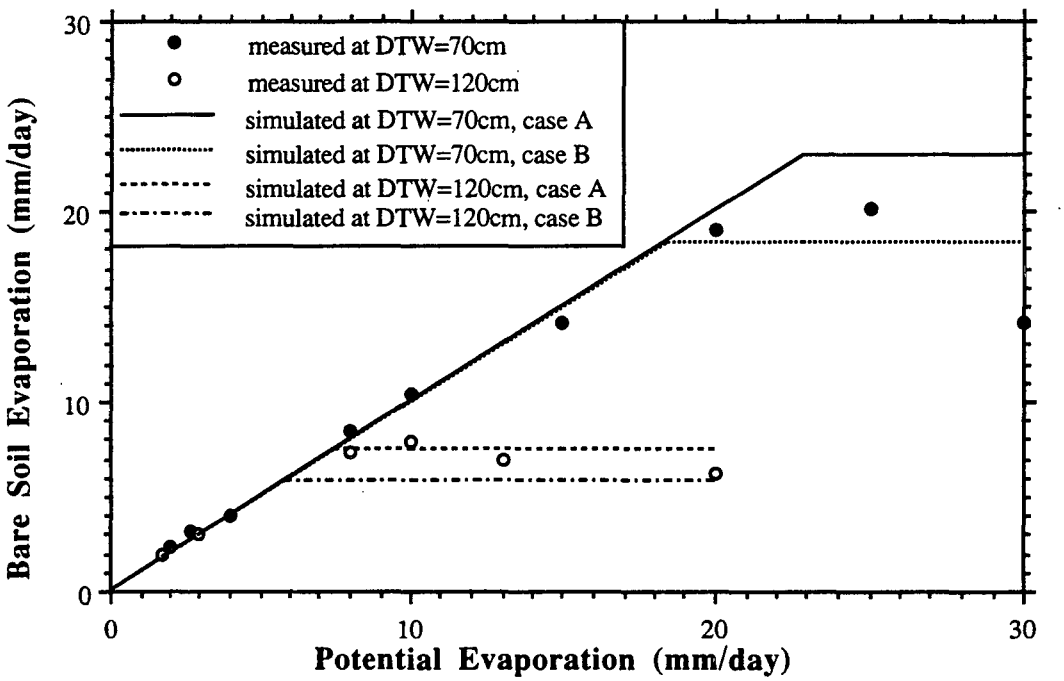

Figure AII.15 Comparison of measured vs. simulated bare soil evaporation rates as a function of potential evaporation, water-table depth, and soil textural composition.

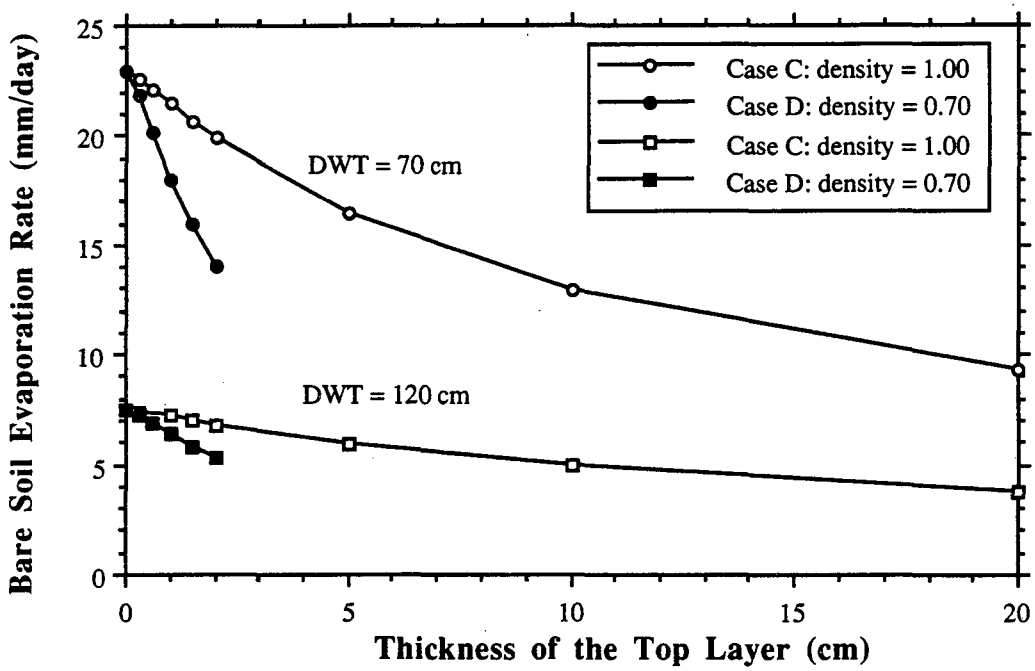

Figure AII.16 Simulated steady state evaporation rates from silty loam at two water table depths as a function of the thickness of a top layer of low bulk density soil.

measured. The soil in the columns was saturated, after which the top was removed and the soil was exposed to a constant evaporativity. After steady-state conditions were attained, external evaporativity was increased to another constant value and the cycle wasrepeated. The results of the experiments and simulations are shown in Fig. AII.15. A sink upper boundary condition was used with the minimum allowable pressure potential in the top element calculated from atmospheric conditions to be approximately -15,000 m (see Eqn. (5.2)). Sixty second time steps were used. As can be seen from Fig. AII.15, the simulations were moderately successful at reproducing laboratory-measured bare soil evaporation rates. However, when potential evaporation reached 30 mm/day, the simulation failed to describe the decline in bare soil evaporation, which was attributed by Hadas and Hillel (1968) to structural changes and resultant conductivity changes due to the drying out of the soil surface. This effect may have been better simulated by a 2-phase (liquid-vapor), non-isothermal model.

Finally, a number of sensitivity studies were performed to estimate the effect of varying the thickness of a reduced bulk density surface layer on evaporation rates. The change in bulk density resulted in a change in the conductivity curve as seen in Fig. AII.14. It was found that the presence of a 2 cm layer of the same composition soil with a dry bulk density of 1.00 g cm^{-3} resulted in a decrease of bare soil evaporation of 13% when the water table was at a depth of 70 cm and 10% when the water table was at 120 cm (Fig. AII.16). When the density of that surface was reduced to 0.70 g cm^{-3}, the decrease in steady-state bare soil evaporation rate was approximately 39% at a depth to water of 70 cm and about 32% at a depth of 120 cm. These dry bulk densities are ones not unlikely to be found in field situations and this example illustrates the potential difficulties involved in modelling bare soil evaporation.

REFERENCES

Arya, L.M., and J.F. Paris, A physioempirical model to predict the soil moisture characteristic from particle-size distribution and bulk density data, *Soil Sci. Soc. Am. J., 45,* 1023-1030, 1981.

Bache, B.W., C.A. Frost, and R.H.E. Inkson, Moisture release characteristics and porosity of twelve Scottish soil series and their variability, *J. Soil Sci., 32,* 505-520, 1981.

Bailey, R.A., W.P. Irwin, and D.L. Jones, Franciscan and related rocks and their significance in the geology of western California, *California Division of Mines and Geology Bulletin, 183,* 177 p., 1964.

Balistrieri, L.S., and T.T. Chao, Selenium adsorption by goethite, *Soil Sci. Soc. Amer. J., 51,* 1145-1151, 1987.

Barraclough, P.B. and P.B. Tinker, The determination of ionic diffusion coefficients in field soils. I. Diffusion coefficients in sieved soils in relation to water content and bulk density, *J. Soil Sci., 32,* 225-236, 1981.

Barraclough, P.B. and P.B. Tinker, The determination of ionic diffusion coefficients in field soils. I. Diffusion of bromide ions in undisturbed soil cores, *J. Soil Sci., 33,* 13-24, 1982.

Bar-Yosef, B. and D. Meek, Selenium sorption by kaolinite and montmorillonite, *Soil Science, 144(1),* 11-19, 1987.

Belitz, K. and F.J. Heimes, Groundwater flow system of the central part of the western valley, in Preliminary assessment of sources, distribution, and mobility of selenium in the San Joaquin Valley, California, *U.S. Geol. Surv. WRI Report 88-4186,* 13-34, 1989.

Benson, S.M., Characterization of the hydrogeologic and transport properties of the shallow aquifer under Kesterson Reservoir, Ph.D. dissertation, University of California, Berkeley, 1988.

Black, T.A., W.R. Gardner, and G.W. Thurtell, The prediction of evaporation, drainage, and soil water storage for a bare soil, *Soil Sci. Soc. Amer. Proc., 33,* 655-660, 1969.

Blake M.C., and D.L. Jones, The Franciscan assemblage and related rocks in northern California: A reinterpretation , in *The Geotectonic Development of California, Rubey v.1,* Prentice Hall, Englewood Cliffs, New Jersey, 1981.

Boast, C.W., Evaporation from bare soil measured with high spatial resolution, in Methods of Soil Analysis, Part 1 - Physical and Mineralogical Methods, A. Klute, ed., 2nd ed., *Agronomy, 9,* pp. 889-900, 1986.

Boast, C.W., and T.M. Robertson, A "micro-lysimeter' method for determining evaporation from bare soil: Description and laboratory evaluation, *Soil Sci. Soc. Am. J., 46,* 689-696, 1982.

Bresler, E., W.D. Kemper, and R.J. Hanks, Infiltration redistribution, and subsequent evaporation of water from soil as affected by wetting rate and hysteresis, *Soil Sci. Soc. Amer. Proc., 33,* 832-840, 1969.

Bresler, E., B.L. McNeal, and D.L. Carter, *Saline and Sodic Soils: Principles-Dynamics-Modeling,* Springer-Verlag, Berlin, 1982.

Brooks, R.H., and A.T. Corey, Hydraulic properties of porous media, *Hydrology Paper No.3,* Colorado State University, Fort Collins, 1964.

Campbell, G.S., A simple method for determining unsaturated conductivity from moisture retention data, *Soil Science, 117,* 311-314, 1974.

Campbell, G.S., *Soil Physics With Basic: Transport Models for Soil-Plant Systems,* Elsevier, Amsterdam, The Netherlands, 1985.

Carpena, O., M.G. Guillén, F.G. Fernández, and M. Caro, Saline soil classification using the 5:1 aqueous extract, *Trans. 9th Int. Cong. Soil Sci., 85, 483-490,* 1968.

Cassell, D.K., and A. Klute, Water Potential: Tensiometry, in Methods of Soil Analysis, Part 1 - Physical and Mineralogical Methods, A. Klute, ed., 2nd ed., *Agronomy, 9,* pp. 563-596, 1986.

Childs, E.C., *An Introduction to the Physical Basis of Soil Water Phenomena,* Wiley (Interscience), New York, 1969.

Childs, E.C., and N. Collis-George, The permeability of porous materials, *Proc. Roy. Soc. London, A 201,* 392-405, 1950.

Clapp, R.B., and G.M. Hornberger, Empirical equations for some hydraulic properties, *Water Resour. Res., 14,* 601-604, 1978.

Dane, J.H., and F.H. Mathis, An adaptive finite difference scheme for the one-dimensional water flow equation, *Soil Sci. Soc. Am. Proc., 45,* 1048-1054, 1981.

Davis, G.H., J.H. Green, F.H. Olmsted, and D.W. Brown, Ground-water conditions and storage capacity in the San Joaquin Valley, California, *U.S. Geol. Surv Water Supply Paper 1469,* 287 p., 1959.

Day, P.R., Particle size fractionation and particle-size analysis, in Methods of soil analysis, Part I. *Agronomy, 9,* 545-567, 1965.

Deverel, S.J., and R. Fujii, Processes affecting the distribution of selenium in shallow groundwater of agricultural areas, western San Joaquin Valley, California, *Water Resour. Res., 24(4),* 516-524, 1988.

Dubrovsky, N.M, Selenium in ground water of the northern part of the western valley, in Preliminary assessment of sources, distribution, and mobility of selenium in the San Joaquin Valley, California, *U.S. Geol. Surv. WRI Report 88-4186,* 67-75, 1989.

Dubrovsky, N.M. and S.J. Deverel, Selenium in ground water of the central part of the western valley, in Preliminary assessment of sources, distribution, and mobility of

selenium in the San Joaquin Valley, California, *U.S. Geol. Surv. WRI Report 88-4186,* 35-66, 1989.

Edwards, A.L., TRUMP: A computer program for transient and steady state temperature distributions in multi-dimensional systems, Rev. II: Springfield Virginia, National Technical Information Service, National Bureau of Standards, 1972.

Elrashidi, M.A., D.C. Adriano, S.M. Workman, and W.L. Lindsay, Chemical equilibria of selenium in soils: A theoretical development, *Soil Science, 144(2),* 141-152, 1987.

Feddes, R.A., E. Bresler, and S.P. Neumann, Field test of a modified numerical model for water uptake by root systems, *Water Resour. Res., 10(6),* 1199-1206, 1974.

Feddes, R.A., S.P. Neumann, and E. Bresler, Finite element analysis of two-dimensional flow in soils considering water uptake by roots: II. Field applications, *Soil Sci. Soc. Amer. Proc., 39,* 231-237, 1975.

Fio, J.L. and R. Fujii, Comparison of methods to determine selenium species in saturation extracts of soils from the western San Joaquin Valley, California, *Geol. Surv. Open-file Report 88-458,* 16 p., 1988.

Flaschka, H.A., A.J. Barnard, Jr., and P.E. Sturrock, *Quantitative Analytical Chemistry: Vol. I,* Barnes and Noble, 1969.

Flexser, S., Lithologic composition and variability of the sediments underlying Kesterson Reservoir as interpreted from shallow cores, LBL-25586, Lawrence Berkeley Laboratory, Berkeley, California, 1988.

Frankenberger, W.T., and U. Karlson, Dissipation of soil selenium by microbial volatilization at Kesterson Reservoir, Final Report to the U.S. Bureau of Reclamation, 1988.

Freeze, R.A., and J.A. Cherry, *Groundwater*, Prentice-Hall, Inc., Engelewood Cliffs, New Jersey, 1979

Fujii, R., S.J. Deverel, and D.B. Hatfield, Distribution of selenium in soil in agricultural fields, western San Joaquin Valley, California, *Soil Sci. Soc. Am. J., 52(5),* 1274-1283, 1988.

Gardner, H.R., Prediction of evaporation from homogeneous soil based on the flow equation, *Soil Sci. Soc. Amer. Proc., 37,* 513-516, 1973.

Gardner, W.R., Some steady-state solutions to the unsaturated flow equation with application to evaporation from a water table, *Soil Science, 85,* 228-232, 1958.

Gardner, W.R., and M. Fireman, Laboratory studies of evaporation from soil columns in the presence of a water table, *Soil Science, 85,* 244-249, 1958.

Gardner, W.R., D. Hillel, and Y. Benyamini, Post irrigation movement of soil water: I. Redistribution, *Water Resour. Res., 6(3),* 851-861; II. Simultaneous redistribution and evaporation,*Water Resour. Res., 6(4),* 1148-1153, 1970.

Gillham, R.W., and J.A. Cherry, Contaminant migration in saturated unconsolidated geologic deposits, in *Recent Trends in Hydrogeology,* T.N. Narasimhan, ed., Geol. Soc. Am. Special Paper 189, 31-62, 1982.

Gilliom, R.J., Geologic source of selenium and its distribution in soil, in Preliminary assessment of sources, distribution, and mobility of selenium in the San Joaquin Valley, California, *U.S. Geol. Surv. WRI Report 88-4186,* 7-11, 1989.

Gupta, S.C., and W.E. Larson, Estimating soil water retention characteristics from particle size distribution, organic matter content and bulk density, *Water Resour. Res., 14,* 1633-1635, 1979.

Hadas, A. and D. Hillel, An experimental study of evaporation from uniform soil columns in the presence of a water table, *Trans. 9th Int. Cong. Soil Sci., 85, 228-232,* 1968.

Hadas, A. and D. Hillel, Steady-state evaporation through non-homogeneous soils from a shallow water table, *Soil Science, 113(2),* 65-73, 1972.

Hall, D.G.M., A.J. Reeve, A.J. Thomasson, and V.F. Wright, Water Retention, Porosity, and Density of Field Soils, *Soil Survey Technical Monograph 9,* Rothamsted Experimental Station, Harpenden, England, 1977.

Hanks, R.J., A. Klute, and E. Bresler, A numeric method for estimating infiltration, redistribution, drainage, and evaporation of water from soil, *Water Resour. Res., 5(5),* 1064-1069, 1969.

Harradine, F., *Soil Survey of Western Fresno County,* University of California Press, Berkeley, 1950.

Hatfield, J.L., A. Perrier, and R.D. Jackson, Estimation of evapotranspiration at one-time-of-day using remotely sensed surface temperature, *Agric. Water Manag., 7,* 341-350, 1983.

Haverkamp, R., and M. Vauclin, A note on estimating finite difference interblock hydraulic conductivity values for transient unsaturated flow problems, *Water Resour. Res., 15(1),* 181-187, 1979.

Hillel, D., *Fundamentals of Soil Physics*, Academic Press, New York, 1980a.

Hillel, D., *Applications of Soil Physics*, Academic Press, New York, 1980b.

Hillel, D., Simulation of evaporation from bare soil under steady and diurnally fluctuating evaporativity, *Soil Science, 120(3),* 230-237, 1975.

Hillel D., On the role of soil moisture hysteresis in the suppression of evaporation from bare soil under diurnally cyclic evaporativity, *Soil Science, 122,* 309-314, 1976.

Hotchkiss, W.R., Generalized subsurface geology of the water-bearing deposits, northern San Joaquin Valley, California, *U.S. Geol. Surv. Open-File Report,* 1972.

Hotchkiss, W.R., and G.O. Balding, Geology, hydrology, and water quality of the Tracy-Dos Palos area, San Joaquin Valley, California, *U.S. Geol. Surv. Open File Report,* 1971.

Hubbert, M.K., The theory of groundwater motion, *J. Geol., 48,* 785-944, 1940.

Jackson, R.D., On the calculation of hydraulic conductivity, *Soil Sci. Soc. Am. Proc., 36,* 380-382, 1972.

Jackson, R.D., B.A. Kimball, R.J. Reginato, and F.S. Nakayama, Diurnal soil-water evaporation: Time-depth-flux patterns, *Soil Sci. Soc. Amer. Proc., 37,* 505-509, 1973.

Johnson, L.W., and R.D. Riess, *Numerical Analysis,* Addison-Wiley, New York, 1977

Koorevar, P., G. Menelik, and C. Dirksen, *Elements of Soil Physics,* Elsevier, Amsterdam, The Netherlands, 1983.

Kohout, F.A., Reorientation of our saline water resources thinking, *Water Resour. Res., 6(5),* 1442-1448, 1970.

Lawrence Berkeley Laboratory, *Hydrological, Geochemical, and Ecological Characterization of Kesterson Reservoir, Annual Report, LBL-24520,* Berkeley, California, 1987.

Lawrence Berkeley Laboratory, *Hydrological, Geochemical, and Ecological Characterization of Kesterson Reservoir, Annual Report, LBID-1420,* Berkeley, California, 1988.

Lettis, W.R., Late Cenozoic stratigraphy and structure of the western margin of the central San Joaquin Valley, California, *U.S. Geol. Surv. Open-File Report 82-526,* 203 p., 1982.

Lindsay, W.L., *Chemical Equilibria in Soils,* Wiley, New York, 1979.

Long, R.H., Analysis of selenium and chloride movement through a shallow pond sediment at Kesterson Reservoir, M.S. thesis, University of California, Berkeley, 1988.

Lund L.J., D. Bakhtar, and G.R. Bradford, sources of selenium and salinity in soils and sediments of the west side of the San Joaquin Valley, in *1985-1986 Technical Progress Report, U.C. Salinity/Drainage Task Force,* Davis, University of California, Division of Agriculture and Natural Resources, 22-30, 1987.

MacFarlane, D.S., J.A. Cherry, R.W. Gillham, and E.A. Sudicky, Migration of contaminants in groundwater at a landfill: a case study, 1. Groundwater flow and plume dileneation, *J. Hydrol., 63(1,2),* 1-29, 1983.

McNeal, J.M., and L.S. Balistrieri, Geochemistry and occurence of selenium: An overview, in Selenium in Agriculture and the Environment, *Soil Sci. Soc. Am. Spec. Publ. No. 23,* L.W. Jacobs, ed., American Society of Agronomy, Madison, Wisconsin, pp. 1-14, 1989.

Moore, R.E., Water conduction from shallow water tables, *Hilgardia, 12,* 383-426, 1939.

Narasimhan, T.N, A unified numerical method for saturated-unsaturated flow, Ph.D. dissertation, University of California, Berkeley, 1975.

Narasimhan, T.N., Physics of saturated-unsaturated subsurface flow, in *Recent Trends in Hydrogeology,* T.N. Narasimhan, ed., Geol. Soc. Am. Special Paper 189, 3-23, 1982a.

Narasimhan, T.N., Numerical modeling in hydrogeology, in *Recent Trends in Hydrogeology,* T.N. Narasimhan, ed., Geol. Soc. Am. Special Paper 189, 273-296, 1982b.

Narasimhan, T.N., and P.A. Witherspoon, An integrated finite difference method for fluid flow in porous media, *Water Resour. Res., 12(1),* 57-64, 1976.

Narasimhan, T.N., and P.A. Witherspoon, Numerical model for saturated-unsaturated flow in deformable porous media, I. Theory, *Water Resour. Res., 13(3),* 657-666, 1977.

Narasimhan, T.N., P.A. Witherspoon, and A.L. Edwards, Numerical method for saturated-unsaturated flow in deformable porous media: 2. The algorithm, *Water Resour. Res., 14(2),* 255-261, 1978.

National Academy of Sciences, Food and Nutrition Board, Recommended dietary allowances, 9th rev. edn., National Research Council, Washington, D.C., 1980.

Neumann, S.P., R.A. Feddes, and E. Bresler, Finite element analysis of two-dimensional flow in soils considering water uptake by roots: I. Theory, *Soil Sci. Soc. Amer. Proc., 39,* 224-230, 1975

Nimah, M.N., and R.J. Hanks, Model for estimating soil water, plant, and atmospheric interrelations: I. Description and sensitivity, *Soil Sci. Soc. Amer. Proc., 37,* 522-527, 1973.

Passerat de Sillans, A., L. Bruckler, J.L. Thony, and M. Vauclin, Numerical modeling of coupled heat and water flows during drying in a stratified bare soil - Comparison with field observations, *J. Hydrol., 105,* 109-138, 1989.

Penman, H.L., Natural evaporation from open water, bare soil and grass, *Proc. Roy. Soc., 193,* 120-145, 1948.

Pinner, A., and P.H. Nye, A pulse method for studying effects of dead-end pores, slow equilibration and soil structure on diffusion of solutes in soil, *J. Soil Sci., 33,* 25-35, 1982.

Poland, J.F., B.E. Lofgren, R.L. Ireland, and R.G. Pugh, Land subsidence in the San Joaquin Valley, California, as of 1972, *U.S. Geol. Surv. Prof. Paper 437-H,* 78 p., 1975.

Porter, L.K., W.D. Kemper, R.D. Jackson, and B.A. Stewart, Chloride diffusion in soils as influenced by moisture content, *Soil Sci. Soc. Amer. Proc., 24,* 460-463, 1960.

Presser, T.S. and I. Barnes, Dissolved constituents including selenium in waters in the vicinity of Kesterson National Wildlife Refuge and the West Grassland, Fresno and Merced counties, California, *U.S. Geol. Surv. Water Resour. Invest. Rep., 85-4220,* 34-47, 1985.

Presser, T.S., and H.M. Ohlendorf, Biogeochemical cycling of selenium in the San Joaquin Valley, California, USA, *Environmental Management, 11(6),* 1988.

Qayyum, M.A., and W.D. Kemper, Salt-concentration gradients in soils and their effects on moisture movement and evaporation, *Soil Science, 93,* 333-342, 1961.

Reynolds, W.D, and D.E. Elrick, Measurement of field-saturated hydraulic conductivity, sorptivity and the conductivity-pressure head relationship using the "Guelph Permeameter," Proc. Nat. Water Well Assoc. Conf. on Characterization and Monitoring of the Vadose Zone, Denver Colorado, Nov. 1985.

Reynolds, W.D., and G.K. Walker, Development and validation of a numerical model simulating evaporation from short cores, *Soil Sci. Soc. Am. J., 48,* 960-969, 1984.

Rhoades, J.D., Monitoring soil salinity: A review of methods, in *Establishment of water quality monitoring programs,* L.G. Everett and K.D. Schmidt eds., Am. Water Resour. Assoc., Minneapolis, 1978.

Rhoades, J.D., Principles and methods of monitoring soil salinity, in *Soil Salinity under Irrigation: Processes and Management,* I. Shainberg and J. Shalhevet, eds., Springer-Verlag, Berlin Heidelberg, 1984.

Richards, L.A., Capillary conduction of liquids through porous mediums, *Physics, 1,* 318-333, 1931.

Ripple, C.D., J. Rubin, and T.E.A. van Hylckama, Estimating steady-state evaporation rates from bare soils under conditions of high water table, *U.S. Geol. Surv. Water-Supply Paper 2019-A,* and others, 1972.

Salhotra, A.M., E.E. Adams, and D.R.F. Harleman, Effect of salinity and ionic composition on evaporation: Analysis of dead sea evaporation pans, *Water Resour. Res., 21(9),* 1336-1344, 1985.

Saxton, K.E., W.J. Rawls, J.S. Romberger, and R.I. Papendick, Estimating generalized soil-water characteristics from texture, *Soil Sci. Soc. Am. J., 50,* 1031-1036, 1986.

Schnabel, R.R., and E.B. Richie, Calculation of internodal conductances for unsaturated flow simulations: A comparison, *Soil Sci. Soc. Am. J., 48,* 1006-1010, 1984.

Schuh, W.M., J.W. Bauder, and S.C. Gupta, Evaluation of simplified methods for determining unsaturated hydraulic conductivity of layered soils, *Soil Sci. Soc. Am. J., 48,* 730-736, 1984.

Schuh, W.M., and J.W. Bauder, Effect of soil properties on hydraulic conductivity-moisture relationships, *Soil Sci. Soc. Am. J., 50,* 848-855, 1986.

Seidell, A., *Solubilities,* 1, 4th ed. American Chemical Society, D. van Nostrand Co., Princeton, New Jersey, 1958.

Shirazi, M.S., and L. Boersma, A unifying quantitative analysis of soil texture, *Soil Sci. Soc. Am. J., 48,* 142-147, 1984.

Sposito, G., *The Surface Chemistry of Soils*, Oxford University Press, New York, 1984.

Staple, W.J., Comparison of computed and measured moisture redistribution following infiltration, *Soil Sci. Soc. Am. Proc., 33,* 840-847, 1969.

Staple, W.J., Predicting moisture distributions in rewetted soils, *Soil Sci. Soc. Amer. Proc., 34,* 387-392, 1970.

Staple, W.J., Boundary conditions and conductivities used in the isothermal model of evaporation from soil, *Soil Sci. Soc. Am. Proc., 35,* 853-855, 1971.

Taylor, J.R., *An Introduction to Error Analysis: The Study of Uncertainties in Physical Measurements,* University Science Books, Mill Valley, California, 1982.

Tidball R.R., R.C Severson, C.A. Gent, and G.O. Riddle, Element associations in soils of the San Joaquin Valley, California, *U.S. Geol. Surv. Open-File Report 86-583,* 1986.

Tokunaga,T.K., Laboratory permeability errors from annular wall flow, *Soil Sci. Soc. Am. J., 52,* 24-27, 1988.

USDA Soil Conservation Service, Soil survey of the Los Banos area, California, Series 1939, 1952.

van Bavel, C.H.M., Lysimetric measurements of evapotranspiration rates in the eastern United States, *Soil Sci. Soc. Amer. Proc., 25,* 138-141, 1961.

van Bavel, C.H.M., and D. Hillel, Calculating potential and actual evaporation from a bare soil surface by simulateion of concurrent flow of water and heat, *Agric. Meteorol., 17,* 453-476, 1976.

Van De Pol, R.M., P.J. Wierenga, and D.R. Nielsen, Solute movement in a field soil, *Soil Sci. Soc. Am. J., 40,* 473-480, 1977.

Veihmeyer, F.J. and F.A. Brooks, Measurements of cumulative evaporation from bare soil, *Trans. Am. Geoph. Union, 35(6),* 1954.

Weres, O., A.F. White, H.A. Wollenberg, and A. Yee, Geochemistry of selenium at Kesterson Reservoir: Possible remedial measures, *Earth Sciences (Lawrence Berkeley Laboratory PUB-431), 8(3),* 1-8, 1985.

Yates, C.C., Analysis of pumping test data of a leaky and layered aquifer with partially penetrating wells, M.S. thesis, University of California, Berkeley, 1988.

van Bavel, C.H.M., Lysimetric measurements of evapotranspiration rates in the eastern United States, *Soil Sci. Soc. Amer. Proc., 25,* 138-141, 1961.

van Bavel, C.H.M., and D. Hillel, Calculating potential and actual evaporation from a bare soil surface by simulateion of concurrent flow of water and heat, *Agric. Meteorol., 17,* 453-476, 1976.

Van De Pol, R.M., P.J. Wierenga, and D.R. Nielsen, Solute movement in a field soil, *Soil Sci. Soc. Am. J., 40,* 473-480, 1977.

Veihmeyer, F.J. and F.A. Brooks, Measurements of cumulative evaporation from bare soil, *Trans. Am. Geoph. Union, 35(6),* 1954.

Weres, O., A.F. White, H.A. Wollenberg, and A. Yee, Geochemistry of selenium at Kesterson Reservoir: Possible remedial measures, *Earth Sciences (Lawrence Berkeley Laboratory PUB-431), 8(3),* 1-8, 1985.

Yates, C.C., Analysis of pumping test data of a leaky and layered aquifer with partially penetrating wells, M.S. thesis, University of California, Berkeley, 1988.

van Bavel, C.H.M., Lysimetric measurements of evapotranspiration rates in the eastern United States, *Soil Sci. Soc. Amer. Proc., 25,* 138-141, 1961.

van Bavel, C.H.M., and D. Hillel, Calculating potential and actual evaporation from a bare soil surface by simulateion of concurrent flow of water and heat, *Agric. Meteorol., 17,* 453-476, 1976.

Van De Pol, R.M., P.J. Wierenga, and D.R. Nielsen, Solute movement in a field soil, *Soil Sci. Soc. Am. J., 40,* 473-480, 1977.

Veihmeyer, F.J. and F.A. Brooks, Measurements of cumulative evaporation from bare soil, *Trans. Am. Geoph. Union, 35(6),* 1954.

Weres, O., A.F. White, H.A. Wollenberg, and A. Yee, Geochemistry of selenium at Kesterson Reservoir: Possible remedial measures, *Earth Sciences (Lawrence Berkeley Laboratory PUB-431), 8(3),* 1-8, 1985.

Yates, C.C., Analysis of pumping test data of a leaky and layered aquifer with partially penetrating wells, M.S. thesis, University of California, Berkeley, 1988.

van Bavel, C.H.M., Lysimetric measurements of evapotranspiration rates in the eastern United States, *Soil Sci. Soc. Amer. Proc., 25,* 138-141, 1961.

van Bavel, C.H.M., and D. Hillel, Calculating potential and actual evaporation from a bare soil surface by simulateion of concurrent flow of water and heat, *Agric. Meteorol., 17,* 453-476, 1976.

Van De Pol, R.M., P.J. Wierenga, and D.R. Nielsen, Solute movement in a field soil, *Soil Sci. Soc. Am. J., 40,* 473-480, 1977.

Veihmeyer, F.J. and F.A. Brooks, Measurements of cumulative evaporation from bare soil, *Trans. Am. Geoph. Union, 35(6),* 1954.

Weres, O., A.F. White, H.A. Wollenberg, and A. Yee, Geochemistry of selenium at Kesterson Reservoir: Possible remedial measures, *Earth Sciences (Lawrence Berkeley Laboratory PUB-431), 8(3),* 1-8, 1985.

Yates, C.C., Analysis of pumping test data of a leaky and layered aquifer with partially penetrating wells, M.S. thesis, University of California, Berkeley, 1988.

LAWRENCE BERKELEY LABORATORY
TECHNICAL INFORMATION DEPARTMENT
1 CYCLOTRON ROAD
BERKELEY, CALIFORNIA 94720